

City Research Online

City St George's, University of London

Citation: Vassie, P. R. (1972). A study of gas evolution in porous electrodes. (Unpublished Doctoral thesis, The City University)

This is the accepted version of the paper.

This version of the publication may differ from the final published version. To cite this item please consult the publisher's version.

Permanent repository link: https://openaccess.city.ac.uk/id/eprint/38541/

Copyright and Reuse: Copyright and Moral Rights remain with the author(s) and/or copyright holders. Copies of full items can be used for personal research or study, educational, or not-for-profit purposes without prior permission or charge, unless otherwise indicated, provided that the authors, title and full bibliographic details are credited, a hyperlink and/or URL is given for the original metadata page and the content is not changed in any way. For full details of reuse please refer to City Research Online policy.

City Research Online: http://openaccess.city.ac.uk/ publications@citystgeorges.ac.uk

A STUDY OF GAS EVOLUTION IN POROUS ELECTRODES

A thesis submitted for the degree Doctor of Philosophy,

of The City University

by

P.R. VASSIE

The author was in receipt of a SRC studentship.

THE CITY UNIVERSITY LIBRARY,
ST. JOHN STREET, LONDON, E.C.1.

68757

Aknowledgements.

The author wishes to aknowledge the advice and encouragement given to him by his supervisor, Dr. A.C.C. Tseung, and to the members of the materials research group for their useful discussions.

The Materials Research Group,
The Department of Chemistry,
The Gloucester Way Annexe,
The City University,
London, E.C.I.

Index.

Summary.	I
The Problem Areas.	4
Chapter I - A Review of the Literature.	6
Chapter 2 - Experimental Techniques.	46
Chapter 3 - The effect of gas evolution on the electrode structure and surface state of carbon and platinum electrodes.	90
Chapter 4 - The effect of electrode structure on the activity of gas evolution electrodes.	242
Suggestions for Further work.	296
References.	
Appendix.	

Index to Figures.

I. Floating half cell. 52

2. Reference electrode. 53

3. Circuit for recording steady state galvanostatic and potentiostatic polarisation curves. 54

4. Circuit, input and response curves for the interrupter technique. 62

5. Circuit for the potentiostatic pulse technique. 68

6. Circuit for the linear sweep technique. 78

7. Galvanostatic hydrogen stripping cell. 81

8. Galvanostatic hydrogen stripping oscilloscope trace. 85

9. Coulter counter cell. 87

IO. Graph for total, faradaic and charging currents v. time. 74

II. Double layer charging curves. 70

I2. Double layer charging data. 72

I3. i v. $t^{0.5}$ plots for platinum foil and black. 75

I4. Input and response traces for the determination of roughness factors. 85

I5. Circuit for galvanostatic hydrogen stripping. 82

I6. Electron micrographs of platinum and carbon blacks. 238

Index to Tables.

I. A comparison of energy conversion devices. IO

2. Rumpf's data for agglomerate strength v. particle size. 23I

3. Fall of anodic currents with time on graphite. IOO

4,5. Effect of hydrogen evolution on hydrogen oxidation performance of platinised graphite. II2,II4

6. Effect of hydrogen evolution on the graphite electrode structure. I25

7. Effect of anodic pretreatments on the oxygen reduction i - E data for graphite. I32

8. Effect of anodic pretreatments on the oxygen reduction data for platinised graphite. I38

9. Electrode potentials of metal/metal oxide couples. I63

IO-I5. Effect of anodic pretreatment on the oxygen reduction i - E data for platinum black. I45- I49

I6-I8. Effect of cathodic pretreatment on the hydrogen oxidation i - E data for platinum black. I5I -3

I9. Effect of cathodic pretreatment on the hydrogen oxidation i - E data for platinised tungsten trioxide. I54

20. Effect of anodic pretreatments on the oxygen reduction i - E data for cobalt nickel oxide. I56

2I. Cathodic i - t curves for preanodised platinum foil. I78

22. Linear sweep data on preanodised platinum foil under oxygen and nitrogen. I8I

23. Transient i - E data on clean and oxidised platinum foil under oxygen and nitrogen. I85

24. Cathodic i - t curves for clean and preanodised platinum. I88

25. i - t data for platinum foil in the range I.0 - 2.0 V. I99

26. Oxygen evolution and oxide formation currents from I.5 - 2.0 V. 207

27. Surface area on platinum blacks. 254

28. Transient and steady state hydrogen oxidation/ evolution i - E data for platinum black. 268

29. The effect of gas bubbles on the gas evolution performance of planar electrodes. 274

30-33. The effect of gas evolution on the double layer peak height of porous and planar electrodes. 276 - 7

34-35. Effectiveness factors for hydrogen evolution/ oxidation on platinum black. 290

36. Hydrogen oxidation/evolution i - E data considering the true electrochemical surface area. 253 48

37. Cathodic i - E curve on preanodised platinum black under oxygen. I65 6

Index to Graphs.

I - 2. The effect of anodic pretreatment on the oxygen reduction performance of silver on graphite electrodes. 96-7

3. Transient oxygen reduction performance on graphite surfaces. I07

4. Oxygen evolution performance on nickel and platinum screens. I08

5. Oxygen evolution performance on graphite cloth. I09

6. Hydrogen evolution performance on graphite powder. III

7. Hydrogen evolution performance on graphite cloth. II6

8-9. Hydrogen evolution performance on nickel and platinum screen. II7

I0-I4. The effect of hydrogen evolution pretreatment time on the hydrogen oxidation performance of graphite electrodes. I3I,II9,I20

I5. Oxygen reduction i - E curve for Co_2NiO_4 I57

I6. Oxygen reduction transient i - E curves for graphite. I6I

I7. Oxygen evolution transient i - E curves for graphite. I62

I8. O.C.V. v. time following anodic pretreatment. I68

I9-20. Transient cathodic i - E curves on clean and oxidised platinum surfaces. I89

2I-22. Effect of oxygen evolution on the oxygen reduction performance of platinum black. I66

23. Oxygen reduction performance on clean and oxidised platinum surfaces. I7I

24. Polarisation and Tafel plots for oxygen

reduction on a Pt-O surface. 183
25. Current-charge-potential-time data for platinum foil at anodic currents. 195
26. Linear sweep oxide formation curve on platinum. 190
27. Relative rate of anodic current decay v. potential for platinum foil. 205
28. Rate of anodic current decay v. log time for platinum foil. 201
29. Rate of anodic current decay v. potential for platinum foil. 202
30. Charge-potential plot for platinum foil in range I.0 - I.5 V. 200
31. Rate of growth of oxide film v. potential for platinum foil. 203
32. Oxide coverage v. potential from I.0 - 2.0 V for platinum foil. 208
33. Rate of growth of oxide film v. potential from I.0 - 2.0 V for platinum foil. 208
34. Oxide formation proportion of the total anodic current v. log time at 2.0 V 203
35. Linear sweep oxide reduction curve on platinum black. 208
36. Test for anodic current separation method. 207
37. Hydrogen evolution i - E curve on platinum foil. 249
38. Hydrogen evolution i - E curve on floating and submerged platinum black. 250
39. Hydrogen evolution i - E curve for platinum black. 252
40. Effect of teflon content on i - E curves for hydrogen evolution on platinum black. 258
41. Cathodic i - t curves in floating and submerged positions. 261

42. Hydrogen evolution/Hydrogen oxidation polarisation curve for platinum black. 261

43. Transient hydrogen evolution/hydrogen oxidation polarisation curve for platinum black. 265

44. The effect of ultrasonic vibrations on the gas evolution performance of planar electrodes. 282

45. Oxide coverage of a platinum foil electrode at 0.85 V after anodic pretreatment at I.8 V. 180

46. Transient hydrogen evolution i - E curve for platinum foil. 266

47. The effect of anodic pretreatment time on the cathodic voltammograms under nitrogen. 2II

Summary.

The chief aim of this work has been to contribute towards the development of a rechargeable metal - air battery. This part of the work is an investigation of factors affecting the rechargeability of the air electrode in particular, the mechanism of gas evolution from porous teflon bonded electrodes in general. Platinum black and silver on graphite electrodes have been chosen as examples since they are the two most commonly used oxygen reduction electrocatalysts in primary metal - air cells.

The problems of using porous electrodes for gas evolution are (a) finding an electrode structure which is not damaged by and makes effective use of the available surface area during gas evolution, (b) finding an electrocatalyst which is stable under strongly anodic conditions, which has a surface oxide which is reduced at potentials > I.2V and which has a low oxygen evolution overvoltage.

Since teflon bonded electrodes have proved to be the most effective for gas dissolution reactions it was decided to use this type of electrode structure. Oxygen and hydrogen evolution currents were drawn from several teflon bonded electrodes using different electrocatalysts (eg. platinum black, silver on graphite, platinised graphite, platinised tungsten trioxide and tungsten carbide) and current collectors (eg. nickel screen, platinum gauze and graphite cloth) and it was found that only graphite based electrodes were damaged by gas evolution. Since these electrodes were damaged by both oxygen and hydrogen evolution and no carbon

monoxide or dioxide was formed it was concluded that the damage was due to mechanical weakness rather than oxidation. By increasing the teflon content of the electrode, graphite electrodes can be made to withstand gas evolution.

All common oxygen evolution electrocatalysts form surface oxides at high positive potentials. These surface oxides lower the oxygen evolution performance and if not reduced at potentials above I.2 V they seriously lower the oxygen reduction performance. Only gold fulfills this condition; the oxide film on platinum remains more than a monolayer thick until the potential is $<$0.85 V while the oxide layer on graphite cannot be completely removed even by hydrogen evolution, which rules out the use of graphite for rechargeable air electrodes.

Graphite and nickel are the materials with the lowest oxygen evolution overvoltage and a recently developed oxygen reduction electrocatalyst, cobalt nickel oxide, with a performance equivalent to silver on graphite, can be used for oxygen evolution taking advantage of the relatively low oxygen evolution overvoltage on nickel.

The oxygen reduction reaction on bare and oxidised platinum foil surfaces was compared with the oxide reduction reaction on oxidised platinum foil surfaces and it was shown that in order to obtain accurate kinetic data for oxygen reduction on an oxide surface it was important to ensure that the transient oxide reduction current had decayed to zero, and that a monolayer of oxide still remained on the electrode.

The kinetics of the oxide formation reaction on platinum foil were studied and shown to obey the Elovich law. However, it was also shown that the oxide film can grow to thicknesses greater than a monolayer and this together with the decay of current with time over long periods conflicts with the currently accepted mechanism for oxygen evolution and oxide formation. A method of separating oxygen evolution and oxide formation currents was developed from an analysis of current - time curves in the potential range I.0 -2.0 V.

A comparison between gas evolution on porous and planar electrodes showed that the percentage reduction in effectively employed surface due to blockage by gas bubbles is of the same order for both types of electrode. The potentiostatic pulse technique was applied to porous electrodes making a correction for double layer charging, the instantaneous currents thus determined enabled the effectiveness factors and intrinsic exchange current densities of porous electrodes to be determined.

The effect of teflon content on gas evolution from a teflon bonded platinum black electrode was minimal. This corresponds to a model postulated for teflon bonded gas evolution electrodes where the factor limiting mass transfer of gas away from the electrode is the pressure needed before gas can escape from the micropores of the electrocatalyst.

The Problem Areas.

1) Electrolytic gas evolution reactions are widely used in industry but comparitively little is known about how they are affected by electrode shape and structure.

2) In industry, planar electrodes are often used when it might be expected that the high surface area exposed by porous electrodes could improve the performance characteristics. For gas dissolution reactions it has been shown that porous electrodes are essential if the reaction rate is to be high enough for viability. Little is known however, as to whether the scale up from planar to porous is quantitative and what factors affect the mass transfer of reactants and products in porous electrodes.

3) In fuel cells and batteries porous electrodes are often used. In some fuel cells gas is produced eg. hydrazine fuel cells and methanol fuel cells, while in the case of batteries it is desirable to have a cell which is rechargeable, and this again usually involves gas evolution; eg. zinc-air cells are high energy density, primary batteries and their versatility could be greatly increased if the electrodes could be made rechargeable. However, it is important that nothing happens to the electrode during the recharge period which is going to effect its discharge characteristics, eg. in aqueous solutions hydrogen evolution proceeds without any type of film formation, while oxygen and chlorine evolution involve oxide films which until stripped off can effect the discharge

characteristics.

4) There is no evidence as to whether the life expectancy of porous electrodes is affected by gas evolution. This is critical if these electrodes are to be used in industry, since electrode replacement is an expensive operation in labour, materials and time.

Chapter 1.

A.	Energy Conversion	6
B.	Porous Electrodes	13
C.	Rechargeable Electrodes	22
D.	The Oxygen Electrode	29
E.	Gas evolution reactions	43

CHAPTER I

A Review of the literature.

A) ENERGY CONVERSION.

A modern industrial society can be viewed as a complex machine for degrading high quality energy into waste heat while extracting the energy needed for creating an enormous number of goods and services. Steadily increasing efficiency of conversion of energy to useful heat, light and work between the years 1890 to 1960 helped to maintain the annual rate of increase in fuel consumption to only 2.7 per cent, which was less than the average annual rate of growth of the gross national product of the U.S.A. . However since 1967 annual increases in fuel consumption have risen faster than the gross national product, indicating that gains in fuel economy are becoming harder to achieve.(I) The use of nuclear fuels will do little to overcome this as nuclear plants have a net efficiency of about 30 per cent compared with about 40 per cent for the best fossil fuel plants. As it is predicted that this trend will continue, resulting in an energy shortage crisis in the next century, it can be seen that research aimed at increasing the efficiency of energy conversion must have a high priority.

The majority of the fuel energy, which appears as waste heat, is released either to an

adjacent body of water or into the surrounding atmosphere. The problem could be partially solved if uses could be found for large quantities of low grade energy. For example low pressure steam can be used for space heating or in the chemical industry as process steam. Nationwide, however, there appears to be no attractive use for the waste heat, which unless limited, has the additional disadvantage of harming the environment.

The internal combustion engine accounts for about I6 per cent of the total fossil fuel consumed in the U.S.A. (All forms of transportation account for 25 per cent of the total.[1]) The net efficiency of the average automobile engine is 25 per cent and the average miles per gallon of fuel is now I2.2,[I] hence an improvement in the energy conversion for automobiles would be of major importance.

Electrical energy is the only form of energy which can be easily made, is convenient to transport and can be used in a controlled manner. Energy is most easily stored in the form of electrical energy which is easily transformed into other forms of energy with nearly IOO per cent efficiency. Since the form of energy most frequently required by man is electricity, it is obvious that methods of direct energy conversion from its primary forms eg. chemical, solar, nuclear and gravitational, is of great importance. The conventional methods, apart from hydro- electric power generation, pass through

the intermediate stage of conversion of heat energy to mechanical energy. Thus, inherent in them is the Carnot limitation, ie. the maximum achieveable efficiency is $\frac{T_I - T_2}{T_I}$ where T_I is the absolute temperature of the input gas and T_2 is the absolute temperature of the gas leaving the heat engine. This effectively limits the maximum efficiency to 60 per cent. Also the moving parts of conventional systems are subject to mechanical failure. The advent of space research has resulted in the development of direct methods of energy conversion because of the simplicity, reliability and lessened weight and volume required in these methods. If the conversion of energy from a primary source to electricity can be made in one step, the efficiency should be higher than were the conversion to occur in many more steps apart from considerations of the Carnot cycle, which intrinsically limits the efficiency of conventional indirect and some direct methods.

A comparative study of the various direct energy conversion systems is a very difficult task. For example it is necessary to know whether the device is required for space or terrestrial, civilian or military applications. The choice of system would then depend on the required power level, the duration of the operation and whether the device is to be used for a stationary or mobile power source.

On a fairly general basis, the following criteria have to be considered in a comparative study of direct energy conversion devices: (I) efficiency, (2) power/weight ratio, (3) power/volume ratio, (4) life expectancy, (5) cost per kilowatt of power produced. Of course, for any particular application it does not follow that all these criteria are important.

There are five chief methods of direct energy conversion.[5,6,7] These are (I) Thermoelectric devices whose operation is based on the Seebeck and Peltier effects, (2) Thermionic devices which convert heat directly to electricity by the heating of an emitter cathode to high temperature and a consequent emission of electrons from it, (3) Photovoltaic systems which convert light to electricity using a pn junction, (4) Magnetohydrodynamic converters in which a high temperature plasma, consisting of a mixture of positive and negative ions, moves through a magnetic field and in a direction perpendicular to it, thus inducing an electric field in a direction mutually perpendicular to the direction of the magnetic field and the direction of motion of the plasma, (5) Electrochemical devices which convert the free energy change of a chemical reaction directly into electricity. These devices give a direct electric current, which although suitable for many outdoor applications eg. cars, lawn cutters, are not suitable for many indoor appliances which are designed to use A.C. current from the mains supply voltage. It would be necessary to convert these

TABLE 1.

A Comparison of Energy Conversion Devices.

Method of energy conversion	Efficiency, %		Power/wt hp lb^{-1}		Power/vol. hp ft^{-3}		Life expectation		Cost/power $ hp^{-1}		Intangible factors	Comments
	Best available till 1969	Maximum feasible	Best available till 1969	Maximum feasible	Best available till 1969	Maximum feasible	Best available till 1969	Maximum feasible	Best available till 1969	Minimum feasible		
Thermoelectric (144)	10	12	0.03	0.1	1.1	2	3 years	Greater than 10 years	400	200	No moving parts, virtually maintenance-free. Noise-free, will operate over wide temperature range. Efficiency independent of size	Cost relatively high. Covers wide range in power levels
Thermionic (145)	22	32	0.03	0.1	1	3	1½ years	Greater than 10 years	400	100	Same as thermoelectric materials problems owing to high temperature and Cs vapor	High temperature necessary—2000°K. Covers wide range of power levels
Photovoltaic (146)	15	25	0.6	1.0	80	130	5 years	Greater than 10 years	70,000	40,000	Simplest device. Long life. High temperature not required	Wide range of power levels. Cost too high. Necessary to develop types other than silicon solar cells. Needs energy storage (fuel cells)
Magneto-hydrodynamic (147-8)	60	70	1.6	2	1,200	20,000	Tests carried out for 1 week	Greater than 10 years	70	45	Same as thermionics but higher temperatures cause more problems	Only for high power levels (>1 Mw). Field in infancy
Low-temperature fuel cells (149)	70	90	0.04	1	3	30	Greater than 2 years	Greater than 10 years	400	100	High efficiency at low temperatures. Easy to operate. No problem of corrosion	H_2-O_2 cells best-developed. Cost of H_2 and its storage are main problems
High-temperature fuel cells (150-2)	60	90	0.2	2	10	50	1 year	Greater than 10 years	100	30	Polarization is low at both electrodes. Carbonaceous fuels may be used in molten carbonate or solid electrolytes	Problems of corrosion. Wide range of power levels
Gas turbine (153)	28		1		70		1 year		25		Many moving parts	Low initial costs, cheap fuel. No cooling or ignition
Internal-combustion engine (153)	27		0.3		7		5 years		3		Many moving parts	Low initial costs. Operates well over wide range of temperatures and pressures
Diesel engine (153)	42		0.2	0.2	8		10 years		3		Many moving parts	Low fuel costs. Hard starting in cold weather (below 5°C)

appliances to D.C. power sources. This can be done by high efficiency rectifiers. Only methods (3) and (5) are free from the Carnot limitation. Table (I) shows a comparison of these direct energy conversion systems together with some of the common indirect conversion devices taking into account the main performance criteria. As most of the work on direct energy conversion devices has taken place in the last few years and considerable improvements are still being achieved, two types of figure are used in the table: the best available to 1969 and the apparent limits of what seem feasible. It should be noted that the figures in the table are dependent on the magnitude of the power output of the device.

The low weight/energy ratio and the reliability of $H_2 - O_2$ fuel cells makes these devices the best for space missions ranging from a few hours to a month and for power levels up to 100 Kw. An analysis of the possible terrestrial uses of electrochemical energy convertors as a source of mechanical power for (1) delivery and industrial trucks, (2) automobiles, (3) construction equipment, (4) light aircraft, (5) locomotives, (6) outboard motors and (7) marine applications was carried out by Adams et al.[2] For an mobile power source high power/weight and power/volume ratios are required. In this respect the best fuel cells have power/weight ratios only one fifth that of the internal combustion engine although the power/volume ratio is comparable. An advantage of

fuel cells over internal combustion engines as a mobile power source is that fuel cells have higher torque characteristics at low speeds whereas the opposite is true with internal combustion engines.[3] The torque at lower speeds is required for acceleration. Furthermore the efficiencies of fuel cells are higher at lower speeds, whereas the converse is true for internal combustion engines. Air pollution is a serious problem in many cities, with fuel cell driven cars this problem could be largely eliminated. There are many medical applications eg. cardiac pacemakers that make use of batteries at present which require replacement after relatively short periods. The implantation of fuel cells in the body which operate with oxygen dissolved in the blood, would significantly increase the life of these pacemakers.[4]

Even if other direct energy conversion devices become more effective than fuel cells eg. (thin film photovoltaics) the storage of the electricity is still mandatory and electrochemical devices provide the only practical way of storing electricity if it is to be available on demand.

For military terrestrial purposes the chief advantage of direct energy conversion devices is that they operate silently due to the absence of moving parts which also results in longer life and in the case of fuel cells, the difficulty of detection by infrared devices.

In an electrochemical energy convertor the reactants, which are commonly gaseous, are transported to the anode and cathode where the anode reaction

produces electrons which are transported through the external circuit to the cathode, where the cathode reaction occurs, using up the electrons. The circuit is completed by the transport of ions from one electrode to the other through the electrolyte. The efficiency of an electrochemical energy convertor is given by:

$$E_I = \frac{\Delta G}{\Delta H} = \frac{-nFE_r}{\Delta H} = I - \frac{T\Delta S}{\Delta H} \qquad (I)$$

where ΔG = free energy change

ΔH = enthalpy change

E_r = thermodynamic reversible cell potential

ΔS = entropy change

T = absolute temperature

Generally, ΔG is quite close to ΔH and hence the maximum efficiency of fuel cells is not much less than 100 per cent. In the practical case the value of E_r and hence ΔG, falls as the current density drawn from the cell increases causing the operating efficiency to fall.

This section summarises the importance of the efficient direct conversion of various energy sources to electricity and its subsequent storage. In this research it is proposed to study electrochemical energy convertors and stores.

B) POROUS ELECTRODES.

An electrochemical energy convertor has an intrinsic maximum efficiency given by equation (I). This is usually about 85 - 100 per cent for fuel cell reactions under standard conditions. For example at 25°C E_I for the reaction

$$H_2 + \tfrac{1}{2}O_2 = H_2O$$

is 83 per cent, and for the reaction

$$CH_4 + 2O_2 = CO_2 + 2H_2O$$

E_I is 92 per cent. For a reaction in which the entropy change is negative it can be seen from equation (I) that E_I decreases with increasing temperature. The converse effect is observed with heat engines and this reduces the advantages of fuel cells over heat engines at high temperatures. This, however, is partially offset since at high temperatures the rate of reaction is increased and the overvoltage decreased thus reducing the need for expensive electrocatalysts. The Faradaic efficiency is defined as

$$e_f = \frac{I}{I_m}$$

where I is the observed current from the fuel cell and I_m is the theoretically expected current assuming that the overall fuel cell reaction proceeds to completion. In most fuel cells e_f is 100 per cent, but sometimes it is less due to side reactions of the reactants and products. The voltage efficiency, e_v, is defined as

$$e_v = \frac{E}{E_r} \qquad (E < E_r)$$

where E is the cell voltage under load. As the load is increased E and hence e_v fall. From these definitions it can be seen that the intrinsic maximum efficiency and the faradaic efficiency depend only on thermodynamic factors while the voltage efficiency is dependent mainly on kinetic factors. Most of the profitable research into fuel cells has the aim of

improving the voltage efficiency (kinetic factors) and hence improving the overall efficiency, e , which is defined as

$$e = E_i \cdot e_f \cdot e_v$$

Attempts to reduce e_v have proceeded along two main lines:

(I) to find cheap electrocatalysts with high exchange current densities, i_o .

(2) to produce electrode structures which have a high surface area/bulk volume ratio and which can sustain high limiting currents.

At present the i_o's of most reactions of interest in fuel cells are $\leqslant 10^{-8}$ A.cm^{-2} . eg. reduction of oxygen, oxidation of hydrocarbons. Using planar electrodes in a hydrocarbon-O_2 fuel cell, a cell potential of 0.5V and with i_o for both electrode reactions as 10^{-10} A.cm^{-2} the current density, i , achieved is only 10^{-5} A.cm^{-2} assuming no concentration and ohmic overpotentials (from Tafel's law.) This is far below the current density required ie. I A.cm^{-2} . Even if the i_o for one electrode is high as in the $H_2 - O_2$ fuel cell the current density under the same conditions is only about 10^{-2} A.cm. Another important factor influencing the performance of fuel cells is the solubility of the fuel and oxygen in the electrolyte which for the common fuels and oxygen is only 10^{-4} moles.l^{-1} . This results in limiting current densities at planar electrodes of the order 10^{-4} A.cm^{-2} . Itis thus essential to use an electrode structure other than planar in order to reduce the activation overpotential and to facilitate mass transfer

to the reaction sites, even if electrocatalysts with high i_o values could be found. The aim of this thesis is to study the electrode structure aspects of electrochemical energy conversion.

As planar electrodes are unsatisfactory an obvious solution to the problem would seem to be the use of rough or porous electrodes. With roughened electrodes the current density can be increased about one hundred times and the limiting current about ten times which is not sufficient improvement. Porous electrodes which consist of either powdered electrocatalyst or electrocatalyst deposited on a conducting support can increase the surface area by about one thpusand times. Research into electrode reactions in porous media is only about five years old. The chief points made so far are:

(I) the reason for the higher power densities of porous electrodes, compared with planar electrodes, is only partly due to the high ratio of real to apparent surface area.

(2) porous electrodes permit a limiting current density much higher than planar electrodes because of the much lower diffusion layer thickness in porous electrodes thus improving the power density.[8]

(3) current densities are not uniform within porous media because the diffusion and ohmic overpotentials vary throughout the length of the pores, hence the contribution of activation, diffusion and ohmic overpotentials to the total is different at different points within the porous structure.[9]

Basically two kinds of porous electrodes have been considered. They are the two phase and three phase systems. The phases present in the former are solid and liquid and this type of electrode is of limited application in fuel cells which usually employ gaseous reactants. In a two phase system the reactant is dissolved in the electrolyte and is transported to the active sites by diffusion and migration. In the three phase system the reactant gas dissolves in the electrolyte at the gas-electrolyte interface and diffuses through the electrolyte to the active sites of the electrode. The two phase systems which are used in the methanol fuel cells have been studied by Newman and Tobias [9] and by Micka [10].

Several physical models have been proposed for three phase electrodes which are known as gas diffusion electrodes. [11-17] In the analysis of these models, which follows, it should be noted that the choice of model will be dependent on the manner of preparation of the electrode eg. teflon is sometimes added to the catalyst particles, which has the effect of decreasing the wetting character of the electrode.

(I) The simple pore model for non wetting electrodes [11]

In this model the electrode is assumed to consist of uniform, parallel, cylindrical pores in which the solid/liquid contact angle is assumed to be 90°. These assumptions enable the total current-overpotential relation, and the current distribution within a pore to be calculated. These results, however, must be considered to be of doubtful application since the model considers

neither the tortuousity, pore interconnection nor pore size distribution of an actual porous electrode.

(2) The thin film model for wetting electrodes.[I2]

The basic assumption is that a comparatively lengthy thin film of liquid extends above the liquid meniscus and is in contact with the solid phase in the pore.

(3) The finite contact angle meniscus model for partially wetting electrodes.[13]

This is intermediate between the above two models and is based on interferometric and reflection studies which showed that the meniscus made a finite contact angle with the electrode surface. It is predicted that close to the region at the upper end of the meniscus the current density should be high since the diffusion path is short. However, this is partly offset by the high ohmic drop in this region due to the thinness of the meniscus.

(4) Stable meniscus models.[I4,I5]

In the above three models cylindrical pores of uniform radius have been assumed. In a pore there is an equilibrium at the gas-electrolyte interface due to the gas pressure, which tends to force the electrolyte out of the pore, and due to the capillary forces of the electrolyte, which tends to flood the pore. Hence there is a critical pore radius and in non homo-porous electrodes ie. actual electrodes, it follows that many of the pores will be non active. This has been overcome in two models: a) the double porosity scale structure in which wide pores face the gas side and

narrow pores face the electrolyte side, producing a stabilized meniscus at the junction of the small and large pores,[I4] b) cone models in which the pores are conical in shape, the wide end facing the gas and the narrow end the electrolyte, thus producing a stabilized meniscus.[I5] Construction considerations make model (a) the more useful (it has been used in the Apollo space program.)

(5) The intersecting pore model[I6]

It is assumed here that the electrode consists of an intersection of micropores with macropores and that due to gas pressure, capillary forces and these intersections, that the entire surface of the macropore is covered wibh a film of electrolyte, and that electrolyte fills the micropores and reactant gas fills the macropores.

From the above analysis it can be seen that two main lines of approach have been taken, namely (I) to determine the distribution of current within the pore with the simplifying assumptions of cylindrical, straight, or uniform pores. (2) to find the influence of pore size distribution, shape, tortuousity and pore interconnections on the electrode performance per unit external area.

Both these theories have usefullness but it is necessary to combine them if a model to approach the practical case is to be developed. Theory (2) has a major disadvantage in that in order to achieve an analytical solution the effects of activation and concentration overpotential on the distribution of

current within a pore have been left out. This means that only the maximum current which could be expected from a certain distribution of pores is obtained.

So far researches on porous electrodes have been predominantly of a theoretical nature there being little or no experimental verification of the above models, except for the finite contact angle meniscus at wetted surfaces. In particular present theories are lacking in that they either consider the current and potential within a single pore or alternatively the electrode kinetic aspect is played down while more importance is attached to the size and distribution of the pores and the entry into them of liquids. So far the two aspects of the theory of porous electrodes have not been joined in mathematical equations mainly due to complexity, so that analytical solutions cannot be derived without prohibitive approximations. Further advances in the theory of porous electrodes will have to involve numerical solutions. Some of the principal questions in porous electrode theory at present are: (I) The current has a very limited penetration down a pore especially in reactions with a high i_o value. This suggests that a considerable downward revision of catalyst costs could be achieved by a device which gives rise to localisation of catalyst in a region where the pore shows its electrochemical activity. This is also likely to be true for reactions with low i_o when the electrode is of the non wetting, teflon bonded type. However, in situations of partial wettability calculations based on the thin film model

predict that the localisation of current to a small area of pore is not great.[18] However, the difficulty is that there is no evidence to support the existance of thin films in fuel cell electrodes. Calculations based on the more reliable finite contact situation for wettable electrodes[13] suggest that the localisation of electrocatalyst is highly desirable. There is also some evidence to suggest that electrolyte pumping may help to remove concentration hold ups in the diffusion of the fuel from the gas-liquid interface in the non wetting situation.[11]

Apart from their use in fuel cells porous electrodes are or could be profitably used in many other electrochemical situations eg. storage batteries, electrosynthesis, preparation of hydrogen and chlorine gases and as counter electrodes in various metal extraction cells. In general porous electrodes are only regularly used in storage batteries, the other systems using simple planar electrodes. The purpose of using porous electrodes in these devices is the same as in fuel cells, namely to improve the voltage efficiency of the cell. However the main difference between the fuel cell case and the other applications is that in the fuel cell electrode gas is consumed, while in most cases, gas is produced in porous electrodes used for the other applications, which results in somewhat different problems with these electrodes, such as mechanical strength of the porous structure and the escape of the gas produced within the small pores in the interior of the electrode. This is also the case

in some fuel cells eg. hydrocarbon-O_2 cells and methanol-O_2 cells produce carbon dioxide, and ammonia-O_2 and hydrazine-O_2 cells produce nitrogen. Porous media are also widely used for gas phase heterogeneous chemical catalysis and occasionally for liquid phase.

Porous electrodes are rarely used for gas evolution and since it may be advantageous to increase the electrochemically active surface area of these electrodes, this work includes a correlation between electrode structure, electrode performance, and surface area. This should give an indication of the feasibility of using these electrodes for rechargeable batteries, as opposed to the introduction of a third electrode into the cell or simply using planar electrodes.

C) RECHARGEABLE ELECTRODES.

The common classification of batteries is into primary and secondary groups. However, this is inappropriate since primary batteries are simply fuel cells which have internal fuel storage. It is the secondary battery which has the unique function of storing electricity and having it available on demand ie. it accepts it and redelivers it, which distinguishes it from primary batteries and fuel cells. This electrochemical device is the only known way of storing electricity and having it available on demand. This facet greatly widens the scope of use of these batteries and for this reason it would be advantageous if methods for recharging fuel cells and primary batteries could be established.

In low temperature $H_2 - O_2$ fuel cells no attempt has been made to make the system rechargeable in situ, possibly due to the high overpotential for the oxygen evolution reaction. As an alternative, attempts have been made to produce a regenerative fuel cell in which the product of the fuel cell reaction is reconverted into its reactants by various methods eg. thermal, photochemical, chemical, radiochemical or electrical. Since there are two stages in a regenerative fuel cell the overall efficiency of such a cell is equal to the product of the efficiencies of the two stages. Electrically regenerative fuel cells are the closest analogy to rechargeable systems in that the fuel cell products are reconverted to the reactants electrically. The difference from a storage (secondary) battery is that the latter are always sealed units, the charging and discharging processes being carried out within the battery itself, while in electrically regenerative fuel cells the fuel cell reaction takes place in one cell and its products are led into another cell, where the regeneration takes place. In fuel cells, because either product or reactants are gases, recharging in situ is not easy since insoluble gases cannot be stored within the cell.

In secondary batteries the function of recharging is to reconvert the products of the discharge reaction, although in the case of batteries this often includes the electrodes themselves eg. lead - acid batteries. In batteries the discharge reaction reactants and products are not usually gases, other than air, hence the fuel storage problem associated with fuel cells is absent.

Hence it should be possible to convert primary batteries to secondary batteries. This, however, has rarely been achieved since often the electrodes are damaged or altered during the recharge cycle thus reducing their performance on the discharge cycle. This has sometimes been overcome by using a third electrode in the system which only operates on the recharge cycle.(I9)

The important quantities in the study of storage batteries are: (I) Electricity storage density which refers to the maximum total amount of electricity which can be withdrawn from unit weight of a substance when it undergoes an electrochemical reaction. This is not a very useful quantity since it says little about the actual behaviour of a substance as an electrode or the possibilities of making an electrode from it. (2) Energy density. This is the energy which may be extracted from unit weight of the substance ie. maximum energy density = electricity storage density $\times$ reversible cell potential

This quantity has the same limitations as (I) in that no account is taken of the weight of the container, electrolyte, grid etc. and also that the cell potential is reduced under load due to overpotential effects. Hence this quantity is dependent on the electrode kinetics.

(3) Power density. This is the rate at which the storer could release energy. ie.

power density = current density $\times$ working potential

The power density depends on the same factors as the

power density of fuel cells. Hence a combination of these three factors, the last being the most important, gives a good guide to the usefulness of a battery.

Based on these three definitions the following factors are desirable in batteries; (I) cell reactions should have a high reversible potential , (2) cell reactions should have a high n value, (3) reactants of low molecular weight should be used, (4) electrode reactions with high $\dot{i}_0$ values should be chosen, (5) a physical electrode structure to give high limiting currents, (6) geometric structures so that ohmic drops are small, (7) a high solution conductance and solubility of dissolved discharge reaction products, (8) highly insoluble reactants to avoid diffusion onto the other electrode and consequent self discharge, (9) the lightest possible construction materials compatible with stability and mechanical strength. These factors are important in both primary and secondary batteries. In addition secondary batteries have the following requirements if they are to have an extensive cycle life: (I) the active cathode must have a very low solubility in the electrolyte in order to minimize the concentration of heavy metal ions in solution which would diffuse to the anode, and plate out producing local action cells conducive to rapid deterioration of the anode. (2) the electrocrystallisation characteristics of the electrode should not involve major changes in molar density to provide the basis for the structural integrity of the porous electrode

and the preservation of desirable microporosity characteristics in going from the state of charge to discharge and vice-versa. (3) the anodic discharge product, usually a hydroxide or salt, should be insoluble to ensure the availability of the product and to reduce the mass transfer problem within the pores when recharging to the metallic state is attempted. (4) all electroactive species in both oxidation states must be stable towards the electrolyte to avoid side reactions or losses through dissolution. (5) the anode oxidation product must not be passivating at reasonably high current densities ie. it must not form dense non conducting films, since the diffusion and migration of metal ions through the oxide or salt layer constitutes the basic transport mechanism in the discharge of these electrodes.

Very few electrochemical systems are capable of meeting the above criteria, hence the small number of commercial secondary batteries. The best known secondary battery at present is the lead-acid type, which although it gives very high current densities per unit volume, has very poor energy and power density characteristics and undergoes a spontaneous discharge causing the phenomena known as sulphation. The more modern silver/zinc cell has very high energy and power densities but can stand only a few hundred charge-discharge cycles. The sodium-sulphur battery gives high current densities but suffers from corrosion problems.

Metal-gas cells represent a hybrid between a fuel cell and a battery, by combining in situ a metal anode with a dynamically supplied gas cathode. The cathodic reactant can be a halogen, nitrogen

dioxide or more usually oxygen from the air. Only oxygen cathodes have reached a developed stage. The attraction of metal-oxygen cells lies in the high theoretical energy densities which are possible. The achievement of a practical system is limited by factors such as the thermodynamic stability towards the electrolyte, kinetic behaviour of the metal, passivation phenomena, etc. . The past five years have witnessed an increasing interest in metal-air cells, particularly the zinc-air cell. Recently zinc-air primary batteries have been marketed by two companies, showing characteristics superior to those of other conventional primary batteries eg. high energy and power densities, good energy/volume ratios and the ability to provide a constant output until 90 per cent of the stored energy has been used. These batteries are about a quarter the volume and an eighth the weight of Leclanche and lead-acid types of comparable capacity and rating.(59) It would be very desirable if these zinc-air cells could be converted to secondary batteries as the present batteries have discharge properties which would make them suitable for overnight recharging similar to heavy duty lead-acid cells. Some research has been done with this aim in mind but two main problems have been found, one associated with each electrode. These are (I) the considerable mass transfer polarization in the case of a soluble anode leads to a rapid reaching of limiting conditions conducive to electrodeposition of the anode metal in dendritic or powdery nonadherent forms.(20) This is the case with zinc in alkaline electrolytes, the dendrites causing shorting

between the electrodes, producing momentary very high currents and hence buckling of the plates, which must be positioned as close to each other as possible to reduce ohmic losses.

(2) One of the chief problems in improving the power density discharge characteristic of this cell was in the cathode. This was solved by using a teflon bonded graphite electrode containing silver, which has proved to have good oxygen reduction characteristics. Unfortunately its recharge ie. oxygen evolution, characteristics are not satisfactory, mainly due to the destruction of the electrode when evolving oxygen. One of the main aims of this project is to find the reason for this breakup and to find possible alternatives to produce an efficient rechargeable cathode for the zinc-air system , which also has good discharge characteristics. At one time porous nickel was used as the air cathode but although this is rechargeable its discharge characteristics are poor.

Other possible types of secondary battery are

(I) Alkali metal-halogen cell [21] which combines the reactions

$$M = M^{+} + e \quad \text{and} \quad X_2 + 2e = 2X^{-}$$

This gives a high reversible cell potential and a high power density because of the high i_0 values for both electrode reactions. This overcomes the main disadvantage of H_2-O_2 cells. The main problem with these cells is one of construction material stability in a molten alkali metal halide.

(2) Storers involving non-aqueous solutions. [22]

It is desirable that batteries should have a high cell potential and consist of reversible (high i_o) electrodes. However, if the cell potential exceeds I.7 V this would cause electrolysis of water thus making aqueous solutions unsatisfactory. This problem can be overcome using non-aqueous electrolytes which decompose only at much higher potentials. From the materials aspect this is better than using molten salts since non-aqueous electrolytes like acetonitrile, cause few corrosion problems. However, problems exist , and a satisfactory oxygen electrode in non-aqueous media has not yet been developed. The main problems are:

(I) water is formed in the oxygen reduction reaction,

(II) the solubility of salts is smaller in non-aqueous solution resulting in lower limiting currents,

(III) voltage losses due to the high resistance in non-aqueous electrolytes.

(3) Batteries based on the electrically regenerative hydrogen-oxygen fuel cell.[23]

Since non carbon rechargeable oxygen electrodes invariably form an oxide film during the recharge cycle, it will be necessary to study the formation and reduction of these films and their effect on the subsequent discharge cycle.

D) THE OXYGEN ELECTRODE.

It has been shown that the oxygen electrode performance is a major obstacle in fuel cells and secondary batteries, for the reasons of low i_o for the oxygen reduction reaction and the oxygen evolution reaction and of low mechanical strength of the commonest

oxygen cathode (carbon) when subjected to oxygen evolution. Hence the oxygen electrode is one of the most important to study.

Although the oxygen electrode has been widely studied there are still doubts about the true mechanism of the oxygen reduction and evolution reactions and only limited progress has been made in finding alternative electrocatalysts to the noble metals. The main work on the electrocatalysis aspect has been with silver supported on graphite electrodes[24] and with semi-conducting metal oxides[25] and doped metal oxides.[26] The silver-graphite electrodes are much cheaper than noble metal electrodes and give a similar oxygen reduction performance, however, as already mentioned, this type of electrode breaks up if oxygen evolution is attempted. Until recently the semi-conducting oxides have not achieved comparable oxygen reduction performances, however, work on some nickel cobalt oxides suggests that this problem could be overcome.[27] It is the intention of this work to study the oxygen evolution characteristics of these compounds as possible alternatives to the noble metals and silver-graphite electrodes for use in secondary zinc-air cells. (The silver graphite electrodes are suitable for fuel cell applications.)

The following is a short survey on the main aspects of the work done on the main oxygen electrode materials.

Carbon electrodes.

Porous carbon structures are made by mixing ground coke with a binder such as pitch and

then heating in the absence of air at about 1000°C causing some of the binder to be pyrolized leaving a porous structure. Porous graphite is made by heating porous carbon to 2500-3000°C in the absence of air.[28] Porous graphite is a more desirable product because it is purer and has better thermal, mechanical and electrical properties than porous carbon. The suitability of various porous carbon structures for fuel cell applications has been reviewed.[29]

Because graphite is a good electronic conductor and because interfering oxide films such as those found on most metals are not present on carbon surfaces,[30] such materials are thought to be suitable for making good inert oxygen electrodes. However, graphite electrodes are not suitable for use in acid solutions especially if an oxidising agent is present, since the electrode swells with the formation of graphitic oxide and finally the electrode breaks up and falls to the bottom of the cell as a black sludge.[31] Similar effects have not been reported in alkaline solutions.

Yeager and Kozawa[32-4] have noted that it is difficult to interpret steady state polarization measurements obtained at porous carbon or graphite electrodes due to complications associated with mass transport and non evenly distributed ohmic drops within the pores of the electrode. To overcome this problem they used porous graphite filled with paraffin wax and pyrolytic graphite. Reproducible polarization curves for the reduction of oxygen on graphite electrodes in the absence of hydrogen peroxide could

not be obtained because graphite is a poor catalyst for the decomposition of hydrogen peroxide and the hydrogen peroxide concentration builds up continuously during a period of cathodic polarization.[35] As the composition of the system changes so do the polarization characteristics eg. the higher the hydrogen peroxide concentration the lower (less noble) the rest potential. The results obtained by a number of workers[36,37] have shown that the potential determining reaction on graphite electrodes in alkaline solution is the O_2/H_2O_2 couple:

$$O_2 + H_2O + 2e \rightleftharpoons HO_2^- + OH^-$$

Oxygen tracer studies using ^{18}O[38] showed that in the reduction of oxygen on carbon electrodes all the peroxide produced comes from the oxygen molecules, and that the reaction has a current efficiency of 100 per cent. Consequently the O-O bond is not broken in the reduction of oxygen on carbon electrodes, and reproducible results cannot be obtained on carbon cathodes until the peroxide composition builds up to a stable value. Yeager[35] has shown the oxygen reduction mechanism on carbon electrodes to be:

$$O_2 + e \rightleftharpoons (O_2^-)_{ads.}$$

$$(O_2^-)_{ads.} + H_2O = (HO_2)_{ads.} + OH^-$$

$$(HO_2)_{ads.} + e \rightleftharpoons HO_2^-$$

Polarization studies on anodic oxygen evolution on graphite were not reproducible and no mechanism has

been suggested.

In order to be used as a fuel cell cathode it was necessary to increase the active surface area and this was originally achieved by pasting finely powdered graphite into a porous carbon body.(32) Since carbon is a poor hydrogen peroxide decomposer the end product of the reduction of oxygen is hydrogen peroxide with a consequent transfer of only two electrons per molecule of oxygen, compared with the four electrons per oxygen molecule for the O_2/H_2O_2 couple. Also the electrode potential for the two electron process is only 0.682 V compared with I.229 V for the four electron process (potentials measured against the hydrogen electrode.) Hence it is important to incorporate an active peroxide decomposing catalyst on the cathode surface. Various metals have been tried, silver and platinum being the most effective. Research on the development of zinc-air batteries has lead to the development of activated carbon electrodes having a long life in alkaline solutions.(39-42)

Early attempts to convert the zinc-air cell into a secondary battery used a catalysed porous nickel diffusion cathode operating on pressurised air.(43) This electrode was satisfactory for recharging, but in the discharge mode was not sufficiently active. Kordesch and co-workers(37) have described various methods of catalysing porous carbon electrodes. In alkaline solutions silver, cobalt and manganese have been most effective, while platinum is by far the best in acid solutions.

Porous Nickel Electrodes.

Various porous metal electrodes

have been employed as oxygen electrodes, notably the high pressure Bacon[44] electrodes made of nickel, the DSK[45] electrodes using Raney silver catalyst, and silver/aluminium alloys. The great advantage of using porous metal electrodes over using porous carbon electrodes are high mechanical strength, good electrical conductivity and the ease with which electrical contacts are made. Unfortunately porous metal structures do not usually have a sufficiently high surface area. Attempts have been made to combine the high surface area of graphite with the good mechanical strength of porous metals,[46] but the mechanical weakness of the graphite is still a major disadvantage, attempts to improve its strength by pressing having little effect when the electrode is used for oxygen evolution.

Pasted Diffusion Electrodes.

Electrode reactions in porous media occur only on a small area of the total surface, hence it is advantageous to make diffusion electrodes as thin as possible. This keeps the diffusion path short and also decreases the size and weight of the cell. This type of electrode was originally made by pasting a slurry of the catalyst onto a metal screen and then drying.[47] The disadvantages of this electrode were its great fragility and wettability. These problems were overcome by using a hydrophobic binder such as teflon.[48] These thin electrodes are particularly effective when used as air electrodes, as the blanketing of the pores by nitrogen is less significant.[46,49]

The Oxygen electrode Reaction on Platinum.

This electrode is used in all earth based fuel cells and metal-air batteries. The advantage of using oxygen from the surrounding atmosphere rather than this or other oxidants in a tank is that the tank and oxidant weights decrease the energy/weight ratio about two to four times. Hence it is the most important reaction in electrochemical energy conversion and storage.

The understanding of the oxygen reduction reaction in the steady state is still fairly limited. The oxygen electrode reaction is one of considerable difficulty with respect to mechanism elucidation and electrocatalysis. These difficulties are:

(I) the range of potential in which the reaction occurs is about I.0-0.5 V, This is in a relatively anodic region where most metals either dissolve or form passivating, catalytically inactive, oxide films. Hence the number of electrocatalysts which can be used for this reaction is severely limited to platinum and the tungsten bronzes in acid solution and somewhat limited in alkaline solutions eg. lithiated nickel oxide, silver, graphite.

(2) the oxygen reduction reaction is slow (low i_0) compared with many other common electrochemical reactions eg. hydrogen oxidation and evolution, chlorine dissolution, silver deposition, reduction of Fe^{3+} to Fe^{2+}.

(3) the anodic region in which the reaction occurs causes substrate changes to occur within it eg. for platinum there is a change in the nature of the surface at about I.0 V which seriously complicates the data.

(4) the reversible oxygen electrode potential, I.23 V, is close to that for several other reactions eg. on platinum the reversible potential for reduction of PtO_2 occurs at I.I3 V and for PtO at I.00 V [2]. Further, the oxygen reduction reaction competes with a similar reaction in which oxygen is reduced to hydrogen peroxide rather than water.

(5) the normal oxygen reduction reaction sometimes produces hydrogen peroxide as an intermediate. [50]

The fact that the effective potential range for oxygen reduction is less than I.0 V means that there is a type of "autopolarization" of about 0.25 V resulting in a severe loss in power. The reason for this is not well understood. Wroblowa et al. [51] have investigated the phenomenal aspects of the observed rest potential on platinum electrodes.

Several explanations have been proposed for the I.0 V rest potential eg.

(I) the formation of hydrogen peroxide as an intermediate. [52] Calculations have shown that the concentration of hydrogen peroxide would not be sufficient to support the observed currents.

(2) that the rest potential is due to one of the oxide couples ie. Pt/PtO or PtO/PtO_2. [53] This explanation does not account for the variation of rest potential with oxygen partial pressure.

(3) the Pt/solution interface is polarizable in the region below I.0 V, the variation in rest potential with oxygen pressure being explained by the replacement of water dipoles in the surface with oxygen atoms, the

difference in dipole moments of metal-O and metal-water dipoles accounting for the variation.[53] This theory does not, however, explain the substantial currents which can flow in the 0.9-I.0 V region. Wroblowa et al[51] have concluded that the I.0 V rest potential is a mixed potential of the cathodic oxygen reduction reaction and an anodic reaction which has not been elucidated. A number of probable anodic reactions were investigated of which only one was consistent with the experimental results. This is the anodic oxidation of an unknown organic impurity which is present in low concentrations and which has a reversible potential of 0.2-0.3 V. This is in fact the observed rest potential of a large number of hydrocarbons in acid solutions on platinum electrodes. This model is also supported by thorough electrolyte purification producing the reversible potential(I.23 V).[54] The slight variation of the I.0 V rest potential (eg. I.00 to I.I5 V) can be explained by the variation of the anodic reaction electrode potential which depends on the specific organic impurity. Various purification schemes have beenused to obtain a temporary reversible electrode potential[54-7] and there is some evidence that the reversible potential is only obtained on oxide covered electrodes.[53]

The importance of the presence of oxide films in mechanistic studies of the oxygen electrode has lead to some research on the nature of the surface of platinum electrodes in the neighbourhood of the reversible potential for the oxygen electrode reaction. The main methods of study have been:

(I) Coulometry [53,60] involving galvanostatic charging curves for the formation and reduction of oxygen layers. This gives the oxygen coverage as a function of potential, but no information on film thickness unless speculative estimates are made for the number of electrons required to form one molecule of the oxide and the density of the oxide. This method does not distinguish between the different oxides (PtO and PtO_2) or between definite films of oxide and adsorbed oxygen. The terminology of oxide film and adsorbed oxygen has been used somewhat vaguely on occasions- an oxide film is where there is at least a monolayer of oxygen in which the oxygen is bound to several metal atoms and the co-ordination number is such that the oxygen must be surrounded by metal atoms on all but one side; the term adsorbed oxygen is used when oxygen is bound to surface metal atoms and the metal atoms have not entered into bonding with oxygen in the plane of adsorption.

(2)Chemical methods. Analytical methods [61] have shown that oxides of platinum do exist on anodically polarized surfaces. The evidence predicts that most of the oxide is PtO. The disadvantage of this method is that the electrode has to be removed from the solution for the subsequent analysis thus introducing the possibility of air oxidation. This, however, is unlikely as comparison with coulometry experiments has shown.

(3) Ellipsometry. [62-4] This technique enables the detection of films and the investigation of their thickness from a fraction of a monolayer upwards. The method is sensitive to I Å and can be used to examine the

electrode in solution. (This is an advantage over the usual electron microscopy and infrared spectroscopy methods of studying catalyst surfaces.) There is a fundamental disadvantage of the method in that there are only two measured parameters related to three unknowns which represent the film thickness, refractive index and electronic conductivity. Hence the method can only be used if a second method is available to provide parallel information on one of the three unknowns. In this case the estimated film thickness as a function of potential has been found coulometrically.[65] It was found that the oxide was PtO and not PtO_2, and that below 0.95 V no film was observed even though the coulometric results predicted one.[78] This was explained as follows:[64] above 0.95 V an oxide film is present, below 0.95 V the film is due to chemisorbed oxygen atoms or OH radicals and is less than a monolayer thick and has optical properties similar to water and hence is not detected by ellipsometry. Ellipsometry has also shown that the film is an electronic conductor.[64]

Mechanism of the oxygen reduction reaction and the oxygen evolution reaction.

This is one of the most difficult and complicated electrode reactions from the point of view of mechanism investigations. The oxygen evolution reaction is less subject to these difficulties because it takes place in a potential region well removed from that in which the complicated alternate reactions, including that of change of substrate, occur. It is always desirable

to study both the anodic and cathodic behaviour of an electrode reaction since information on the mechanism of one process can be instructive about the mechanism of the other and vice versa. For example, some mechanistic criteria, such as stoichiometric number, cannot be evaluated unless both processes are studied, and also in the application of the principle of microscopic reversibility. This principle can be extended away from equilibrium if the evidence suggests a continuity of mechanism, at significant overpotentials, compared with that at the reversible potential.

Because of the complexity of the oxygen reduction reaction mechanism a considerable amount of the information about this mechanism has been inferred from the study of the four electron oxygen evolution process. This is a justified approach for the oxygen reduction reaction occurring at potentials higher than about 0.95 V but around this potential there is a change of substrate from oxide to bare metal and hence at potentials below this value the oxygen reduction reaction occurs on a substrate different from that on which the oxygen evolution reaction occurred, making comparison between the two processes invalid.[79] Hence the mechanism of the oxygen reduction reaction at potentials less than 0.95 V requires seperate study.

The oxygen evolution reaction is not in itself an easy reaction to study for two main reasons: (I) it takes place in a potential region which in acid solution makes most electrode materials unstable, (2) the reaction is highly irreversible (low i_0) on nearly all

electrocatalysts hence, owing to competing reactions of impurities with higher i_0 values, great difficulty in obtaining reversible potentials has been encountered, thus necessitating stringent electrolyte purification.

There are two chief approaches as to the mechanism of the oxygen evolution reaction; one involves a hydrogen peroxide intermediate; the other proposes that the intermediates are oxides, hydroxide or oxyhydrates and that there is no peroxide intermediate. The latter mechanism is supported by the fact that oxides are known to form at the potentials of oxygen evolution [64] and tracer studies have shown that oxygen evolved on Pt-O^{18} surfaces contained the heavy isotope. The peroxide mechanism was inferred from cathodic studies and such data from steady state, long time cathodic measurements in which hydrogen peroxide may be produced cannot have direct implication for the anodic reaction mechanism owing to the change of substrate. More recent work by Bockris et al. [67-69] has shown that Langmuir adsorption is likely and Temkin adsorption improbable, and that the rate determining step is the charge transfer reaction from water to form OH radicals. The probable mechanism for the oxygen evolution reaction is

$$M + H_2O = MOH + H^+ + e \quad \text{(rate determining step)}$$

$$2MOH \rightleftharpoons MO + M + H_2O$$

$$2MO \rightleftharpoons 2M + O_2$$

Applying the principle of microscopic reversibility the mechanism of the oxygen reduction reaction on an oxide

surface can be inferred from the mechanism of the anodic oxygen evolution reaction. Thus the rate determining step is the charge transfer from adsorbed hydroxyl or oxygen radicals to water after initial chemical reactions of oxygen involving adsorption on the oxide substrate. There is also a considerable amount of evidence proposing a mechanism where the oxygen is first reduced to hydrogen peroxide (2 electron process) which is itself reduced to water in another two electron process.[70-72] Since the standard potential for the O_2/H_2O_2 couple at 25°C is 0.68 V, it is possible, at potentials more negative than this, that both reactions ie. O_2/H_2O, four electron process and O_2/H_2O_2, two electron process, occur simultaneously. This would explain the presence of hydrogen peroxide. Experiments using a rotating platinum disc electrode with a platinum ring have enabled a quantitative estimation of the amount of hydrogen peroxide formed during oxygen reduction to be made.[73,74] This has shown that in purified sulphuric acid solutions no hydrogen peroxide is formed at potentials above 0.1 V hence above this potential the oxygen is reduced directly to water in a four electron process. In unpurified sulphuric acid solutions the ring current is appreciable over the entire potential range 0.7 V -0.0 V showing that oxygen is reduced to both water and peroxide in parallel reactions and that the peroxide is not further reduced at the disc.[74] In purified alkaline solutions[75] this technique has shown that oxygen is reduced to water and peroxide in

parallel reactions and that the peroxide is further reduced at the disc, thus showing it to be a true intermediate. Further evidence for the cathodic reaction on oxide surfaces being the reverse of the anodic evolution reaction is the intersection of the anodic and cathodic Tafel lines at the reversible potential, I.23 V and determinations of stoichiometric number on oxide surfaces is approximately four.(68)

Carbon and platinum are the most commonly used oxygen electrodes although both suffer from disadvantages especially when used for oxygen evolution. Carbon electrodes, although cheap, disintegrate while platinum electrodes are expensive and form oxide films in common with all other metals. These electrocatalysts will be studied since no other materials are easily available with comparable exchange currents for the oxygen reduction reaction.

E) GAS EVOLUTION REACTIONS.

As already mentioned electrodes undergoing this type of reaction are important in a number of applications, notably: (I) rechargeable air electrodes for metal-air batteries, (2) electrically regenerative fuel cells, (3) fuel cells using liquid fuels eg. methanol and hydrazine, (4) manufacture of chlorine and related processes, (5) preparation of pure hydrogen, (6) as counter electrodes in the electrolytic extraction of some metals, and (7) in various electro oxidations and reductions in organic electrosynthesis. Considering this wide range of applications suprisingly little work has been done on this type of electrode eg. little has

been done to improve their efficiency such as using porous electrodes. Porous graphite electrodes are used in preparation of chlorine and in some of the other applications although they must be frequently replaced. However they are generally used for their chemical inertness rather than to supply a higher surface area. Similarly in methanol and hydrazine fuel cells no work has been done on the effect of electrode structure on the evolution of gases. Most of the work done on gas evolution electrodes has been of a mechanistic nature. The oxygen evolution reaction which has already been described is perhaps the most important, the others of importance being chlorine and hydrogen and to a lesser extent, carbon dioxide and nitrogen evolution.

The standard potential for the Cl_2/Cl^- couple at 25°C is I.36 V and as such it might be expected to take place simultaneously with oxygen evolution. However, the former reaction is much more reversible than the latter so that practically, except at high overpotentials, the amount of oxygen evolved is very small. Never the less in this potential region it is obvious that the chlorine evolution reaction occurs on an oxide surface if a platinum electrode is used and this is a complicating factor as it is in the study of the oxygen electrode reaction. Nearly all the work done on the chlorine evolution electrode has been to elucidate its mechanism and carbon and platinum have been the chief electrode materials used. (77)

The hydrogen evolution reaction is one of great industrial importance (76) and also one of great importance in the development of modern electrochemistry. The

mechanism of and electrocatalysis of this reaction have been widely studied and are now both fairly well understood. Its technological importance is well known eg. it is a standard method of preparing pure hydrogen and also of preparing heavy water since hydrogen is evolved faster than deuterium. Also this reaction plays a dominant role in the corrosion of metals in acidic solutions and since it can occur on a wide range of metals in acid media it has enabled a detailed study of the effect of the substrate on the kinetics of the reaction to be made. The dependence of i_o, for a given metal for this reaction, on other factors is somewhat insignificant eg. i_o is not dependent on concentration or type of electrolyte and, more important, was affected neither by pretreatment of the electrode ie. there are no competing reactions resulting in surface films as there are in the oxygen and chlorine evolution reactions, nor by the state of aggregation ie. i_o for solid and liquid gallium were the same. These factors make the hydrogen evolution reaction both a useful and relatively simple gas evolution reaction to study from the electrode structure aspect. However as oxygen evolution is one of the commonest cases of this type of reaction and is significantly different from hydrogen evolution in that it occurs on an oxide film and oxygen has widely different physical properties to hydrogen eg. density and diffusion coefficient; it is also important to study this reaction in porous materials.

chapter 2.

2.1.	Materials used.	46
2.2.	Electrode fabrication	50
2.3.	Half cell testing.	51
2.4.	Correction for ohmic overvoltage.	59
2.5.	Correction for mass tranfer overvoltage.	61
2.6	Linear Sweep Voltammetry	76
2.7.	Measurement of electrocatalyst surface area	77
2.8.	" " roughness factors of planar electrodes	84
2.9.	" " volume of gas evolved from electrode	86
2.10.	The Coulter counter	86
2.11.	Determination of electrical resistance of catalyst powders	89.

Chapter 2.

Experimental Techniques.

2.I. Materials used in Electrochemical Half-cell Testing.

Electrolytes.

The two electrolytes used were 5N potassium hydroxide and 5N sulphuric acid. Both solutions were prepared from 'analar' grade chemicals and conductivity water of resistance greater than 4 MΩ.cm. . These solutions were purified by anodic and cathodic pretreatment between two large platinum foil plates of area 20 cm^2 at a constant current of 5 mA for IO hours. Although this purification procedure made little difference to the results on porous electrodes it was found to be essential when working with platinum foil electrodes (see chapter 3).

Gases.

Four gases were used ie. oxygen, air, hydrogen and nitrogen. The oxygen, nitrogen and hydrogen were white spot grade supplied by B.O.C.. The air supply was obtained directly from the atmosphere without purification.

Electrocatalysts.

(I) graphite
(2) carbon black
(3) silver on graphite or carbon black
(4) platinised graphite
(5) platinum black
(6) platinised tungsten trioxide
(7) cobalt nickel oxide
(8) tungsten carbide
(9) platinum foil

The sources and/or preparation of these electrocatalysts is as follows:

(I) British Petroleum coarse graphite powder (surface area 5 m^2/g) was ground under vacuum in a vibratory ball mill for 8 hours resulting in a fine graphite powder of B.E.T. surface area 500 m^2/g.

(2) Active graphite supplied by Acheson Industries which had a B.E.T. surface area of 510 m^2/g and 93% of the surface area was attributable to pores below 50 Å radius.

(3) Carbon blacks were supplied by the Cabot Corporation. The samples used are given in the table below.

Types	Sterling MT	Vulcan XC 72R
B.E.T. Surface area	7 m^2/g	220 m^2/g
Particle Diameter by B.E.T.	462 mμ	15 mμ
Electrical Resistivity	Medium	Low $\ll$ 0.25Ωcm

(4) Silver deposited on graphite or carbon black supports can be prepared in three ways:

(a) by grinding the coarse support with a silver compound, such as silver nitrate, under vacuum in a vibratory ball mill. This produces a silver deposit which X ray diffraction shows is very highly dispersed (I65).

(b) by impregnation. This consists of evacuating the support (graphite or carbon black), soaking the support with the impregnating solution (silver nitrate), drying and finally heating to reduce the silver nitrate to

silver metal (210°C).

(c) by freeze drying (see below).

(5) platinised graphite was prepared by soaking graphite powder in a solution of chloroplatinic acid, drying and finally heating in a stream of hydrogen at 80°C in a tube furnace to reduce the chloroplatinic acid to platinum. The sample prepared had a platinum content of 5% by weight and a surface area of 498 m^2/g.

(6) platinised tungsten trioxide was prepared by impregnation of a slurry of tungsten trioxide with chloroplatinic acid solution, followed by freeze drying and reduction in hydrogen, initially at 50°C ie. below the melting point of chloroplatinic acid, for one hour and then at 80°C for two hours.

(7) cobalt nickel oxide (Co_2NiO_4) was prepared by freeze drying a solution containing cobalt(II) and nickel(II) nitrates. The solid solution formed was decomposed by heating under vacuum giving the metal oxides which were heated in air at 400°C for five hours. The resulting oxide has been shown to possess a spinel crystal structure.(166) The sample used had a surface area of 40 m^2/g and an electrical resistance of 10Ωcm.

(8) Tungsten carbide was supplied by British Ropes Ltd. and had a B.E.T. surface area of 1 m^2/g.

(9) platinum foil was supplied by Englehard Ltd.

(10) the platinum black was catalyst grade supplied by Johnson Matthey Co.Ltd.

Another sample was prepared in the laboratory by the reduction of hexachloroplatinate with formaldehyde in alkaline solution.(169)

$$(PtCl_6)^{2-} + 2HCHO + 6OH^- \rightarrow Pt + 2HCOO^- + 4H_2O + 6Cl^-$$

$$(PtCl_6)^{2-} + HCHO + 6OH^- \rightarrow Pt + CO_3^{2-} + 4H_2O + 6Cl^-$$

The platinum black is assumed to form by an initial nucleation process with subsequent development of the platinum crystallites by an electrogrowth mechanism. The surface area of the platinum black prepared is very sensitive to preparation parameters such as reactant concentration, order of addition, pH, temperature and presence of oxygen. These parameters can be varied to give the desired product.

The common chemicals used in these preparations were of analar quality, except for chloroplatinic acid, tungsten trioxide and tungsten carbide which were laboratory reagent grade.

In general it has been found better to prepare electrocatalysts, especially supported electrocatalysts, by the freeze drying technique rather than powder impregnation. With any impregnation method, during drying the salt (eg. H_2PtCl_6 or $AgNO_3$) tends to crystallise from solution producing concentrated areas of salt. This problem is overcome by freeze drying,(130) resulting in a much better dispersion of platinum or silver. The general method of freeze drying can be summarised as follows: the powder to be impregnated is slurried with the salt solution eg. chloroplatinic acid or silver nitrate, and then quickly sprayed into liquid nitrogen before the suspended powder has time to settle. In this way the intimate mixture between powder and solution is frozen in. The ice was then removed by sublimation below the triple point for water by evacuating at

room temperature, so preventing any melting which would result in the growth of chloroplatinic acid or silver nitrate crystallites. It is important that an efficient vacuum pump is used so that the water vapour is removed as soon as it is formed in order to keep the ice below the triple point. When all the ice has sublimed the chloroplatinic acid is reduced to platinum by warming in a hydrogen atmosphere or silver nitrate is decomposed by heating to 210°C. The greater the degree of dispersion of supported electrocatalysts the easier the surface migration of adsorbed species and the lower the electrical contact resistance between the two phases.

2.2. Electrode Fabrication.

Weighed amounts of the electrocatalyst powder and an aqueous polytetrafluoroethylene (P.T.F.E.) dispersion (I.C.I. grade G.P.I, 60% solids of particle diameter 0.2-0.5 micron) were slurried together and painted onto either platinum gauze (80 mesh, 18 s.w.g.) nickel gauze (100 mesh) or graphite cloth screens, (manufactured by Morganite Modmor Ltd. from carbon fibres resistance 1 ohm/square). After drying at 70°C for one hour the electrodes were cured at 300°C for one hour. This procedure removes the wetting agent present in the teflon dispersion and causes its partial sintering, thus increasing the strength and hydrophobic nature of the electrode. The curing temperature is critical since at temperatures above 330°C the P.T.F.E. is transformed into a glassy state, rendering the electrode completely hydrophobic and consequently inactive. Electrodes containing carbon were cured under nitrogen since carbon is slowly

oxidised at 300°C.

The electrocatalyst loading was calculated from the weight changes of the screen before and after fabrication, assuming that the components of the catalyst - P.T.F.E. slurry were transferred to the screen in the same proportion as in the original slurry. Complete transfer of the mix was not possible. The dispersion of the electrocatalyst powder in the P.T.F.E. suspension was sometimes improved by using an ultrasonic vibrator. Electrocatalyst loadings were usually within the range 4-20 mg.cm^{-2} and the most satisfactory P.T.F.E. content has been shown to be 25-35% by weight of the electrocatalyst. (158)

The platinum, nickel and graphite cloth screens act as current collectors and when the electrode is used for oxygen reduction or hydrogen oxidation they contribute only a negligible current. However when the electrode is used for oxygen or hydrogen evolution they can contribute a significant current and a correction is necessary.

2.3. Half cell testing.

(a) Cell design.

The cell design shown in Fig. I is a modification of the floating electrode cell described by Giner. (196) The working electrode was spot welded into a piece of gold foil wedged at one end. The geometric area of exposed electrode was measured. The electrode thus mounted was clamped between a pair of teflon rings on the central tube of the upper compartment. The reference electrode system was housed inside this tube which terminated in a 'U' shaped luggin capillary which

Fig. 1 Floating Electrode Cell

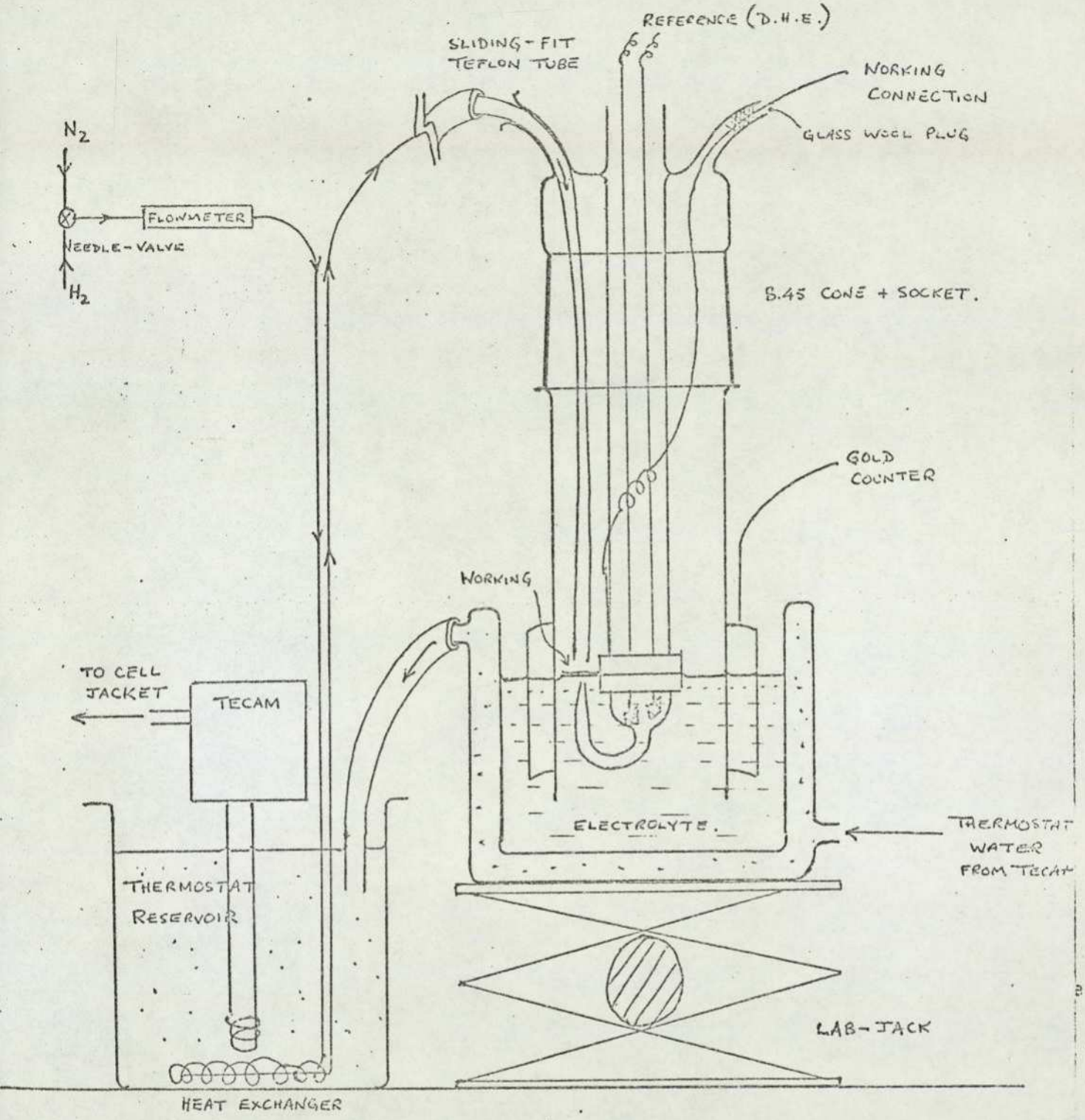
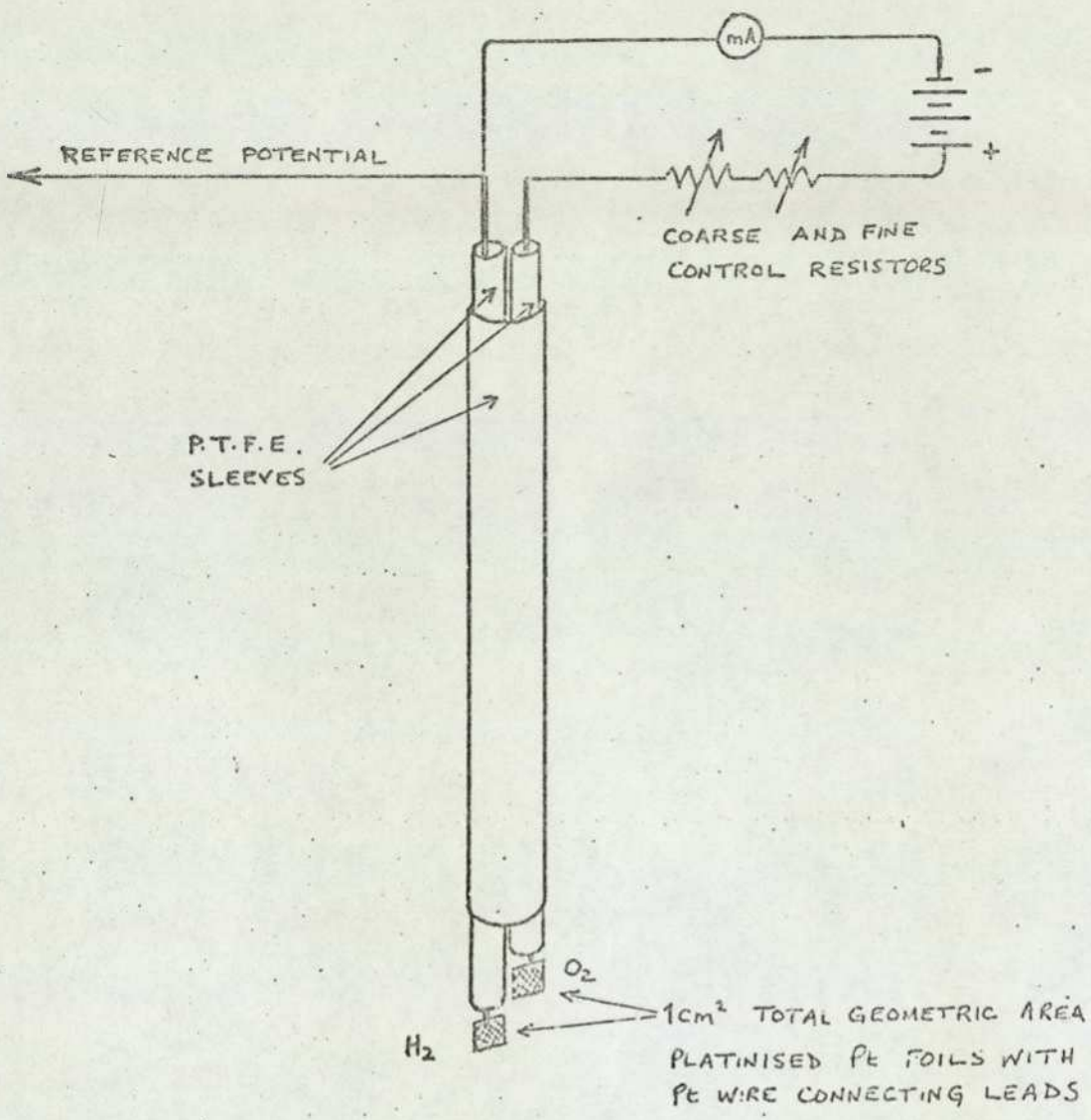
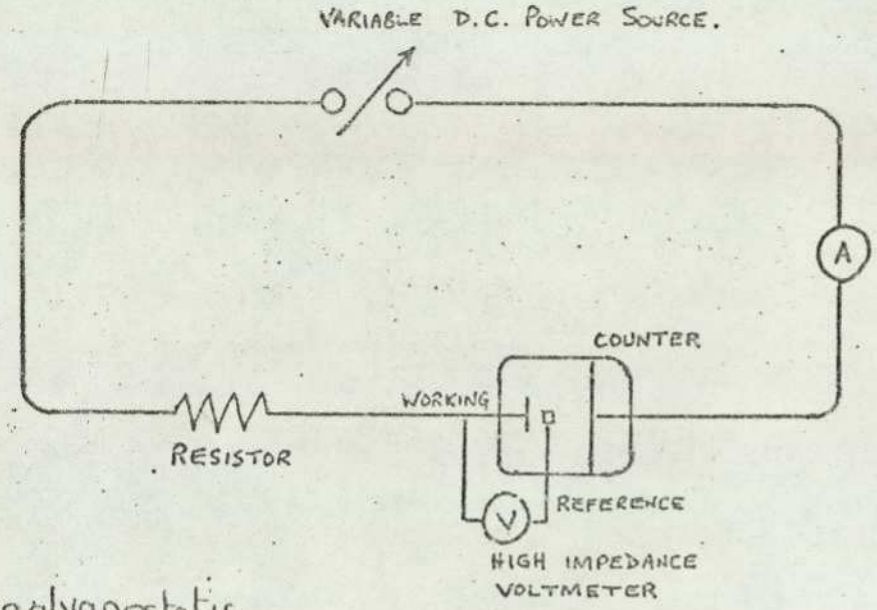


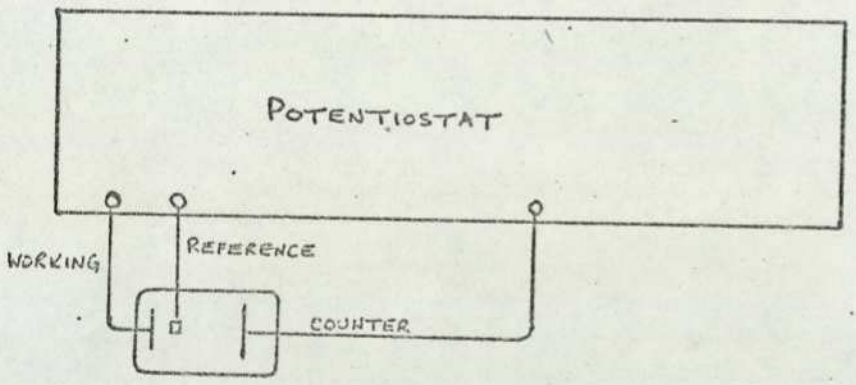
Fig. 2. The Dynamic Hydrogen Reference Electrode.



.3. Circuits for steady state potentiostatic and galvanostatic polarisation curves.



(a) galvanostatic



b) potentiostatic.

reached to just under the working electrode which floats on the electrolyte surface. In this cell the electrode compartment is sealed off from the atmosphere outside by the electrolyte and the electrode compartment can be fed with any gas required, either bubbled through the electrolyte or simply blown through the chamber. The gas flow rate was controlled by a needle valve and calibrated 'gap meter' (Gallenkamp). The electrolyte temperature can be varied by the thermostated water bath supplying the jacketed lower cell assembly.

(b) The reference electrode system.

The dynamic hydrogen reference electrode system (D.H.E.) was used.[171] Fig. 2. This consists of two vertically staged platinised platinum electrodes, each of area 0.5 cm^2 between which a constant current of 2 $mA.cm^{-2}$ was passed. The lower electrode, connected to the negative battery terminal, evolved hydrogen while the oxygen evolved from the upper electrode escaped upwards and did not interfere with the electrode evolving hydrogen. The potential of the working electrode is measured against the potential of the lower reference electrode. The voltage of this reference electrode, measured against a normal bubbling hydrogen reference electrode in the same electrolyte (R.H.E.), remained constant at -25 mV $\pm$ 4 mV over a few months before replatinising became necessary.

(c) Method for determining steady state potentiostatic polarisation curves.

(I) The cell was set up as in Fig. 3 and the system allowed to reach a steady temperature.

(II) The required atmosphere is obtained by passing

oxygen, nitrogen, hydrogen or air and the open circuit voltage (O.C.V.) measured with a high impedance digital voltmeter (D.V.M.) (II megohm).

(III) The potentiostat was set to the O.C.V. and switched to the cell.

(IV) The potentiostat was then set at the desired potential and the current measured when it became steady. This procedure was repeated at different potentials as the polarisation increased and again at the same potentials as the polarisation was decreased.

(V) The correction for the ohmic overvoltage was made by the interupter method (see below).

(d) Method for determining galvanostatic steady state polarisation data.

The procedure is the same as for the potentiostatic method except that the potentiostat is used to apply a constant potential across a standard resistance thus producing a constant current. A suitable constant current is applied to the cell and the potential between the working and reference electrode is measured, when steady, with the D.V.M. . This is repeated at different constant currents and the current-potential curve plotted. (see Fig. 3).

(e) The potentiostat.

This was a chemical electronics TR40-3A model which had the following specifications:

Maximum output current	3.0 A
Current measurement accuracy	±I% full scale deflection
Output voltage	40 V
Control voltage span	+3 to -3 V (accuracy ±0.5 mV)
Control voltage stability	± 0.I mV

Long term drift — Continually monitored and corrected with potentiostat controls.

Rise time (to 90% of selected voltage) — 0.3 microsec.

Response time (to 100% selected voltage) — 10 microsec.

Input current — $I \times 10^{-10}$ A

A potentiostat is used to maintain a constant potential between the test electrode and a given reference electrode. A potentiostat has an inbuilt standard voltage adjustable to any value and the ability to measure the potential between the test and reference electrodes. The two potentials are electronically compared and the current flowing in the power circuit is automatically adjusted by an operational amplifier so that the electrode potential is maintained at the same value as the standard. This implies that a current must flow through the reference electrode but with modern instruments this is very small, although it is necessary to check that the reference electrode is not polarised.

(f) Origins of errors in steady state half cell testing.

(I) Electrocatalyst loading.

Possible errors are the accuracy of weighing, measurement of electrode geometric area and the assumption that each component in the catalyst mix is transferred to the electrode in the same proportions. This last error can not be estimated and depends mainly on an efficient dispersion procedure. The maximum error in the geometric electrode area was ± 0.2 cm^2 in 1 cm^2 ie. 20% and the error in the electrocatalyst loading $\pm$ 5%.

Another possible error which is difficult to assess is whether the electrocatalyst - P.T.F.E. mix has been pasted evenly over the whole current collector surface. This depends largely on the skill of the maker and a rough guide to uniformity was achieved by visual inspection.

(II) Dispersion of electrocatalyst on support.

This should be quite reproducible for samples prepared by freeze drying but significant errors are probable in samples prepared by powder impregnation.

(III) Current and potential measurements.

The current was measured to $\pm$ 2% of full scale deflection and the potential to $\pm$ 0.5% hence the error in these measurements is very small except at very low currents and potentials.

(IV) The correction for ohmic overvoltage.

During the estimation of the iR drop the main source of estimatable error was imposed by the inaccuracy of reading the oscilloscope grid. Measurement limits were to $\pm$ 0.2 cm. iR drops were usually in the region of 0.05 - 0.2 ohm. Using a current of 10 mA, measured across a 100 ohm standard resistor, and oscilloscope vertical sensitivities of 200 $mV.cm^{-1}$ and 1 $mV.cm^{-1}$ for current and voltage measurements respectively the iR drop was measured to within 0.02 ohm, resulting in errors of 10 - 40%. When measuring the actual voltage drop of an electrode it is sometimes difficult to assess the difference between the voltage drop due to ohmic effects and that due to activation effects and this can result in errors greater than those estimated above.

From the above account it can be seen that the chief origins of error are the electrocatalyst preparation, electrode fabrication and the measurement of the ohmic overvoltage. Hence the accuracy of a single current-voltage scan is high, being limited only by the accuracy of the iR correction, while the reproducibility using either (a) another sample from the same 6 cm^2 original electrode, (b) a new electrode fabricated from the same batch of electrocatalyst, or (c) a new electrode fabricated from a different batch of electrocatalyst is much poorer, especially for (b) and (c). The scatter of the results shows that the reproducibility is usually better than $\pm$ 15% for a given electrocatalyst batch. Different batches pose a much greater problem in that the B.E.T. surface areas of different batches of the same material often vary substantially.

2.4. The correction for ohmic overvoltage.

An ohmic overvoltage exists wherever there is a resistance to current flow, eg. connecting wires, resistance of working and counter electrodes, and the electrolyte resistance. The resistance of connecting wires and the counter electrode are very low and this usually applies to the working electrode also. Hence the main source of ohmic overvoltage is the electrolyte resistance which, in these experiments, was also quite low (5N sulphuric acid and 5N potassium hydroxide). The electrolyte resistance is minimised by using a luggin capillary, the tip of which is located close to the working electrode surface. The resistance between the luggin and the working electrode can be determined in three ways:

(a) from the luggin - electrode geometry it is possible to calculate the iR drop from the relationship (I72)

$$\eta_{iR} = \frac{i L}{K}$$

where i = current

K = specific conductivity of the electrolyte

L = I.67 d

where d is the external diameter of the luggin capillary tip placed at a distance of 2 d from the working electrode surface. This method is likely to be unreliable at high currents when the electrolyte resistance will vary over the luggin - capillary gap.

A similar method is to measure the electrode potential as a function of luggin gap and then extrapolate the results to give the potential at zero gap. (I73) At high currents the potential- gap relationship is not linear, thus making extrapolation difficult. Both these methods depend on the accurate determination of the luggin tip-working electrode gap, and while this is simple for a planar electrode it is virtually impossible for a porous electrode whose surface is rough and ill defined.

(b) by using an A.C. conductivity bridge (I74) connecting the working electrode to one arm and completing the circuit by placing a probe at the luggin tip.

(c) by the interupter method (I84) where a steady D.C. polarising current is interupted at mains frequency (50 Hz) by means of a fast acting, mercury wetted relay producing a train of square current waves through the cell. The components of the total overpotential can be

estimated as a result of their different time dependence of decay or growth. Thus ohmic polarisation is instantaneous while activation and mass transfer polarisation require finite times to grow or decay. Hence when the potential between the working and reference electrodes is displayed on an oscilloscope and the voltage - time curve traced, this will differentiate between the three component overpotentials. (See Fig. 4). From the current flowing and the vertical portion of the voltage - time trace, the working electrode - luggin gap resistance can be calculated from Ohm's law and then used to correct the electrode potential. The circuit diagram for this method is shown in Fig. 4. The ohmic drop depends on the electrode reaction and when measuring the ohmic drpp it is important to ensure that the electrode is undergoing the same electrode reaction as that for which the correction is to be used eg. gas evolution reactions often result in a higher ohmic drop due to partial insulation by gas bubbles. If the electrocatalyst has a high resistivity it is possible that only a fraction of the electrocatalyst resistance will be included in the interupter determination.

In this work the electrolytes were highly conducting and the luggin - working electrode distance was short ($\sim$0.2 cm) resulting in ohmic resistances from 0.05 to 0.30 ohm.

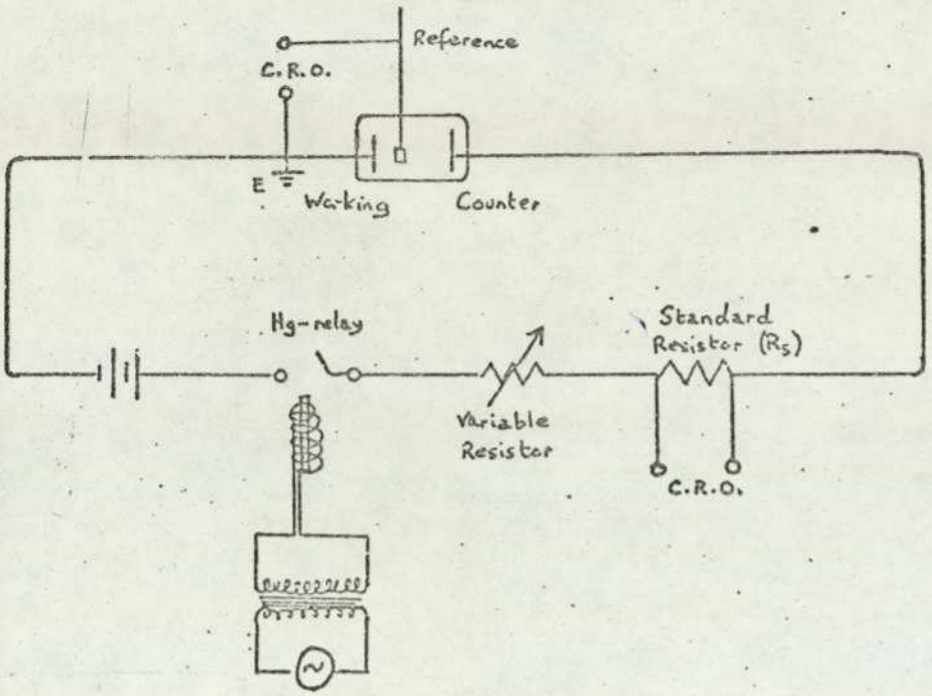
2.5. The correction for mass transfer overvoltage.

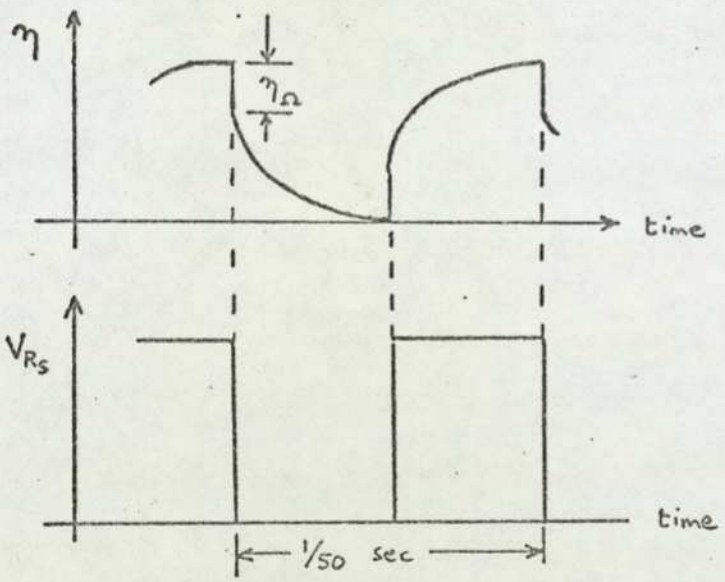
Two methods have been used for planar electrodes:

(I) The rotating disc electrode.

By rotating the electrode horizontally under

ig. 4 Circuit and traces for interrupter technique





carefully controlled hydrodynamic conditions the limiting current for a process under mass transfer control is given by (I75)

$$i_L = W^{0.5} \left[0.62\, n\, F\, C_O\, D^{2/3} \nu^{-1/6} \right]$$

where i_L = limiting current

W = angular velocity of electrode

n = number of electrons involved in the electrode process

F = the Faraday

C_O = bulk concentration of reactant

D = diffusion coefficient of reactant species

ν = kinematic viscosity of the electrolyte

Thus for a process operating under mass transfer control the plot of i_L v $\sqrt{W}$ is a straight line. Current limitations arrising from other sources of polarisation will be independent of rotation speed. Hence by increasing the rotation speed at a fixed potential it is possible to eliminate mass transfer which is indicated when the limiting current is no longer dependent on rotation speed. At very low and high rotation speeds modifications of the above equation are used. (I76,I77) The rotation speed can only be increased to a certain level dependent on the cell design before turbulence sets in. Hence very fast reactions are difficult to treat by this method and in order to eliminate the mass transfer component of the overpotential it is necessary to extrapolate the linear plot of I/i_L v $I/\sqrt{W}$ to $I/\sqrt{W} = 0$ when the rotation speed is infinite. It is not possible to study porous teflon

bonded electrodes by this technique.

(II) The potentiostatic and galvanostatic pulse techniques.

Consider an electrode, immersed and equilibrated in an electrolyte solution containing a reactant at concentration, C_O. At the instant of applying a current or overpotential to this electrode the i - η relationship will be governed solely by the charge transfer reaction (neglecting ohmic and double layer charging effects). Mass transfer effects will be negligible at this instant, but will become more significant as the reaction time increases. After an infinite time the steady state condition will be attained.

In principle the transient behaviour of an electrode, either at constant current or overpotential under mass transfer free conditions prevailing at zero time, can be measured using an oscilloscope. However, it is not possible to take measurements at exactly zero time due to double layer charging effects. The electrode behaves as a condenser and at the instant of applying the potential or current a very small, but finite, time is required to charge the electrode. This time depends on the capacity of the electrode double layer and consequently, on the electrode surface area, and can be as long as several micro seconds. Hence at the instant of polarisation and over the first few micro seconds the current is at least partly non-faradaic. During this short time some mass transfer polarisation occurs, especially with very fast electrode reactions and hence it is desirable to keep the electrode area low to minimise the double layer

charging time.

Two procedures may be used to interpret electrode transients:

(I) Measurements are taken at the shortest time interval at which double layer charging is complete and a certain amount of mass transfer polarisation accepted. The double layer charging time can be measured from the electrode transient in the absence of any reacting species.

(II) A more accurate measurement can be obtained from the mathematical relationship for the transient. It can be shown that, for a stationary electrode, at constant overpotential, whereby the reactant arrives solely by diffusion from the bulk electrolyte, which extends to infinity in a perpendicular direction to the electrode surface ie. semi-infinite linear diffusion, the current transient is given by:

$$i = i_0 \left[\exp\left(\frac{-\alpha n F \eta}{RT}\right) - \exp\left(\frac{(1-\alpha) n F \eta}{RT}\right) \right] \exp\left(\lambda^2 t\right) . \operatorname{erfc}\left(\lambda t^{0.5}\right)$$

The first two terms are identical to the equation for a reaction controlled solely by electron transfer and are independent of time. The last two terms correct the equation for mass transfer where

$$\lambda = \frac{i_0}{nF} \left[\frac{\exp\left(\frac{-\alpha n F \eta}{RT}\right)}{C_O^o D_O^{o.5}} + \frac{\exp\left(\frac{(1-\alpha) n F \eta}{RT}\right)}{C_R^o D_R^{o.5}} \right]$$

where i_0 = exchange current density

α = transfer coefficient

C_O^0 and C_R^0 are the bulk concentrations of reactant and product respectively.

D_O and D_R are the diffusion coefficients of the reactant and product respectively.

At $t = 0$, $\exp(\lambda^2 t).\mathrm{erfc}(\lambda t^{0.5})$ is unity ie. mass transfer effects are absent. As $t \to \infty$, $\exp(\lambda^2 t).\mathrm{erfc}(\lambda t^{0.5}) \to 0$ ie. mass transfer effects become more dominant as the time increases. For short time intervals when $(\lambda t^{0.5}) \ll I$ the term $\mathrm{erfc}(\lambda t^{0.5})$ can be expanded to

$$1 - 2\left(\frac{\lambda t^{0.5}}{\pi^{0.5}}\right)$$

Hence a plot of i v. $t^{0.5}$ at short times is linear. If this plot is extrapolated to $t^{0.5} = 0$ then the i intercept is the current at zero time ie. in the absence of mass transfer effects. Since the term $(\lambda t^{0.5})$ depends on i_0 it follows that for very fast reactions the time interval at which $(\lambda t^{0.5}) \ll I$ may be too short to make reliable measurements.

A similar $\eta - t^{0.5}$ relationship can be derived when a constant current pulse is applied and the overpotential-time transient recorded.

The above relationships are derived under the simplest possible diffusion conditions viz. semi infinite linear diffusion. This type of diffusion is obtained with planar electrodes but with more complicated electrode structure the derivatives become increasingly complex and it is unlikely that an analytical relationship can be derived for highly complex porous

electrodes. Also the equations do not apply when other forms of mass transfer are possible and measurements should be confined to short time intervals to minimise mass transport by convection or vibrations.

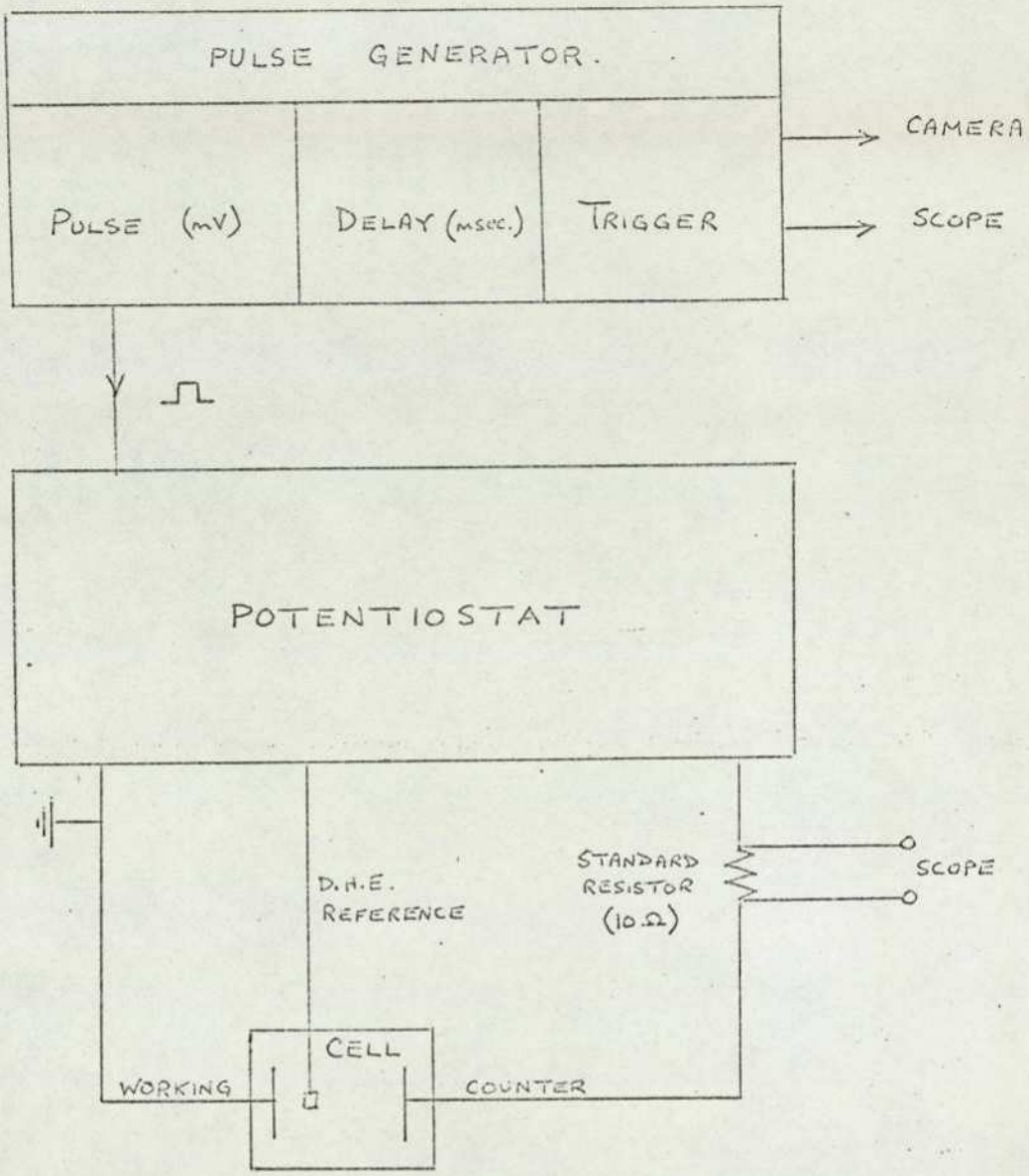
Apart from the application of potential or current pulses, methods are available in an alternating component of overpotential superimposed on the steady state condition.. By postulating an equivalent circuit for the electrode reaction and measuring impedance and phase shifts between i and η, kinetic data can be obtained for the process.[197] These methods are very useful but the analysis of data becomes increasingly involved as the complexity of the reaction increases.

Mass transfer through porous media is more complex than mass transfer to a planar electrode and therefore is unlikely to obey the laws of semi infinite linear diffusion. Hence the mathematical treatment cannot be used unless the i - t or η - t relationships can be empirically established. However it is sometimes essential to use porous electrodes in applied studies and in these cases the less precise method of eliminating mass transfer overpotential must be used.

The experimental procedure for measuring electrode transients is as follows:

The electrode is mounted in the floating electrode half cell containing the appropriate electrolyte. In the case of teflon bonded porous electrodes the electrode was electrochemically floodedin order to ensure that all the electrocatalyst area was being used. The electrode was then left to equilibrate in the chosen atmosphere until the O.C.V. was steady.

FIG. 5 SCHEMATIC CIRCUIT DIAGRAM FOR POTENTIOSTATIC PULSING.



The potentiostat was set to this value and switched to the cell and a single potential jump applied to the electrode by means of a pulse generator (Chemical Electronics, RBI). The change in cell current with time was measured across a suitable known resistance in series with the cell and displayed on an oscilloscope. This trace was photographed using a 35 mm camera with (Sdatron CD1400 cx1442-3) the pulse generator, oscilloscope and camera being suitably synchronised. This procedure was repeated for varying values of potential jump. A schematic circuit diagram of the system is shown in Fig. 5.

The possible errors are:

(a) potential measured with a digital voltmeter and accurate to $\pm$ I mV in I V ie. O.I%.

(b) potential measured across a standard resistance in the counter electrode circuit using an oscilloscope. $\pm$0.4 cm in 4 cm

(c) an error which is less easily estimated is encountered when it is required to measure the current at very short times when the possibility exists that non faradaic currents are present. This problem is only likely to be significant for high surface area porous electrodes since for planar electrodes the non faradaic double layer charging current is known to decay to zero very quickly.

$$t_c = C_D . R$$

where t_c = time constant

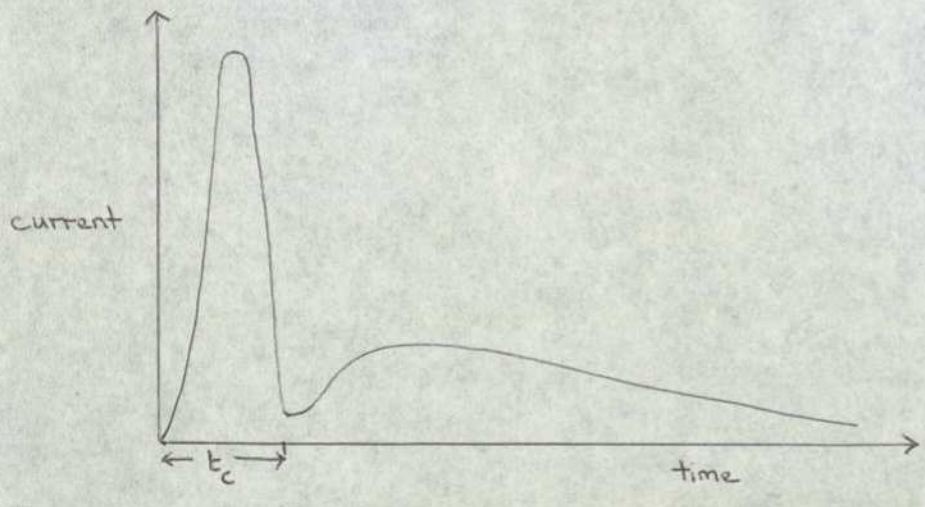
C_D = double layer capacity

R = electrolyte resistance between luggin tip and working electrode

C_D is low for a planar electrode and since R is low

* On this basis, for the porous electrodes used in the present study, the time constant should be ~ 500 μsec, assuming complete electrocatalyst utilisation. The response time of the potentiostat is 10 μsec so it follows that even for planar electrodes accurate measurements cannot be made at times less than 10 μsec.

statically in a potential region where no faradaic processes occur eg. 0.50 V (under nitrogen) in 5N sulphuric acid electrolyte for the platinum electrodes and 5N potassium hydroxide for the graphite electrode which had been pre-electrolysed and well purged with nitrogen. Anodic and cathodic pulses were then applied using the pulse generator (±50 - 100 mV) and the response recorded on the oscilloscope. Tests were repeated for varying electrode surface areas. Typical traces are shown in Figs. 11 for platinum foil, platinum black and graphite electrodes. The general shape is shown below.



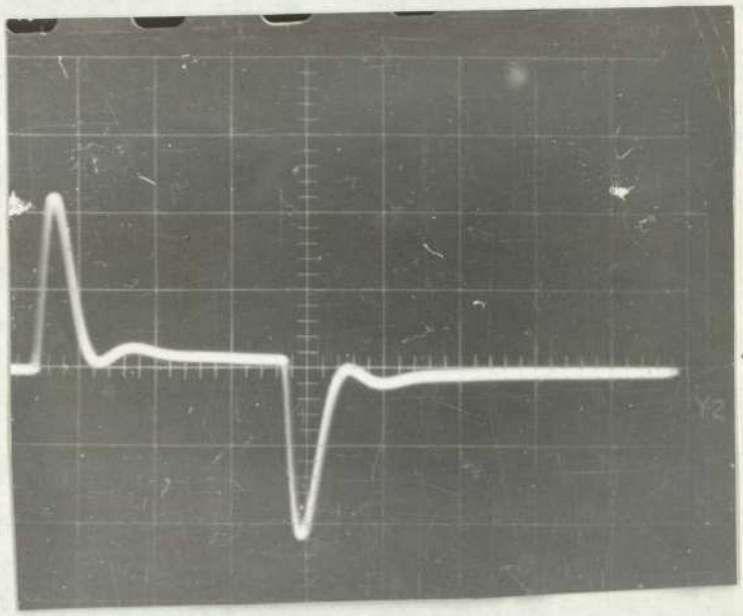
The sharp spike on the trace is due to the charging of the double layer and the double layer charging time t_c can be measured as shown. The minimum of the trace and the continuation of the trace to longer times can be explained in three ways:

(I) An oscillatory effect in the potentiostat - pulse generator - cell circuit. (Chemical Electronics Ltd. report that this is a definite possibility.)

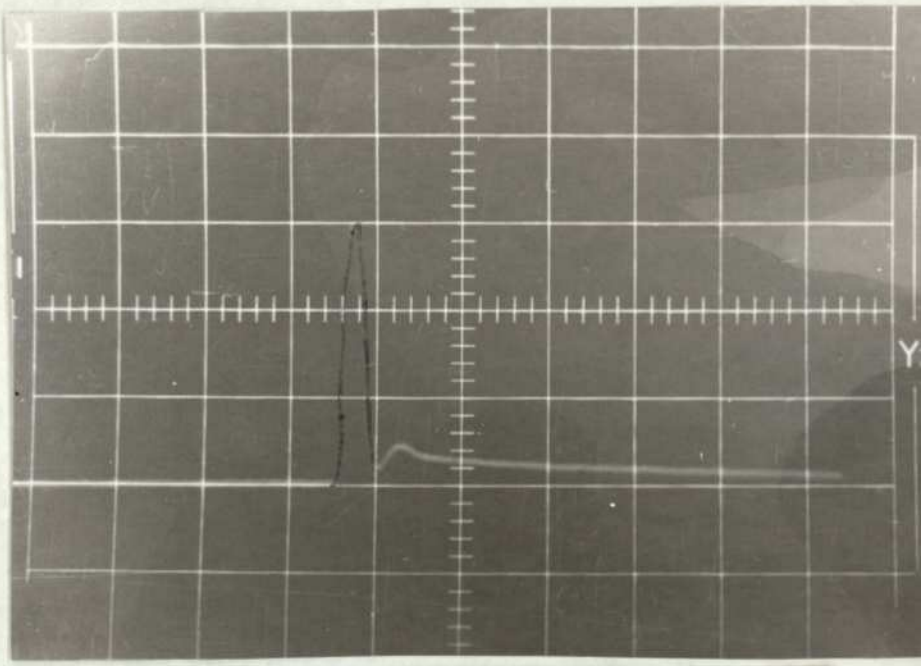
Fig 11.

Double Layer
Charging Curves

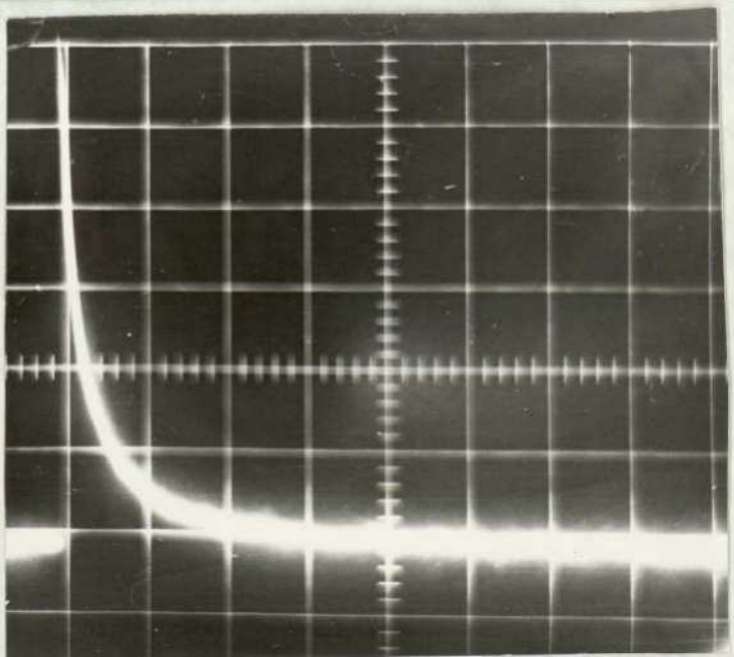
(a)
platinum foil
X axis 40μs/cm



(b)
platinum black
X axis 20μs/cm



(c)
graphite
X axis 1ms/cm



(2) In a porous electrode most of the surface is charged during t_c but some of the surface in the pores which is not easily accessible requires a considerably longer time before it is fully charged.
(3) It could be due to a pseudocapacity effect.

Although there is some evidence (I33) that inaccessible pores take longer to charge than readily accessible surface this explanation seems improbable in this case since curves of similar shape were observed for platinum foil electrodes of roughness factor I.6.

In any event the readings taken after t_c are reasonably free from non faradaic effects providing they are greater than I0% of the double layer charging peak current, since the height of the smaller maximum was found to be $\sim$ I0% of the peak charging current, at times within the initial 2 msec.

The effect of varying the applied pulse amplitude from 50 to I00 mV had the effect of doubling the height of the double layer charging peak and the remainder of the trace without affecting t_c.

The effect of varying the electrode surface area had no effect on t_c which is to be expected for planar electrodes since t_c in this case is probably due to the response time of the electric circuit. However, varying the surface area of porous electrodes suprisingly has no effect on t_c eg. doubling the surface area has the effect of doubling the charging peak height but leaving t_c unchanged. The area of the curve from $t = 0$ to $t = t_c$ is the double layer charge and can be approximated as $0.5\, i_p\, t_c$ where

i_p = peak charging current. Since the double layer capacity is proportional to the surface area of the electrode it follows that doubling the surface area should result in a doubling of the double layer charge as observed. This doubling is achieved by increasing i_p, t_c remaining constant.

Hence it appears that this is a reasonable method of determining the time to charge the double layer of a porous electrode and that within the limitations mentioned, currents measured at longer times can be said to be virtually free from non faradaic effects. The results of double layer charging experiments are shown in Fig.12.

Fig.12.

Electrode	t_c	I_p (mA)	Surface area cm^2	Pulse amplitude
platinum foil	25µs ± 5µs	60	3.2	± 50 mV
		I20	3.2	± I00 mV
		I20	6.4	± 50 mV
		I80	9.6	± 50 mV
platinum black	I00µs ± 20µs	925	I unit	± I00 mV
		460	I unit	± 50 mV
		900	2 units	± 50 mV
		I380	3 units	± 50 mV
graphite	I ms ± 0.2 ms	I60	I unit	± 50 mV
		320	I unit	± I00 mV

Note: (I) area of platinum foil corrected for surface roughness.

(2) I unit of surface area for platinum black electrode = 0.5 cm^2 geometric area of a teflon bonded electrode of loading 5.2 mg/cm^2 and B.E.T surface area of platinum black = 8.1 m^2/g

(3) I unit of surface area of graphite electrode = I.0 cm^2 of a teflon bonded graphite electrode of loading 8.0 mg/cm^2 but of unknown B.E.T. surface area.

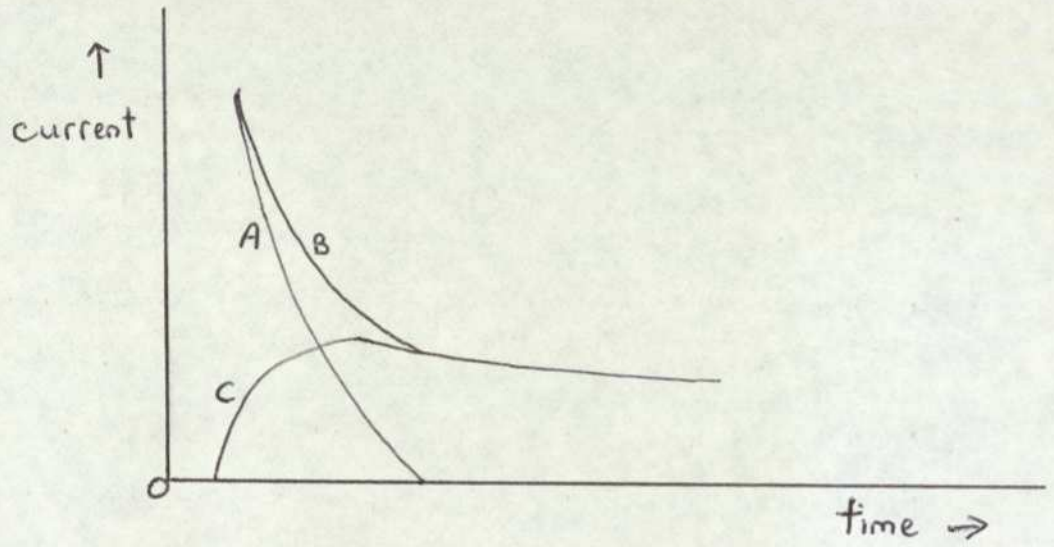
In the double pulse method (189) the problem of double layer charging at short times is overcome by applying two constant current pulses. The first is as short as possible eg. Iμs and adjusted in magnitude so as to just charge the double layer. The second pulse is of much smaller magnitude and longer duration. The overvoltage resulting from the second pulse is measured directly with an oscilloscope.

The problem of double layer charging is most acute for very fast electrode reactions when diffusion effects are well established before the double layer is fully charged. In a potentiostatic circuit the most serious problem is the ohmic resistance between the electrode and the luggin capillary, which impedes the setting up of potentiostatic conditions. In addition, the internal resistance of the circuit results in a longer time constant before potentiostatic conditions are set up. As potentiostatic circuits involve feedback, there is a stability problem which limits the response time of the circuit to values greater than 3μsec. (190) With galvanostatic circuits it is predominantly the double

layer charging which impedes the establishment of galvanostatic conditions. The charging time of the double layer condenser is relatively long because the charging current is limited by the constant current applied to the system.

The effect of double layer charging can be conveniently summarised by Fig. IO.

Fig.IO.



A - charging current

B - total current ie. charging and faradaic currents

C - faradaic current

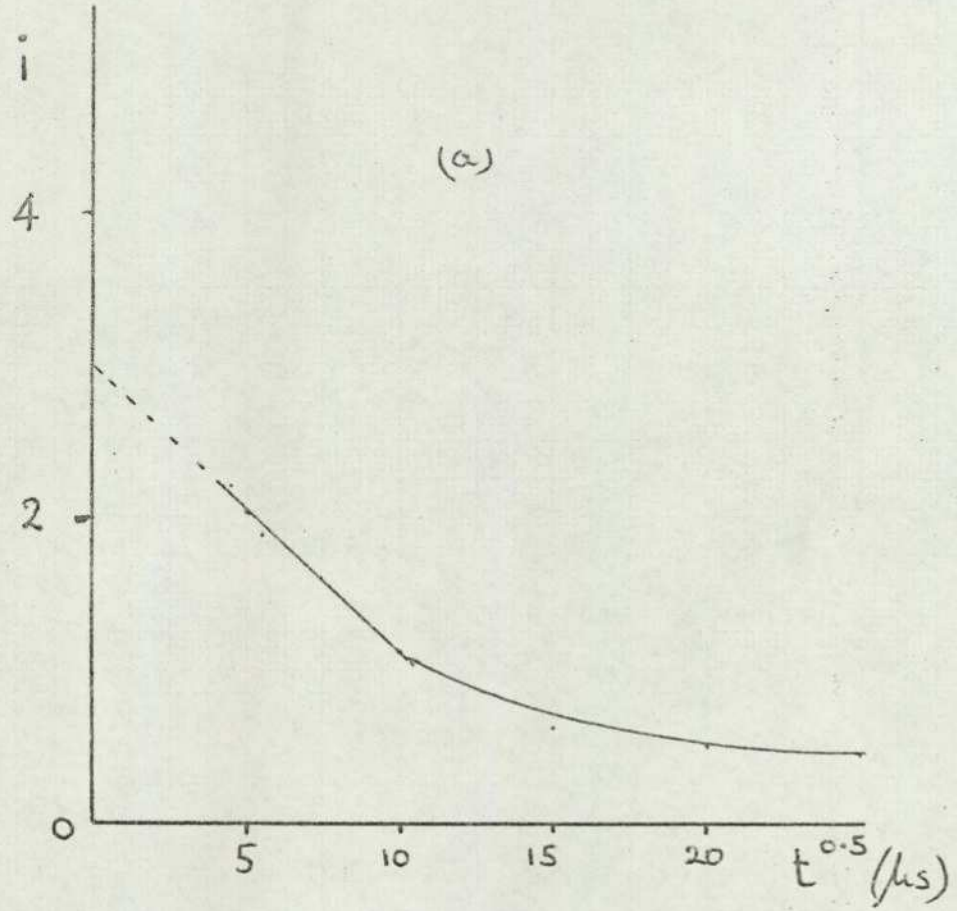
For fast electrode reactions such as hydrogen evolution or oxidation there is likely to be a significant error in measuring the current free from mass transfer overvoltage since in the time taken to charge the double layer or for the potentiostat response to settle the mass transfer overvoltage reaches a finite value. Hence the current can be measured immediately after double layer charging is complete or the faradaic current at zero time can be estimated from an extrapolation of an $i - t^{0.5}$ plot to $t^{0.5} = 0$.

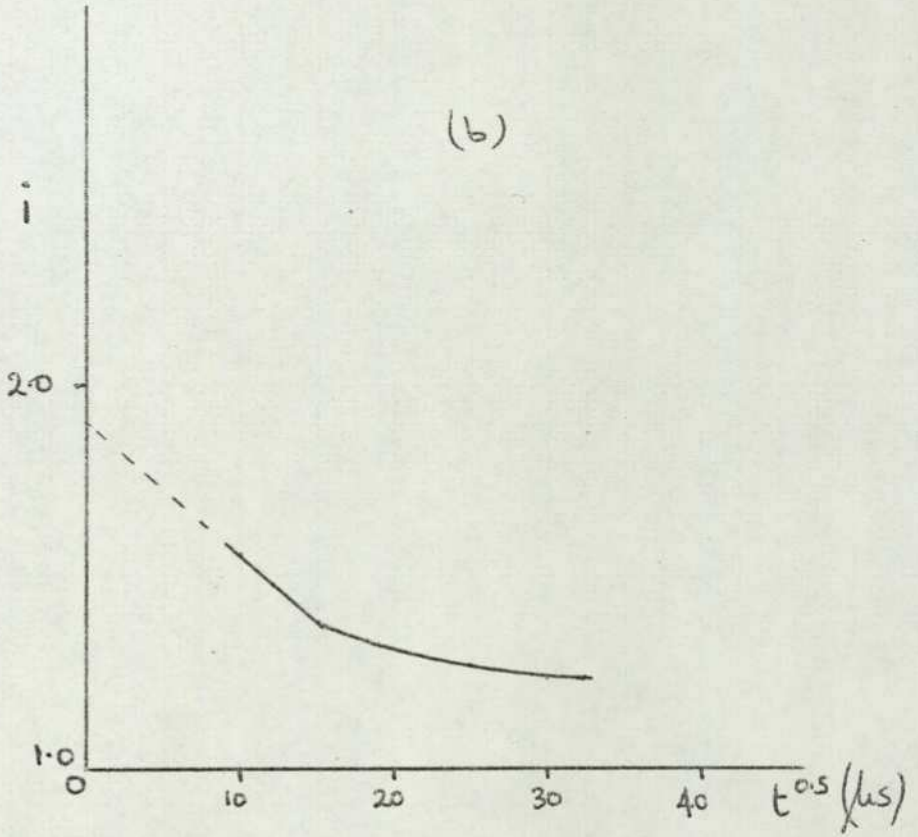
Fig. 13. $i - t^{0.5}$ plots for H_2 evolution on (a) platinum foil and (b) teflon bonded platinum black.

Electrolyte 5N H_2SO_4
Temp. 21°C
Atmosphere H_2

OCV 0.030V
Pulse Amplitude −50mV
Resistance 0.12 ohm

Electrocatalyst S.A. = $8 m^2 . g^{-1}$
" loading = $8 mg . cm^{-2}$
Current Collector Pt gauze
O.C.V. 0.023V
Pulse Amplitude − 50mV
Resistance 0.11 ohm





A comparison of these two methods for the hydrogen evolution reaction on platinum foil and teflon bonded platinum black shows that the error involved in measuring the current following completion of double layer charging rather than extrapolating an $i - t^{0.5}$ curve was about 25% for platinum foil and 20% for teflon bonded platinum black. (Fig. B)

2.6. Linear Sweep Voltammetry.

A useful technique for studying electrode processes is the application of a linearly changing voltage function to a stationary working electrode. The resultant current - potential plot or voltammogram consists of a pattern of current maxima along the potential axis, whose heights and positions are characteristics of the electrode process. The occurrence of maxima for any given electrode process is a mass transfer effect and is predicted from theoretical considerations of simplified diffusion conditions (I78) eg. linear diffusion. The exact profile of the voltammogram is affected by parameters such as temperature, electrolyte composition, voltage scan rate (I79) and the number of voltage cycles.

Linear sweep voltammetry has many applications in electrochemistry. (I78) In the study of electrochemical reaction mechanisms it can be used to measure kinetic parameters such as i_0 and α, using single sweeps on plane electrodes, and to determine the reversibility by comparing cathodic and anodic sweeps.

By selecting a sufficiently slow sweep rate the steady state polarisation curve may be automatically plotted. In this work the linear sweep generator (Chemical Electronics) was used in conjunction with the

potentiostat and floating half cell, and the results recorded on an X - Y pen recorder (Bryans Model 2IOOI). The technique was usually employed to determine current-voltage curves under reproducible conditions when a steady state current could not be obtained due to oxide film formation or gas bubble formation. A schematic diagram of the system is shown in Fig. 6.

2.7. Measurement of electrocatalyst surface area.

In order to find the intrinsic exchange current density it is necessary to know the surface area of the electrocatalyst in the electrode.

There are two main approaches to determining the electrocatalyst surface area:

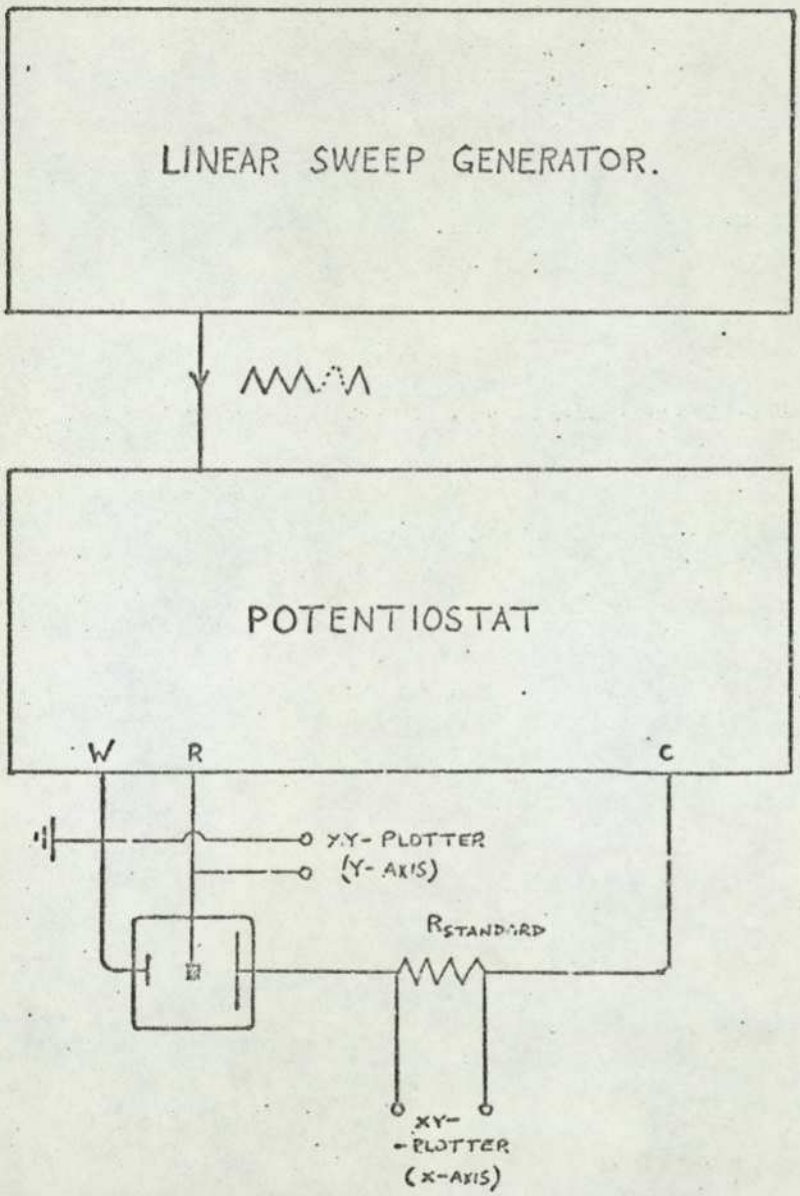
(I) The total surface area which can be determined by tests on the electrocatalyst alone, such as gas adsorption, electron microscopy or X ray diffraction.

(II) The electrochemical surface area ie. the electrocatalyst area that is available for reaction, excluding areas not in electrolyte contact, areas which are inert, or ohmically insulated due to high resistivity in the catalyst layer which is determined by tests on the electrode itself, such as hydrogen or oxygen stripping.

When the total surface area equals the electrochemical surface area the electrocatalyst is being used at maximum efficiency and the current density will be essentially uniform. The electrocatalyst utilisation factor, U, is defined as

$$U = \frac{\text{Electrochemical surface area}}{\text{Total surface area}} \times 100$$

6. Circuit for Linear Sweep Voltammetry.



In the present investigations the total surface area was determined by the gas adsorption technique. The physical adsorption of many gases on solid surfaces at temperatures close to the gas boiling point follows an 'S' shaped isotherm. This shape is a result of multimolecular layer formation as opposed to monolayer formation observed for chemisorbed gases eg. Langmuir adsorption.(180) Brunauer, Emmett and Teller(181) have derived an equation for this isotherm by considering the adsorption process as a condensation of gas onto the solid surface and then applying a modified Langmuir treatment. The relationship is

$$\frac{x}{q(1 - x)} = \frac{1}{q_m C} + \frac{C - 1}{q_m C} \cdot x$$

where x = the relative pressure ie. P/P_0 where

P = actual pressure

P_0 = saturated vapour pressure of the liquid adsorbate

q = quantity of gas adsorbed at a given value of x

q_m = the monolayer capacity

C = a constant involving the heats of adsorption of successive adsorbed layers

From the above equation a plot of $\frac{x}{q(1 - x)}$ v. x gives a straight line of slope $\frac{C - 1}{q_m C}$ and an intercept of $\frac{1}{q_m C}$. The value of q_m is given by $q_m = \frac{1}{\text{slope} + \text{intercept}}$

From a knowledge of q_m and the cross sectional area of the adsorbed molecule the powder surface area can be determined. The B.E.T. equation holds between relative

Fig. 8.

Typical Oscilloscope trace for galvanostatic H_2 stripping

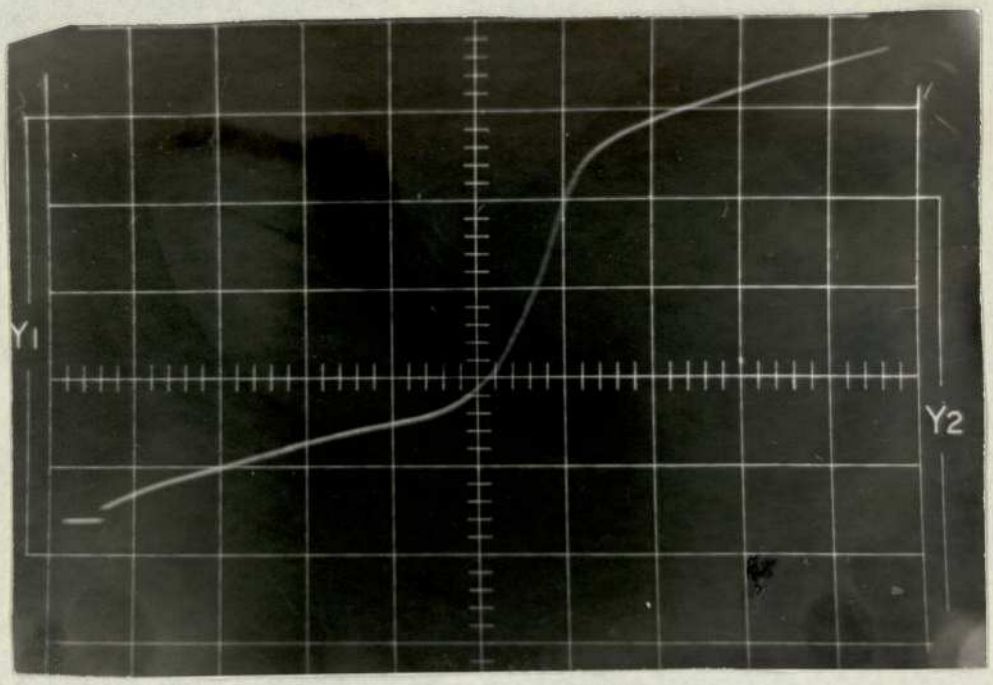
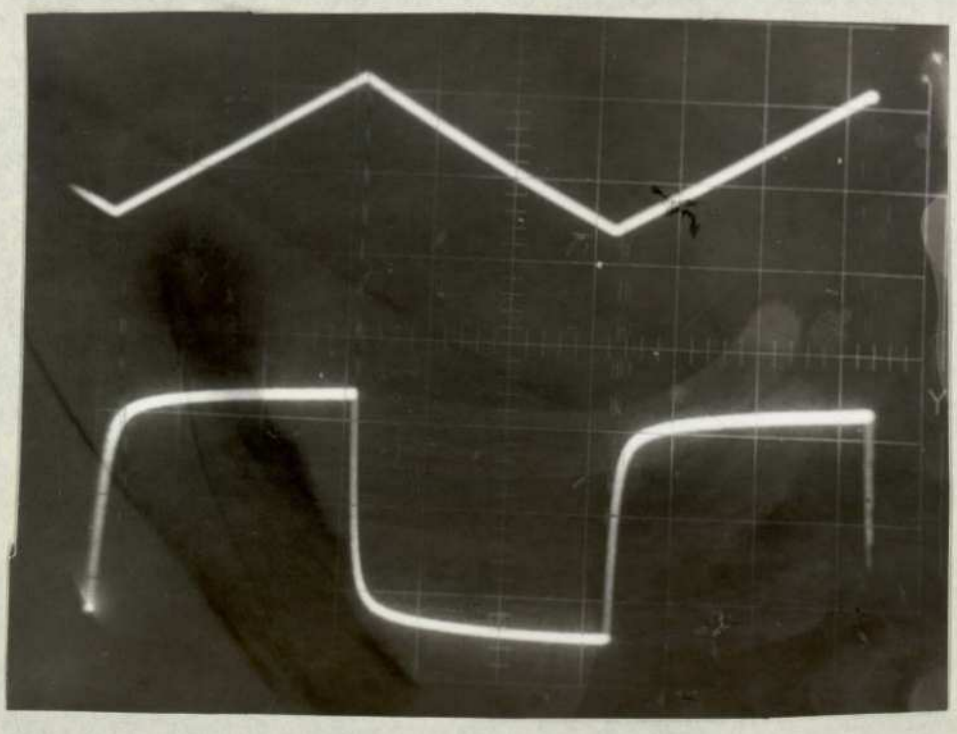


Fig. 14. Typical input and response curves for the determination of roughness factor



pressures of 0.05 and 0.25. Below 0.05 the surface contains active adsorption centres and is not homogeneous and above 0.25 the heats of adsorption of the outer layers vary markedly from the initial layers and capillary condensation occurs at $x \rightarrow I$. For nitrogen adsorption at its normal boiling point (78°K) this relative pressure range corresponds to nitrogen partial pressures of 20 - 200 torr.

The isotherm data can be obtained by two methods:

(a) the volume of gas adsorbed is measured as a function of pressure with the sample contained in a vacuum system. (I82)

(b) the weight of adsorbate is determined using a microbalance. (I83)

In this study the latter method was applied.

The gravimetric determination of the adsorbed layer is much more accurate than the volumetric method which is prone to large "dead space" errors. The error in the linearity of the B.E.T. plot in this work was greatest for samples of surface area $< 20\ m^2/g$. The estimated error in B.E.T. plot linearity for the platinum black samples is $\pm$ 20% and for the high surface area graphite sample $\pm$ 10%.

The electrochemical surface area was measured by equilibrating the electrode with hydrogen in the cell shown in Fig. 7 and then passing a constant anodic current and recording the potential - time response using an oscilloscope. The potential is approximately constant until all the hydrogen has been stripped from the electrode when the potential rises sharply through a double layer region until some other process can support the current when a potential arrestment will occur. The product of the constant anodic current and

7
1. 13. Galvanostatic Hydrogen Stripping Cell.

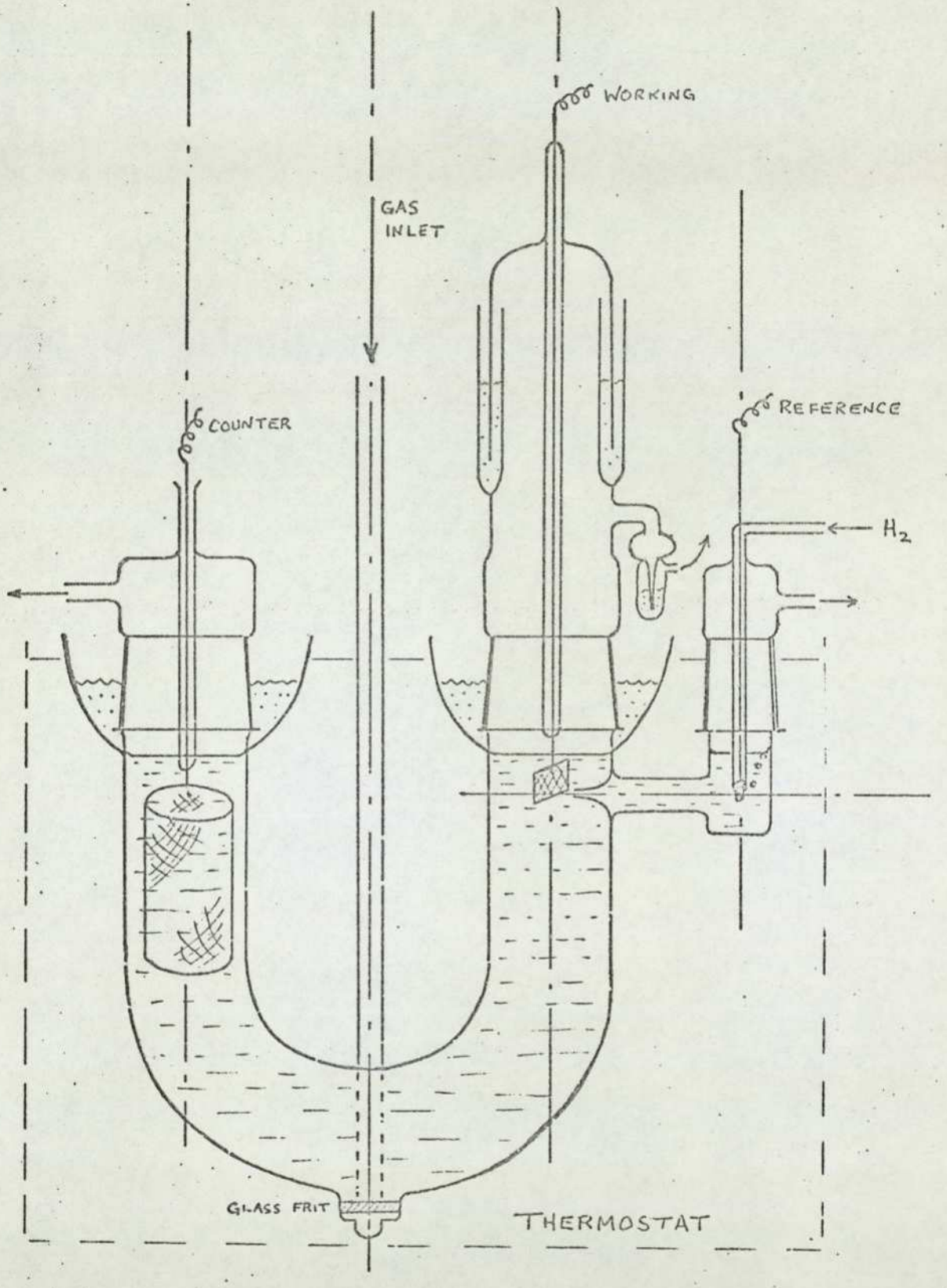
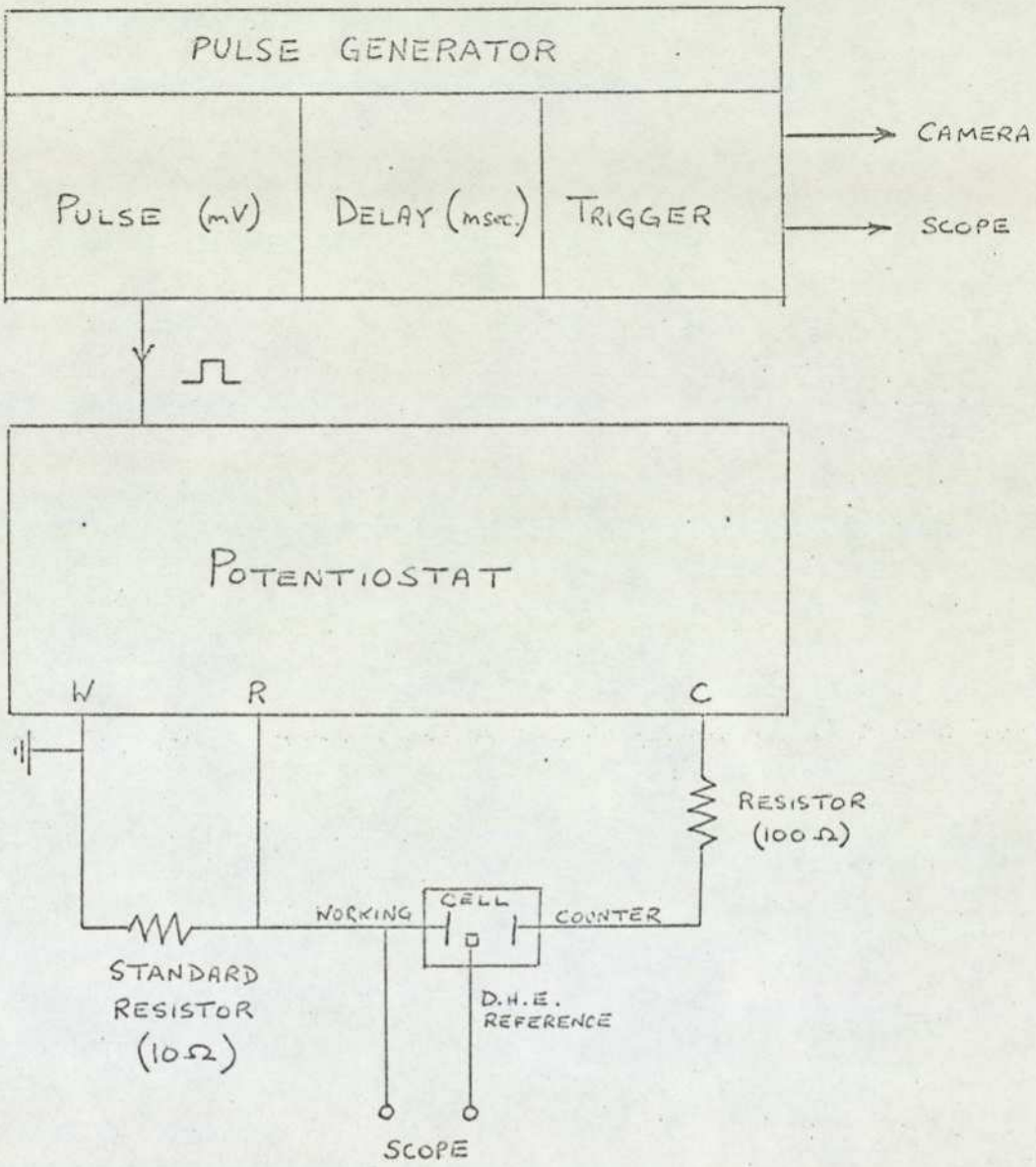


FIG. 15 SCHEMATIC CIRCUIT DIAGRAM FOR GALVANOSTATIC PULSING.



the time taken to strip the hydrogen completely gives the quantity of electricity involved. From this it is possible to determine the amount of surface hydrogen from Faraday's Law and with a knowledge of the electrocatalyst active site area ie. 8.9 A^{o2} (187) it is then possible to determine the electrochemical surface area, assuming the platinum : hydrogen ratio is I :I.

During this stripping process, hydrogen is prevented from diffusing from the bulk electrolyte to the electrode by purging with nitrogen prior to stripping, and by choosing anodic currents that result in short stripping times. The apparatus used for this process is shown in Fig. 15 and is specially designed to ensure rapid equilibration of the gas.

The possible errors are:

(a) in the oscilloscope time reading. From the start of the constant current pulse to the time when all the adsorbed hydrogen has been oxidised is not sharply defined and the resulting maximum error is ± 0.5 cm in 5 cm ie. IO%. This results in a IO% error in the charge measurement.

(b) the error in the constant current is quite small eg. ± 0.2 mA in IO mA or 2%.

(c) errors which are difficult to assess are, whether the bulk electrolyte is free from dissolved hydrogen when the constant current pulse is applied, whether the nitrogen purging has any effect on the adsorbed hydrogen, whether electrochemical flooding produces electrolyte contact with all the electrode surface.

An alternative method of determining the

electrochemical surface area is by recording a fast linear sweep and measuring the area under the hydrogen oxidation peak. The disadvantage of these methods is that they can only be used for materials which are efficient hydrogen oxidation electrocatalysts.

A typical potential - time response curve to the step galvanostatic input in a teflon bonded platinum black electrode is shown in Fig. 8 .

2.8. Determination of the Roughness Factor of Planar Electrodes.

This can be determined by double layer capacity measurements since the double layer capacity is directly proportional to the surface area. In the absence of faradaic currents the double layer capacity is given by

$$i_c = C_D \frac{dE}{dt}$$

where i_c = double layer charging current density

C_D = double layer capacity

E = potential

t = time

If a triangular wave of small peak to peak amplitude (< 100 mV) is applied to a working electrode which behaves as a pure condenser ie. without faradaic current or ohmic resistance, the current response is in the form of a square wave. The peak to peak amplitude of the square wave represents the current required for charging and discharging the double layer. This method is conveniently applied by superimposing a triangular wave on a potentiostatically controlled voltage, selected to avoid faradaic currents. This was achieved using the potentiostat and pulse generator previously mentioned

and the resulting square wave was displayed on an oscilloscope. From the double layer capacity of the electrode it is possible to estimate the surface roughness factor of the electrode, assuming the smooth surface has a capacity of I7 μF.cm^{-2}, based on the capacity measurements on smooth liquid mercury surfaces.(198)

ie. $\frac{C_D}{I7}$ = roughness factor

(I7o)

This method has a wider application than galvanostatic hydrogen stripping in that it can be used for any conducting surface subject to the following limitations:

(a) the double layer capacity is sensitive to impurities.

(b) a potential region in which no faradaic processes occur must be chosen.

(c) the ohmic resistance, r, which in any real system always exists in series with the capacitance, is small so that the time constant rC_D is small. The high values of C_D in porous electrodes limits the application of this technique to fairly low surface area electrodes.

In this investigation, a triangular wave of amplitude 50 mV and a scan rate of 2 - 6 V/sec were used, giving a triangular wave which was superimposed on a D.C. voltage of 500 mV. The cell was purged with nitrogen before taking measurements to ensure the absence of faradaic processes. The method was used to determine the roughness factor of a platinum foil electrode. The The values obtained were in the range I.5 - I.9. (See Fig. 14).

The main error in this determination is in the determination of i_c using the oscilloscope.

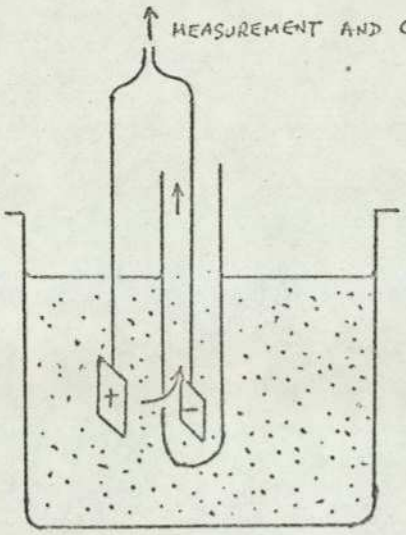
If the response curve is a close approximation to a square wave then the maximum error is ±0.4 cm in 6 cm or 7%.

2.9. Comparison of volume of oxygen produced during the passage of anodic currents and the anodic charge passed.

A gas burette is used to measure the volume of gas formed and the gas produced at the reference electrode and counter electrode escapes into the atmosphere because there is an effective gas lock between the working electrode compartment and the reference and counter electrode compartments. The charge passed was determined by plotting a current - time curve and measuring the area enclosed by it in the case of a potentiostatic study or simply from the product of time and current in the case of a galvanostatic study. Unfortunately the gas burette was not sufficiently sensitive to measure small volumes or rapid changes in volume. This could be achieved by replacing the gas burette with some thin glass tubing which could be calibrated.

2.10. Determination of the particle size distribution of an electrocatalyst using a Coulter counter. (168)

In this method the powder to be measured is dispersed in a solvent contained in the outer compartment of the apparatus shown in Fig. 9. The inner compartment is connected to the outer by means of a small orifice of known dimensions. The dispersed powder is pumped through the orifice and by monitoring the change in current flowing between the two electrodes on



THE COULTER COUNTER PRINCIPLE Fig. 9

either side, the powder may be classified according to particle size.

The change in resistance as the particle passes through the orifice is given by

$$\Delta R = \frac{\rho_o V}{A^2}\left[\frac{1}{1-(\rho_o/\rho)} - \frac{A_I}{A}\right]$$

where ρ_o = electrolyte resistivity

ρ = effective particle resistivity

V = particle volume

A = orifice area normal to axis

A_I = projected area of particle as it is orientated when passing through orifice, (projected parallel to orifice axis).

For a given sample and electrolyte all factors on the right hand side of this equation are constant with only V and A_I changing with particle size. If the particle diameter is below 30% of the orifice diameter A_I/A can be neglected. ρ_o/ρ is independent of the particular electrolyte - solid suspension tested for a given particle size and a reasonably conducting electrolyte. Hence $\Delta R \propto V$ irrespective of the material of the particle. In general this holds for porous particles, the response referring to an envelope volume of the particle.

If n is the number of pulse (ie. particles) recorded above a given threshold sensitivity (ie. possessing a minimum particle diameter) and assuming the particles are spherical and of density, δ, then

net outer surface of particles = $\sum \pi d^2 n$

net mass of particle = $\sum \frac{\pi}{6} d^3 \delta n$

where d = diameter of particle

Hence the mean aggregate specific surface area, S_{av}

$$S_{av} = \frac{6 \Sigma d^2 n}{\delta \Sigma d^3 n}$$

and the mean particle diameter, d_{av}

$$d_{av} = \frac{6}{\delta S_{av}}$$

The lower limit of particle size measurement by this technique is 0.2 micron. This method was used to determine the particle diameter of Johnson Matthey platinum black, which was shown to be less than 0.2 micron (ie. aggregate size is less than 0.2 micron). Hence this technique is only suitable for course electrocatalyst.

2.II. Determination of the electrical conductivity of a powdered electrocatalysts.

The powder was packed and pressed into a glass tube of known dimensions with two conducting metal probes. The resistance between the probes was measured with an Avo meter. (I67)

Chapter 3

3.1 The effect of O_2 evolution on the O_2 reduction performance of carbon based electrodes. 90

3.2. Reasons for electrode degradation 99

3.3. The effect of O_2 evolution on the carbon surface state 131

3.4 Alternatives to carbon electrodes for rechargeable air electrodes 140

3.5. O_2 reduction and O_2 evolution on graphite in the absense of H_2O_2 159

3.6. The effect of oxide films on the performance characteristics of rechargeable air electrodes 161

3.7 O_2 reduction on Pt-O films and the electrochemical reduction of Pt-O films. 170

3.8. The effect of surface oxides on the O_2 evolution reaction on platinum 191

3.9 The strength of porous materials 218

Chapter 3

The Effect of Gas Evolution on the Electrode Structure and Surface State of Carbon and Platinum Electrodes.

3,I.I. Introduction.

3.I.1. The effect of oxygen evolution on the oxygen reduction performance of carbon based electrodes.

Graphite or carbon is a material widely used for electrodes as it is quite a good electrical conductor, is cheap, and is generally chemically inert. However, it is known to corrode under certain conditions, notably in its most common application, the anodic electrolytic production of chlorine and chlorates. It has been shown that a graphite anode evolving chlorine from a chloride solution is slowly oxidised to CO and CO_2 [101,102] thus causing a change in the characteristics of the electrode comprising a change in nature of the graphite surface and an increase in surface area. Various explanations have been given for this corrosion:

(I) the chemical action of active oxygen formed at the anode during electrolysis, [102] and the action of oxygen containing oxidising agents such as hypochlorous acid. [103] As a result the individual graphite grains become separated from one another and crumble away leading to mechanical destruction of the anode.

(2) the degree of graphitization of the carbon eg. artificial graphite electrodes are more wear resistant than charcoal electrodes. [100,107]

(3) the destruction rate is increased by increase in temperature, decrease in electrolyte concentration,

increase in pH, and is more severe in chlorate production than in chlorine production, (104,108) possibly due to a higher hypochlorous acid concentration. (105)

This destruction is not limited to the outer layer of the electrode but may permeate deeply into it causing internal losses (up to 40% of the total loss.) (103) This is suprising since the current density falls rapidly with distance from the surface (pore entrance) and should be low in the interior of the electrode. Investigations into the causes of this internal wear have suggested that it is due to chemical attack by hypochlorous acid. (105) More recent work on this phenomenom suggests that the destruction is due to unstable graphite surface oxides, formed on oxygen evolution in alkaline or neutral solutions, decomposing to give CO_2, (102) and not to hypochlorous acid which has been shown to be absent. (104) In acid solutions no oxygen is evolved and the wear is only slight. (102) Electrode wear is greater in chlorate baths than in chlorine baths, since the sodium chloride concentration is lower in the former case both at the electrode exterior and interior resulting in an increase in oxygen evolution. (104) The presence of chromate ions in chlorate cells has been shown to increase the electrode wear. (106) Studies of chlorine evolution in saturated brine show that in electrodes made of graphite powder and pitch binder, the latter is the more severely corroded causing graphite loss. (100) In aqueous chloride solutions, anodic polarisation can cause both oxygen and chlorine evolution. At high

overpotentials mainly chlorine is evolved, at lower overpotentials near the Cl_2/Cl^- reversible couple potential, more oxygen is evolved. In porous electrodes the potential at the surface is much greater than the potential in the interior, hence chlorine is evolved on the surface and oxygen in the interior ie. oxygen causes electrode damage and an increase in surface area which accentuates the problem. (108)

No work appears to have been published on related phenomena for the oxygen evolution reaction on graphite electrodes in alkaline solutions. Oxygen evolution in acid solutions causes degradation due to the formation of graphite intercalation compounds. (100) Internal wear is an important feature of the behaviour of graphite anodes as it causes an increase in their specific electrical resistance resulting in an increase in consumption of graphite and electrical energy.

Ifthe graphite surface oxide mechanism is correct then degradation of graphite electrodes would be expected to occur on oxygen evolution from aqueous solutions containing no chloride ions. If corrosion of the chlorine electrode is due chiefly to chemical attack by hypochlorous acid then the oxygen evolution electrode should not be significantly degraded. Statements that graphite is attacked by nascent oxygen during oxygen evolution do exist in the literature, (112) but no experimental data is given.

In this investigation potassium hydroxide solutions are used since this electrolyte is widely used in metal-air batteries and in some fuel cells,

and also because graphite is chemically unstable in strongly acid solutions. For fuel cell and metal-air battery applications it is necessary for the electrode to be very thin ($\sim$2mm), whereas in electrolysis cells graphite electrodes of substantial thickness are used ($\sim$ I5cm). Hence structural damage to such a thin electrode would be far more serious in that the electrode life would be very short. In the thick electrodes only the surface region ($\sim$ 5mm) is being effectively used at any time and as this region is destroyed fresh electrode is exposed; hence by using sufficiently thick electrodes a substantial life can be obtained. This, however, does not solve the problem for fuel cells and batteries where the weight and volume of the cell are of major importance, and where it is necessary to use closely spaced electrodes to reduce the cell iR drop. It is also reported (II2) that platinum is the only metal which can survive alternating use as an anode for oxygen evolution and a cathode for oxygen reduction. The silver-graphite electrodes which are used as cathodes in modern fuel cells are oxidised to carbon dioxide and silver oxide which dissolves in the electrolyte, when used as anodes. Hence an alternative solution must be found. It is possible to design a cell with three electrodes, one reversible hydrogen electrode and two oxygen electrodes (one for dissolution and one for evolution.) One of the advantages of such a rechargeable H_2-O_2 cell is that the hydrogen and oxygen formed during recharging can be used

in the discharge stage.(109) This process has been used before in the form of a regenerative fuel cell which uses two seperate cells to effect the recharge. This, however, was not developed on a commercial basis since the efficiency of the electrolysis cycle was less than 50%.(110,111) The three electrode cell provides a definite improvement on the two electrode regenerative cell, but even so, systems which necessitate gas storage are by nature bulky, hence limiting these cells to non mobile applications. In these three electrode storage cells(112-4) the oxygen evolution electrode is chosen to have a low over-potential eg. nickel, and a high resistance to corrosion in the porous state. The overall efficiency of such a system is comparable with that of a hydro-electric storage plant, lead-acid and alkaline storage batteries.(112) Although this type of gas storage cell is not suitable for mobile applications, since it would introduce prohibitive increases in weight and volume, it is very suitable for stationary plants since its storage capacity can be increased stepwise by adding more hydrogen and oxygen containers. For mobile applications it would be desirable if a system, not involving gas storage, could be developed. The metal-air cells fulfill this objective but at present problems exist at both electrodes during recharging. As three electrode cells are unsuitable and electrode and electrolyte replacement expensive,(20) rechargeable air electrodes must be sought.

3.I.2. Experimental.

Potentiostatic, steady state, oxygen reduction

current-voltage curves were plotted before and after galvanostatic, anodic oxygen evolution treatment at various currents, for various times, at 22°C, in 5N potassium hydroxide, using an air atmosphere. The electrode used was a silver-graphite (Acheson) teflon bonded electrode.

3.I.3 Results and Discussion.

It was observed that the current increased slowly with time when the electrode was first placed in the electrolyte, however a steady value was reached after about two hours if the electrode was held at about 850 mV. This suggests that the electrolyte permeates the pores slowly, taking some time to achieve a stable interface, probably because graphite has a hydrophobic surface. It is necessary to study this ageing effect in order to interpret the results correctly.

Graphs I and 2 show the effect of galvanostatic, anodic pretreatment, at current densities up to 40 $mA.cm^{-2}$, on the oxygen reduction polarisation curve. Electrode damage occured at anodic current densities greater than I3$mA.cm^{-2}$. Graph 2 shows the effect of potentiostatically holding the electrode at a potential slightly anodic to the reversible oxygen electrode potential for a long time, on the oxygen reduction polarisation curve. In this test only very small currents passed and electrode damage was not visible. The oxygen reduction polarisation curves have been corrected for the small iR drop between the working electrode and the Luggin capillary using the

GraphI.

The effect of anodic pretreatment on the oxygen reduction perfomance of a teflon bonded silver - graphite electrode.

Electrolyte 5N KOH

Atmosphere Air

Pressure I atmosphere

Temperature 22°C

O.C.V. I.OI V

Electrocatalyst silver on Acheson graphite

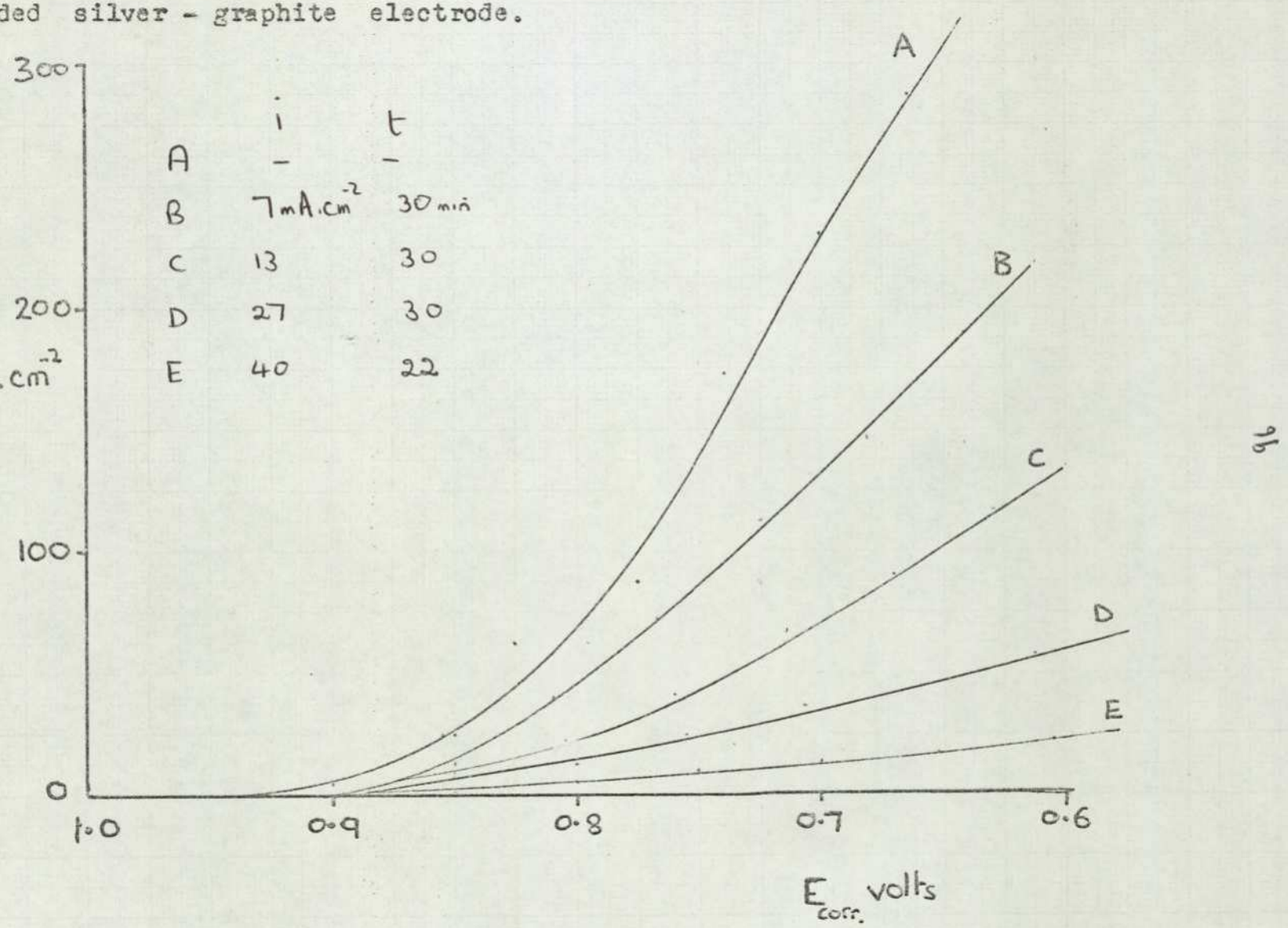
Current collector nickel screen

Electrocatalyst loading

9 mg.cm^{-2}

Electrocatalyst S.A.

510 m^2/g



Graph 2.

Oxygen reduction performance of a teflon bonded silver graphite electrode before and after anodic pretreatment in which no oxygen was evolved.

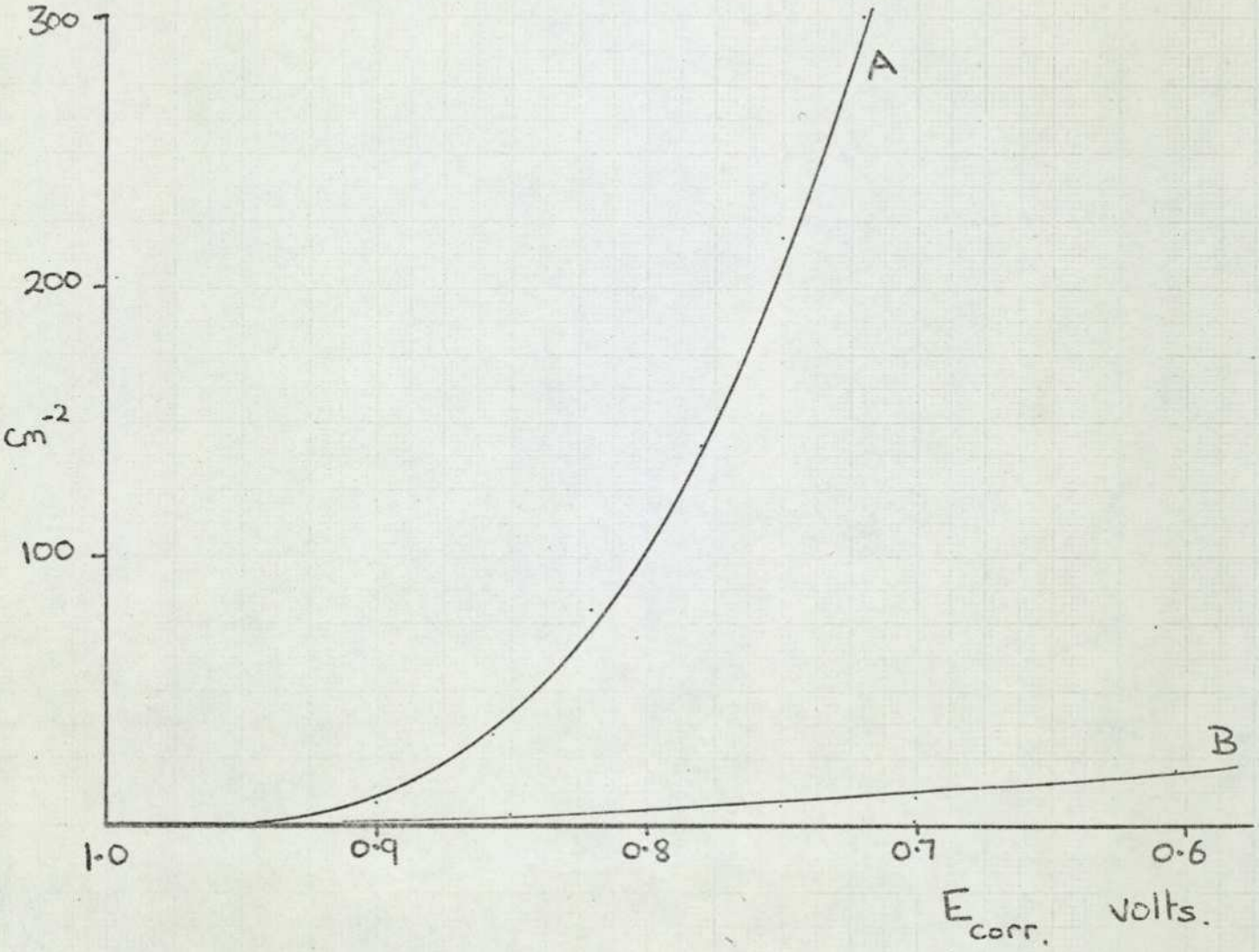
Electrolyte 5N KOH

Atmosphere air
Pressure I atmos.
Temperature 21°C
O.C.V. I.0I V
Electrocatalyst silver on graphite
Current collector nickel screen
Loading II mg.cm^{-2}
Electrocatalyst S.A. 5I0 m^2/g

Anodic pretreatment

A - none

B - I.40 V for I9.5 hours
(i= 2.4 - 0.6 mA.cm^{-2})



67

interupter technique. As the iR correction is small, it will be used in the following text only where it is essential to the comprehension of the results.

These experiments show that the oxygen reduction performance is reduced substantially by anodic current densities as low as 7.5 $mA.cm^{-2}$ applied for thirty minutes. The reduction in performance is 40% at 800 mV, 61% at 900 mV, and 35% at 700 mV. For subsequent periods of anodic pretreatment, the oxygen reduction current continued to fall eg. anodic pretreatment of 15 $mA.cm^{-2}$ for thirty minutes caused the oxygen reduction current to fall by a further 40%. At the end of the galvanostatic anodic pretreatments the oxygen reduction current was only 8% of its original value at 800 mV. Visible electrode degradation was observed during this sequence, in the form of electrocatalyst falling off the current collector to the bottom of the cell.

Potentiostatic, anodic pretreatment at I.40 V for 19.5 hours, at currents in the range 2 $mA.cm^{-2}$ to 0.05 $mA.cm^{-2}$ resulted in a fall of 94% in the oxygen reduction current at 800 mV although there was no visible damage. These experiments show that the greater the anodic current the greater the visible electrode degradation and that below a certain anodic current no visible damage occurs, although the oxygen reduction performance is reduced. These results show that oxygen evolution causes electrode degradation which severely reduces the oxygen reduction performance of the electrode. The reasons for this are not definitely known at present.

For instance, it might be caused by oxidation of the graphite to carbon dioxide, or by the formation of solid graphitic oxides, or by mechanical rupture due to high oxygen pressures in the graphite pores. The fact that the oxygen reduction performance falls when no visible damage is observed does not rule out any of these possibilities, since even at low current densities mechanical pore rupture could be occuring within the electrode, resulting in disruption of the critical teflon bonded electrode structure, without visible signs of damage. The fact that the oxygen reduction performance after anodic pretreatment, recovered partially on the passage of high cathodic currents, ($100\ mA.cm^{-2}$) and that the anodic current at a given potential fell rapidly with time (see Table 3) suggests the possibility of some form of graphite oxidation.

The drastic fall in oxygen reduction performance, after potentiostatic treatment at I.40 V for I9.5 hours, was not caused by the electrode flooding. This was shown by running a blank, without the anodic pretreatment, but left in contact with the electrolyte for 24 hours.

Brief tests on solid graphite plate electrodes show that these are also degraded by oxygen evolution, although not so rapidly, presumably because of their relatively low porosity.

3.2 Possible reasons for electrode degradation.

3.2.I Introduction.

These are:

(I) oxidation of graphite to CO and CO_2

Table 3.

The decay of anodic currents from a teflon bonded silver-graphite electrode held at constant potentials.

I.35 V		I.50 V		I.65 V	
$mA.cm^{-2}$	t	$mA.cm^{-2}$	t	$mA.cm^{-2}$	t
I00	2 secs	I00	2 secs	I08	2 secs
7.5	30 secs	I0	30 secs	38	30 secs
5.2	I min	6.7	I min	36	I min
3.3	2	5.I	2	34	2
2.5	3	4.I	4	34	3
2.I	4	3.6	6	33	4
I.6	6	3.4	8	3I	5
0.90	25	3.3	I0	23	I05
0.82	30	3.I	I2		

Electrolyte	5N potassium hydroxide
Atmosphere	Air
Pressure	I atmosphere
Temperature	20°C
O.C.V.	I.0I V
Electrocatalyst	silver on graphite
Current collector	nickel screen
Loading	II $mg.cm^{-2}$
Electrocatalyst S.A.	5I0 m^2/g
Ohmic resistance per. cm^2.	0.20 ohm

(2) oxidation of graphite to solid graphitic oxides;
(3) disruption of the teflon bonded structure due to high gas pressures within the porous electrode;
(4) evolution of gases from the current collector.

(I) When carbon is in contact with oxygen physical and chemisorption (II6) may be detected. Physically adsorbed oxygen can be desorbed under vacuum but chemisorbed oxygen cannot. (II7) When a sample of chemisorbed oxygen on carbon is heated, oxygen is not detected but CO and CO_2 are, indicating thermal breakdown of the chemisorbed oxygen layer. (II6) The presence of surface carbon-oxygen complexes is well known (II8,II9) and the mechanism for the combustion of carbon involves these complexes. (I20) These surface carbon-oxygen complexes have been reported to play a major part in the electrochemical combustion of carbon. (I04) The formation of oxide complexes as intermediates in the electrochemical combustion of carbon to CO and CO_2, in chloride solutions, has been reported. (I02) Very little work has been done on the electrolytic combustion of carbon in aqueous solutions containing no chloride ions.

It is proposed to investigate this possibility by analysing the electrolyte and the atmosphere for CO_2 after holding the electrode in an anodic region.

(2) Graphitic oxides are formed by the action of oxidising mixtures on graphite. (I2I) Pyrolysis of graphitic oxide produces CO, CO_2 and O_2, although with slow decomposition rates no oxygen was observed. (I22) Surface layers of graphitic oxide have been reported

on graphite surfaces held in an anodic region,[102] but it is not known whether subsequent electrode degradation is due to the formation of this oxide or its decomposition to CO and CO_2. Although the latter seems more feasible, the formation of graphitic oxide could alter the activity of the electrode surface for the oxygen reduction process. Investigations at low anodic currents, at which no electrode damage is observed, should help to elucidate this point. Graphitic oxide has been shown to be a non-conductor of electricity.[123]

(3) It is proposed to investigate this possibility by hydrogen evolution studies, since this should eliminate the possibility of degradation caused byoxidation effects. The hydrogen evolution reaction on carbon has only been studied in bisulphate melts.[124]

(4) This point can be investigated by using different current collectors, preferably those which do not evolve gas to a significant extent in the potential range of the experiment.

3.2.2 Experimental.

(a) The electrolyte (5N KOH) was tested for the presence of carbonate ions after evolving gas at an anodic potential (2.0V) for a given time. This was compared with the carbonate content of another sample of electrolyte which was exposed to the atmosphere for the same length of time under the same conditions but no electrolysis was carried out. This test should give a clear indication as to whether or not carbon dioxide is formed during electrolysis.

(b) The gas produced when a similar electrolysis

was carried out under an inert atmosphere eg. nitrogen, was tested for the presence of oxygen. It has been reported that under certain conditions carbon dioxide is the chief product with only traces of oxygen formed. This simple qualitative test should elucidate this point.

(c) A constant anodic current was passed for a given time and the volume of gas formed was measured using a gas burette. This volume can be compared with the theoretical volume for oxygen evolution under the prevailing conditions. If carbon dioxide were formed this would dissolve in the electrolyte resulting in a smaller volume.

(d) The electrode was held potentiostatically at potentials between I.26-I.36 V where no gas evolution or visible degradation are observed. Steady state and transient measurements on the oxygen reduction polarisation curve can then distinguish between whether the catalytic surface has been changed or whether the electrode structure has been damaged.

(e) Oxygen evolution studies of other electrocatalysts on the same current collector show whether gas evolution from the current collector is important. Aconfirmatory test was carried out by evolving oxygen on current collectors which are poor oxygen evolution electrocatalysts.

These tests (a-e) have been carried out using both teflon bonded graphite electrodes and teflon bonded silver-graphite electrodes.

(f) If the electrode degradation is due to oxidation effects hydrogen evolution should not cause similar effects. If the damage is due to mechanical weakness in the porous structure or to weak binding to the current collector, hydrogen evolution would be expected to cause similar damage. A platinised graphite electrode was held at potentials at which hydrogen evolution occurred and then the hydrogen oxidation polarisation curve recorded in a hydrogen atmosphere was compared with the curve obtained before hydrogen evolution. Nickel screen and graphite cloth were used as current collectors. Hydrogen evolution on plain graphite was not easy as it is associated with a high overpotential.

3.2.3. Results.

(a) Analysis of 5N potassium hydroxide electrolyte for the presence of carbonate ions.

A current of 100 $mA.cm^{-2}$ was passed through the test electrode for four hours. The blank was placed in a similar cell adjacent to the test electrode system. Both electrolyte solutions were treated with excess dilute hydrochloric acid and any gases formed passed over anhydrous calcium sulphate to absorb water vapour and then over soda lime to absorb carbon dioxide. The soda lime was weighed before and after adding the hydrochloric acid.

Blank	Test	
0.1610g	0.1632g	increase in weight of soda lime.
0.00	0.1640g	theoretical increase in weight if all the oxygen

produced by the current was converted to carbon dioxide and the electrolyte was previously free of carbonate ions.

Solubility of carbon dioxide in 100 ccs. of water at 21°C is 0.164g.

Weight of carbon dioxide calculated from the weight of oxygen formed, by Faraday's Law, Converted to carbon dioxide

$$C + O_2 = CO_2$$

(b) Qualitative test for the electrolytic formation of oxygen and carbon monoxide.

Anodic currents were passed in a nitrogen atmosphere and the gas collected in a microburette over pyrogallol solution. Although gas was clearly seen to form no increase in volume was detected indicating that the gas is oxygen, which is absorbed by the pyrogallol. The gas evolved on anodic polarisation did not contain enough carbon monoxide to register on a 10-300 p.p.m. Drager tube.

(c) Quantitative test for the volume of oxygen produced.

A constant anodic current of 25 $mA.cm^{-2}$ was applied to the electrode and the volume, pressure and temperature of the gas produced, measured after given times. The volume of gas corrected to S.T.P. was the same as that predicted for oxygen evolution by Faraday's Law. If any carbon dioxide had been formed it would have dissolved in the alkaline electrolyte and the volume of gas collected in the gas burette would be less than predicted.

eg. w

eg. when $i = 100\ mA.cm^{-2}$ is passed for I hour the volume of oxygen that should, theoretically, be produced (Faraday's Law) at S.T.P. = 20.9 ml. The volume of gas actually collected, (22.0 ml at 20 C and 750 mm) corrected to S.T.P. was found to be 20.7 ml.

(d) The effect of oxygen evolution at very low rates.

When graphite or silver-graphite teflon bonded electrodes are held at potentials between I.26 and I.36 V no gas is observed to form even though small anodic currents pass. Using the gas burette attached to the cell and holding the electrode in this potential range for periods up to 24 hours confirmed that no gases were produced. After this pretreatment the steady state and transient oxygen reduction polarisation curves were recorded and compared with similar curves before anodic treatment. (See graphs 2 and 3.) No visible damage to the electrode occured during the anodic pretreatment.

(e) Oxygen evolution at comparable potentials and current densities on platinum black using nickel and platinum screen as current collectors, hydrogen evolution on platinised tungsten trioxide using platinum screen as current collector and oxygen evolution on cobalt nickel oxide on nickel screen as current collector have not resulted in damage to the electrode (see 3.4).

Graphs 4 and5 show the oxygen evolution polarisation curves for three current collectors ie. nickel and platinum screen and graphite cloth. Using these results it is possible to determine what proportion of the oxygen evolution current of teflon

Graph 3.

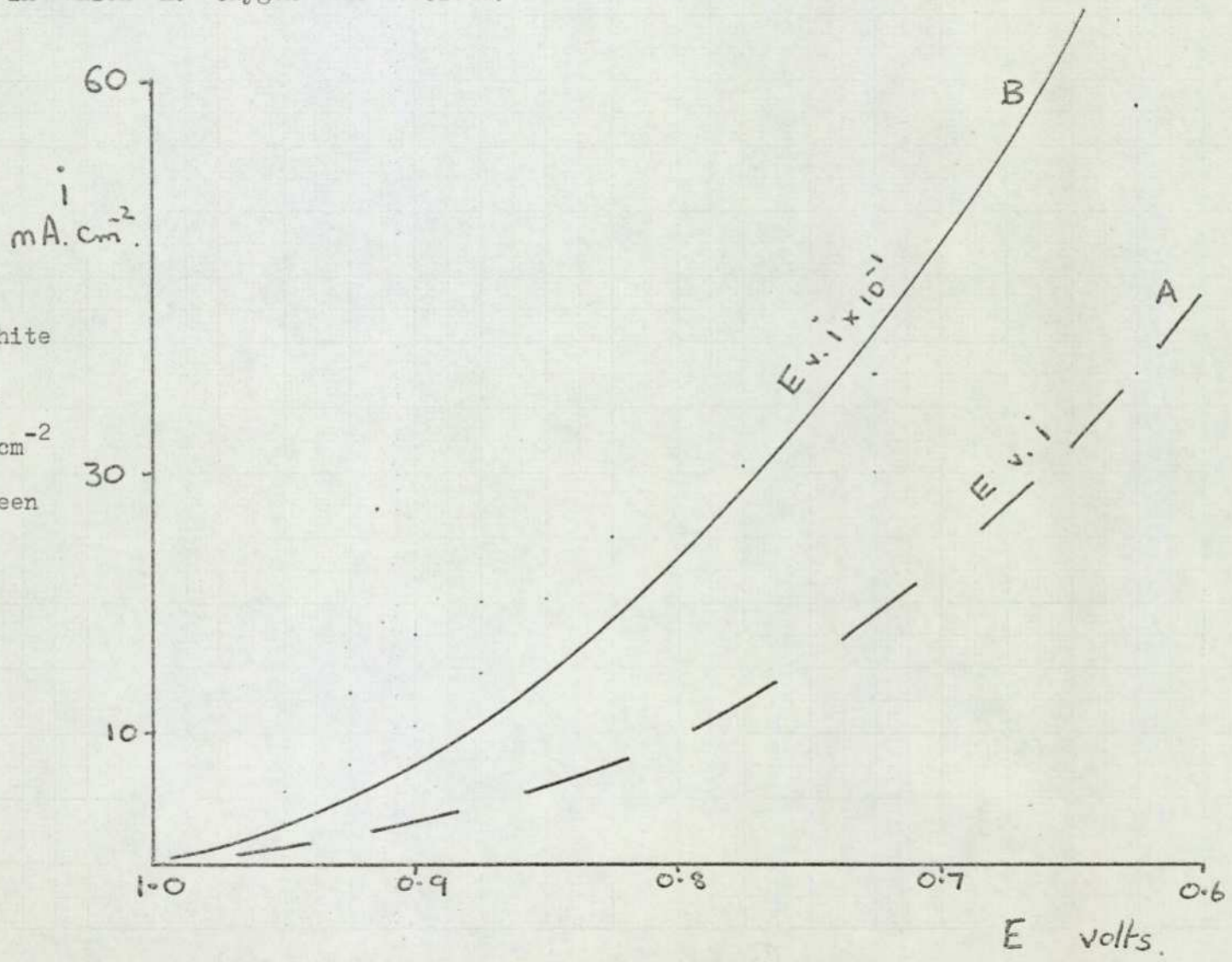
Transient oxygen reduction performance of a teflon bonded silver graphite electrode before and after anodic pretreatment in which no oxygen was evolved.

Electrolyte	5N KOH
Atmosphere	air
Pressure	I atmos.
Temperature	22°C
O.C.V.	I.02 V
Electrocatalyst	silver on graphite
Electrocatalyst S.A.	5I0 m^2/g
Electrocatalyst loading	II $mg.cm^{-2}$
Current collector	nickel screen
Time	I msec.

Anodic pretreatment

A - none

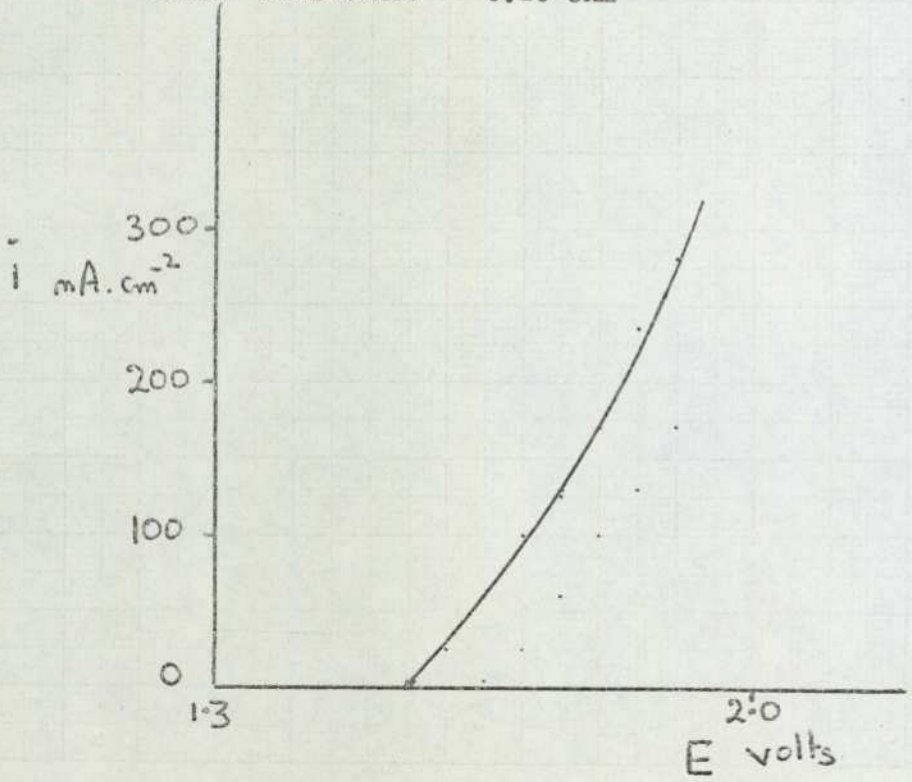
B - I.40 V for I9.5 hours
(i = 2.4 - 0.6 $mA.cm^{-2}$)



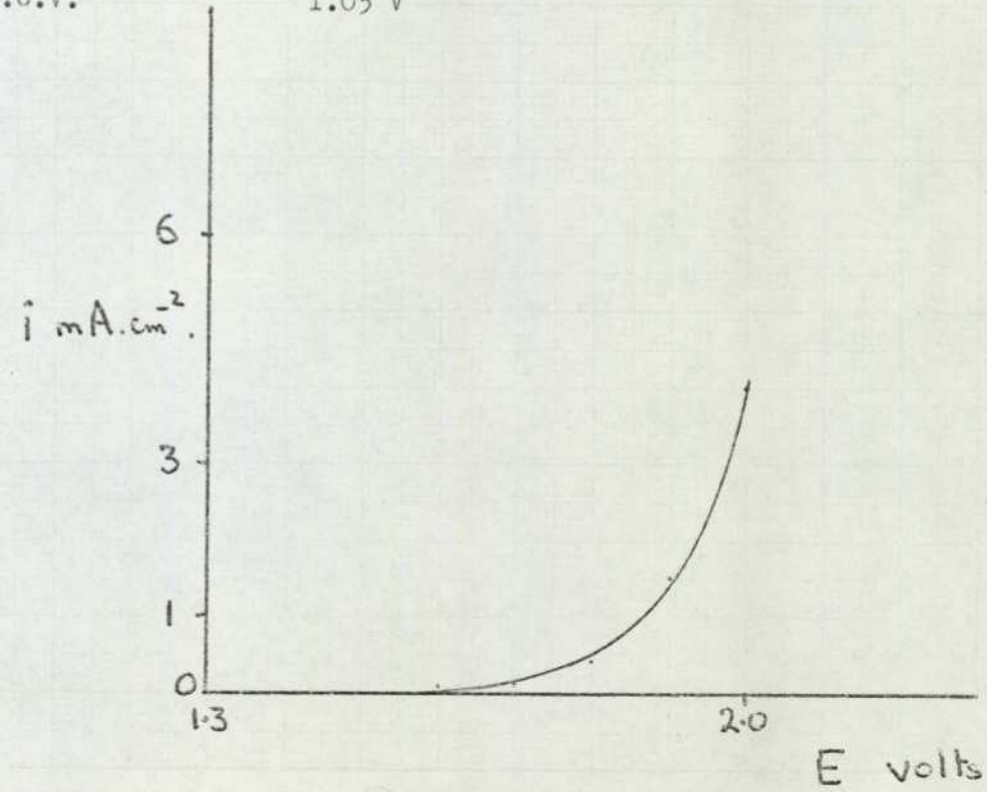
Graph 4.

Steady state oxygen evolution performance on nickel and platinum current collectors.

Electrolyte	5N KOH
Atmosphere	air at I atmosphere
Temperature	2I°C
Electrocatalyst	nickel screen
O.C.V.	0.99 V
Ohmic resistance	0.20 ohm



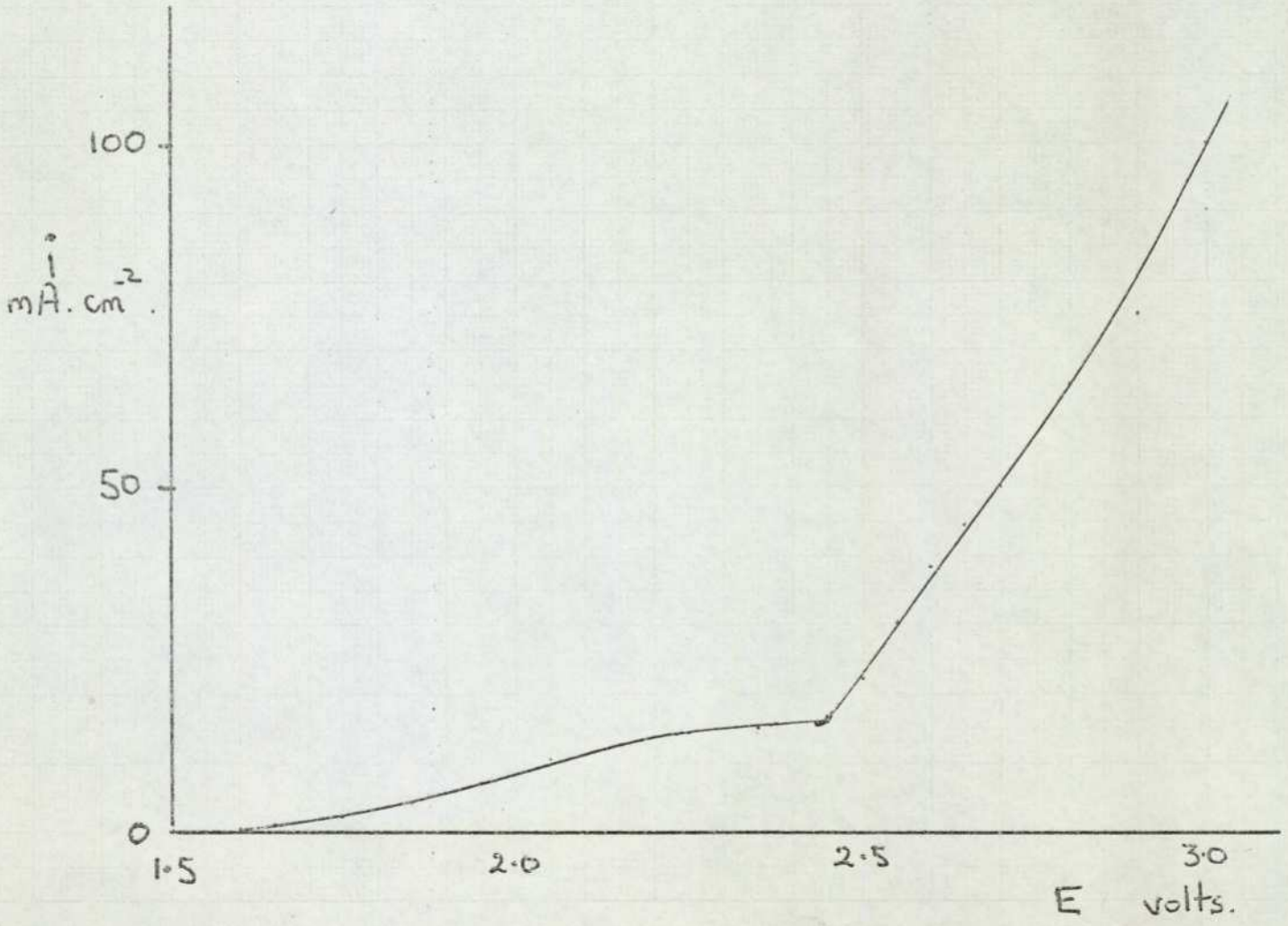
Electrocatalyst	platinum screen
Ohmic resistance	0.I5 ohm
O.C.V.	I.03 V



Graph 5.

Oxygen evolution performance on graphite cloth current collector.

Electrolyte	5N KOH
Atmosphere	oxygen
Pressure	I atmos.
Temperature	22°C
O.C.V.	I.0 V
Electrocatalyst	graphite cloth
Ohmic resistance	0.43 ohm



bonded electrodes can be attributed to the electro-catalyst and what proportion to the current collector.

(f) Graph 6 shows a hydrogen evolution polarisation curve for a teflon bonded graphite electrode on a graphite cloth current collector. Hydrogen gas bubbles were first observed at a current density of 4.3 $mA.cm^{-2}$ at a potential of -250 mV and electrode damage in the form of graphite falling off the electrode was observed at 33 $mA.cm^{-2}$ and -475 mV. This electrode was not active for hydrogen oxidation in a hydrogen atmosphere, hence the effect of hydrogen evolution on the hydrogen oxidation performance could not be measured. Consequently a teflon bonded, platinised graphite electrode using graphite cloth as a current collector was employed. This electrode was held for fixed times at potentials at which hydrogen evolution occurred. After each hydrogen evolution pretreatment the steady state hydrogen oxidation polarisation curve was measured and compared with a similar curve measured before any pretreatment (Tables 4 and 5). This experiment was repeated using nickel screen as the current collector. The steady state polarisation data for hydrogen evolution on the graphite cloth current collector are shown in graph 7. The graphite cloth was not observed to be physically damaged by hydrogen evolution, although it was not possible to test this by the hydrogen oxidation reaction since graphite is non active for this reaction. The steady state polarisation data for hydrogen evolution on nickel screen are given in graph 8. With gas evolution studies, steady state polarisation curves are best obtained by a controlled linear

Graph 6.

Steady state hydrogen evolution polarisation curve for teflon bonded graphite on graphite cloth.

Electrolyte	5N KOH
Atmosphere	hydrogen
Pressure	I atmos.
Temperature	22 C
O.C.V.	-0.I8 V
Electrocatalyst	graphite
Loading	I2 mg.cm^{-2}
Electrocatalyst S.A.	500 m^2/g
Ohmic resistance	0.35 ohm

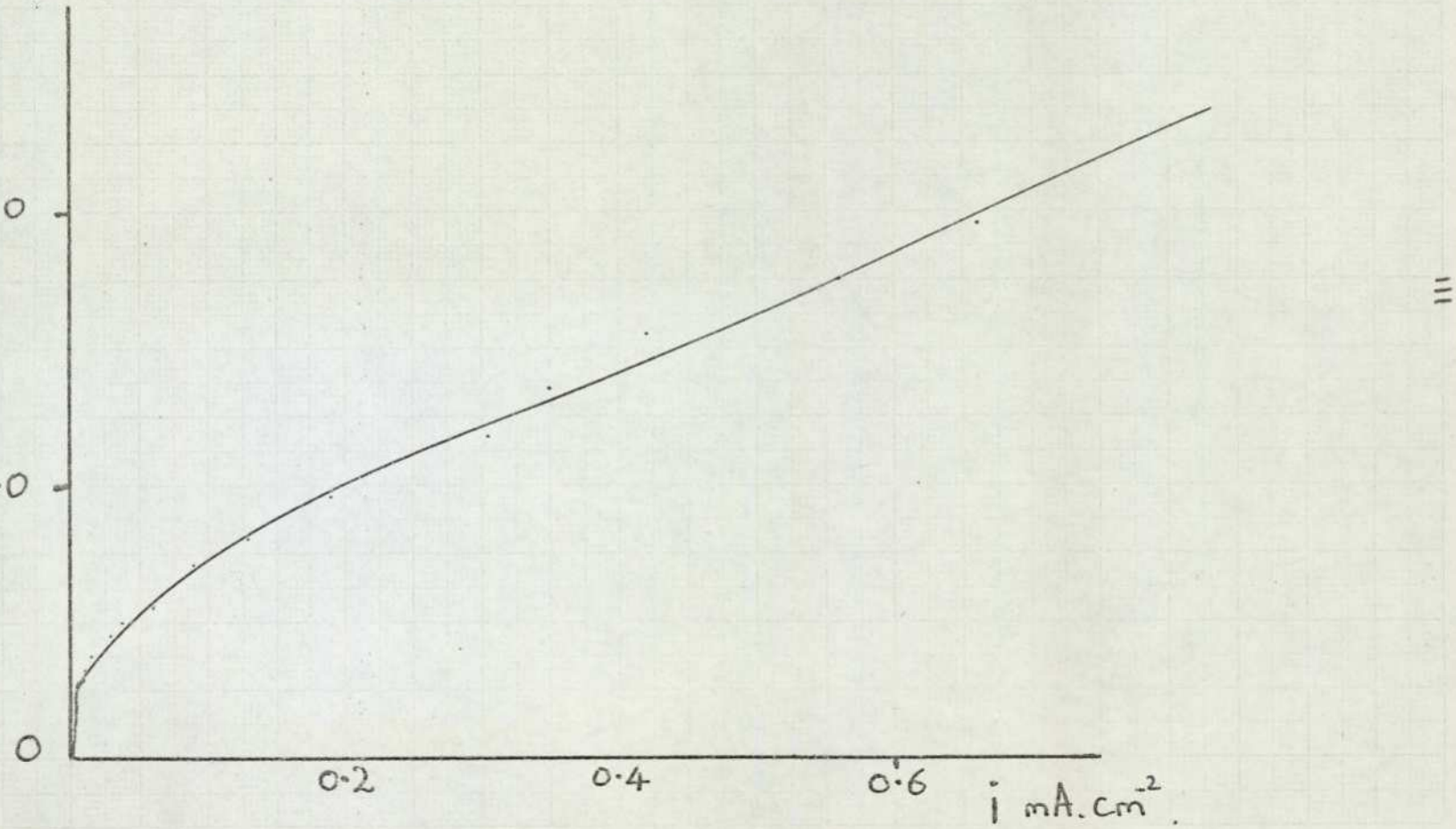


Table 4.

The effect of hydrogen evolution pretreatments on the steady state hydrogen oxidation polarisation data for a teflon bonded platinised graphite electrode.

E (mV)	i (mA)										
	A	B	C	D	E	F	G	H	I	J	K
+80	2.8	2.8	2.8	2.9	2.9	3.0	3.3	3.I	3.3	3.4	3.4
90	5.4	5.6	5.5	5.6	5.5	5.9	6.0	6.0	6.I	5.9	6.0
I25	I5	I5	I5	I5	I5	I5	I6	I5	I6	I5	I6
200	36	36	36	35	36	36	36	36	36	36	36
300	64	63	63	63	63	64	64	64	64	63	63

	i (mA)								
	L	M	N	O	P	Q	R	S	T
80	3.3	3.4	3.4	2.I	2.7	2.0	I.6	I.2	I.0
90	5.9	6.I	5.8	4.5	4.5	3.7	3.0	2.5	2.3
I25	I6	I5	I5	I3	I2	9.0	7.0	6.5	4.9
200	36	36	33	3I	30	25	I7	I5	I2
300	63	62	58	56	55	47	32	27	22

Electrolyte	5N potassium hydroxide
Atmosphere	Hydrogen at I atmosphere
Temperature	22 C
O.C.V.	+0.070 V
Electrocatalyst	platinised graphite
Electrocatalyst loading	I3 mg.cm^{-2}
Electrocatalyst S.A.	500 m^2/g
Current collector	graphite cloth
Ohmic resistance	0.30 ohm
Electrode area	2.0 cm^2

Key to table 4.

	Mean cathodic current(mA)	Potential (mV)	Time	Observations
A	-	-	-	No pretreatment
B	2.2	+6I.5	45 secs	
C	8.0	+4I	45	
D	I9	+I.6	45	
E	28	-3I	45	
F	40	-76	45	
G	60	-I50	45	
H	90	-250	45	
I	I30	-400	45	
J	I85	-600	45	Visible destruction first observed.
K	200	-600	6.5 min	
L	230	-750	I	
M	295	-I000	IO	
N	400	-I550	IO	
O	80	-250	60	
P	I60	-600	30	
Q	390	-I575	I3	
R	350	-I575	26	
S	325	-I575	45	
T	305	-I575	80	Electrode fully submerged in electrolyte.

Table 5.

The effect of hydrogen evolution pretreatments on the steady state hydrogen oxidation polarisation data for a teflon bonded platinised graphite electrode.

E (mV)	i ($mA.cm^{-2}$)										
	A	B	C	D	E	F	G	H	I	J	K
35	3.2	2.I	3.7	3.I	3.8	4.2	5.0	5.0	-	-	-
40	I0.0	8.6	I0.0	9.0	9.7	9.2	I0.0	I0.3	I.2	I.0	0.73
45	-	-	-	-	-	-	-	-	2.3	I.9	I.5
50	23	22	22	22	2I	2I	20	20	3.5	2.7	2.2
60	-	-	-	-	-	-	-	-	6.0	4.4	3.7
70	48	48	47	47	45	42	40	37	8.0	6.I	5.I
I00	86	85	82	82	80	74	70	62	I5	II	9.3
I50	I50	I49	I40	-	-	-	-	-	26	I9	I6
200	202	20I	I96	I93	I89	I77	I63	I45	38	27	23
300	320	3I9	308	303	296	282	262	229	62	45	37
400	425	425	425	425	4I2	395	364	308	85	6I	50
550	570	570	570	565	560	530	490	425	I25	89	72

	i ($mA.cm^{-2}$)		
	L	M	N
40	-	0.66	0.46
45	-	I.2	0.97
50	-	I.7	I.5
60	3.6	2.6	-
70	4.8	3.6	2.8
I00	8.6	5.7	4.4
I50	I4	8.5	-
200	I9	II.0	8.4
300	28	I5	I2
400	36	I9	I5
550	49	26	20

Key to table 5.

	Mean cathodic current density ($mA.cm^{-2}$)	Time	Potential (mV)	Observations
A	-	-	-	-
B	5	I5 min	+25	
C	7.3	IO	+23	
D	I5	5	+I4	
E	33	5	+9	Very slight degradation
F	62	5	-I6	Degradation
G	93	32	-40	Degradation
H	II6	40	-80	Degradation
I	260	30	-I80	Rapid degradation
J	44	IO	-I50	Degradation
K	53	IO	-2IO	Degradation
L	I40	I4	-350	Rapid degradation
M	400	IO	-500	Rapid degradation
N	870	7	-750	Rapid degradation

Electrolyte	5N potassium hydroxide
O.C.V.	+0.026 V
Electrocatalyst loading	7 $mg.cm^{-2}$
Current collector	nickel screen
Ohmic resistance	0.IO ohm
Atmosphere	hydrogen at I atmosphere
Temperature	22°C
Electrocatalyst S.A.	500 m^2/g

Graph 7.

Steady state hydrogen evolution polarisation curve on graphite cloth.

Electrolyte 5N KOH

Atmosphere hydrogen

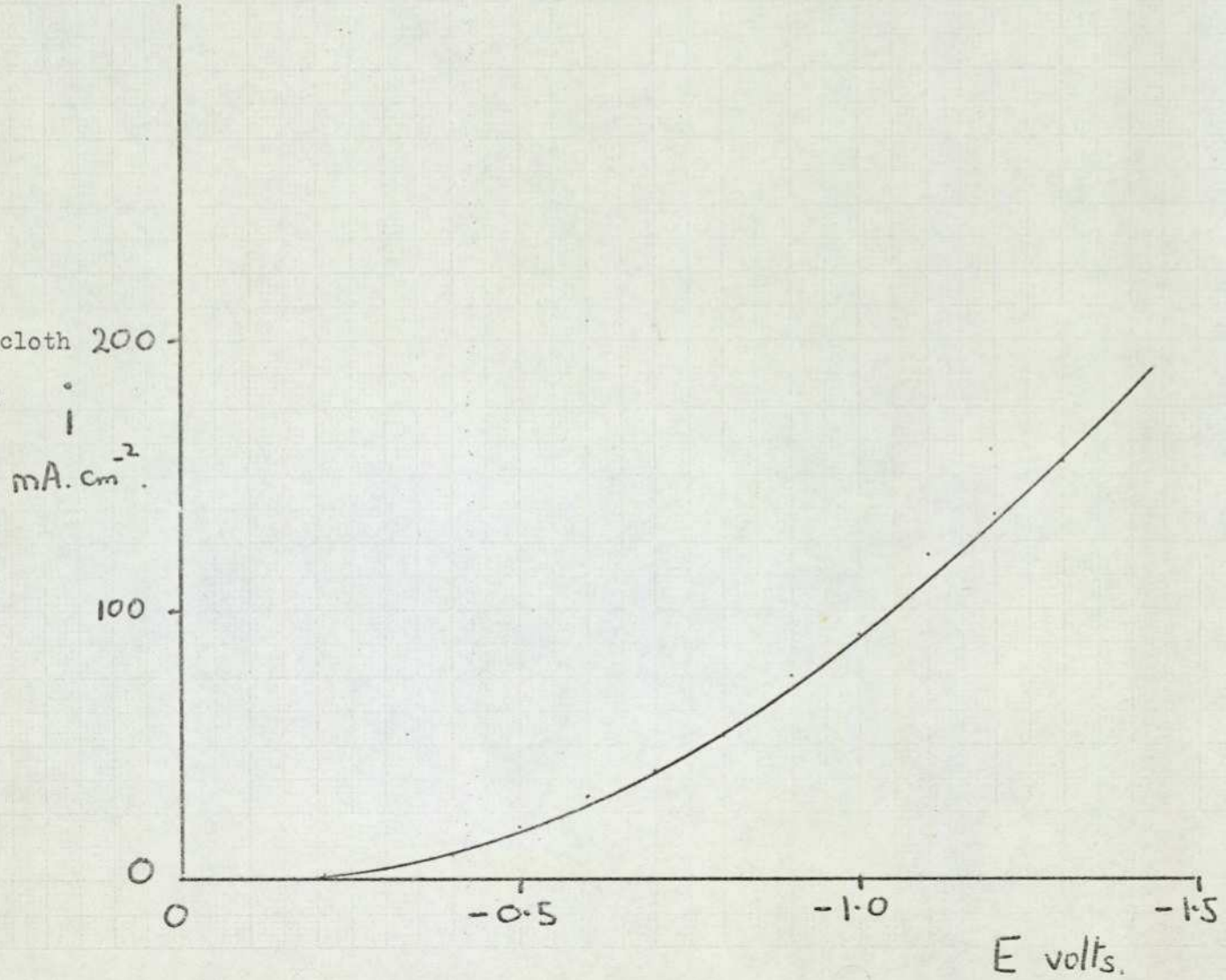
Pressure I atmos.

Temperature 2I C

O.C.V. -0.I7 V

Electrocatalyst graphite cloth

Ohmic resistance 0.30 ohm

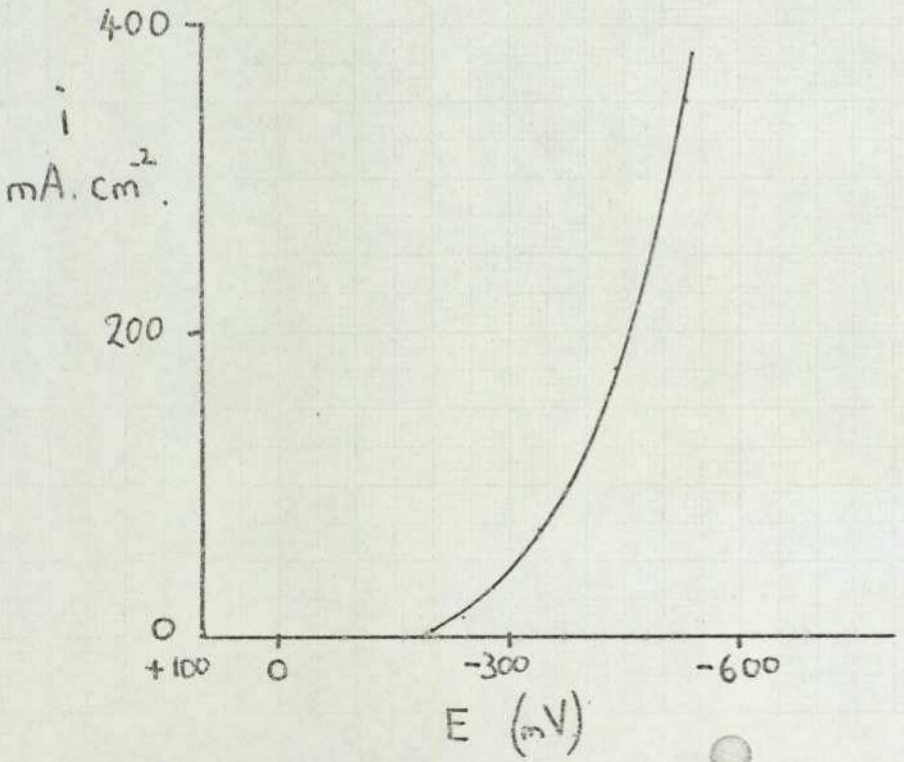


Graph 8.-9

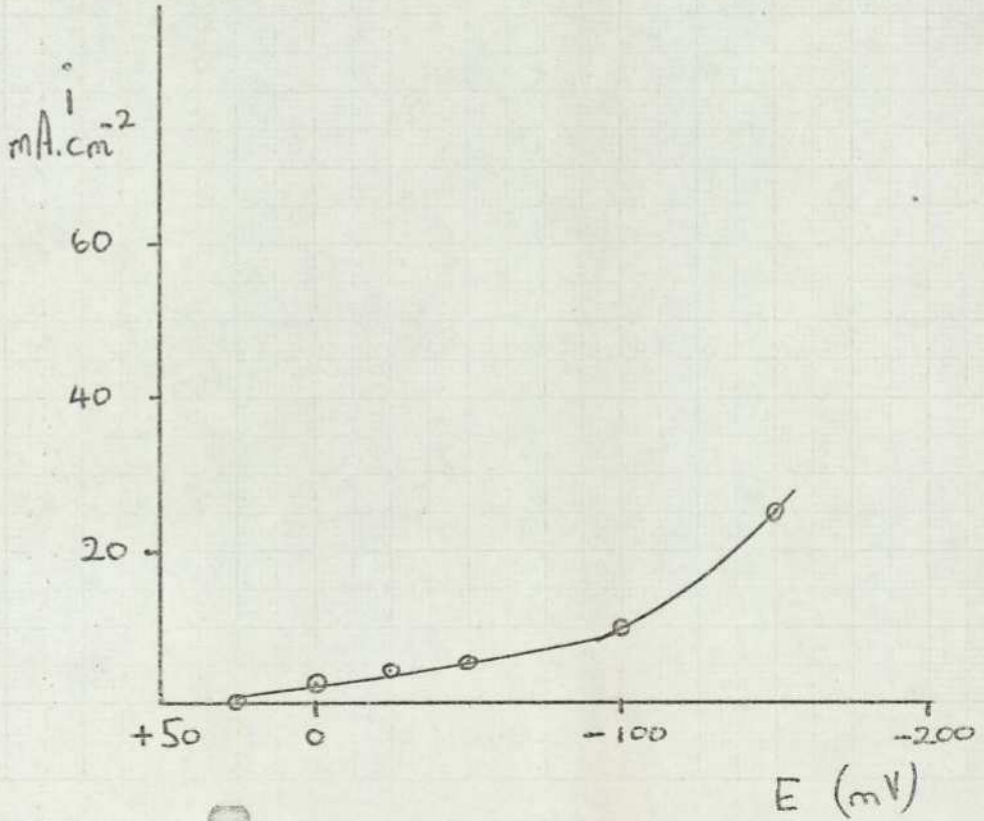
Linear sweep hydrogen evolution polarisation curves for nickel screen and platinum

(a)

Electrolyte	5N KOH
Atmosphere	hydrogen at I atmos.
Temperature	2I°C
O.C.V.	+0.I4 V
Electrocatalyst	nickel screen
Resistance	0.I0 ohm
Sweep rate	900 mV/min



Electrolyte	5N H_2SO_4
Atmosphere	hydrogen at I atmos.
Temperature	2I°C
O.C.V.	+0.026 V
Electrocatalyst	platinum screen
Resistance	0.I0 ohm
Sweep rate	900 mV/min



voltage sweep since in these processes the current often varies as a complex function of time.

In order to determine whether the fall in hydrogen oxidation performance after hydrogen evolution pretreatment is due primarily to (I) loss of electrocatalyst from the electrode or (2) disruption of the teflon bonded electrode structure, the transient and steady state hydrogen oxidation performance was measured before and after pretreatment (graphs 13-14) on platinised graphite using a nickel screen current collector.

3.2.4. Discussion.

(a) The analysis of the electrolyte for carbonate ions and the qualitative tests for oxygen and carbon monoxide in the product gases, supports the assumption that very little, if any, carbon monoxide and carbon dioxide are formed, and that the gas produced is almost entirely oxygen. The results are confirmed by the quantitative measurement of the volume of gas produced, which within the limits of experimental error, was equal to the amount of oxygen produced, as predicted by Faraday's Law, for the quantity of electric charge passed. Any carbon dioxide formed by the reaction of electrolytically produced oxygen and the graphite electrode material would have been dissolved in the electrolyte, resulting in a lower than predicted volume of gas products.

(b) The anodic pretreatment of electrodes at low overpotentials ie. I.26-I.36 V, shows that fall of the oxygen reduction performance is not caused by damage to the electrode structure resulting from gas evolution since no gas is observed to form and there are no

Graph I3.

The effect of hydrogen evolution pretreatments on the steady state hydrogen oxidation performance of a teflon bonded platinised graphite electrode.

Data and Key for graphs I3 and I4.

Atmosphere	hydrogen at I atmos.
Temperature	2I C
Resistance	0.20 ohm
Electrolyte	5N KOH
Electrocatalyst	platinised graphite
Electrocatalyst S.A,	500 m^2/g
Electrocatalyst loading	I0 $mg.cm^{-2}$
Current collector	nickel screen
O.C.V.	+25 mV

transient currents measured after I msec

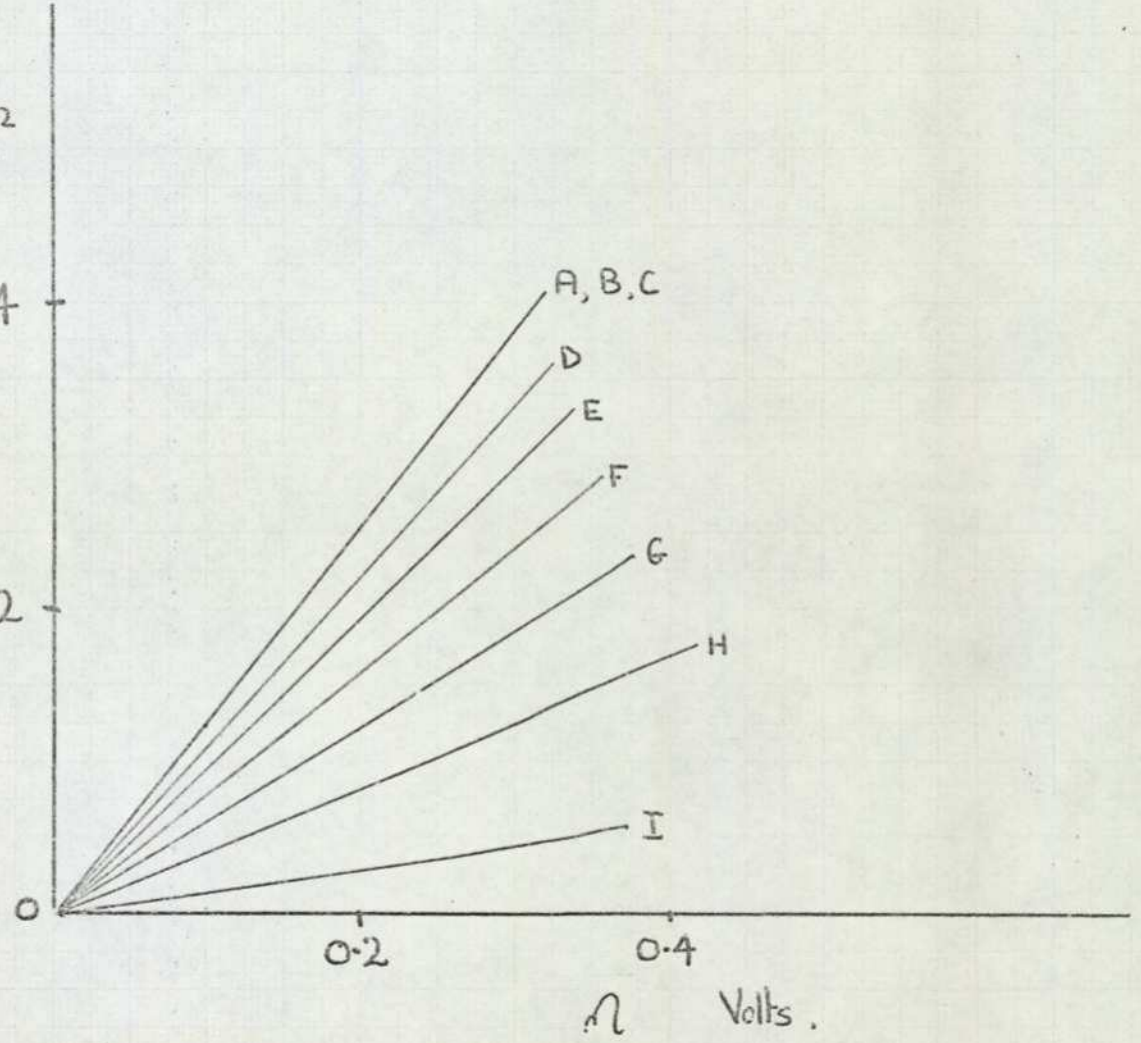
Cathodic current density

I20 $mA.cm^{-2}$ slight degradation observed

Key	Time
A	-
B	30 min
C	30 min
D	I20 min
E	60 min
F	60 min

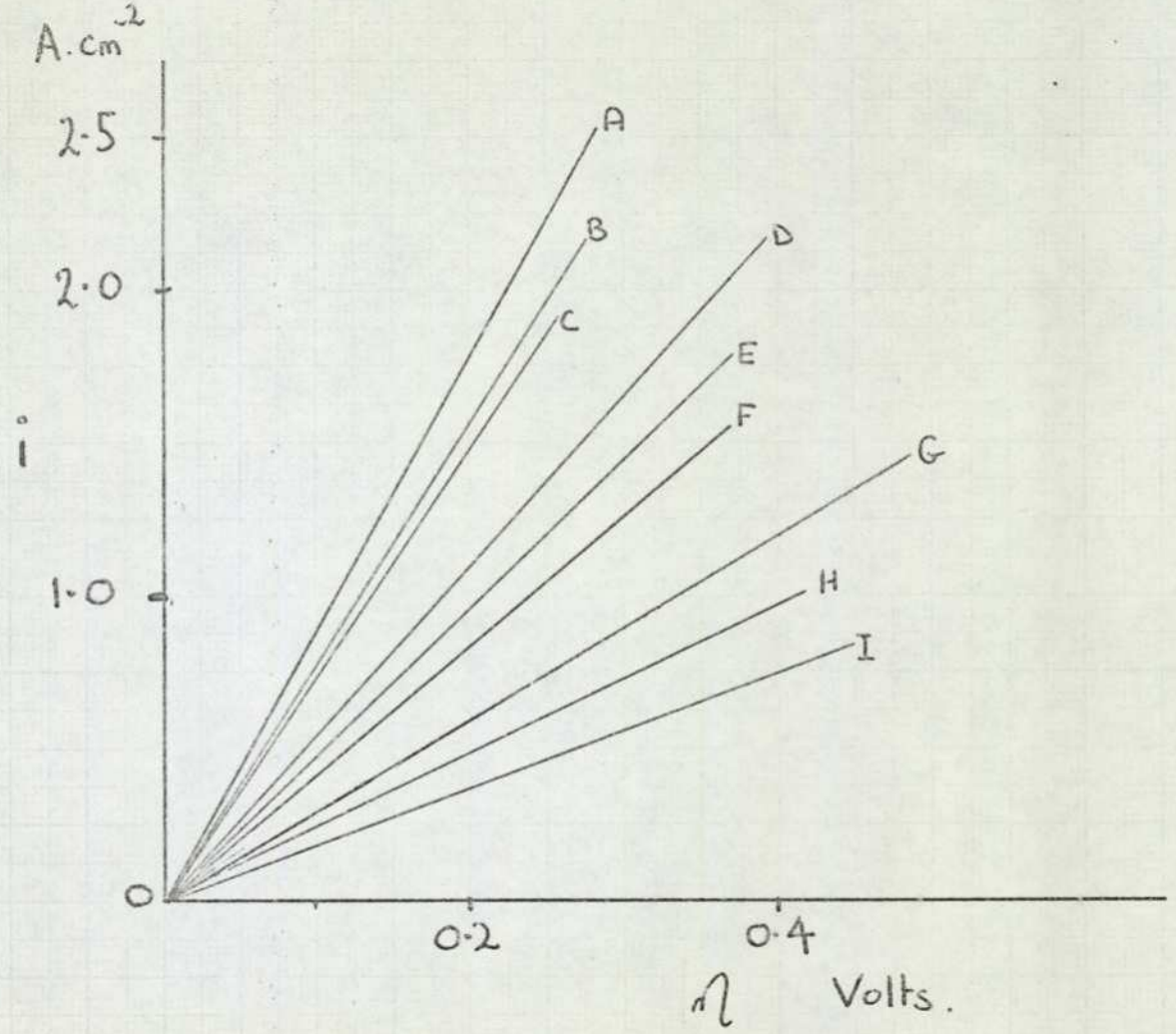
Cathodic current density 250 $mA.cm^{-2}$
rapid degradation observed

G	I0 min
H	I0 min
I	20 min



Graph I4.

The effect of hydrogen evolution pretreatments on the transient hydrogen oxidation performance of a teflon bonded platinised graphite electrode.



visible signs of electrode damage, which would be expected from the magnitude of the performance reduction. Also, the transient performance of the electrode after I msec was reduced substantially and by a similar amount, to the steady state performance, suggesting that the activity of the electrode surface had been reduced by the anodic pretreatment rather than hindrance of oxygen mass transfer by damage to the teflon bonded electrode structure. These results are consistent with the formation of carbon-oxygen surface complexes, possibly a surface layer of graphitic oxide. Graphitic oxide is a non conductor of electricity and even a partial coverage of the graphite surface would be expected to result in a substantial loss of electrode performance. Surface oxide formation can also explain the decay of the oxygen evolution current with time (table 3).

(c) Oxygen and hydrogen evolution tests on teflon bonded platinum black, platinised tungsten trioxide and cobalt nickel oxide, on platinum or nickel screen current collectors resulted in no electrode degradation even at high current densities eg. 0.5 $A.cm^{-2}$. Since these electrodes are all prepared in the same way as teflon bonded graphite electrodes and all the electrocatalysts are powders of similar surface area, it would be likely that if gas evolution from the screen was the reason for the electrode damage, then all these electrodes would behave similarly in this respect.

Comparing the results in graphs I and 4 on silver-graphite and nickel screen electrodes, it can be seen that damage to the silver-graphite electrode was

first observed at about I.50 V when the current had been flowing for about 20 mins at I3 $mA.cm^{-2}$. This can be compared with a current of 0.2 $mA.cm^{-2}$ on nickel screen after about I5 secs at the same potential. Since the anodic current on nickel screen decays with time, after 20 mins it would be substantially lower. The rate of gas evolution from the nickel screen under these conditions was very low in comparison to the total current and gas evolution from the current collector would not explain the electrode degradation.

Platinum screen and graphite cloth are also poor oxygen evolution electrocatalysts (see graphs 4 and 5) giving only low currents at I.90 V. Hence if gas evolution from these current collectors was the cause of electrode degradation this would only occur at higher potentials. Tests on teflon bonded platinum black on platinum screen and graphite cloth current collectors at potentials up to 2.2 V have shown that no degradation occurs. Hydrogen evolution on teflon bonded platinum or platinised tungsten trioxide on platinum screen involves a considerable current contribution from the platinum screen at low over-potentials without electrode degradation. Hence it seems improbable that vigorous gas evolution from the current collector is the cause of electrode damage on graphite based electrodes.

This comparison between the current densities on the current collector and current collector/electro-catalyst system at the same potential gives the maximum contribution of the current collector to the overall electrode current density at a given potential since only part of the screen surface will be wetted

by the electrolyte in the current collector/electro-catalyst system.

(d) So far it has been shown that surface carbon-oxygen complexes are formed at low anodic overpotentials and that at higher anodic overpotentials oxygen gas is produced and the electrodes are physically damaged. This damage is not due to carbon combustion or gas evolution on the current collector and the fall in oxygen reduction performance is observed even when no electrode degradation and gas evolution is visible during the anodic pretreatment. The questions posed are (I) is the fall in performance due mainly to the carbon-oxygen complexes or to the electrode degradation, and (2) is the formation of carbon-oxygen complexes a necessary condition for electrode degradation.

To investigate the second question hydrogen evolution tests were carried out on teflon bonded graphite electrodes using graphite cloth as current collector. Damage was first observed at -475 mV when the current was 33 $mA.cm^{-2}$ (graph 6) ; at the same potential the hydrogen evolution current density on the current collector was I2 $mA.cm^{-2}$ (graph 7). As with all these gas evolution tests the rate of destruction increased with increasing anodic current density. Platinised graphite electrodes gave more useful results since the electrode was much more active, especially for the hydrogen oxidation reaction. The results in table 4 show that these electrodes, using a graphite cloth current collector, first show

signs of destruction at about 90 mA.cm^{-2}. At lower currents no damage was observed and the hydrogen oxidation performance remained constant.

Sometimes hydrogen evolution tests at low current densities for short times do not cause any electrode damage while hydrogen evolution for longer times at the same current densities does cause damage. Tests ofup to two hours duration have been carried out on platinised graphite on graphite cloth in the current range 10-60 mA.cm^{-2} (table 6). At currents less than 30 mA.cm^{-2} no destruction was observed in two hours, while at currents between 30-60 mA.cm^{-2} destruction was observed between six and sixty minutes after the application of the cathodic current, the higher the current the sooner the degradation occured. This suggests that at lower hydrogen evolution current densities no degradation occurs even after long periods. A possible explanation for these results is that at low current densities the pressure of hydrogen produced in the pores is not sufficient to cause degradation but is sufficient to permit the escape of hydrogen from the interior of the electrode by diffusion through the electrolyte ie. concentration of hydrogen in the electrolyte in the interior of the electrode is higher than in the bulk solution due to the higher hydrogen gas pressure. Although more exhaustive tests are required this could mean that this type of electrode could be used for recharging purposes if the recharge rate is low.

Forty five seconds hydrogen evolution pretreatment at 90 mA.cm^{-2} did not affect the hydrogen

Table 6.

The effect of hydrogen evolution pretreatments at low constant currents for varying times on the endurance of a teflon bonded platinised graphite electrode.

Time	Cathodic current density ($mA.cm^{-2}$)	Observations
I hour	IO	No degradation
I hour	IO	No degradation
I hour	20	No degradation
I hour	20	No degradation
¼ hour	30	No degradation
½ hour	30	Slight degradation
I4 min	40	Slight degradation
6 min	60	Slight degradation

Electrolyte	5N potassium hydroxide
Temperature	2I°C
Atmosphere	hydrogen
O.C.V.	0.075 V
Electrocatalyst	platinised graphite
Electrocatalyst loading	I2 $mg.cm^{-2}$
Electrocatalyst S.A.	500 m^2/g
Current collector	graphite cloth
Resistance	0.25 ohm

oxidation performance although electrode damage was observed. Suprisingly even after pretreatments K,L,M and N,(see table 4) 100-200 $mA.cm^{-2}$ for 1 - 10 minutes where substantial degradation resulted, the hydrogen oxidation polarisation curve was unaffected over a wide potential range. This indicates that either the teflon bonded structure is not entirely disrupted by hydrogen evolution or that this structure has little affect on the hydrogen oxidation performance. The latter is improbable since the hydrogen oxidation performance of a flooded platinum black electrode is very poor in comparison with the teflon bonded electrode because of the slower mass transport of hydrogen to the active sites. Pretreatments O and P, ~40 - 80 $mA.cm^{-2}$ for 30 - 60 minutes, resulted in small losses in hydrogen oxidation performance while Q,R,S and T, 0 - 80 minutes at -1.575 V, which resulted in severe electrode damage produced an electrode with much poorer hydrogen oxidation characteristics. The electrode damage is also reflected in the fall in hydrogen evolution current with time at the same potential. The reduction in hydrogen oxidation performance was most marked after pretreatments Q and R, even though similar currents flowed for a shorter time than in S and T. This is probably because the graphite cloth, which is made from carbon fibres, traps a considerable amount of the electrocatalyst between the fibres, thus making it difficult to remove all the electrocatalyst from the current collector, cf. nickel and platinum foil and screen current collectors. In pretreatments B - I although no electrode damage was observed, it seems likely that

this could have occurred if the current had flowed for a longer time (table 6). This can be seen from O, where electrode damage occurred at only 40 $mA.cm^{-2}$. This is an example of a general phenomenom observed in gas evolution on these electrodes ie. when degradation has been initiated it can be maintained at considerably lower gas evolution rates.

A significant quantity of electrocatalyst must be lost from the electrode before the hydrogen oxidation performance is affected. This suggests that the subsequent loss of performance is simply due to the loss of electrocatalyst resulting in a lower electrocatalyst loading. This also explains why initially no loss in hydrogen oxidation performance was observed ie, with teflon bonded electrodes the gas dissolution performance increases with electrocatalyst loading up to a certain level beyond which increases in electrocatalyst loading have little affect. This is because these electrodes use the available electrocatalyst surface area most usefully only when they are very thin. The critical loading is usually about 7 $mg.cm^{-2}$ and the electrodes used in this study were made with loadings of about 10-15 $mg.cm^{-2}$, hence the initial losses of electrocatalyst during hydrogen evolution do not affect the hydrogen oxidation performance.

The results in graphs I3 and I4 show that the transient hydrogen oxidation performance of platinised graphite on nickel screen after hydrogen evolution pretreatment, which resulted in slight electrode destruction but no loss of hydrogen oxidation steady

state performance, was slightly reduced. This is consistent with the above results since the transient performance is due to the use of the entire electrode-electrolyte interfacial area and any loss of electrocatalyst would reduce this area. It can be seen from the results that as the quantity of electrocatalyst which had fallen off the electrode increased, the transient hydrogen oxidation performance decreased. Also the height of the double layer capacity peak at very short times is reduced as electrocatalyst is lost.

The results of a similar experiment using nickel screen instead of graphite cloth as current collector produced very similar results (see table 5). The first visible signs of electrode degradation occurred at a current of 33 $mA.cm^{-2}$ and this resulted in a slight fall in the steady state hydrogen oxidation performance. At lower hydrogen evolution currents (B,C,D) no loss of performance occurred. In general the fall in performance was dependent on the amount of electrocatalyst lost from the electrode eg. pretreatment I produced very rapid degradation and a major drop in the hydrogen oxidation performance. After this pretreatment the electrode was so weakened that further steady electrode destruction occurred at currents as low as 44 $mA.cm^{-2}$. At the end of the experiment only a little electrocatalyst remained on the nickel screen. In a separate test the electrode was completely submerged in the electrolyte and although this had little effect on the current at which degradation was first observed, it did facilitate the degradation at higher currents, probably enabling electrocatalyst to be

lost from the top of the electrode more easily.

These results are only approximate since the errors in the geometric electrode area, electrocatalyst loading and oscilloscope readings are all about 10-15%. However if the electrocatalyst loading was measured after each pretreatment then the effect of this parameter on the steady state and transient hydrogen oxidation performance could be determined. This would assume that the electrocatalyst and teflon were lost from the electrode in the same proportion as they were originally present, and the electrode would need to be thoroughly washed and dried, thus introducing possible errors, before the loading was measured.

Graphs 10-12 clearly show the fall in hydrogen oxidation performance with time at a given constant hydrogen evolution current density. Even at 40 $mA.cm^{-2}$ when hydrogen evolution causes only slight electrode damage, the performance drops by about 40% after 200 minutes.

The conclusions that can be made so far are:
(1) electrode degradation is caused by both hydrogen and oxygen evolution and is probably due to the mechanical weakness of carbon electrodes.
(2) This electrode degradation reduces the oxygen reduction and hydrogen oxidation performances.
(3) Oxygen evolution at low currents causes a fall in oxygen reduction performance without causing electrode damage. This is probably due to the formation of surface carbon-oxygen complexes. Section 3.3. studies this effect in more detail.

Graphs I0, II and I2
The effect of time of hydrogen evolution pretreatment on the hydrogen oxidation performance of a platinised graphite teflon bonded electrode.

cathodic current density
250 mA.cm^{-2}

Key	Time
A	-
B	5 min
C	I0 min
D	I5 min
E	20 min

Data for graphs I0 - I2.

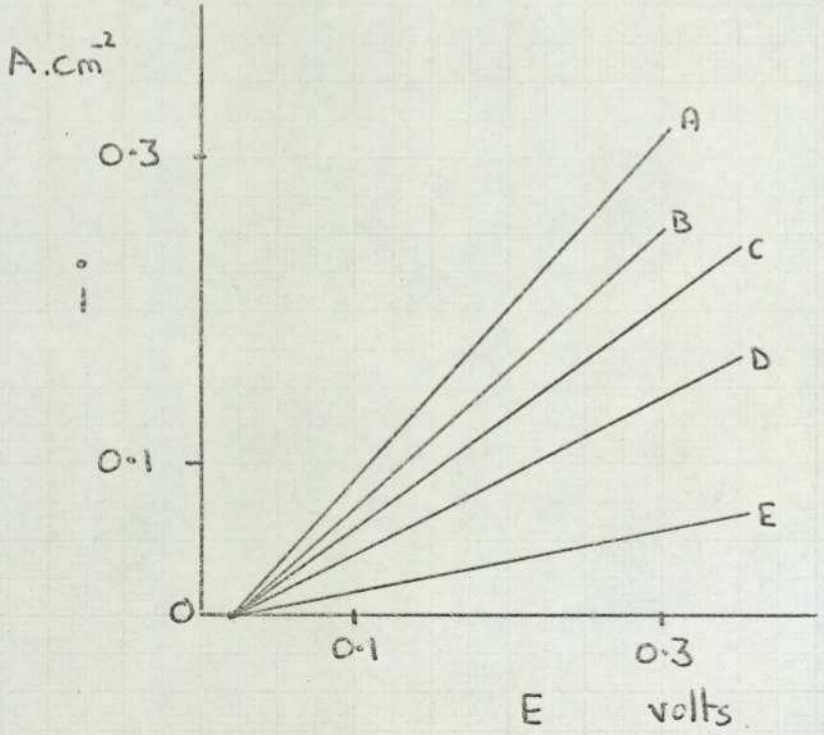
O.C.V.	+22 mV ± 2mV
Temperature	2I°C
Atmosphere	hydrogen at I atmos.
Electrolyte	5N KOH
Electrocatalyst	platinised graphite
Electrocatalyst loading	7 mg.cm^{-2}
Electrocatalyst S.A.	500 m^2/g
Current collector	nickel screen
Resistance	0.I0 ohm ± 0.05 ohm

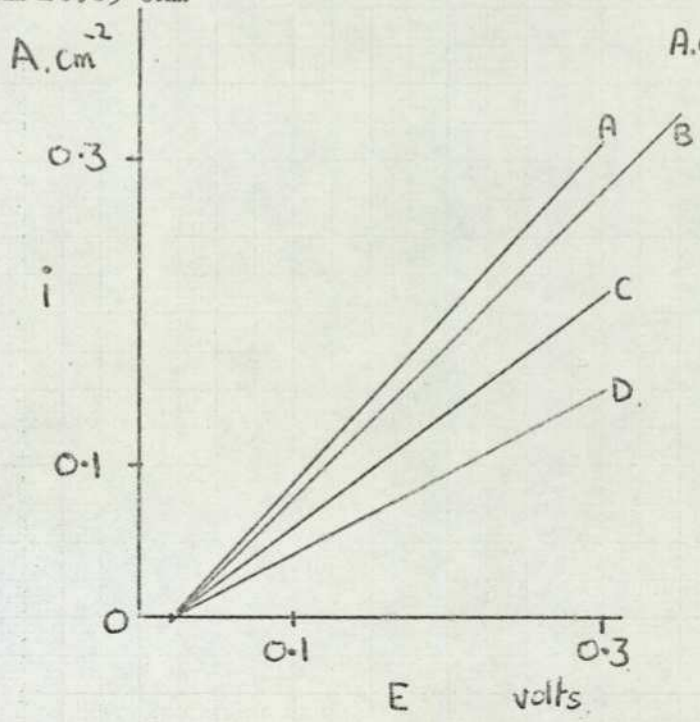
Graph II.
Cathodic current density
I20 mA.cm^{-2}

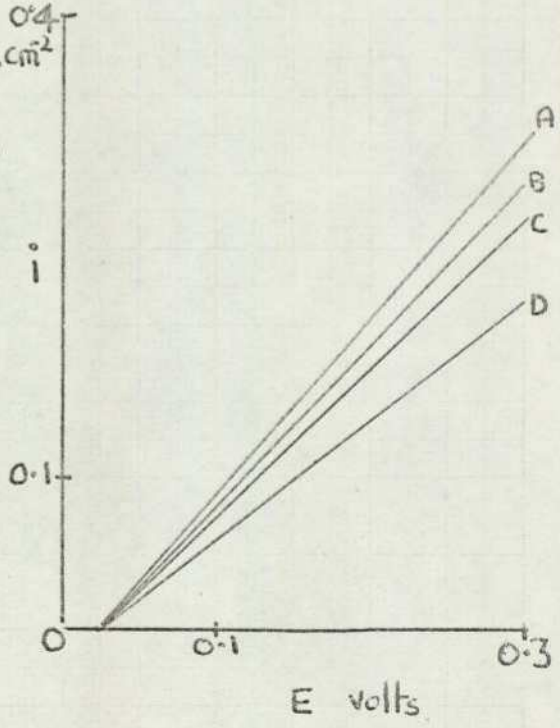
Key	Time
A	-
B	I5 min
C	60 min
D	I20 min

Graph I2.
Cathodic current density
40 mA.cm^{-2}

Key	Time
A	-
B	I5 min
C	60 min
D	I20 min







3.3. The Effect of Oxygen Evolution on the Carbon Surface.

3.3.I. Experimental.

Teflon bonded graphite and platinised graphite electrodes on both nickel screen and graphite cloth current collectors were subjected to various anodic pretreatments and the steady state oxygen reduction performance subsequently determined. Attempts were made to reduce any carbon-oxygen complexes by passing cathodic currents ie. hydrogen evolution. It was hoped that the electrolytic reduction of these surface complexes would restore the electrode surface to its original form, thus making it possible to distinguish between the effects of the surface oxygen complexes and the electrode degradation, on the lowering of oxygen reduction performance.

3.3.2. Results and Discussion.

Table 7 shows the effect of various anodic/cathodic pretreatments on the steady state oxygen reduction polarisation data for teflon bonded graphite on graphite cloth.

These results indicate that:

(I) The electrode, as prepared, has certain surface groups, probably carbon-oxygen complexes, which can be reduced by evolving hydrogen on it (see A and B). These surface groups lower the activity of the surface for the oxygen reduction reaction.

(2) Oxygen evolution at low current densities reduces the oxygen reduction activity of the electrode without causing any visible damage. The fall in performance

Table 7.

The effect of anodic pretreatments on steady state oxygen reduction performance of a teflon bonded graphite electrode.

E (mV)	i ($mA.cm^{-2}$)										
	A	B	C	D	E	F	G	H	I	J	K
925	I.2	I.3	I.2	0.86	0.29	-	-	0.63	-	0.9	-
900	2.7	3.9	3.I	2.I	0.43	2.0	2.0	I.4	-	2.4	2.5
850	8.6	I2	9.0	6.9	0.86	8.0	8.3	2.9	8.0	7.I	7.I
800	I6	23	I6	I2	I.3	I4	I4	4.7	I4	I3	I2
750	26	34	25	I9	I.9	2I	2I	8.0	20	I9	I8
700	36	47	33	25	3.I	28	28	I2	28	26	24
650	47	59	-	32	4.0	35	34	I6	35	33	30
600	58	70	5I	39	8.6 to 34	4I	40	2I	4I	40	36
500	-	-	-	-	-	-	-	33 to 49	-	-	-

E (mV)	i ($mA.cm^{-2}$)										
	L	M	N	O	P	Q	R	S	T	U	V
925	-	-	I.0	0.7	0.33	-	0.77	0.3I	-	-	0.69
900	2.0	0.36	2.I	I.8	0.57	-	2.0	0.52	2.0	0.84	I.7
850	5.2	0.46	6.3	5.4	I.I	2.6	5.3	I.I	4.7	2.4	3.5
800	8.7	0.7	I2	I0	3.0	4.7	II	2.2	9.3	3.8	5.5
750	I3	I.4 to 5.0	I7	I4	6.3	6.9	I7	5.5	I4	5.3	7.5
700	I8	6.7 to II.0	23	2I	9.2	9.3	23	7.0	I9	6.7	I0.0
650	25-29	I6	30	27	I3	I2	29	9.2	23	8.I	I2
600	35	2I	36	32	I9	I4	35	II	27	9.5	I4
500	-	27-42	50	42	50	20-47	-	38	-	I3	I8

Key to table 7.

	Pretreatment process	Current density ($mA.cm^{-2}$)	Potential (V)	Time (min)	Comments
A	No pretreatment	-	-	-	-
B	H_2 evolution	4	-0.23	IO	no degradation
C	O_2 evolution	20 - 8	I.45	IO	no degradation
D	O_2 evolution	36 - 27	I.75	IO	no degradation
E	O_2 evolution	I72-I00	3.00	5	visible degradation
F	H_2 evolution	300	-I.I5	5	visible degradation
G	O_2 evolution	360-I40	3.IO	2	visible degradation
	O_2 reduction	-	0.35	0.5	no degradation
H	O_2 evolution	350-I40	3.IO	2	visible degradation
I	no pretreatment	-	-	-	O_2 reduction reverse direction
J	left overnight	-	-	-	-
K	O_2 evolution	85-I4	I.57	I.5	visible degradation
L	O_2 evolution	290-I00	2.85	I	visible degradation
M	O_2 evolution	330-I30	3.IO	I	visible degradation
N	left overnight	-	-	-	-
O	O_2 evolution	I00-I3	I.70	3	visible degradation
P	O_2 evolution	280-I40	3.IO	I	visible degradation
Q	O_2 evolution	270-I40	3.IO	3	visible degradation
R	no pretreatment	-	-	-	O_2 reduction reverse direction
S	O_2 evolution	230-II0	3.IO	I5	visible degradation

Key to table 7 (cont.).

	Pretreatment process	Current density ($mA.cm^{-2}$)	Potential (V)	Time (min)	Comments
T	no pretreatment	-	-	-	O_2 reduction reverse direction
U	O_2 evolution	205-I00	3.IO	3	visible degradation
V	H_2 evolution	200	-I.O	5	visible degradation

Electrolyte	5N potassium hydroxide
Atmosphere	Oxygen at I atmosphere
Temperature	2I°C
O.C.V.	+0.96V
Electrocatalyst	graphite
Electrocatalyst loading	I5 $mg.cm^{-2}$
Electrocatalyst S.A.	500 m^2/g
Current collector	graphite cloth
Chmic resistance	0.35 ohm

depends on the anodic charge passed (see C and D).

(3) Oxygen evolution at very high overpotentials causes a large drop in oxygen reduction performance at potentials $>$ 0.60 V. However at about 0.60 V the current increases steadily with time eventually reaching a value which is only slightly less than the original current at that potential. This suggests that the oxide groups formed during the anodic pretreatment are being reduced at around 0.60 V. Since visible electrode damage occurred during the pretreatment it can be said that the main cause of the loss of oxygen reduction performance was due to the formation of surface oxides and not to disruption of the electrode structure. (see E, H and I). It should be noted, however, that several oxide species are probably formed depending on the potential and it appears that only those formed at high potentials eg. above 2.7 V, are easily reduced at potentials in the range 0.5 - 0.6 V.

(4) After holding the electrode at 0.6 V subsequent hydrogen evolution slightly increases the electrode activity even though it causes electrode degradation. It is possible that hydrogen evolution reduces another different oxide species (see F).

(5) Oxygen evolution at 3.10 V followed by holding the electrode at 0.35 V had little effect on the oxygen reduction performance ie. the oxide surface groups were reduced when the electrode was held at 0.35 V (see GG)

(6) Although oxides are formed at all potentials in the range 1.00 - 3.10 V it appears that this process has a much greater effect on the oxygen reduction

performance at potentials greater than about 2.7 V. It is possible that this is due to the formation of a different oxide species and this is supported by the fact that only oxides formed above ~2.7 V can be reduced at 0.6 V (see K,L,M,N,O,P,Q and R).

(7) As this process of oxygen evolution followed by oxide reduction at about 0.6 V was repeated, the oxygen reduction performance gradually declined, probably due to the electrocatalyst lost during oxygen evolution. At the end of this series of tests the electrode was subjected to hydrogen evolution in order to ensure the reduction of all the surface oxide groups formed at high potentials. Hence the loss of oxygen reduction performance from R to V is due to electrode degradation (see R,S,T,U, and V).

(8) The formation of oxides on these electrodes at potentials $>\sim$2.7 V results in a change in the open circuit voltage ie. the O.C.V. of these electrodes is normally in the range 0.95 - 0.97 V, oxygen evolution pretreatment at 3.10 V causes the O.C.V. to rise to about 1.08 V after equilibration. The O.C.V. was measured after holding the electrode at potentials in the range 0.90 - 0.50 V. At potentials $>$ 0.70 V the O.C.V. remained 1.08 V and the oxygen reduction performance was severely depressed; at potentials in the range 0.70 - 0.50 V the O.C.V. gradually fell to less noble values (0.95 V) and the oxygen reduction performance recovered. On returning to higher potentials eg. 0.80 V, the O.C.V. and oxygen reduction performance were maintained.

The main conclusions are:

(a) The loss in oxygen reduction performance is caused mainly by the formation of oxide surface groups and secondly by electrode damage.

(b) Oxides formed at potentials > 2.7 V can be reduced at potentials < 0.6 V and hence they need not result in any permanent performance loss, oxides formed at potentials < 2.7 V cannot be reduced in this way and hence result in a permanent and cumulative performance loss. The electrode damage resulting from oxygen evolution also causes a permanent and cumulative drop in performance. In zinc-air and other cells in which graphite cathodes are used the potential is never likely to reach values as high as 2.7 V and hence the formation of the reducible oxide groups is of little significance in this connection. Nevertheless a considerable amount of the current research on carbon is concerned with the detection and effects of various surface groups and in this respect the electrochemical formation and reduction of surface oxide groups, which has not previously been reported, should be of interest.

The results in table 8 for platinised graphite, teflon bonded electrodes used at potentials < 2.0 V confirm the above conclusions. The anodic pretreatments in this experiment were carried out as follows: the potential was increased gradually from I.0 V to the final value so that the high transient currents normally observed over the first minute were avoided. The results obtained followed a similar pattern to those in table 7. One difference was that the oxygen reduction current recovered somewhat in the potential

Table 8.

The effect of anodic pretreatments on the steady state oxygen reduction performance of a teflon bonded platinised graphite electrode.

.E(mV)	i(mA.cm^{-2})							
	A	B	C	D	E	F	G	H
1000	1.3	0.9	0.4	0.2	0.14	-	-	-
975	3.7	2.8	1.5	0.7	0.31	-	-	-
950	8.5	6.0	3.6	1.5	0.65	0.21	0.17	0.16
900	29	21	12	4.0	1.9	0.65	0.40	0.25
850	60	45	23	7.5	3.3	1.2	0.56	0.32
800	101	73	39	11	5.0	1.7	0.79	0.40
750	135	100	54	16	7.1 to 13	2.5	1.1 to 1.9	0.5 to 0.8
700	185	137	69	21	18	5.2	2.7	1.1
600	280	202	104	33	28	8.7	3.6	1.7
500	380	265	148	49	41	14	5.7	2.1

Electrolyte	5N potassium hydroxide
Atmosphere	oxygen at 1 atmosphere
Temperature	21 C
O.C.V.	1.04 V
Electrocatalyst	platinised graphite
Electrocatalyst loading	16 mg.cm^{-2}
Electrocatalyst S.A.	500 m^2/g
Current collector	nickel screen
Ohmic resistance	0.20 ohm

Key to table 8.

	$i(mA.cm^{-2})$	E (V)	Time (min)	Comments
A	-	-	-	No pretreatment
B	20 - I.5	I.27	25	No visible degradation
C	20 - 3.6	I.35	I7	No visible degradation
D	20 - 6.0	I.45	23	No visible degradation
E	20 - I2	I.55	22	Visible degradation
F	62 - 49	I.65	I5	Visible degradation
G	I40 - IC0	I.75	I5	Visible degradation
H	230 - I30	I.85	24	Visible degradation

region 0.80 - 0.70 V and it is thought that this is due to reduction of platinum oxides formed during the anodic pretreatment. N.B. Platinum oxides are reduced in this potential region. Hydrogen evolution at -0.10 V had little effect on the oxygen reduction performance which is to be expected since the surface oxides were formed at low potentials (less than 2.0 V) and most of the hydrogen evolution current at -0.10 V is due to hydrogen evolution on the platinum.

The electrode damage was observed in two forms: (I) very small particles of graphite, too small to be seen individually, fell off the electrode and gave the solution a brownish yellow colouration. The particles did not sediment over a period of one week ie. colloidal graphite. This colouration was most pronounced near the electrode during oxygen evolution.
(2) small, visible graphite particles fell from the electrode and sank to the bottom of the cell.

3.4. Possible Alternatives to Carbon based Electrodes in Rechargeable metal-air Cells.

3.4.I. Introduction.

It has been shown that carbon based air electrodes are completely unsatisfactory for use in a rechargeable cell [125]. An alternative electrode must have similar oxygen reduction characteristics and be unaffected by oxygen evolution.

Various electrodes have been used as oxygen or air electrodes eg.

(a) Bacon dual porosity sintered nickel electrodes,[44]

which use oxygen at high pressure and temperature.
(b) DSK raney silver-aluminium electrodes (I27), which use oxygen at ambient temperature and pressure.
(c) Porous noble metal (I26) and nickel electrodes (I29).
(d) Kordesch composite electrodes (46) which use the high mechanical strength of nickel screen and porous nickel, the high surface area of activated carbon and the hydrophobic properties of teflon to produce an air breathing cathode.
(e) Teflon bonded gas diffusion electrodes using porous noble metals, (I28) powdered graphite, (I36) supported noble metals (I37) and semiconducting metal oxides (I86) as electrocatalysts.

For metal-air cells (a) would not be suitable as it operates on oxygen at high temperatures and pressures, (b) uses too much silver to be economically viable and (c) are not air breathing electrodes ie. low performance, (d) are air breathing and use inexpensive materials but suffer from the disadvantages of carbon electrodes. (e) appear to be the most suitable except that graphite and noble metals are unsatisfactory electrocatalysts. Supported noble metals (not a carbon support) and semiconducting oxides provide the most likely answer. Possible supports for alkaline media are nickel oxide and boron carbide although these are unlikely to be as good as graphite which is an active support ie. it is not simply an electronically conducting extender of high surface area , it also takes part in the electrode reaction, nor are they as cheap as graphite. Semiconducting metal oxides have not been sufficiently active oxygen

reduction electrocatalysts for them to be considered for use in commercial batteries. However, recent work in these laboratories has resulted in an electrode of satisfactory oxygen reduction characteristics.(166)

The stability of teflon bonded electrodes, which do not contain carbon, to anodic polarisation has been investigated. The number of materials which can be used for oxygen evolution is limited, especially in acidic solutions, because of the high positive potentials at which the process occurs. Many metals dissolve at these high potentials and in acid solution only the noble metals are stable. Semiconducting oxides are usually stable in alkaline solution but only a few are stable in acid solution eg. tin oxide. For stable metals the oxygen evolution process causes an oxide film to cover the metal surface. This oxide film can be difficult to remove and generally has a much lower oxygen reduction activity than the bare metal surface. Oxygen evolution on semiconducting metal oxides usually results in raising the oxidation state of the metal. In this section the stability of three types of teflon bonded electrode have been tested when being used for oxygen or hydrogen evolution. The criteria of stability are (a) mechanical strength and (b) the activity of the electrode surface for the oxygen reduction or hydrogen oxidation reactions. The electrocatalysts tested were platinum black, platinised tungsten trioxide and cobalt nickel oxide.

3.4.2. Experimental.

The platinum black electrodes were tested for the effects of hydrogen and oxygen evolution in both

acid and alkaline media. After gas evolution the hydrogen oxidation and oxygen reduction steady state polarisation data were measured and compared with the readings obtained before gas evolution. The platinised tungsten trioxide electrodes were tested in a similar way except that only acid electrolyte and the hydrogen electrode reaction were studied. (Tungsten trioxide is soluble in alkali.) The cobalt nickel oxide was tested only in alkaline media and for the oxygen electrode reaction. (Cobalt nickel oxide is soluble in acids.)

The effect of rapidly switching on and off gas evolution currents on platinum black electrodes and the long term endurance of these electrodes under conditions of gas evolution were investigated. The rapid on - off switching was achieved using a suitably programmed pulse generator.

3.4.3. Results.

(I) Platinum black.

These electrodes were not damaged by oxygen evolution current densities up to I.0 $A.cm^{-2}$, by extensive periods of up to two days of continuous oxygen evolution at high current densities, by rapidly switching the current on and off at repetition rates of the order of one second, for periods of up to one hour, or by intermittent use over two months with an average weekly running time of seventy eight hours. These results apply for acid and alkaline electrolytes and for nickel screen or platinum screen current collectors. In order to obtain anodic currents as high as I.0 $A.cm^{-2}$ it was necessary to use potentials up to 2.2 V. The rapid switching of the current was

achieved using a pulse generator.

The second criterion of stability ie. whether oxygen evolution affects the oxygen reduction performance was also studied under the above anodic conditions. The oxygen reduction performance was found to vary in two ways: (I) after anodic pretreatment the performance in the potential region I.0 - 0.80 V was significantly depressed. In the potential region 0.80 - 0.60 V the current was observed to increase with time until it reached the same value as prior to the anodic pretreatment. When the potential was then returned to the 0.80 - I.0 V region the current had returned to its initial value.
(2) Over an extended period of time there was a permanent but slight fall in performance, eg. after two months use the performance was about 80 % of the initial performance.

Tables I0,II and I2 show the results for platinum black on nickel screen in 5N potassium hydroxide electrolyte. In each case the oxygen reduction polarisation data shown were recorded after holding the electrode at 0.6 V for ten minutes. Similar results for platinum black on platinum screen in 5N sulphuric acid electrolyte are shown in tables I3,I4 and I5.

For the hydrogen evolution studies the use of a nickel screen current collector has the advantage that nickel has a higher overpotential for hydrogen evolution than platinum and consequently contributes little to the total current at low overpotentials (see graph 8). However, the use of acid solutions necessitating platinum screen current collector is more

Table IO

The effect of galvanostatic anodic pretreatments on the oxygen reduction performance of a teflon bonded platinum black electrode.

E(mV)	i($mA.cm^{-2}$)						
	A	B	C	D	E	F	G
975	I.I	I.0	I.0	I.0	I.0	I.0	I.0
950	4.2	4.0	4.0	4.0	3.9	3.9	3.9
900	23	22	22	22	22	2I	2I
850	79	80	78	78	80	78	78
800	I39	I37	I37	I36	I36	I35	I35
750	I85	I84	I85	I83	I84	I84	I82
700	2I2	2I0	2I0	209	208	208	208

Key

	A	B	C	D	E	F	G
anodic current density ($mA.cm^{-2}$)	-	I0	20	50	I00	200	500

time ←—— one hour ——→

A - no pretreatment

Electrolyte	5N potassium hydroxide
Atmosphere	oxygen at I atmosphere
Temperature	2I°C
O.C.V.	I.04 V
Electrocatalyst	platinum black
Electrocatalyst S.A.	$8.1\ m^2.g^{-1}$
Electrocatalyst loading	$6\ mg.cm^{-2}$
Current collector	nickel screen
Ohmic resistance	O.I0 ohm

Table II.

The effect of rapid switching of the anodic current on the oxygen reduction performance of a teflon bonded platinum black electrode.

E (mV)	i(mA.cm^{-2})				
	A	B	C	D	E
950	3.0	3.0	3.0	2.9	2.9
900	I6	I6	I6	I6	I5
850	70	69	69	70	68
800	I28	I28	I28	I27	I25
750	I72	I70	I72	I70	I70
700	200	I98	20I	200	I98

Key

	constant anodic current density (mA.cm^{-2})	on time off time (sec)	frequency (Hz)	total time (hours)
A	-	-	-	-
B	I0	0.5	I	I
C	50	0.5	I	I
D	250	0.5	I	I
E	500	0.5	I	I

Electrolyte	5N potassium hydroxide
Atmosphere	oxygen at I atmosphere
Temperature	2I°C
O.C.V.	I.04 V
Electrocatalyst	platinum black
Electrocatalyst S.A.	8.1 $m^2.g^{-1}$
Electrocatalyst loading	6 mg.cm^{-2}
Current collector	nickel screen
Ohmic resistance	0.I0 ohm

Table I2.

Comparison of initial oxygen reduction performance with the oxygen reduction performance two months later after the anodic passage of II7,000 coulombs.cm^{-2}.

E (mV)	i(mA.cm^{-2})	
	before	after
950	3.4	2.8
900	I9	I5
850	72	58
800	I32	I07
750	I75	I40
700	205	I68

maximum anodic current = I000 mA.cm^{-2}

average switching frequency = 3 times a day over the two month period.

Electrolyte	5N potassium hydroxide
Atmosphere	oxygen at I atmosphere
Temperature (average)	20°C
O.C.V.	I.04 V
Electrocatalyst	platinum black
Electrocatalyst S.A.	8.1 $m^2.g^{-1}$
Electrocatalyst loading	6 mg.cm^{-2}
Current collector	nickel screen
Ohmic resistance	0.I0 ohm

Table I3.

Oxygen reduction polarisation data before and after constant current oxygen evolution pretreatment at $0.5\ A.cm^{-2}$ for one hour for a teflon bonded platinum black electrode.

E (mV)	$i(mA.cm^{-2})$ before	after
950	2.0	2.0
900	7.I	7.0
850	25	25
800	50	49
750	6I	60
700	70	70

Table I4.

Oxygen reduction polarisation data before and after rapid switching of a constant anodic current of $0.5\ A.cm^{-2}$ for a teflon bonded platinum black electrode.

on time = 0.5 sec frequency = I Hz total time = I hour

E (mV)	$i(mA.cm^{-2})$ before	after
950	2.4	2.3
900	8.6	8.3
850	30	30
800	58	59
750	70	70
700	82	80

Data for tables I3 and I4, also I5.

Electrolyte	5N sulphuric acid
Atmosphere	oxygen at I atmosphere
temperature	2I C
O.C.V.	I.05 V
Electrocatalyst	platinum black
Electrocatalyst S.A.	$8 m^2 . g^{-1}$
Electrocatalyst loading	6 $mg.cm^{-2}$
Current collector	platinum screen
Ohmic resistance	O.IO ohm

Table I5.

Comparison of oxygen polarisation data for a teflon bonded platinum black electrode before and after two months intermittent anodic pretreatment.

E (mV)	i($mA.cm^{-2}$) before	after
950	2.5	I.9
900	9.0	7.I
850	32	25
800	60	48
750	7I	54
700	8I	64

anodic charge passed	I03,000 $coulombs/cm^2$
maximum anodic current	I $A.cm^{-2}$
average switching frequency	3 times per day
average temperature	20°C

common in practice. Both types of electrode were subjected to hydrogen evolution and then the hydrogen oxidation polarisation data were recorded. The results were very similar for both current collectors and those for platinum screen are shown in tables I6, I7 and I8. These results show that the electrode is not permanently damaged by hydrogen evolution, although over a long period of intermittent hydrogen evolution the performance does fall by about 30 %. This could be due to other factors eg. partial flooding of the electrocatalyst, poisoning of the electrocatalyst.

(2) Platinised tungsten trioxide.

The results in table I9 indicate that there was no electrode damage and no loss in hydrogen oxidation performance after passing hydrogen evolution currents up to 380 $mA.cm^{-2}$ for periods of one hour.

(3) Cobalt nickel oxide.

The results in table 20 show that these electrodes were not damaged by oxygen evolution currents up to I $A.cm^{-2}$ and that no oxide films were formed which were stable in the oxygen reduction potential region ie. there was no loss in the oxygen reduction performance. Graph I5 shows the steady state oxygen evolution polarisation curve for this electrode. The O.C.V. following oxygen evolution was increased to high values eg. after oxygen evolution at I.60 V the O.C.V. was I.52 V and steady. for 5 min. However when a potential less than I.52 V was applied the O.C.V. decreased and when the oxygen reduction potential region was reached the O.C.V. had returned to its normal value of I.03 V ie. all the high oxidation state cobalt and nickel species

Table I6.

Hydrogen oxidation polarisation data for a teflon bonded platinum black electrode after constant current hydrogen evolution pretreatments for one hour.

E (mV)	i(mA)				
	A	B	C	D	E
32	3.0	3.0	3.I	3.I	2.9
35	I0.5	I0	I0	I0	I0
40	22	22	22	2I	2I
50	47	48	47	47	45
6I	73	75	76	73	74
75	I08	I08	I07	I05	I05
90	I47	I46	I45	I42	I43
I50	295	295	298	295	296
200	400	398	399	397	400
250	5I0	509	5I0	5I0	508
300	635	635	633	635	633

Electrode area = 0.50 cm^2

Key

	constant cathodic current density ($mA.cm^{-2}$)	comments	time (hours)
A	-	no pretreatment	-
B	I0	-	I
C	50	-	I
D	250	-	I
E	I000	-	I

Table I7.

The effect of rapidly switching cathodic hydrogen evolution currents on the hydrogen oxidation performance of a teflon bonded platinum black electrode.

E (mV)	i(mA) before	i(mA) after
32	2.9	3.0
35	I0	I0
40	2I	2I
50	45	44
6I	74	72
75	I05	I05
90	I43	I42
I50	296	292
200	400	395
250	508	505
300	633	633

Pretreatment

constant current = I $A.cm^{-2}$

on time-off time = 0.5 sec

frequency = I Hz

total time = I hour

Table I8.

Hydrogen oxidation polarisation data before and after two months intermittent hydrogen evolution pretreatment in which 208,000 coulombs.cm^{-2} were passed.

E (mV)	i (mA) before	i (mA) after
35	9.3	6.7
40	20	I4
50	42	29
60	69	48
I50	282	I9I
200	380	260
300	6I2	435

maximum current = I A.cm^{-2}

average switching frequency = 2/ day

average temperature = 20 C

Data for tables I6,I7 and I8.

Electrolyte	5N sulphuric acid
Atmosphere	hydrogen at I atmosphere
Temperature	2I°C
O.C.V.	0.030 V
Electrocatalyst	platinum black
Electrocatalyst S.A.	8.1 $m^2.g^{-1}$
Electrocatalyst loading	6 mg.cm^{-2}
Current collector	platinum screen
Ohmic drop	0.I0 ohm
Electrode area	0.50 cm^2

Table I9.

The effect of hydrogen evolution pretreatments on the hydrogen oxidation performance of a teflon bonded platinised tungsten trioxide electrode.

E (mV)	i(mA.cm^{-2})					
	A	B	C	D	E	F
20	I0	9.7	9.7	9.6	9.9	9.7
25	I7.5	I6	I6	I6	I6	I6
30	25	24	25	25	26	25
35	3I	3I	29	29	30	29
50	50	49	49	50	50	49
75	77	77	79	76	75	75
I00	I04	I05	I03	I03	I0I	I03
I25	I25	I2I	I24	I20	I23	I20
I50	I47	I46	I49	I47	I46	I47
I75	I67	I62	I67	I65	I64	I65
200	I84	I84	I83	I8I	I83	I8I

[redacted]

Key

	constant cathodic current (mA.cm^{-2})	time (hours)	comments
A	-	-	no pretreatment
B	25	I	no electrode damage
C	62	I	no electrode damage
D	I25	I	no electrode damage
E	250	I	no electrode damage
F	375	I	no electrode damage

Data for table I9.

Electrolyte	5N sulphuric acid
Atmosphere	hydrogen at I atmosphere
Temperature	21°C
O.C.V.	+0.018 V
Electrocatalyst	platinised tungsten trioxide
Electrocatalyst loading	9 mg.cm^{-2}
Current collector	platinum screen
Ohmic resistance	0.I5 ohm

Data for table 20.

Electrolyte	5N potassium hydroxide
Atmosphere	oxygen at I atmosphere
Temperature	20°C
O.C.V.	I.035 V
Electrocatalyst	cobalt nickel oxide
Electrocatalyst S.A.	40 m^2/g
Electrocatalyst loading	I0 mg.cm^{-2}
Current collector	nickel screen
Ohmic resistance	0.I0 ohm

Table 20.

The effect of anodic pretreatments on the oxygen reduction performance of a teflon bonded cobalt nickel oxide electrode.

E (mV)	i(mA.cm^{-2})						
	A	B	C	D	E	F	G
I000	0.I9	-	-	-	-	-	-
950	3.I	3.I	3.0	3.0	3.0	3.0	3.0
900	25	24	24	24	24	25	24
850	60	58	59	59	58	58	58
800	96	94	95	96	96	94	93
750	I46	I45	I44	I45	I44	I43	I44
700	202	200	200	202	202	200	I98

Key

	Potential (V)	Anodic current (mA.cm^{-2})	Time (min)	
A	-	-	-	no pretreatment
B	I.40	9.0-2.6	I5	
C	I.60	30-24	I5	
D	I.70	I54-I33	I5	
E	I.80	520-497	I5	
F	I.90	866-8I8	I5	
G	I.95	I000-932	60	

Graph I5.

Oxygen evolution polarisation curve for a teflon bonded cobalt nickel oxide electrode.

Electrolyte 5N KOH

Atmosphere oxygen

Pressure I atmos.

Temperature 20°C

O.C.V. I.035 V

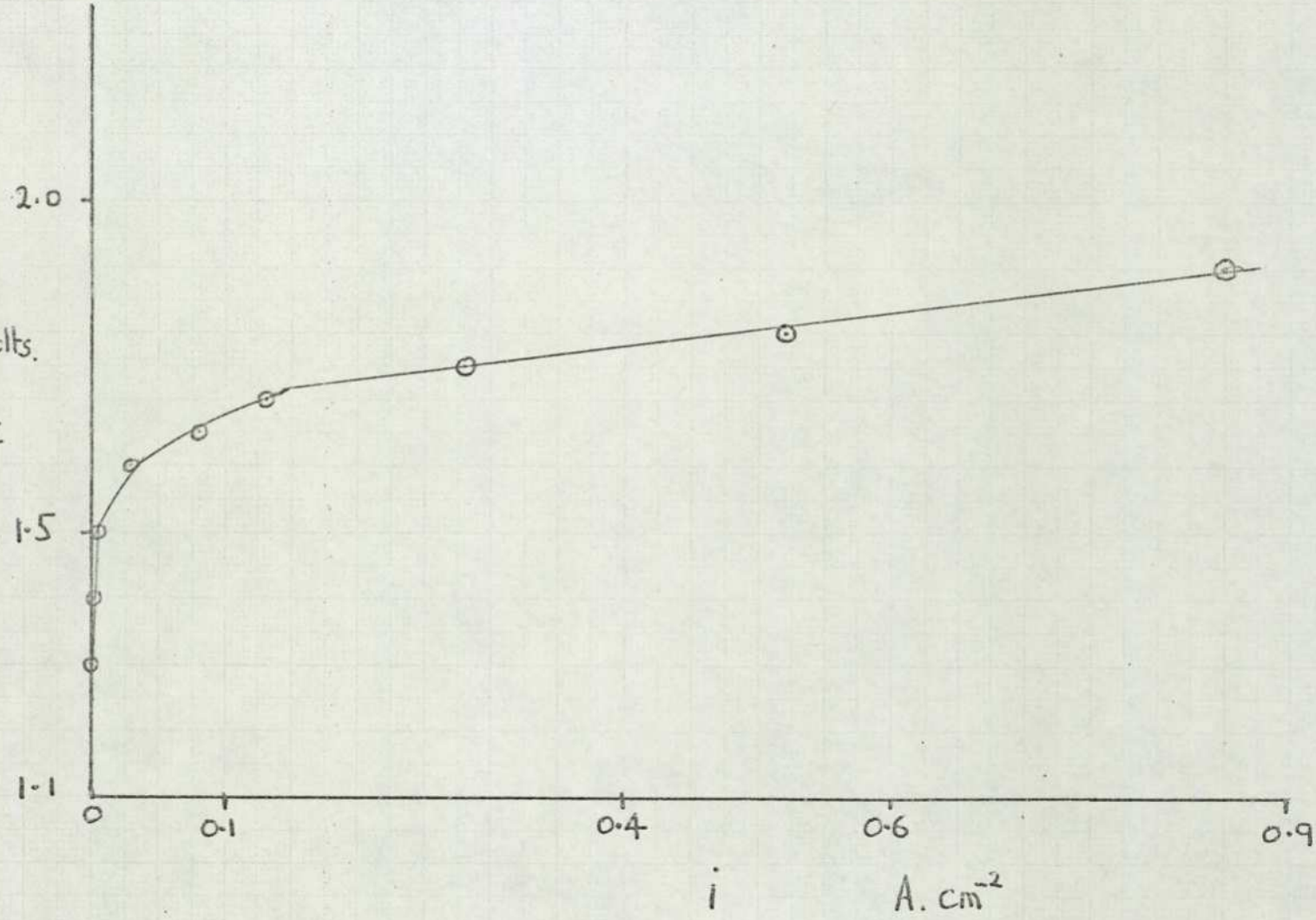
Electrocatalyst cobalt nickel oxide

Electrocatalyst S.A. 40 m^2/g

Electrocatalyst loading I0 $mg.cm^{-2}$

Current collector nickel screen

Ohmic resistance 0.I2 ohm



had been reduced to their stable state at I.00 V.

3.4.4. Discussion.

The results show that none of these electrodes are physically damaged by oxygen or hydrogen evolution even under quite severe conditions. Over a long period ie. two months, there is a significant fall in performance but this is probably not caused by the gas evolution since teflon bonded electrodes which have not been subjected to gas evolution show similar effects over a long period of time. Wetting and poisoning problems, which can be improved by using electrodes backed with teflon tape and by carefully purifying the gases and electrolyte, are probably responsible.

The platinum black electrodes form a surface oxide during oxygen evolution which limits their effectiveness as rechargeable oxygen electrodes but no surface films are formed during hydrogen evolution which are stable in the hydrogen oxidation potential region, thus making them satisfactory as rechargeable hydrogen electrodes.

Teflon bonded platinised tungsten trioxide electrodes would make suitable rechargeable hydrogen electrodes since hydrogen evolution causes neither electrode degradation nor a change in the electrocatalyst surface state which is maintained in the hydrogen oxidation potential region.

Teflon bonded cobalt nickel oxide electrodes would make suitable rechargeable oxygen or air electrodes for the following reasons:

(a) Oxygen reduction performance is equivalent to that of silver/graphite electrodes used at present in

commercial zinc/air cells.

(b) Unlike carbon based electrodes, oxygen evolution results in no electrode degradation.

(c) Oxygen evolution causes no change in the surface state of the electrocatalyst which is maintained in the oxygen reduction potential region. cf. carbon based and noble metal black electrodes.

The electrode materials are far cheaper than noble metal black electrodes and at least as cheap as silver/graphite electrodes. Electrode fabrication techniques for all three types of electrode are similar. Hence, cobalt nickel oxide is the best, known, rechargeable oxygen or air electrode at the present time.

3.5. Oxygen Reduction and Oxygen Evolution on Teflon Bonded Graphite Electrodes in the Absence of H_2O_2

3.5.1. Introduction.

Yeager et al.[34] have noted that it is difficult to interpret steady state polarisation measurements at porous graphite electrodes because of problems associated with mass transport in the pores of the electrode and because of a varying hydrogen peroxide concentration. Since carbon is a poor catalyst for hydrogen peroxide decomposition the hydrogen peroxide concentration builds up continuously during cathodic polarisation, thus changing the polarisation characteristics. Anodic oxygen evolution data is also affected by the presence of hydrogen peroxide since this is decomposed at the same potentials at which oxygen evolution occurs. These problems can be overcome by using the potentiostatic pulse technique to eliminate most mass transfer effects and to limit the quantity of hydrogen peroxide formed

by cathodic polarisation.

3.5.2. Experimental.

Potentiostatic transients were measured over a range of oxygen reduction and oxygen evolution potentials, the 5N potassium hydroxide electrolyte containing no hydrogen peroxide.

3.5.3. Results and Discussion.

The O.C.V. was measured before and after the oxygen reduction transients were recorded as this is a useful guide to the amount of peroxide formed.[35] The O.C.V. was found to fall by 2mV to less noble values after the I msec transient run and by 6 mV after the 4 sec steady state run. Graph I6 compares the oxygen reduction polarisation data after I msec and 4 sec. The I msec transients should eliminate most of the mass transfer polarisation while the effect of hydrogen peroxide is negligible on the I msec transient results. The results were corrected for the ohmic overpotential by the interrupter method.

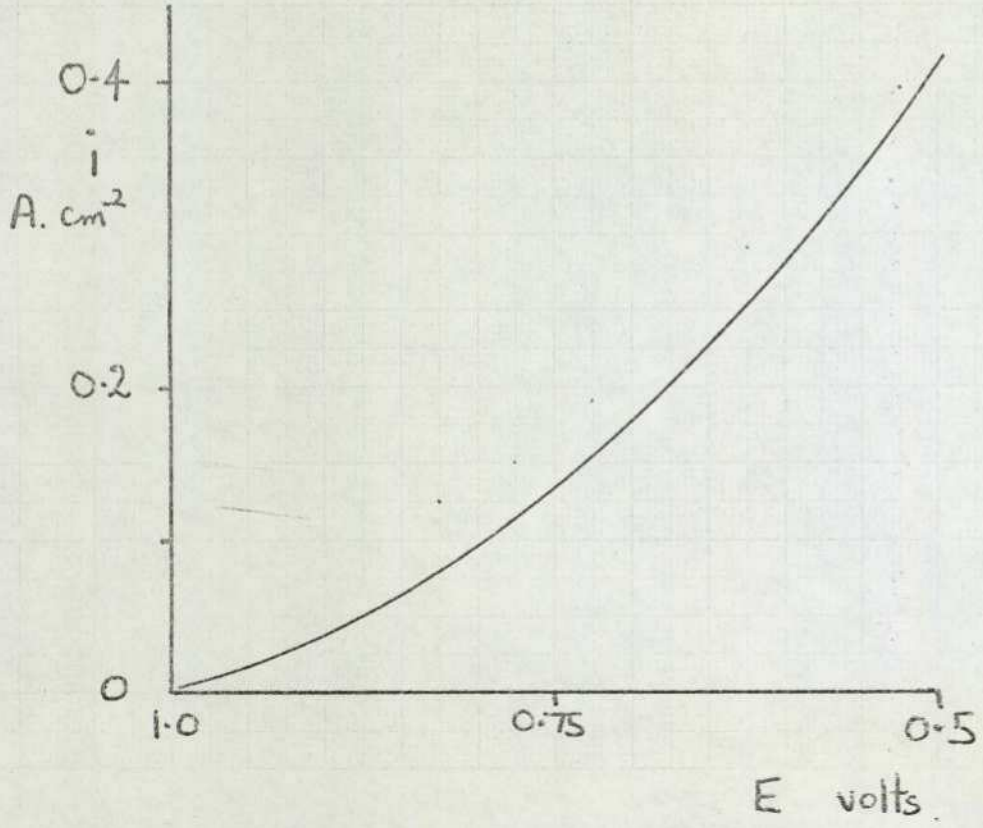
The oxygen evolution transients (graph I7) are complicated by the fact that the anodic currents decay with time, probably due to the formation of graphitic oxides and to the contribution of the nickel screen whose current also decays. This makes it difficult to separate the oxygen evolution and oxide formation currents, especially at short times and to allow for the effect of the oxide surface on the oxygen evolution reaction. It appears that a large proportion of the total transient current (I msec) at low overpotentials is due to oxide formation since it falls rapidly with time to relatively very low values.

Graph I6.

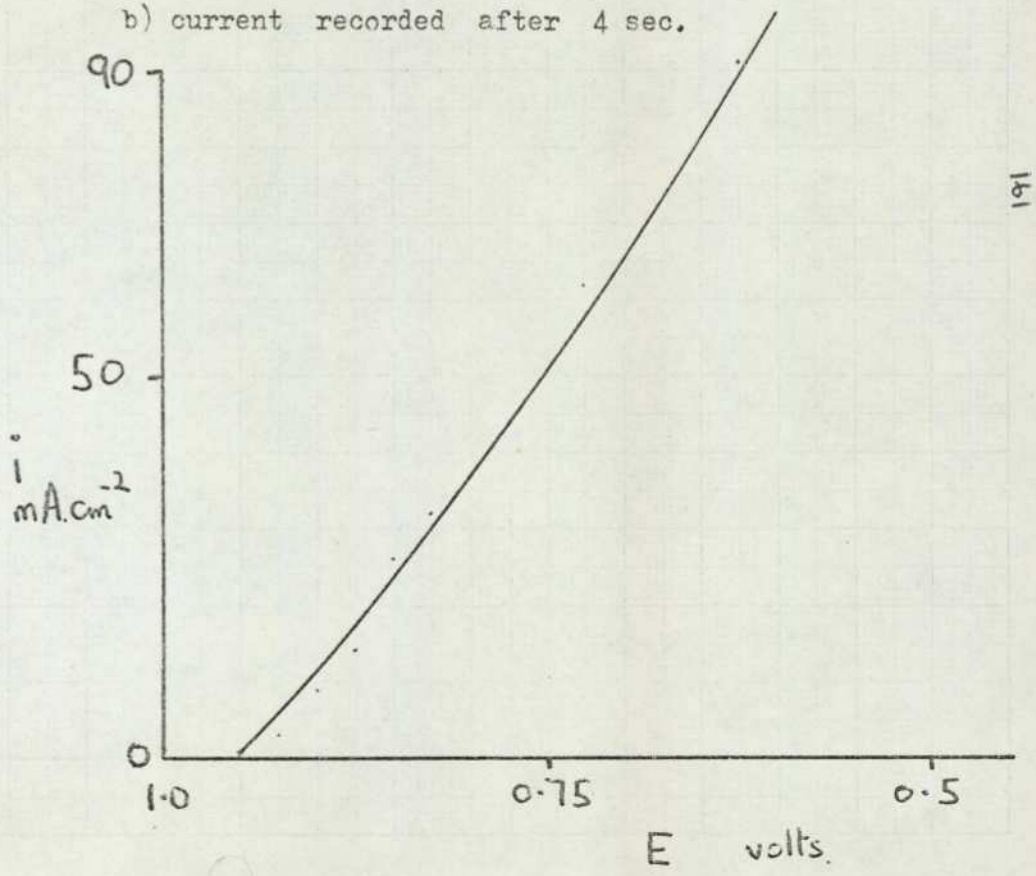
Oxygen reduction transients for a teflon bonded graphite electrode measured after Imsec and 4 sec.

Electrolyte	5N KOH
Atmosphere	oxygen
Pressure	I atmos.
Temperature	2I°C
Ohmic resistance	0.2 ohm
Current collector	nickel screen
Electrocatalyst S.A.	390 m^2/g
Electrocatalyst loading	I0 $mg.cm^{-2}$
Electrocatalyst	graphite
O.C.V.	I.02 V

a) current recorded after I msec.



b) current recorded after 4 sec.



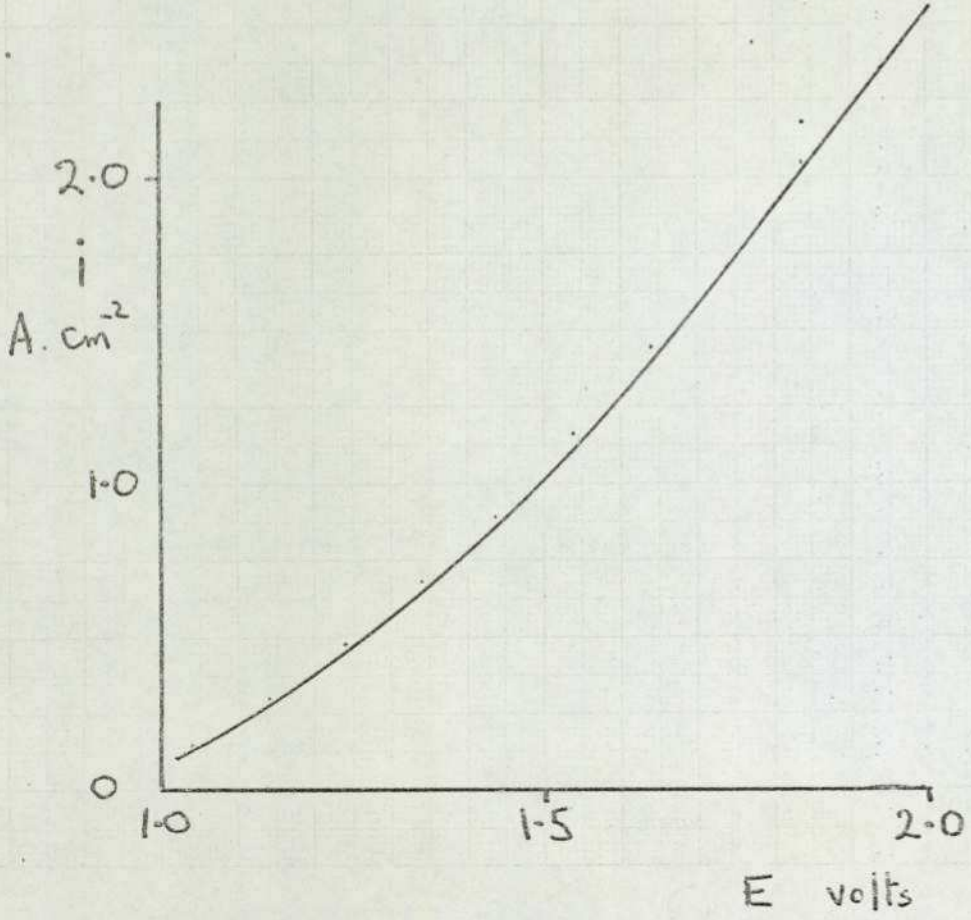
Graph I7.

Oxygen evolution transients for a teflon bonded graphite electrode measured after I msec and 4 sec.

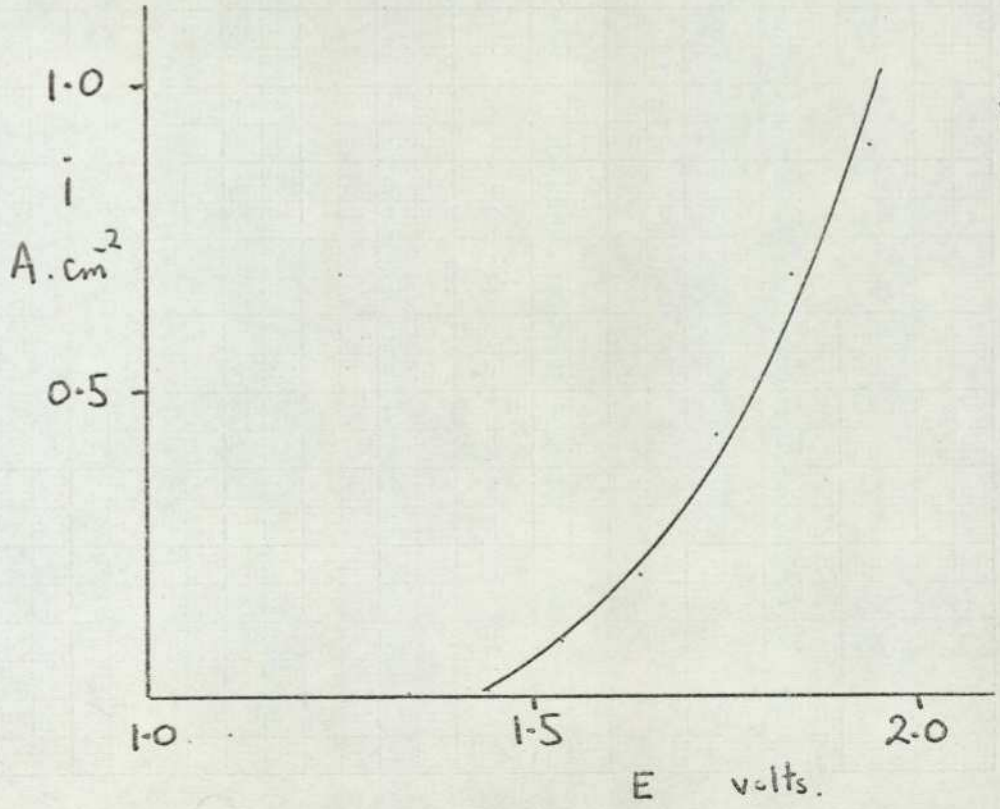
Electrolyte	5N KOH
Atmosphere	oxygen
Pressure	I atmos.
Temperature	22°C
O.C.V.	I.02 V

Electrocatalyst	graphite
Electrocatalyst S.A.	390 m^2/g
Electrocatalyst loading	I0 $mg.cm^{-2}$
Current collector	nickel screen
Ohmic resistance	0.2ohm

a) current recorded after I msec.



b) current recorded after 4 sec.



The results recorded after 4 sec. do not eliminate the mass transfer effects within the pores but the oxide formation current should have decayed to low values. Possible solutions to these problems would be to: (I) eliminate the use of nickel current collector by using graphite cloth or a thin sheet of graphite. (2) initially pretreat the electrode at 2.00 V to produce a stable graphitic oxide layer.

3.6. The Effect of Oxide Film Formation on Rechargeable Oxygen Electrodes.

3.6.I. Introduction.

The potential range in which the oxygen reduction and oxygen evolution reactions occur is about 0.5 - I.9 V. Reference to tables of standard potentials shows that this range is in a relatively anodic region where most metals either dissolve or form passivating oxide films. This is especially true in acid solutions where only the noble metals, tungsten bronzes and tin oxide are not corroded. Several other electrocatalysts such as lithiated nickel oxide and silver can be used in alkaline solution. Obviously any material which dissolves in the electrolyte in this potential range is unsuitable as a rechargeable oxygen electrode. However, even the noble metals, silver and semi-conducting oxides which do not dissolve have the complication that they are themselves oxidised during the oxygen evolution cycle. With metals this takes the form of an oxide film while in semiconducting oxides the oxidation state of the metal is increased. This oxidation is often an essential step in the oxygen evolution reaction mechanism. For rechargeable

TABLE 9.

Electrode Potentials For Metal | Metal Oxide Couples.

Atomic No.	Metal	Oxide Formation Reaction	Potential v. N.H.E. Volts.
75	Re	$2Re + 3H_2O = Re_2O_3 + 6H^+ + 6e$	0.227 − 0.0591 pH
76	Os	$Os + 2H_2O = OsO_2 + 4H^+ + 4e$	0.687 − "
77	Ir	$2Ir + 3H_2O = Ir_2O_3 + 6H^+ + 6e$	0.926 − "
78	Pt	$Pt + H_2O = PtO + 2H^+ + 2e$	0.980 − "
79	Au	$2Au + 3H_2O = Au_2O_3 + 6H^+ + 6e$	1.457 − "
80	Hg	$Hg + H_2O = HgO + 2H^+ + 2e$	0.926 − "
43	Tc	$Tc + 2H_2O = TcO_2 + 4H^+ + 4e$	0.272 − "
44	Ru	$2Ru + 3H_2O = Ru_2O_3 + 6H^+ + 6e$	0.738 − "
45	Rh	$2Rh + H_2O = Rh_2O + 2H^+ + 2e$	0.796 − "
46	Pd	$Pd + H_2O = PdO + 2H^+ + 2e$	0.917 − "
47	Ag	$2Ag + H_2O = Ag_2O + 2H^+ + 2e$	1.173 − "
48	Cd	$Cd + H_2O = CdO + 2H^+ + 2e$	0.005 − "
26	Fe	$Fe + H_2O = FeO + 2H^+ + 2e$	−0.047 − "
27	Co	$Co + H_2O = CoO + 2H^+ + 2e$	0.095 − "
28	Ni	$Ni + H_2O = NiO + 2H^+ + 2e$	0.116 − "
29.	Cu	$2Cu + H_2O = Cu_2O + 2H^+ + 2e$	0.471 − "
30	Zn	$Zn + H_2O = ZnO + 2H^+ + 2e$	−0.439 − "
81.	Tl	$2Tl + H_2O = Tl_2O + 2H^+ + 2e$	0.485 − "
82	Pb	$Pb + H_2O = PbO + 2H^+ + 2e$	0.248 − "
49.	In	$2In + 3H_2O = In_2O_3 + 6H^+ + 6e$	−0.190 − "
50	Sn	$Sn + H_2O = SnO + 2H^+ + 2e$	−0.091 − "

oxygen electrodes this is not important providing the oxide is formed and decomposed at a potential greater than I.26 V ie. the reversible oxygen electrode potential. Unfortunately this is not usually the case and since these oxide films are generally very poor oxygen reduction electrocatalysts and are not electronic conductors, the electrode cannot be used for this reaction until the potential has been reduced to low values to strip off the oxide or hydrogen has been evolved on the electrode surface. In addition, some metal oxides are unstable and dissolve in the electrolyte making electrodes containing these metals unsuitable for recharging.

Table 9 shows the standard electrode potentials of a number of metal/metal oxide couples. All data for this table is taken from the Pourbaix atlas of

From this table it can be seen that only gold is free from oxide at the reversible oxygen electrode potential. Under anhydrous conditions silver is also free from oxide at this potential. Apart from these metals only iridium, platinum and mercury form their lowest oxide at potentials greater than 0.90 V. Hence even if the oxygen electrode system were intensively purified in order to achieve the reversible oxygen electrode potential, the oxygen reduction performance at low overpotentials would still be very poor for the vast majority of metals due to the presence of oxide films. These films are often nonconductors and poor oxygen reduction electrocatalysts.

For metals of atomic number 76-79 platinum is the most active for oxygen reduction in potassium hydroxide electrolyte because while an oxide surface

inhibits the reduction of oxygen to hydrogen peroxide it promotes the catalytic conversion of hydrogen peroxide to water. This is probably because the negative dipoles of the oxide film inhibit the first stage which occurs only through an electron transfer process while the oxide film can participate in the chemical conversion of hydrogen peroxide to water. (I32)

$$H_2O_2 + Pt\text{-}O = Pt + O_2 + H_2O$$

For this reason platinum, which has an oxygen surface coverage of about 25% at its rest potential (I34) is more effective as an oxygen reduction electrocatalyst than gold which has a very low oxygen surface coverage of about 3% at its rest potential (I33) which inhibits the second stage of the reaction. Platinum appears to have the optimum oxygen surface coverage of this group of noble metals, causing severe inhibition of neither reaction. However, after anodisation at I.9 V gold is ten times more active than platinum at 0.9 V (I35,I33) because the platinum still has a high coverage of oxide (said to be a monolayer at I.IO V (78)) which is not reduced until lower potentials are reached while the gold oxide was fully reduced at potentials higher than I.0 V. It has been reported that for platinum it is necessary to reduce the potential below 0.55 V to completely reduce the oxide (94). Hence the importance of the formation and reduction of oxide films on metals and their effect on the oxygen reduction performance of rechargeable electrodes can be clearly seen.

3.6.2. Experimental.

The steady state oxygen reduction polarisation

data for a teflon bonded platinum black electrode were compared before and after anodic pretreatment at 2.00 V for ten minutes. After this pretreatment the electrode was left overnight to reach equilibrium before taking the oxygen reduction polarisation measurements. This procedure was repeated recording the oxygen reduction polarisation data by linear sweep voltamograms at moderately fast sweep rates (0.5 V/min). This is a more accurate and reproducible method of plotting i/E curves when i varies with time. Experiments were carried out in air and oxygen atmospheres.

3.6.3. Results.

After oxygen evolution the rest potential is raised to a value of about I.45 V. This rest potential decays with time and after leaving overnight had fallen to I.0I7 V which was steady within ± I mV over a period of thirty minutes. This is not much different from the O.C.V. before anodic pretreatment ie. I.045 V. Care was taken to ensure that the O.C.V. was constant otherwise the current varies with time during the polarisation run, due to the reduction of higher platinum oxides eg. PtO_2 or PtO_3. The results are compared in table 37.

Before pretreatment the O.C.V. under air and oxygen differed by about IO mV, the air electrode having the lower value. After pretreatment and equilibration the O.C.V. under air and oxygen was the same (±2 mV). The steady state polarisation curve under an oxygen atmosphere shows that the oxygen reduction is inhibited at potentials above 0.65 V after anodic pretreatment. The linear sweep voltamograms

TABLE 37.

Steady State Oxygen reduction i-E data on clean and preanodised teflon bonded platinum black electrodes.

(a) preanodised.				(b) clean		clean	
E volts.	i	E volts	i	E volts	increasing i mA	decreasing i mA	
1.021	1 μA	0.600	200 mA	1.020	0.040	0.09	Electrolyte 5N H_2SO_4
1.002	3-1	0.576	253	1.000	0.080	0.24	Temp. 20°C
0.983	5-3	0.550	284	0.975	0.19	0.73	Atmosphere O_2
0.971	9-6			0.950	0.48	1.53	O.C.V. clean 1.04V
0.958	14-9			0.925	1.1	3.6	O.C.V. oxide 1.027V
0.945	24-15			0.900	2.6	6.5	Electrode Area 0.4cm^2
0.933	31-18			0.875	5.8	11.3	Electrocatalyst S.A. 16$m^2.g^{-1}$
0.920	36-22			0.850	11.5	18	" loading 5$mg.cm^{-2}$
0.908	41-25			0.800	30	41	Current Collector Pt gauze
0.896	48-38			0.750	62	71	Resistance 0.08ohm.
0.884	62-49			0.700	105	118	
0.871	90-68			0.650	153	163	
0.858	112-103			0.550	277	270	
0.852	144-130						
0.845	185-182						
0.839	245-255						
0.826	440-590						
0.808	1.58-1.73mA						
0.788	4.0-4.6						
0.770	10.5-12.0						
0.752	21.5-25.0						
0.726	49-53						
0.701	83-87						
0.676	118-121						
0.651	152-153						
0.626	183-187						

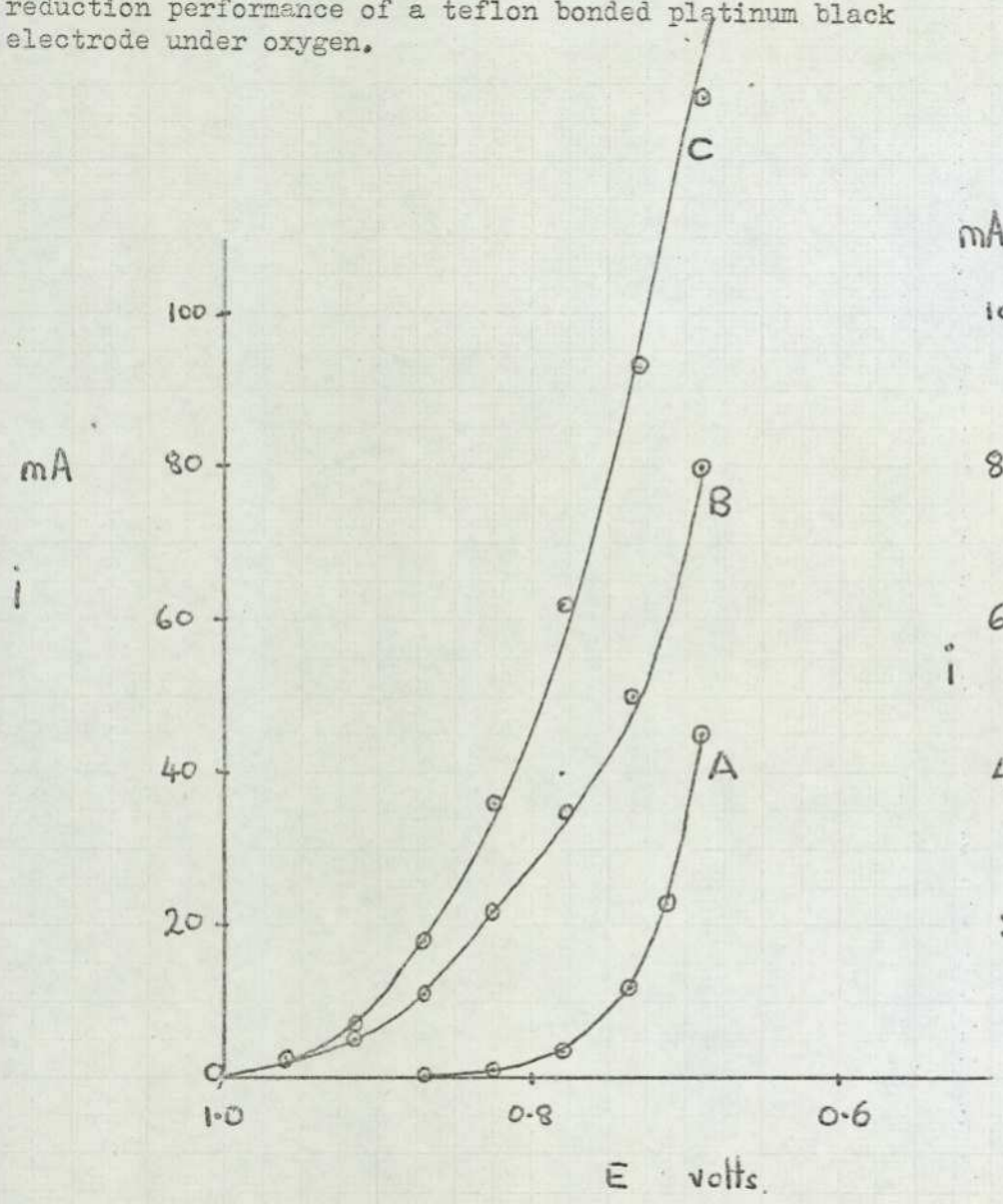
recorded under oxygen and air atmospheres (graphs 21 and 22) show clearly that the oxygen reduction performance is inhibited over four sweeps (two forward and two reverse) after pretreatment.

3.6.4. Discussion.

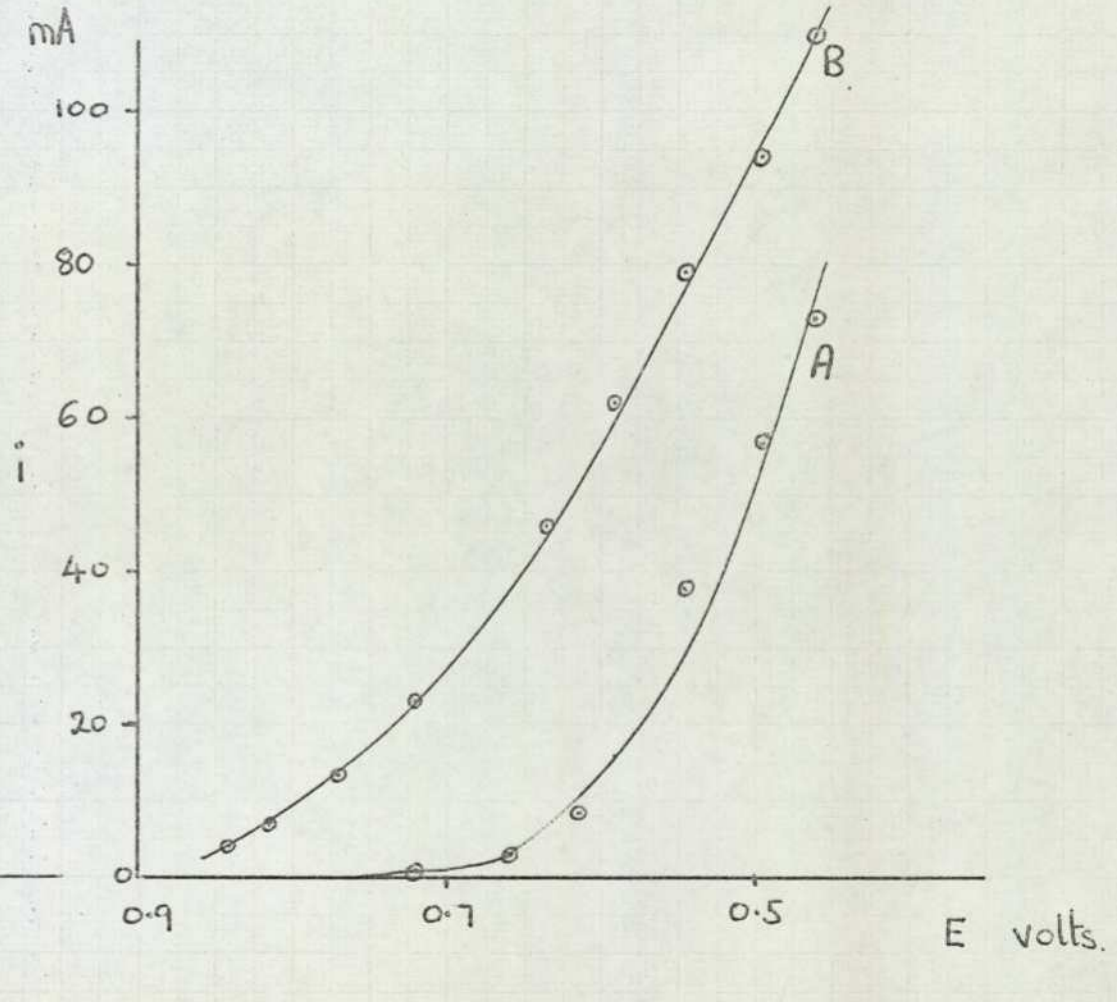
When platinum is held at a potential of 2.00 V three surface oxides are formed (PtO, PtO_2 and PtO_3). Following this anodic pretreatment the O.C.V. is increased to about 1.45 V and this value falls steadily with time. (Graph 18) If the electrode is switched to a potential in range $0.85\ V < E < 1.0\ V$ for five minutes and then back to open circuit the O.C.V. remains significantly greater than the O.C.V. prior to anodic pretreatment. If the electrode is switched to a potential less than 0.8 V for five minutes the O.C.V. returns to a value close to the original. This indicates that the oxide film is only reduced at potentials less than 0.85 V.

The decrease in the O.C.V. with time indicates that some of the oxides are decomposing. The final steady O.C.V. could correspond to a clean surface or to a PtO surface. If it were a clean surface the oxygen reduction performance would be expected to be the same as before the anodic pretreatment. The limits of the domains of relative stability of platinum and its oxides are shown in table 9, and it can be seen that at the steady O.C.V. after anodic pretreatment the only stable oxide is PtO, the other two oxides decomposing spontaneously at higher potentials. The steady state current which was measured after 30 secs. at each potential, increased with time when $845\ mV > E > 660\ mV$. This is due to the reduction of the surface oxide.

Graph 22. The effect of anodic pretreatment on the oxygen reduction performance of a teflon bonded platinum black electrode under oxygen.



Graph 2I. The effect of anodic pretreatment on the oxygen reduction linear sweep voltammograms of a teflon bonded platinum black electrode under air.



Graph 2I. Data.

Electrolyte	5N H_2SO_4
Atmosphere	air
Temperature	2I C
O.C.V. (anodised)	I.02 V
O.C.V. (clean)	I.03 V
Electrocatalyst	platinum black
Electrocatalyst S.A.	I6 m^2/g
Electrocatalyst loading	6 $mg.cm^{-2}$
Current collector	platinum screen
Sweep rate	550 mV/min
Resistance	0.I5 Ohm
Pretreatment	3 min at 2.00 V

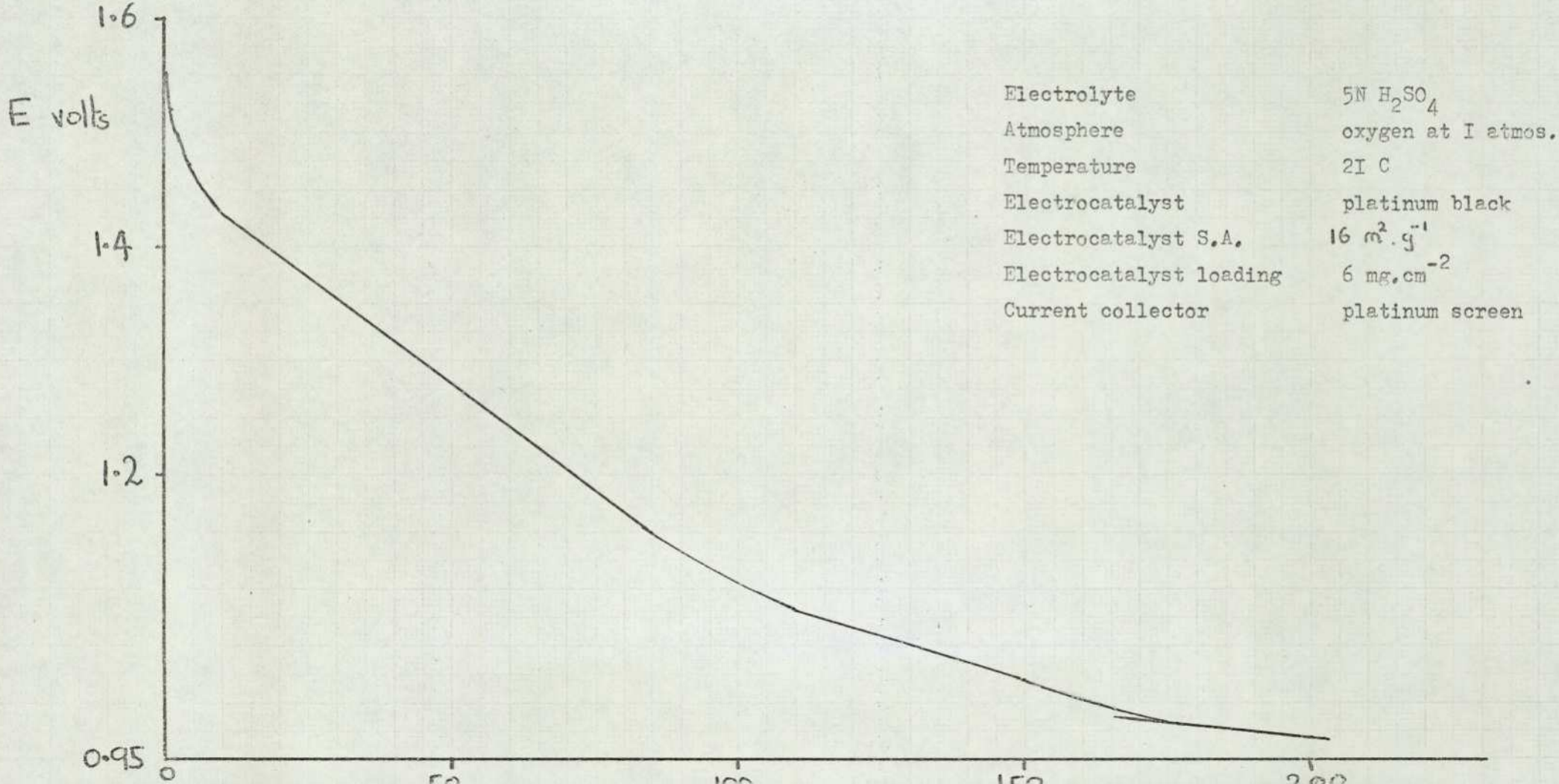
A first sweep following pretreatment
B third and subsequent sweeps after anodic pretreatment

Graph 22. Data.

Electrolyte	5N H_2SO_4
Atmosphere	nitrogen at I atmos.
Temperature	22 C
O.C.V. (anodised)	I.02 V
Electrocatalyst	platinum black
Electrocatalyst S.A.	I6 m^2/g
Electrocatalyst loading	6 $mg.cm^{-2}$
Current collector	platinum screen
Resistance	0.I5 ohm
Sweep rate	400 mV/min
Anodisation time	3 min

A first sweep following anodic pretreatment
B second sweep following anodic pretreatment
C fourth sweep " " " (alloxide reduced

graph 18 Open circuit potential - time curve following anodic pretreatment (5 min at 2.00 V).



Electrolyte	5N H_2SO_4
Atmosphere	oxygen at I atmos.
Temperature	2I C
Electrocatalyst	platinum black
Electrocatalyst S.A.	16 $m^2.g^{-1}$
Electrocatalyst loading	6 $mg.cm^{-2}$
Current collector	platinum screen

The steady state current fell with time when 1.02 V > E > 845 mV due to a reduction in the thickness of the oxide film which has been shown to be a linear function of potential.(78) This suggests that above 845 mV the platinum oxide film is passive, while at lower potentials it is spontaneously reduced to the bare metal.

A comparison of the polarisation data before and after anodic pretreatment shows that at potentials above 850 mV the current after anodic pretreatment is more than two orders of magnitude smaller than before the pretreatment. This is especially significant when one considers that the current is decaying with time. In the potential range 850-660 mV the performance gradually recovered reaching the original level at about 625 mV. A polarisation curve recorded after the oxide had been stripped off showed that the reduction in performance due to the oxide was only temporary. It can be seen that if platinum were to be used as a rechargeable oxygen electrode in, for example, a metal-air battery it would be ineffective for oxygen reduction after recharging at the normal operating potential ie. zinc-air cells are operated at about 1.4 V and have an O.C.V. of 1.6 V. Hence it would be necessary to apply a heavy polarisation to the battery, initially after recharging, to reduce the PtO, although unless this procedure is timed carefully, a large current will be drawn from the cell, reducing its discharge time at a given current. From the results in table 37. it can be seen that a potential less than 700 mV is required for rapid oxide reduction. Although this is a

disadvantage it does not preclude the use of this type of electrodatalyst as rechargeable oxygen electrodes, cf. carbon based electrodes, and is much superior to employing a third electrode in the cell.

The linear sweep voltamograms show that the current at 900 mV after pretreatment is nearly two orders of magnitude less than before pretreatment under oxygen while under air at 700 mV the current after pretreatment is two orders of magnitude less than before pretreatment (graph 23). Possible reasons for this difference are: (a) oxygen reduction currents on the oxide surface under oxygen are greater than under air. (b) pretreatment for oxygen atmosphere was twice as long at the same potential as the pretreatment under air, hence there is more oxide on the electrode tested under oxygen resulting in a higher oxide reduction current than that for the electrode tested under air. The fact that the oxygen electrode required more sweeps to remove all the oxide than the air electrode can be explained by (b) above, in both cases - oxygen electrode I.02 V - 0.65 V, air electrode I.02 V - 0.45 V. Because of the interference by anodic oxide films it was decided to study some aspects of the formation and reduction of these films on platinum in greater detail.

3.7. Oxygen Reduction on Platinum Oxide Films and the Electrolytic Reduction of these Films.

3.7.I. Introduction.

The growth of anodic oxide films on platinum depends on the polarisation potential, temperature, duration of anodisation, and especially on the surface state of the electrode, which can be altered by

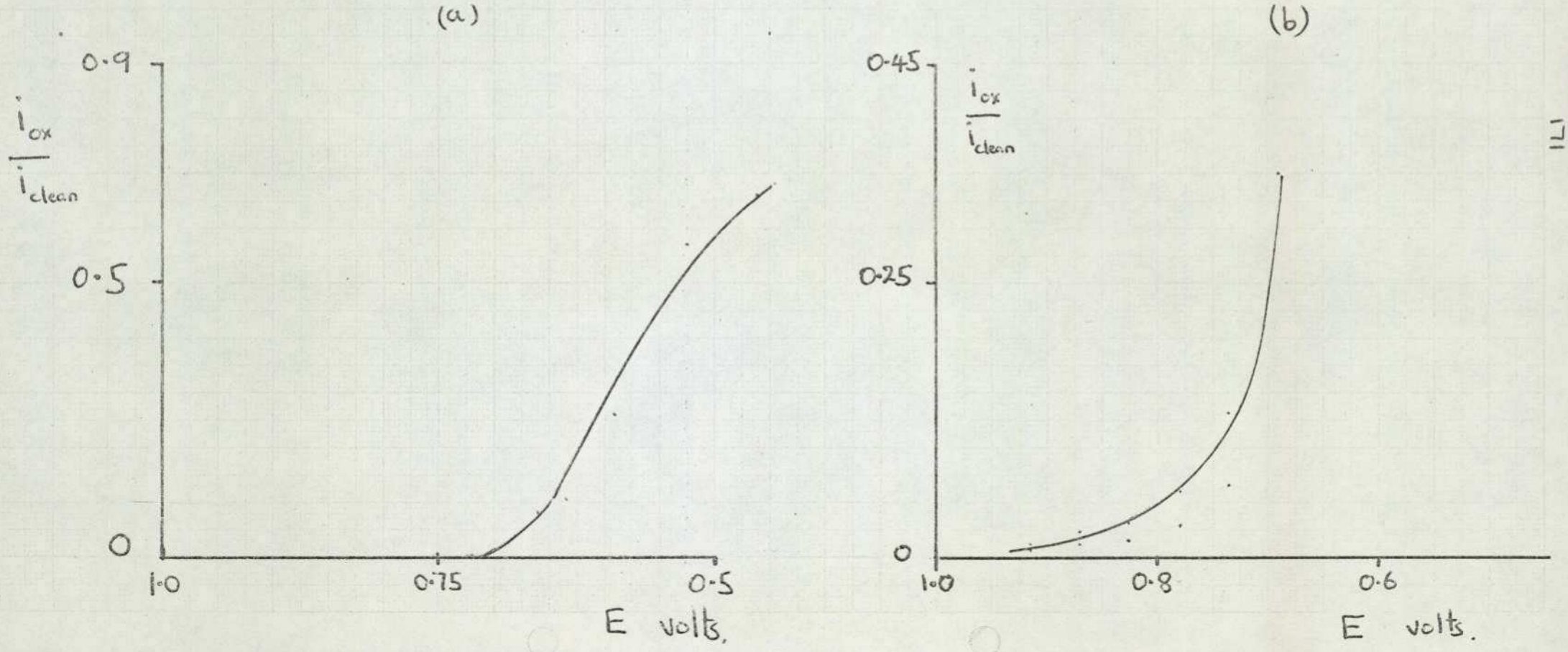
Graph 23.

Comparison of oxygen reduction on clean and anodised surfaces under air and oxygen atmospheres.

Electrolyte $5N\ H_2SO_4$
Temperature $20^\circ C$
Electrocatalyst platinum black
Electrocatalyst S.A. $16\ m^2.g^{-1}$
Electrocatalyst loading $6\ mg.cm^{-2}$
Current collector platinum screen
Ohmic resistance 0.I0 ohm

a) Atmosphere Air at I atmos.
Sweep rate 550 mV/min.

b) Atmosphere oxygen at I atmos.
Sweep rate 400 mV/min.



pretreatment. If any of these conditions is not stipulated reproducible results will not be obtained. Although there have been many investigations of the anodic oxide film formed on platinum, there is still little agreement on its nature or extent, often because the conditions of formation and reduction of the film have not been fully stipulated.

The enhanced catalytic activity of platinum after anodisation, for a number of electrochemical processes, has been explained as being due to facilitated electron transfer from the oxidised platinum surface by the oxygen bridge mechanism [80] or alternatively a chemical reaction is responsible in which the reagents react directly with the oxidised surface, which is unstable in the presence of reducing agents. [81] The enhanced activity of platinum which has been oxidised and then reduced is said to be due to the formation of a thin platinised layer. [82] This theory is supported by the marked roughening on the platinum surface under a-c conditions [83] and disputed by Gilman [84] who has shown that only a small increase in area is produced by one polarisation cycle and then only if the oxide is reduced very quickly. Feldberg et al [85] attributed the enhanced activity to a layer of PtOH while Wieke and Welbus [86] have suggested impurity desorption.

The effect of an oxide film of platinum has usually been shown to inhibit the oxygen reduction reaction [87,88] although sometimes it has been shown that the reaction rate was accelerated. [89] The mechanism of the oxygen reduction reaction on a clean platinum

surface is confused because some workers claim the formation of hydrogen peroxide [90] while others have shown its absence. [88] It is evident from the literature that a wide variation of results has been obtained under different conditions in acid electrolytes even when the platinum has not been anodised. This situation has resulted from the insufficiently precise specification of the experimental conditions. Recent work under high purity conditions has shown that oxygen reduction on clean platinum and oxidised platinum is kinetically different [68] and that hydrogen peroxide [74] is produced by adsorbed impurities in a reaction which occurs parallel to the main reduction of oxygen direct to water. Hence the importance of specifying the purity level of the electrolyte and reactant can be seen.

Appleby [91] has studied the oxygen reduction reaction in 85% ortho phosphoric acid on platinum foil which had previously been subjected to a variety of pretreatments. Three different surfaces were produced, each having different oxygen reduction kinetics:

(I) a fully oxidised surface produced by anodising at 2.00 V;

(2) an oxide free surface, considered to have oxygen adsorbed in less than monolayer quantity, and

(3) an active surface consisting of a partially reduced oxide film. This active platinum surface was found to be a better oxygen reduction electrocatalyst than either the oxidised or the oxide free surfaces. However neither the active or oxidised surfaces are stable with time at about 800 mV, both being gradually converted to the oxide free surface. Under typical fuel cell operating conditions it was shown that the oxide

free surface was superior to the oxidised surface but inferior to the active surface although the performance of the latter declined as it was converted to the oxide free state. The nature of the active surface has not been definitely characterised although it probably involves dermasorbed oxygen in the disordered outermost layers of the platinum.

It has been shown [92] that anodisation of platinum causes a penetration of oxygen into the metal lattice deeper than the dermasorbed layer, in a similar way to the action of concentrated nitric acid. [93] The higher the anodisation potential the more deeply the oxygen penetrates. This dissolved oxygen has been used to explain the different properties of anodised and clean platinum electrodes and the fact that initially the amount of charge required to form a monolayer of adsorbed oxygen anodically is not equal to the charge needed to reduce the monolayer cathodically. [94]

Another explanation for the temporary enhanced activity of platinum following an oxidation - reduction cycle is that rearrangement of the platinum atoms occurs when strong platinum-oxygen bonds are formed in the surface film. [95] When the oxygen atoms are removed on reduction the rearranged platinum atoms take a finite time to return to their regular lattice positions, the time increasing with the potential and duration of the anodisation.

Two models have been proposed for the growth of anodic oxide films on platinum: (I) The high field ionic conduction model [78] in which the overpotential appears across the anodic oxide film and the log of

the ionic current density is proportional to the field in the oxide, (2) The place exchange model.[64] At present neither model has sufficient experimental backing. If the high field model is applicable then oxygen evolution would be due to an electronic tunnelling current which flows through the oxide film to the metal once its potential is high enough. Optical measurements on the high field model suggest that a monolayer starts to form at I.0 V and is complete at I.I V. There is little experimental evidence for the place exchange model except that the film thickness is a linear function of potential, a fact which is true for both models.

At very high anodic potentials eg. 2.I V multilayer oxide films have been reported.[96,97] The growth rate of these films is very slow compared with monolayer films and at potentials above 2.I9 V cease to form at all. Reduction of these multilayer oxide films results in large increases in the roughness factor of the electrode surface. The lowest potential recorded for the formation of multilayer oxide films is I.8 V.

Anodic oxide films on platinum often inhibit electro-oxidation processes eg. oxidation of ethylene.[98] Hence the rate at which these films can be removed by hydrogen gas dissolved in the electrolyte is of some significance. The reaction has been shown to proceed at a rate inversely proportional to the oxide coverage.[99] This has been interpreted as being due to the inhibition of the electrochemical oxidation of hydrogen by adsorbed oxygen species. Hence as the oxide

is reduced the inhibition of hydrogen oxidation is reduced resulting in an increase in the rate of oxide reduction.

In the present work it was decided to investigate the stability of the oxide film formed by the pre-anodisation of platinum. The potential range in which the oxide film is passive is to be determined and with this information the oxygen reduction kinetics on the oxide film are to be studied in the passive potential region and compared with the oxide reduction polarisation data in both passive and active potential regions.

As an extension of this work the process for oxide formation by the electrolytic discharge of water molecules is to be investigated in an attempt to find the rate law for oxide film growth. With this information it is hoped to elucidate some of the problems associated with the oxygen evolution reaction by investigating the rate of decay of the oxygen evolution current and attempting to relate it to the growth of an oxide film.

3.7.2. Experimental.

Potentiostatic transient measurements in the potential range 0.6 V - I.0 V were made on a pre-anodised electrode in oxygen and nitrogen atmospheres in order to determine the proportion of the current on an oxide surface that is due to oxygen reduction and the proportion that is due to oxide reduction. The separation of these two components is important in the study of oxygen reduction on oxide surfaces.

Linear sweep voltamograms in the oxygen reduction potential region on preanodised electrodes under oxygen and nitrogen atmospheres were recorded. This should be a better method of seperating the two currents since in the region where the oxide film is passive the oxide reduction current decays with time to very low values of the order of $\mu A.cm^{-2}$. However, it is important to know the limit of this passive region and the current decay characteristics under oxygen and nitrogen.

3.7.3. Results and Discussion.

Current-time data for oxide/oxygen reduction under oxygen and nitrogen in the potential range I.00 V - 0.70 V for platinum foil electrodes preanodised for one minute at I.80 V, are shown in table 2I. The time period over which measurements were taken was 5 sec. to about 4 min. These results show that at potentials $\geq$ 0.90 V the current at times up to 3 min. is almost the same under oxygen or nitrogen. At potentials $\leq$ 0.80 V the current under oxygen is higher than that under nitrogen the difference increasing with time ie. at 0.80 V after I0 sec. the current under nitrogen is 0.76 of the current under oxygen while after 2 min. the current under nitrogen is only 0.I5 of the current under oxygen. The explanation is that the oxide film is not reduced until the potential falls below about 0.80 V and that at higher potentials almost the entire current is due to a reduction in the thickness of the oxide film. If any oxygen reduction on the oxide surface occurs the resulting current must be very small in comparison with the oxide reduction current. The most likely reason for the difference in current observed with oxygen and nitrogen

Table 2I.

Cathodic current - time curves for a preanodised platinum foil electrode under oxygen and nitrogen.

Time (sec)	700mV		800mV		900mV		950mV	
	O_2	N_2	O_2	N_2	O_2	N_2	N_2	O_2
	$i(\mu A.cm^{-2})$							
5	I73	34.7	23.I	I9.2	8.03	6.74	3.06	3.06
I0	I50	20.2	I6.4	I2.5	4.4	4.04	2.02	I.9I
I5	I34	-	I3.8	9.6	3.25	2.88	I.54	I.44
30	II5	I2.5	II.9	6.0	I.82	I.64	0.96	0.96
60	94	4.8	II.7	3.85	I.I5	0.96	0.29	0.57
I20	75	3.I	I2.7	2.4	0.76	zero	0.I5	0.38
I80	63	2.3	-	I.92	0.57	-	zero	0.28
300	52	I.73	-	-	-	zero	-	-
360	-	-	-	I.25	0.38	-	-	-
600	-	-	I3.I	-	-	-	-	-

Electrolyte 5N H_2SO_4

Temperature 2I°C

Atmospheres oxygen and nitrogen at I atmos.

Electrocatalyst platinum foil

Resistance 0.I0 ohm

Anodic pretreatment I min at I.80 V then held at I.05 V till i = 0

atmospheres at potentials $\geq$0.90 V as the time increases is that as oxide is reduced some bare platinum metal is exposed on which oxygen reduction occurs. In the study of the reversible oxygen electrode on a platinum oxide surface about the potential I.26 V it has been reported that in order to obtain the cathodic oxygen reduction data these measurements must be taken quickly, and immediately following preanodisation.[68] At potentials less than about 0.80 V the oxide film is reduced spontaneously and consequently this limits the potential to the range I.26 - 0.85 V. However even within this range the oxide film thickness varies with potential, hence when the potential is lowered a current flows which is due to (a) oxide reduction and (b) oxygen reduction on the oxide surface and/or (c) oxygen reduction on the bare metal surface. With increasing time (a) falls to near zero and the current is due to either (b) or (c) depending on whether a complete monolayer film still exists. The decay of (a) to zero can take up to five minutes, hence if the cathodic measurements are made quickly after preanodisation a significant proportion of the current would be due to oxide reduction. This is especially true at potentials above about I.07 V where the higher platinum oxides are spontaneously reduced.[68] Damjanovic and Appleby[155] wait until an approximate steady state is achieved before recording the current. This method allows the oxide reduction current some time, one minute in Appleby's experiments, to decay. However this time is not sufficient for the oxide reduction current to decay to zero and since this current is initially much greater than the oxygen

reduction current on a clean surface it remains significant even after 4 min. If readings in the potential range I.26 V - 0.85 V are to be made after, say 5 min., it is necessary to check that the surface is still covered with a monolayer after this time. This seems likely since the oxide is not spontaneously decomposed at potentials $\geqslant$ 0.85 V. The coverage can be determined by measuring the area under the oxide reduction current - time curve. Assuming that the oxide surface is PtO, a monolayer corresponds to about 640 μ.coulombs.cm.$^{-2}$ (I55) (Graph 45)

The importance of the influence of oxide reduction currents on oxygen reduction polarisation data on a platinum oxide surface is emphasised in table 22 where linear sweep polarisation curves on preanodised platinum black electrodes, recorded under oxygen and nitrogen, are compared with a similar curve on a clean platinum surface under oxygen. Using a sweep rate 0.40 V/min. it was shown at potentials $>$ 0.80 V the curves for the oxide surface under oxygen and nitrogen were almost identical and that at 0.70 V the current under nitrogen is still approximately 25% of that under oxygen. These currents on the oxide surface at potentials $>$0.80 V are more than an order of magnitude smaller than equivalent oxygen reduction currents on a clean surface. Hence it is essential to check that the oxide reduction current has decayed to zero and that there is at least a monolayer coverage when the oxygen reduction current is recorded. The oxide coverage is determined by pretreating the electrode for one minute at I.80 V, followed by holding it at the required potential for a certain time before a cathodic potential sweep was

Graph 45.

Linear sweep oxide stripping curve for a platinum foil electrode pretreated for I min. at I.80 V and then held at 0.85 V for 5 min.

Electrolyte	5N H_2SO_4
Temperature	20°C
Atmosphere	nitrogen
Pressure	I atmos.
Electrocatalyst	platinum foil
Resistance	0.06 ohm
Sweep rate	0.8 V/min.

Area under curve between 0.50 V and 0.85 V = II60 $\mu c.cm^{-2}$

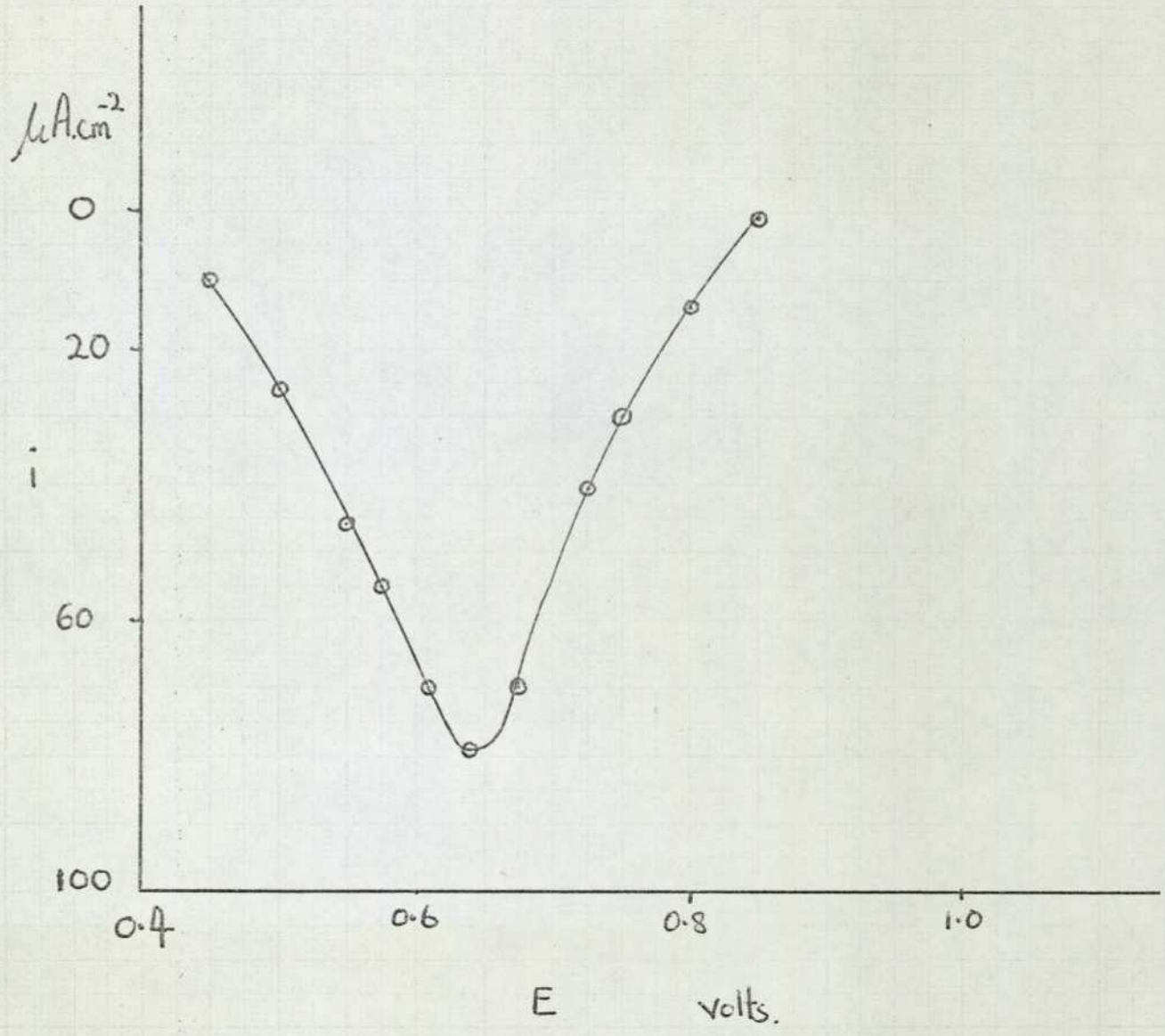


Table 22.

Linear sweep voltammogram data on preanodised platinum black under oxygen and nitrogen.

clean surface under oxygen		oxide surface under oxygen		oxide surface under nitrogen	
$i(mA.cm^{-2})$	mV	$i(mA.cm^{-2})$	mV	$i(mA.cm^{-2})$	mV
3.4	960	0.2	915	0.4	922
6.0	915	0.8	870	I.2	880
20.6	870	2.2	825	2.0	838
52	825	7.0	780	4.2	796
I02	780	25	735	8.0	754
I68	735	86	690	I6	7I2
248	690				

Electrolyte	5N H_2SO_4
Temperature	2I°C
Atmospheres	oxygen and nitrogen at I atmos.
Electrocatalyst	platinum black
Sweep rate	0.4. V/min
Pretreatment	5 min at 2.00 V then held at I.05 V till i = 0

applied and the area under the curve measured. These results confirm that at potentials > 0.85 V a monolayer of oxide exists even after times of up to 5 min. The current-voltage and Tafel plots for oxygen reduction on a platinum oxide surface after the oxide reduction current had decayed to zero are shown in graph 24. Comparing the results with those of Damjanovic [68] and Appleby [155] it can be seen that the Tafel slopes and exchange current densities are in reasonable agreement considering that Damjanovic used 1N $HClO_4$ and 1N KOH and Appleby, 85% orthophosphoric acid, and that there were small differences in temperature. Appleby [155] also shows that at low temperatures ie. 25°C, a monolayer of oxide exists on platinum after several minutes at 850 mV v. a bubbling hydrogen electrode in the same solution (H.R.E.) following a similar anodic pretreatment. Since Appleby states that PtO is unstable in 85% orthophosphoric acid it would be expected that the coverage in 5N H_2SO_4 would be at least as great. The current densities for oxygen reduction in this work were about an order of magnitude greater than those of Appleby and this could be attributed to the high viscosity of his electrolyte.

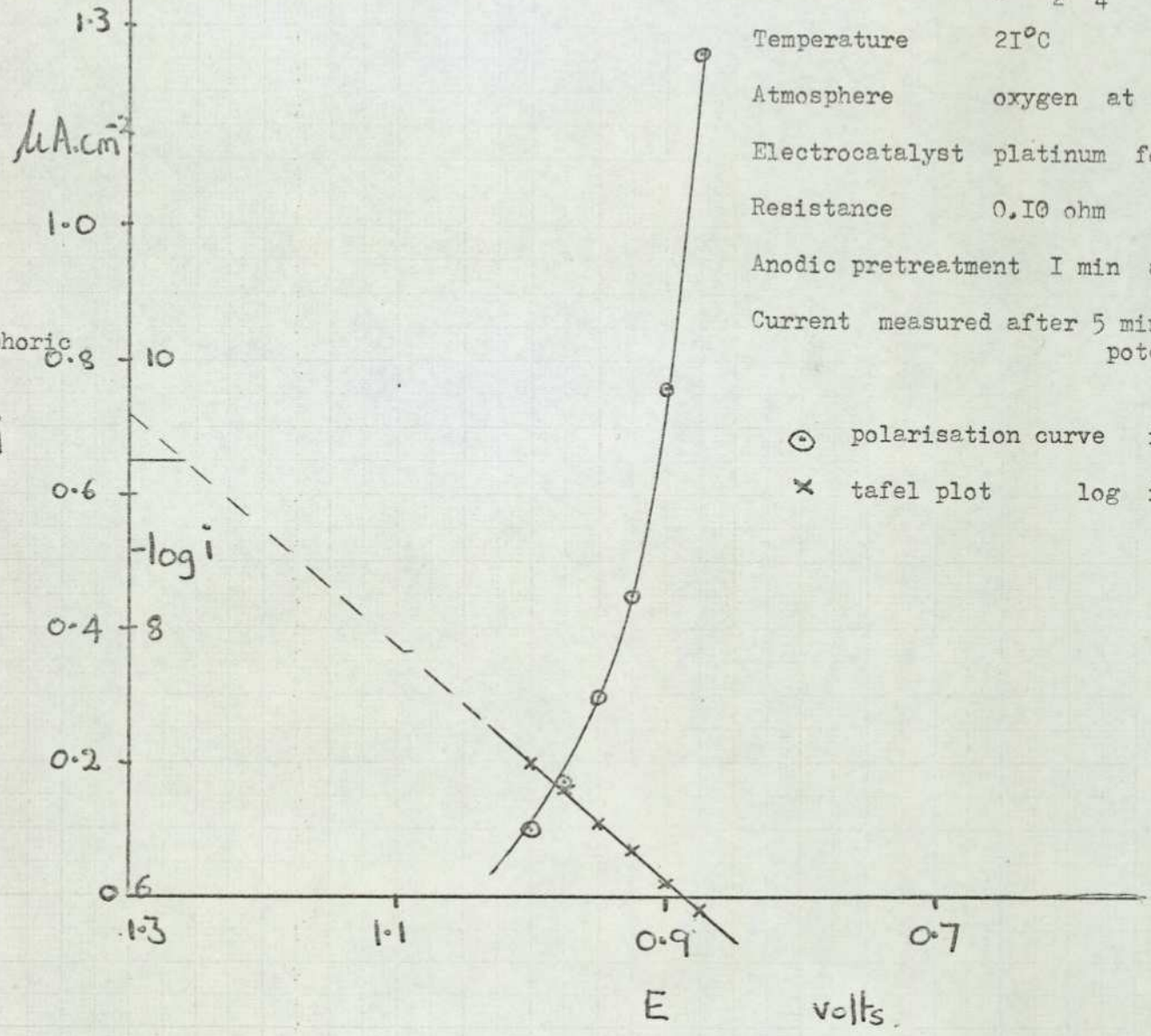
The results of this study do not, however, agree so favourably with those of Damjanovic et al who base their conclusions on measurements made in the potential range 1.02 V - 0.79 V. It has already been shown that at potentials below about 0.85 V the oxide is completely reduced, leaving the bare metal surface and it seems suprising that tafel points in the region below 0.85 V still fall on the straight line, especially considering that oxide reduction currents and oxygen reduction currents

Graph 24.

Polarisation and Tafel plots for oxygen reduction on a preanodised platinum foil electrode.

	i_o (A.cm^{-2})		Temp°C
Appleby (155)	-	-2.03	25.I
Damjanovic (68)	4×10^{-10}	-	25
Present study	4.2×10^{-10}	-	2I

	tafel slope (mV)	Electrolyte
Appleby	-I22	85% orthophosphoric acid
Damjanovic	I00	IN $HClO_4$
Present study	II4	5N H_2SO_4



Electrolyte 5N H_2SO_4

Temperature 2I°C

Atmosphere oxygen at I atmos.

Electrocatalyst platinum foil

Resistance 0.I0 ohm

Anodic pretreatment I min at I.80 V

Current measured after 5 min at a given potential

⊙ polarisation curve i - E

× tafel plot log i - E

on bare metal are much greater than the oxygen reduction currents on the oxide surface. The current densities for oxygen reduction on the oxide surface in Damjanovic's study were about an order of magnitude greater than those obtained in this investigation. At potentials less than 0.85 V Damjanovic's current densities were almost two orders of magnitude greater. This suggests that these results contain a contribution due to oxide reduction at potentials $>$ 0.85 V and also to oxygen reduction on the bare metal at potentials lower than this.

This work shows the great care that must be observed when measuring oxygen reduction currents on anodically pretreated platinum surfaces, ie. measurements should only be made in the range from I.00 V to 0.85 V since at higher potentials the oxygen reduction current is very small eg. 10^{-7} - 10^{-9} $A.cm^{-2}$ and consequently difficult to measure unambiguously, while at lower potentials the oxide film is continuously removed leaving the bare metal surface, resulting in higher currents than the true oxygen reduction current on the oxide surface, because of the oxide reduction and oxygen reduction on the bare metal surface.

The results in table 23 show current-time data over the initial 100 msec. at potentials in the range I.00 to 0.75 V on platinum foil electrodes pretreated for one minute at I.80 V in oxygen and nitrogen atmospheres and similar results for a bare platinum surface under oxygen. The preanodised electrodes give almost identical current-time curves under either oxygen or nitrogen over the entire potential range and for a given time and

Table 23.

Transient cathodic polarisation data for clean and preanodised platinum foil under oxygen and nitrogen atmospheres.

(a) Clean surface under oxygen.

Time (msec)	Potential (mV) 750mV	850mV	950mV	1000mV
	i(mA/cm^2)			
0.1	16.8	9.2	4.5	2.21
0.2	7.2	4.4	1.83	0.87
0.4	3.36	1.72	0.77	0.38
1.0	1.54	0.72	0.34	0.115
4	0.48	0.25	0.14	0.048
10	0.21	0.105	0.042	0.024
40	0.096	0.05	0.023	0.0095
100	0.029	0.011	-	-
490	0.014	-	-	-

(b) Preanodised surface under oxygen.

Time (msec)	Potential 750mV	850mV	950mV	1000mV
	i(mA/cm^2)			
0.1	31.7	20	10.6	5.4
0.2	25.0	15.3	6.7	3.3
0.4	19.2	10	3.4	1.73
0.9	11.0	4.8	0.77	0.384
4	3.1	1.34	0.39	0.144
9	1.7	0.76	0.15	0.057
40	0.52	0.19	0.075	0.019
90	0.31	0.076	-	-
470	0.067	0.038	-	-
970	0.029	-	-	-

Table 23 (cont.)

(c) Preanodised surface under nitrogen.

Time (msec)	Potential 750mV	850mV	950mV	1000mV
		i($mA.cm^{-2}$)		
0.1	29.5	19.1	11.5	5.4
0.2	23.4	14.8	6.9	3.4
0.4	19.2	10	3.3	1.83
0.9	11.4	4.3	0.86	0.48
4	2.86	1.43	0.39	0.144
9	1.71	0.76	0.15	0.057
40	0.48	0.17	0.067	0.023
90	0.27	0.057	-	0.0096
470	0.096	-	-	-
970	0.038	-	-	-

Electrolyte 5N H_2SO_4

Temperature 21°C

Atmospheres Oxygen and nitrogen at 1 atmos.

Electrocatalyst Platinum foil

Resistance 0.10 ohm

Pretreatment 1 min at 1.80 V then held at 1.05 V till i = 0

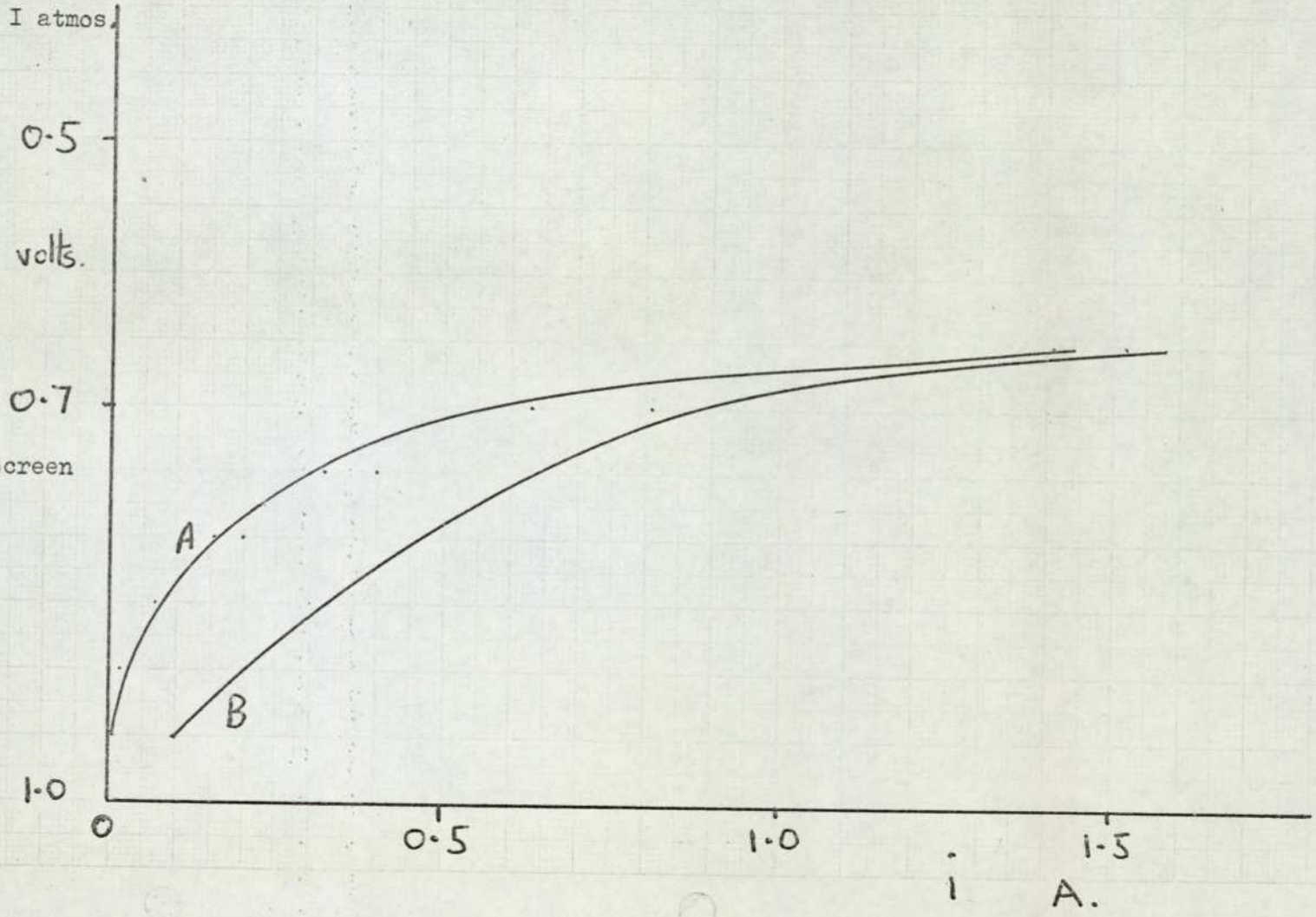
graph 20. Transient oxygen reduction polarisation curves on clean and anodised platinum surfaces.

Electrolyte	5N H_2SO_4
Atmosphere	oxygen at I atmos.
Temperature	2I C
O.C.V.	I.04 V
Electrocatalyst	platinum black
Electrocatalyst S.A.	16 $m^2.g^{-1}$
Electrocatalyst loading	6 $mg.cm^{-2}$
Electrode area	0.50 cm^2
Current collector	platinum screen
Ohmic resistance	0.06 ohm

current measured after 0.2 msec.

A clean surface

B anodised surface (5min at 2.00 V)



181

potential the current density on the clean platinum surface was about half that on the preanodised surface. These results support the view that the oxide reduction current is much greater than the oxygen reduction current on a preanodised platinum surface and consequently that it is essential to let the oxide reduction current decay to zero before taking readings.

Table 24 shows current-time curves on clean and preanodised platinum surfaces in the potential range I.26 - I.0I V. These results show that in this region the oxygen reduction current on an oxide surface is too low to be detected and that the current from the electrode which was not preanodised is only slightly less than the preanodised electrodes because the oxide coverage at I.26 V is greater than at I.05 V.

This work is in agreement with the work on platinum black which also showed that the oxide reduction current decayed with time at potentials above 0.85 V but that below this potential the oxide film was continuously stripped off. Also, transient i-E curves for preanodised and clean platinum black under both oxygen and nitrogen were almost identical. (see graphs 19-20).

Oxygen reduction currents on anodised surfaces are very low compared with oxygen reduction on the clean surface even if platinum black is used, (Graph 35) which increases the surface area about a thousand times and although the oxide reduction currents are much greater they fall to zero with increasing time at potentials above 0.85 V. Hence if platinum black electrodes are to be used as rechargeable air/oxygen electrodes their

Table 24.

Cathodic current - time curves for a preanodised and clean platinum foil electrode under oxygen and nitrogen.

Time (sec)	I.II V . oxide surface under O_2	I.II V . oxide surface under N_2	I.0I V . oxide surface under O_2	I.0I V . oxide surface under N_2	I.2I V . oxide surface under O_2	I.2I V . oxide surface under N_2
			$i(\mu A.cm^{-2})$			
5	4.8	4.6	7.3	6.7	2.5	2.5
I0	2.7	2.5	3.8	3.5	I.7	I.7
I5	I.9	I.7	2.5	2.I5	I.2	I.3
30	0.77	0.62	I.03	0.90	0.53	0.60
60	0.I9	0.I9	0.47	0.40	0.I9	0.I9
I20	zero	zero	0.27	0.27	zero	zero
I80	-	-	0.I9	0.I5	-	-
240	-	-	zero	zero	-	-

E = I.I6 V

Time (msec)	clean surface under oxygen	oxide surface under oxygen	oxide surface under nitrogen
	$i(mA.cm^{-2})$		
0.I	3.0	9.6	9.6
0.2	4.2	6.I	6.25
0.4	I.72	2.7	2.9
0.9	0.39	0.77	0.87
4	0.24	0.29	0.29
9	0.096	0.I7	0.I7
40	0.039	0.057	0.057
90	0.0I4	0.028	0.028

Electrolyte 5N H_2SO_4 Resistance 0.I0 ohm

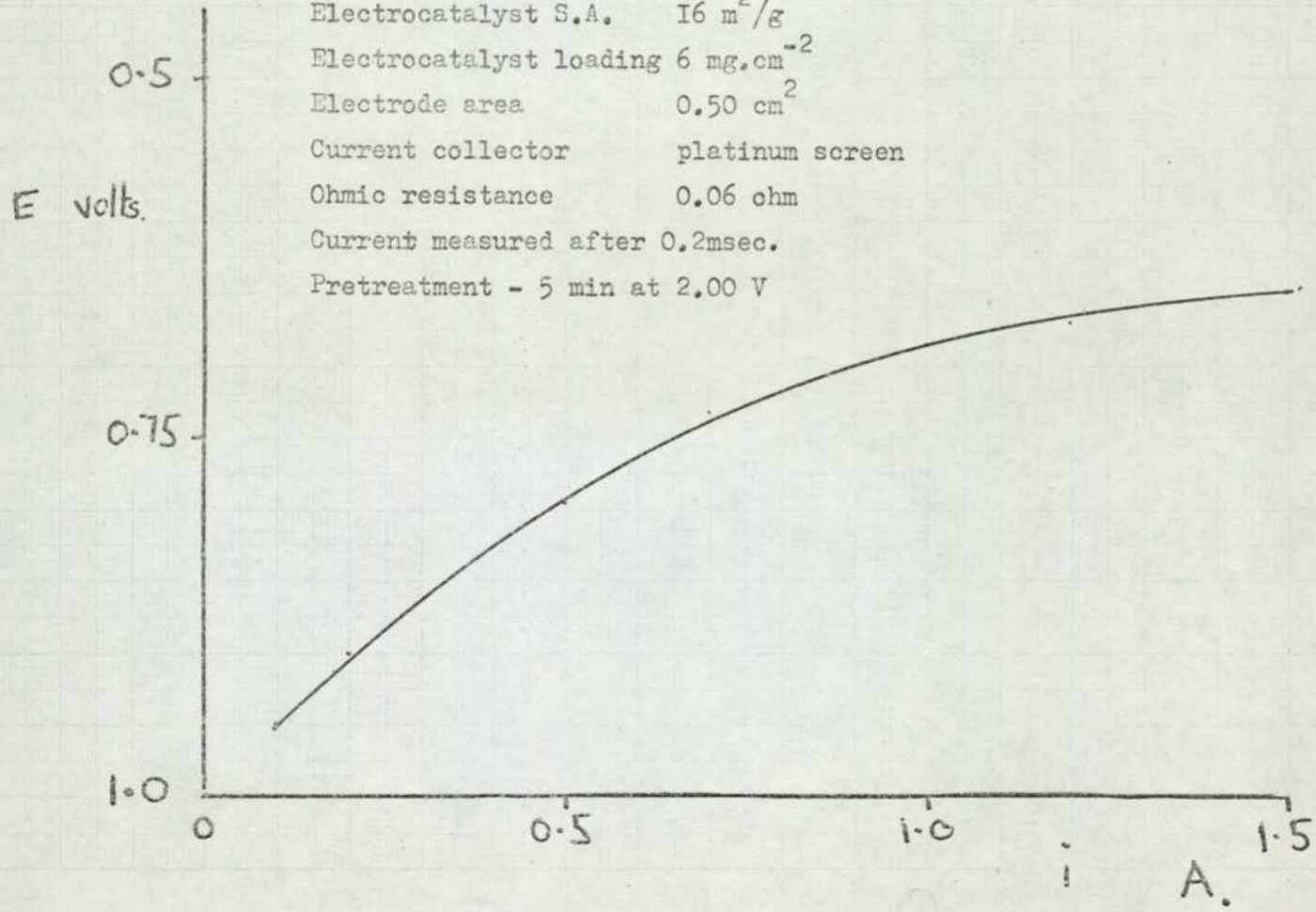
Temperature 2I°C Anodic pretreatment I min at I.8 V then held at I.26 V till i= 0

Atmospheres O_2 and N_2 at I atmos.

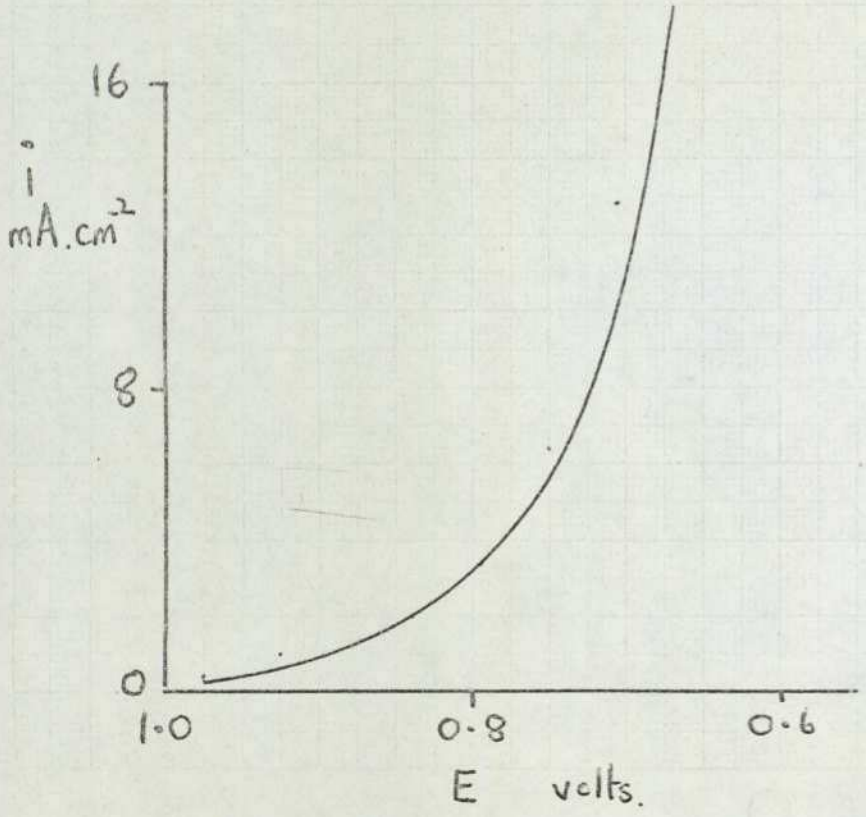
Electrocatalyst platinum foil

graph 19. Transient oxide reduction polarisation curve on anodised platinum black.

Electrolyte	5N H_2SO_4
Atmosphere	nitrogen at I atmos.
Temperature	2I°C
O.C.V.	I.0I V
Electrocatalyst	platinum black
Electrocatalyst S.A.	I6 m^2/g
Electrocatalyst loading	6 $mg.cm^{-2}$
Electrode area	0.50 cm^2
Current collector	platinum screen
Ohmic resistance	0.06 ohm
Current measured after	0.2msec.
Pretreatment - 5 min at	2.00 V



Graph 35 - Linear sweep oxide reduction polarisation curve on an anodised teflon bonded platinum black electrode.



Electrolyte	5N H_2SO_4
Atmosphere	nitrogen
Pressure	I atmos.
Temperature	2I°C
O.C.V.	I.0I V
Electrocatalyst	platinum black
Electrocatalyst S.A.	16 $m^2.g^{-1}$
Electrocatalyst loading	6 $mg.cm^{-2}$
Current collector	platinum screen
Ohmic resistance	0.I5 ohm
Sweep rate	400 mV/min
Pretreatment	I min at 2.00 V

discharge performance following recharging will be very poor at potentials greater than 0.85 V which is the normal operating voltage. At lower potentials the performance will improve with time as the oxide film is steadily reduced.

3.8. The Effect of Surface Oxides on the Oxygen Evolution Reaction on Platinum.

3.8.I. Introduction.

It has been observed that the anodic oxygen evolution current on platinum at a given potential falls with time and this has been attributed to the increasing depth of oxide coverage with time causing the gradual deactivation of the active centres.(54) If the mechanism of the oxygen evolution reaction is

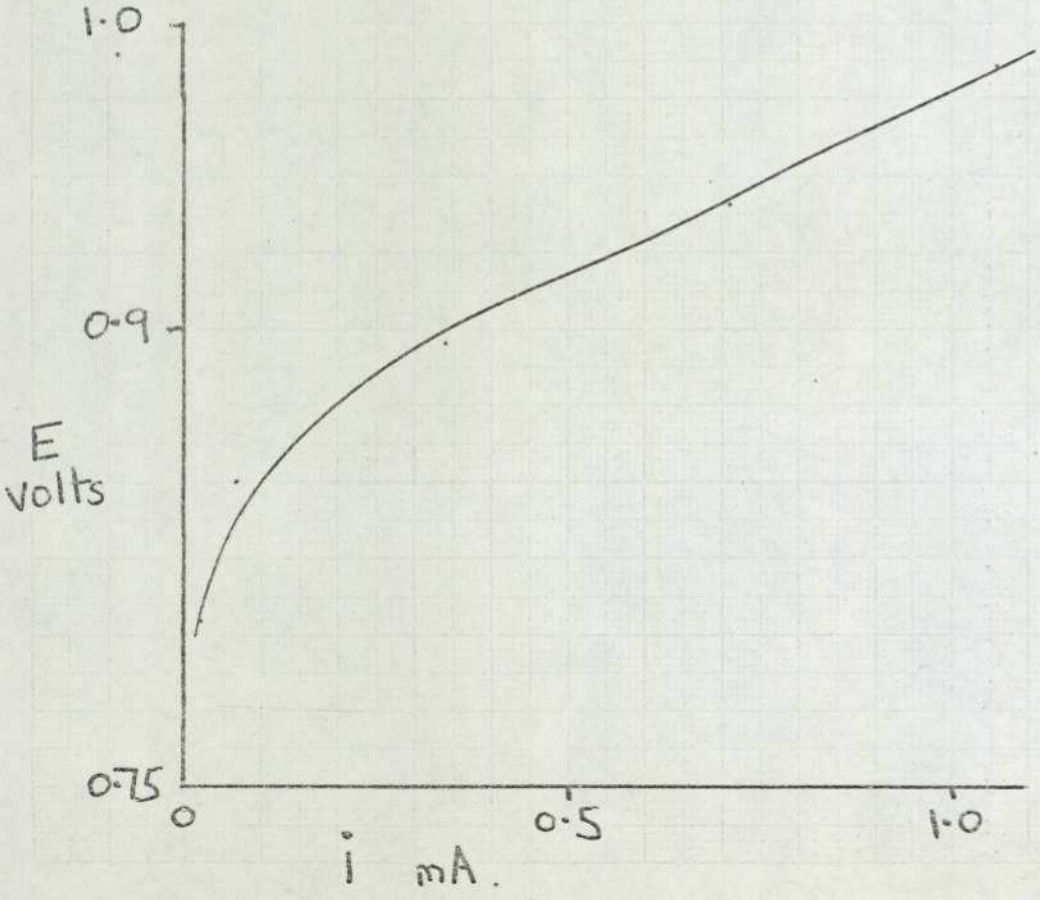
(I) $4M + 4H_2O \rightleftharpoons 4MOH + 4H^+ + 4e$

(II) $2MOH = MO + MH_2O$

(III) $2MO = 2M + O_2$

where (I) is the rate determining step then the surface oxide should be removed as fast as it is formed and the current should not vary with time. Since (II) and (III) are chemical reactions the electric current is due entirely to (I) which is the oxide formation reaction, which also occurs in the potential range I.0 - I.4 V before any oxygen is evolved. If the above mechanism is correct, irrespective of the rate determining step, it implies that there must be a rapid increase in the rate of oxide formation at about I.45 V when oxygen evolution is observed, although this seems unlikely since in the potential range I.2 - I.4 V the oxide formation current does not vary with potential (graph 26)

graph 266. Linear sweep voltammogram for oxide formation on a clean platinum surface.

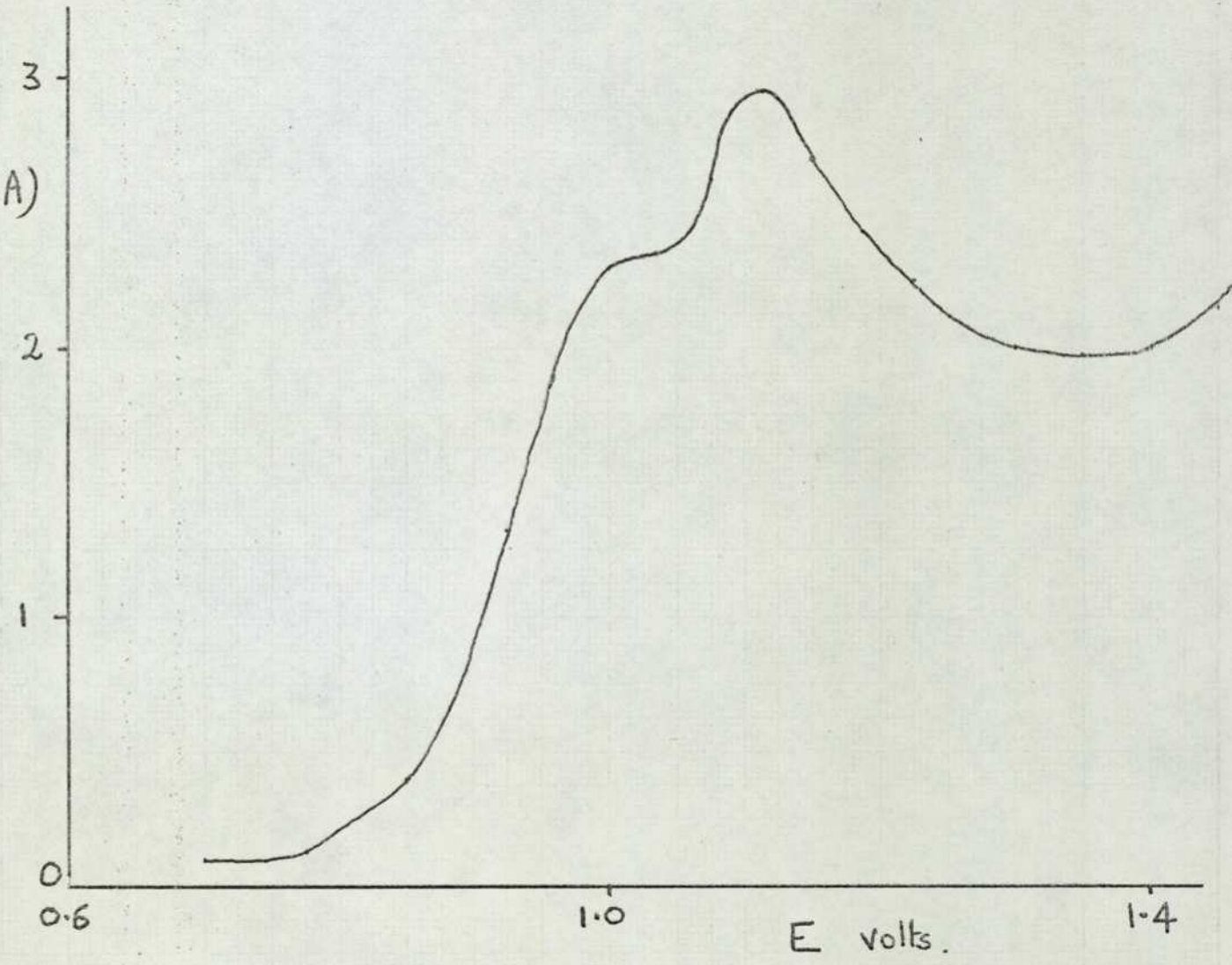


Electrolyte	5N H_2SO_4
Atmosphere	nitrogen
Pressure	I atmos.
Temperature	21°C
O.C.V.	0.70 V
Electrocatalyst	platinum black
Electrocatalyst S.A.	16 $m^2.g^{-1}$
Electrocatalyst loading	6 $mg.cm^{-2}$
Current collector	platinum screen
Ohmic resistance	0.15 Ohm
Sweep rate	400 mV/min
Electrode area	0.50 cm^2

GRAPH 26(a)

Anodic Linear Sweep Voltammogram for a teflon bonded platinum black electrode

Electrolyte	5N H_2SO_4
TEMP.	21°C
Atmosphere	N_2
Electrocatalyst S.A.	16 $m^2 g^{-1}$
" loading	5.5 $mg.cm^{-2}$
current collector	Pt gauze
sweep rate	1v/min.
resistance	0.16 ohm



and no new oxide species is known to form in the region of I.45 V. Reactions (II) and (III) are not potential dependent although they could be dependent on the surface oxide concentration. However if, at about I.45 V, the rates of reactions (II) and (III) increased then oxide would be decomposed and the rate of (I) would increase resulting in a higher current. Never the less it is difficult to find possible explanations of this phenomenom.

Bockris (I56) has analysed various possible oxygen evolution reaction mechanisms and from the values of anodic and cathodic Tafel slopes and stoichiometric numbers has concluded that only three are possible. All three mechanisms possess only one electrochemical step ie. reaction (I) which is said to be unambiguously the rate determining step for each mechanism. However this does not explain the fall in current with time or why no oxygen is evolved at potentials less than I.45 V. Hence the oxygen evolution reaction mechanism still poses problems of considerable complexity.

A possible explanation for these problems could be achieved if the formation of nonstoichiometric platinum oxides is assumed or if platinum oxide (PtO) and platinum dioxide (PtO_2) are assumed to exist together at the same potential. Platinum oxides could quite easily be nonstoichiometric because platinum is a very noble metal and its oxidation may not go to completion resulting in an excess of platinum ions. The oxides PtO and PtO_2 are formed at similar potentials and hence are likely to coexist. A mechanism involving these species would explain the good electrical

conductivity of the electrode surface since pure PtO or PtO_2 should be poor conductors.

If an oxide such as PtO_{I+x} is assumed to form where the value of x is dependent on the potential then the fall in current with time at a constant potential can be explained on the basis of a thickening film at constant x. As the film grows ionic conduction becomes harder, the resistance increases and the current falls.

The explanation of the overvoltage observed before oxygen is evolved could be explained by assuming that the x value at a certain potential reaches a limiting value (maximum value). At lower potentials the favoured reaction is either $Pt \rightarrow PtO$ or $PtO \rightarrow PtO_2$ but at the critical potential the oxygen evolution reaction is favoured because nearly all the surface platinum has been converted to PtO_2. At higher potentials the oxide ions formed can either contribute to film growth by a diffusion mechanism or they can be discharged as oxygen molecules. The latter process is the easier and hence most is evolved as oxygen and the proportion going to oxide film growth falls as the film grows thicker.

It is proposed to study the current decay of platinum over a large time range (secs - minutes) in the oxide formation and oxygen evolution potential regions, and to show whether all the current in the oxygen evolution region can actually be correlated with the quantity of oxygen formed. This should be true if multilayer oxide films do not form below 2.0 V.[96,97] The current decay curves should determine whether the

decay is due to oxide coverage and whether or not the decay law is the same for oxygen evolution and oxide formation.

3.8.2. Experimental.

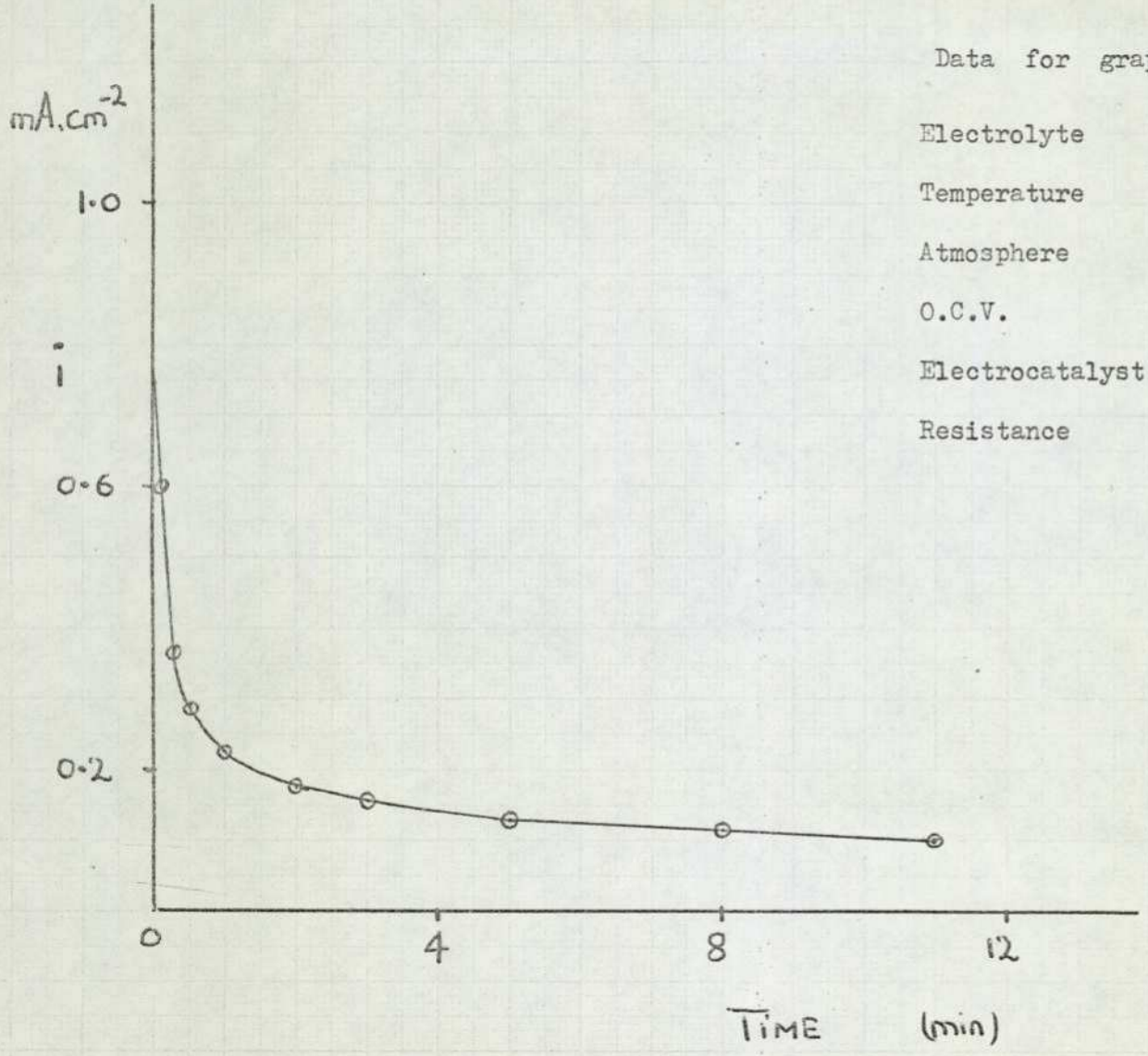
Potentiostatic current-time curves were recorded in the oxide formation and oxygen evolution potential regions in the time range I sec - 5 secs on platinum foil in a nitrogen atmosphere by the pulse technique and by normal ammeter clock measurements in the range 5 secs - I5 min. on electrode surfaces which had been pretreated to contain (a) no surface oxide and (b) a fixed amount of surface oxide.

The charge passed, calculated from current-time curves, was compared with the charge required to produce the volume of oxygen, corrected to S.T.P., collected in a gas burette.

3.8.3. Results and Discussion.

The current-time curves for a platinum foil electrode in the time range 5sec - I5 min., at constant potential between I.6 and 2.0 V are plotted in graph 25. The slopes of these curves were measured at various times. The slope represents the rate of current decay with time at a given time. This is equivalent to the rate of oxide formation in the potential range I.0 - I.4V. The curves show that in the oxide formation region the current falls to very low values as the time increases, while in the oxygen evolution region a significant current is observed even at long times. The area under the curve enclosed by the time period 0 - I0 min. was measured and plotted against the potential (graph 30). This curve was linear in the potential

Graph 25. (a) Current - time curve at I.90 V for platinum foil.

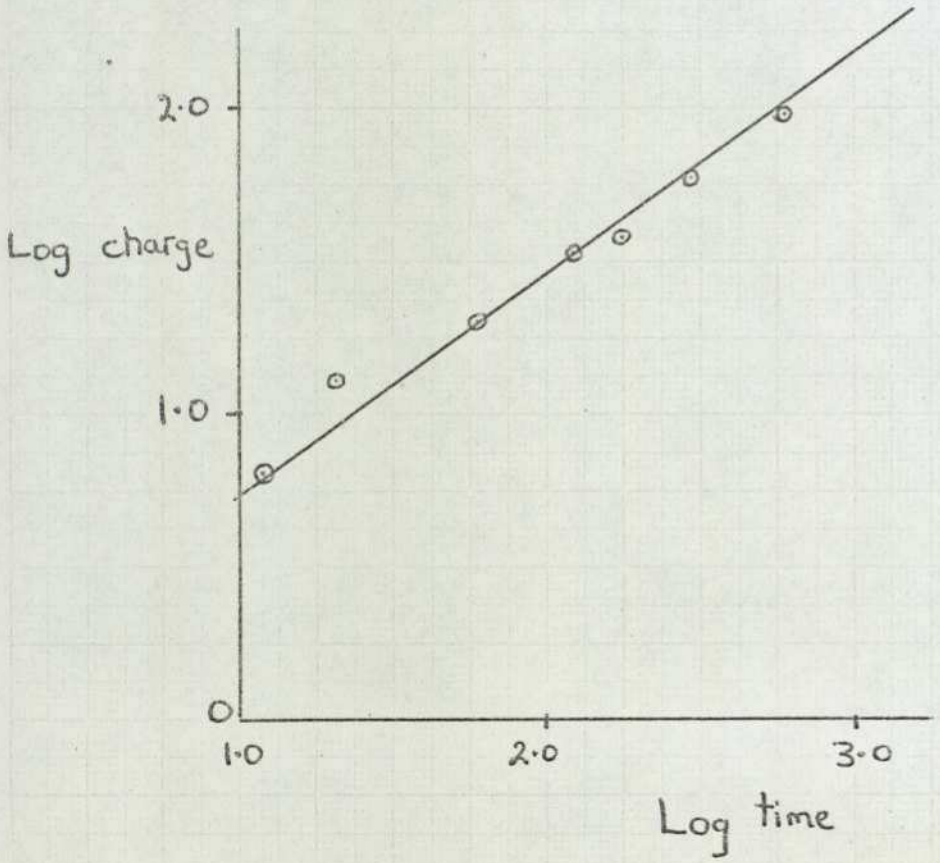


Data for graph 25 (a) to (h).

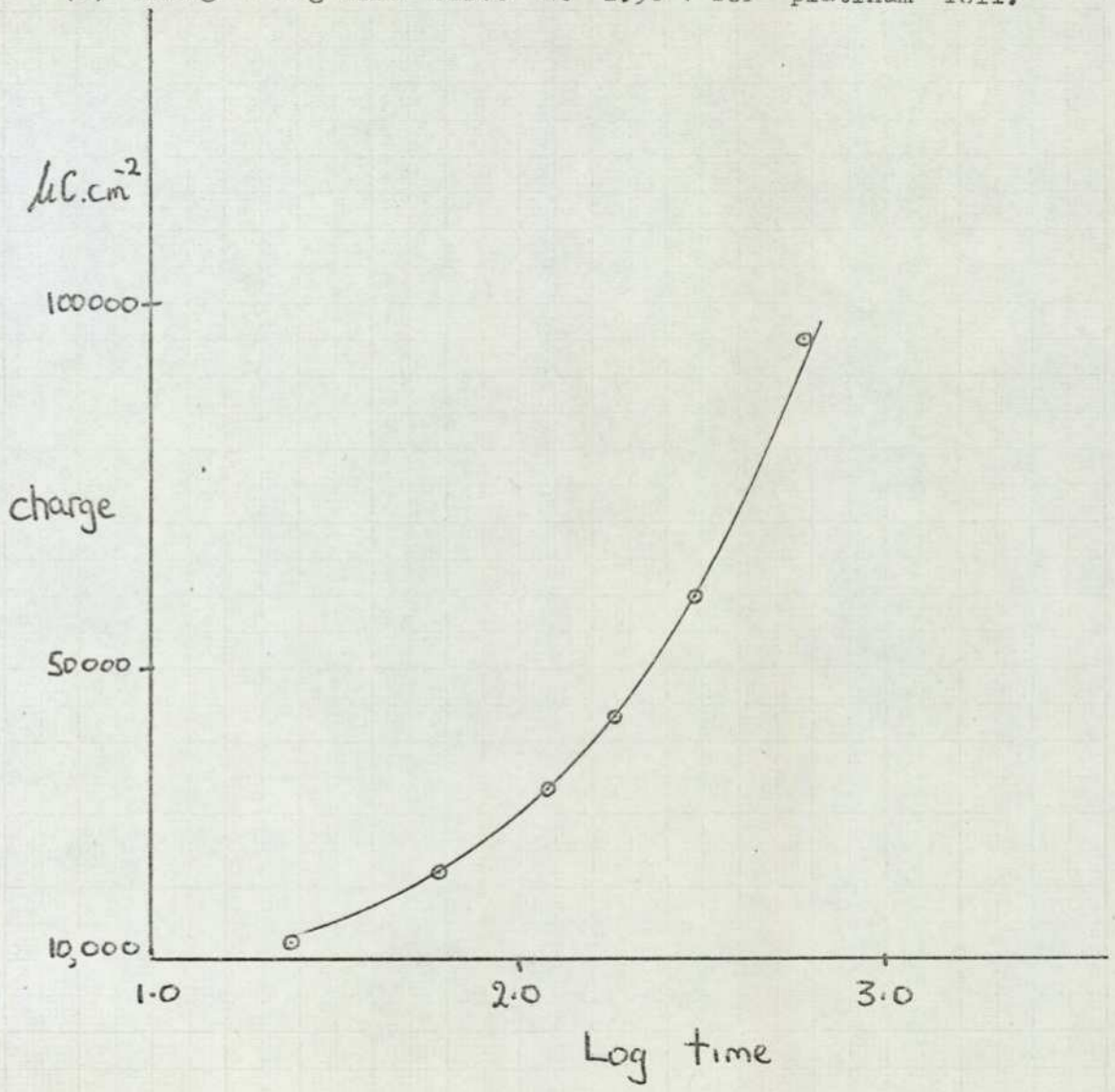
Electrolyte	5N H_2SO_4
Temperature	2I C
Atmosphere	nitrogen at I atmos.
O.C.V.	0.9 V
Electrocatalyst	platinum foil
Resistance	0.08 ohm

Graph 25.

(b) log charge - log time curve at I.9 V for platinum foil.

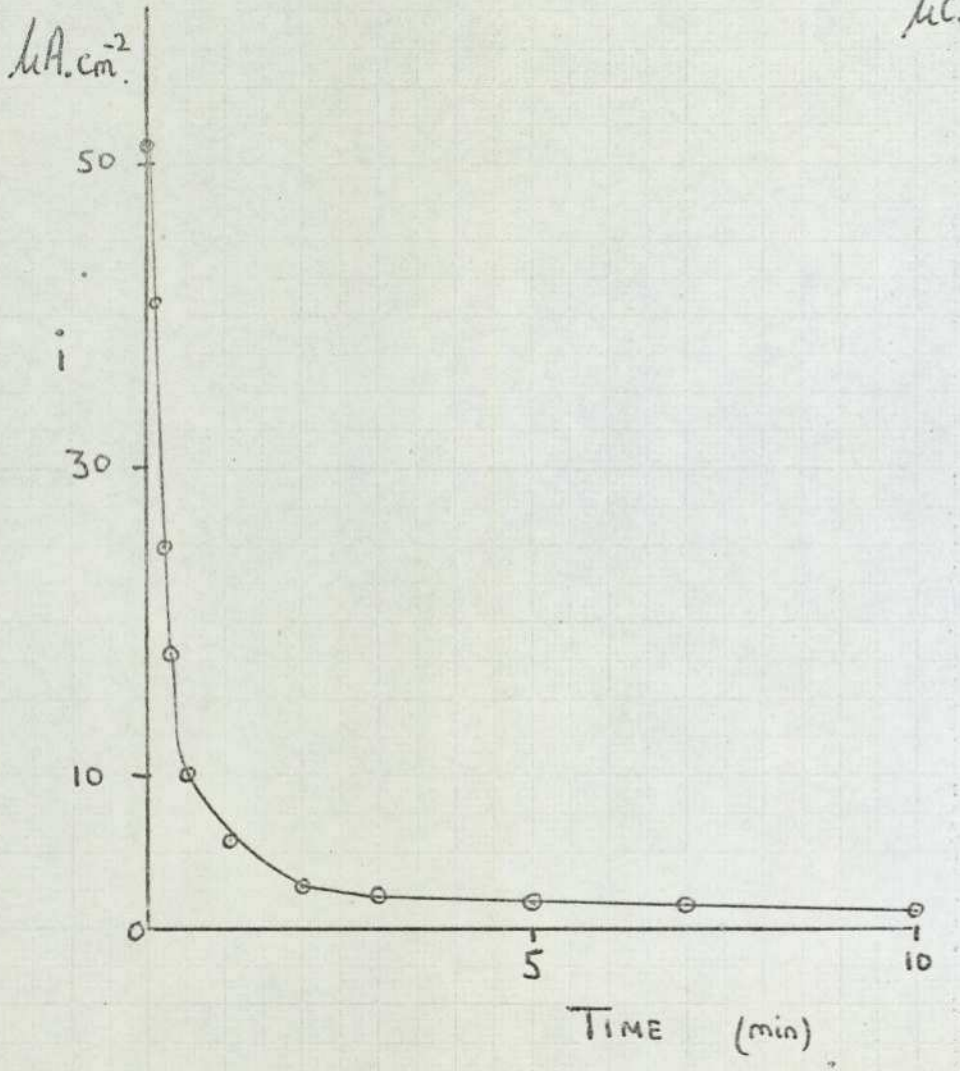


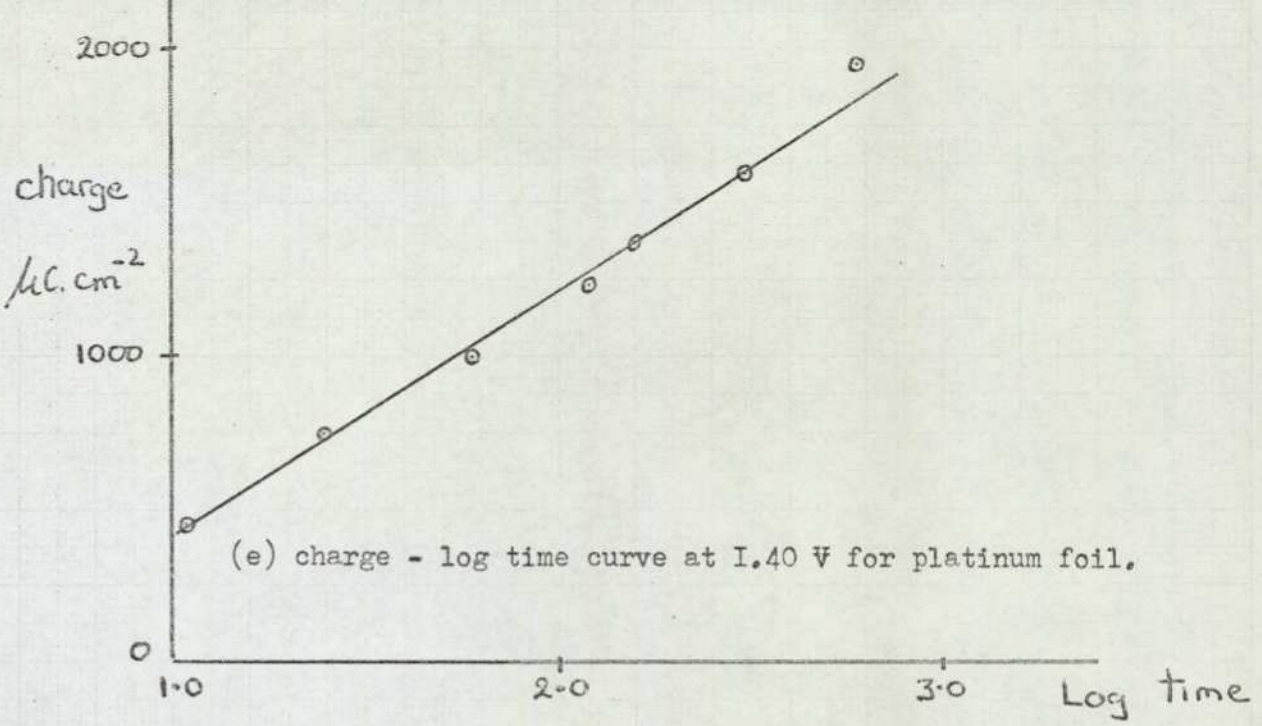
(c) charge - log time curve at I.90 V for platinum foil.



Graph 25.

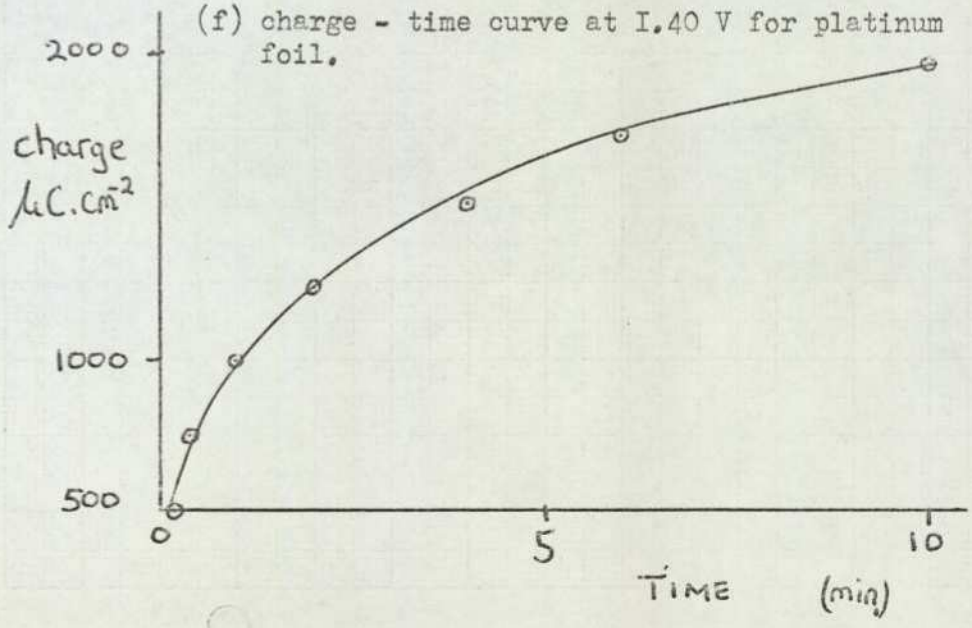
(d) current - time curve at I.40 V for platinum foil.





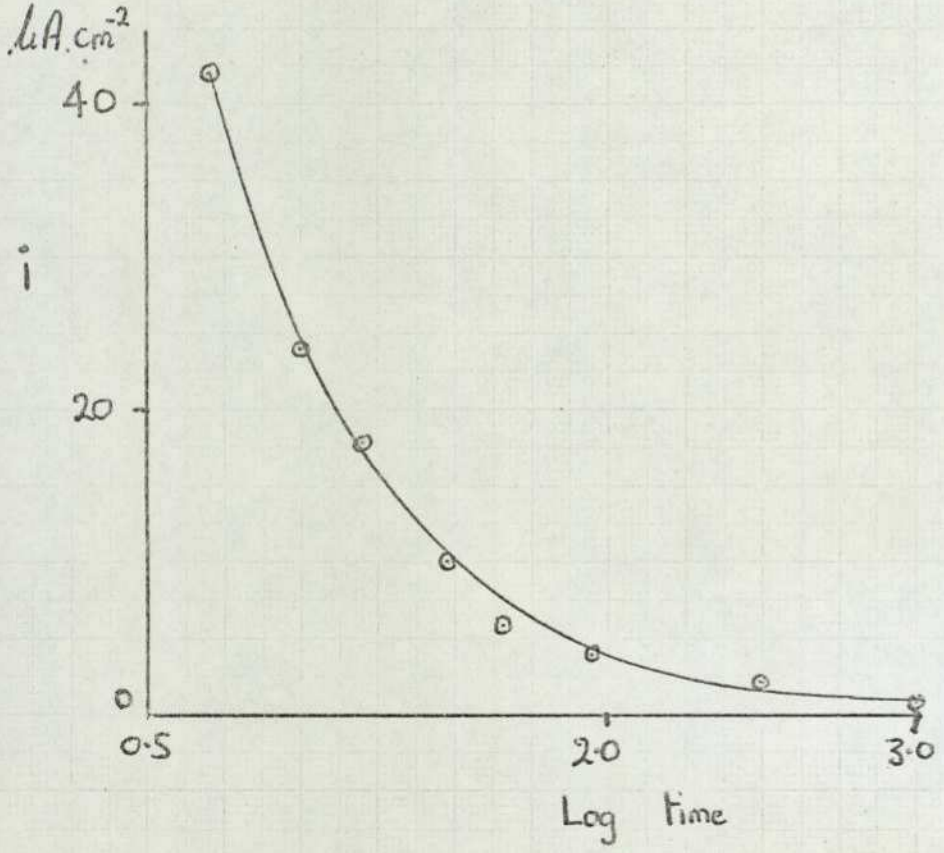
(e) charge - log time curve at I.40 V for platinum foil.

(f) charge - time curve at I.40 V for platinum foil.



Graph 25.

(g) current - log time curve at I.40 V for platinum foil.



(h) current - log time curve at I.90 V for platinum foil.

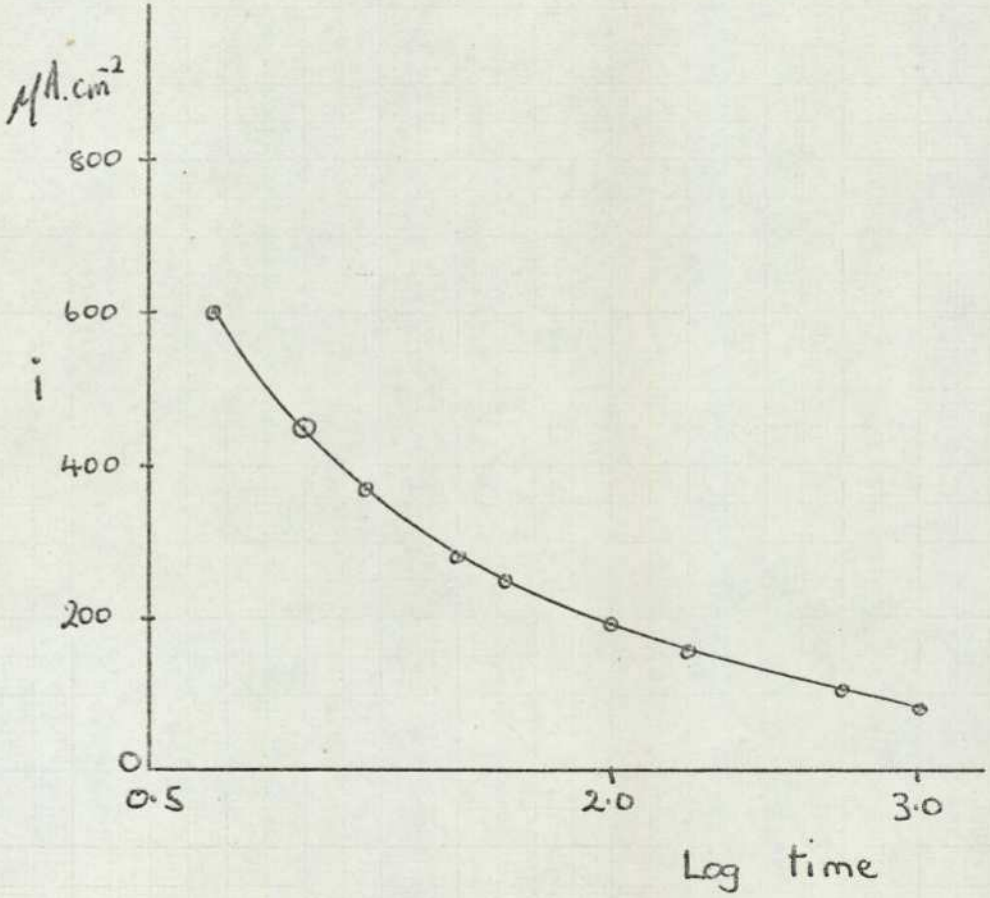


Table 25.

Current - time data at constant potentials in the range I.0 - 2.0 V for a platinum foil electrode.

Potential	I.05 V	I.I0 V	I.20 V	I.30 V	I.40 V	I.5I V
Time (sec)			i (mA)			
5	40	4I	90	I20	2I0	300
I0	28	26	55	80	I70	I60
I5	22	20	40	6I	90	II0
30	I5	I3	24	36	47	58
45	I2	I0	I8	26	33	-
60	I0.2	8	I4.5	20.5	26.5	33
75	-	7	I2	I7	22	-
90	-	6.3	I0.5	I5	I9	23
I20	7	5.7	9	II.5	-	I9
I80	-	4.2	6.8	8.6	II.3	I4
240	4.I	3.9	-	-	9.5	-
300	3.4	3.5	4.6	6.0	7.8	I0.0
600	-	-	-	-	-	6.5
I050	-	-	-	-	-	5.0
660	0.5	I.4	-	3.9	4.8	-
900	-	I.I	-	-	-	-
720	-	-	3.I	-	-	-
960	-	-	2.8	3.2	-	-
I50	-	-	-	-	I2.5	-

Electrolyte	5N H_2SO_4	Resistance	0.08 ohm
Temperature	2I°C	Electrode area	5.0 cm^2
Atmosphere	nitrogen at I atmos.		
O.C.V.	0.9 V		
Electrocatalyst	platinum foil		

Table 25 (cont.)

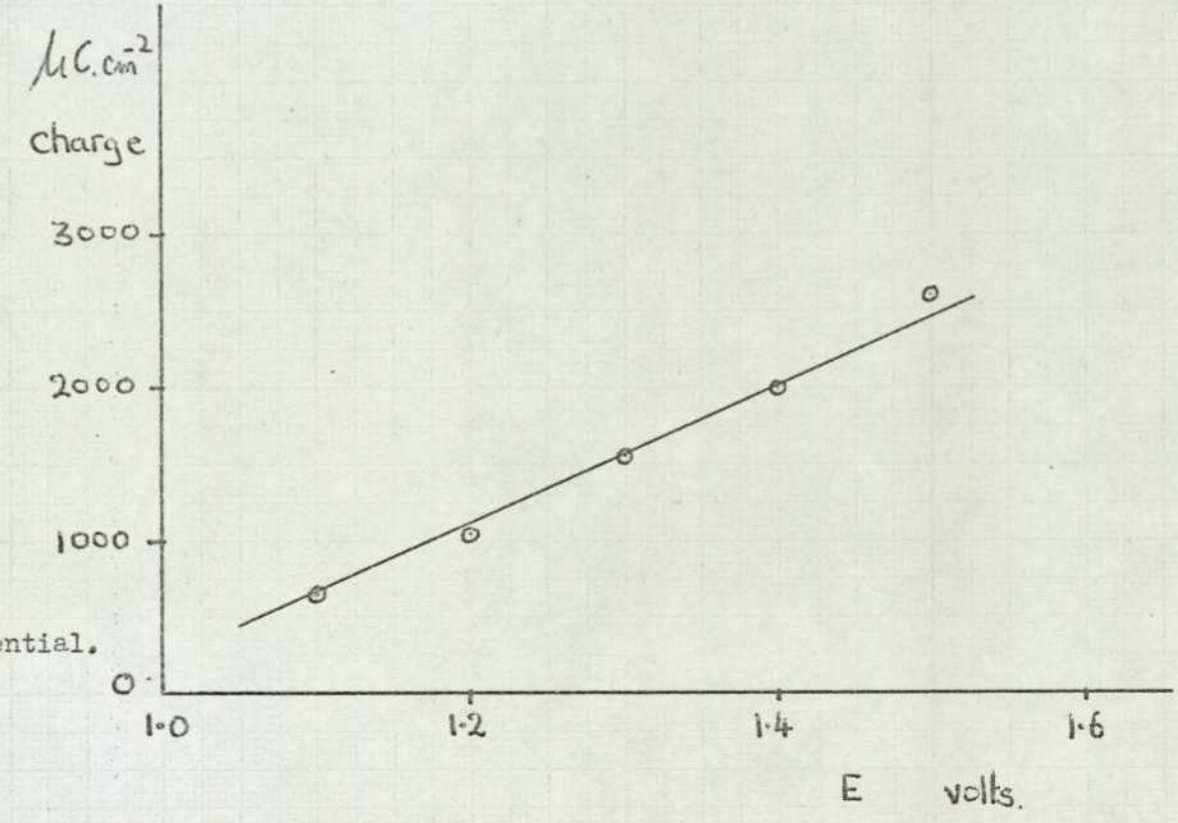
Potential	I.60 V	I.70 V	I.80 V	I.90 V	2.00 V
Time (sec)			i (mA)		
5	500	500	I000	3000	II,000
I0	220	300	800	2200	7000
I5	I60	235	650	I850	-
30	94	I55	450	I430	5250
45	67	I23	390	I240	4800
60	46	I03	340	II20	-
75	-	-	-	-	-
90	42	-	-	-	3900
I20	35	7I	255	870	3600
I80	27.5	58	2I3	770	3200
240	23	50	I90	-	3000
300	20	-	I76	640	2800
600	I3.3	-	-	-	2300
I050	-	-	-	-	-
900	II	-	-	440	-
720	-	30	-	-	-
I200	-	-	I07	-	-
660	-	-	-	440	-
20	-	-	-	-	6000

Graph 30.

Charge v. potential plot for a platinum foil electrode in the range I.0 V - I.5 V.

Electrolyte	$\frac{1}{2}$N H_2SO_4
Temperature	2I°C
Atmosphere	nitrogen
Pressure	I atmos.
O.C.V	0.9 V
Electrocatalyst	platinum foil
Resistance	0.08 ohm

charge measured after IO min. at a given potential.



region I.05 - I.50 V confirming the previously reported linear relationship between potential and oxide coverage.[68] The deviation from this linear relationship at potentials greater than I.50 V suggests a different reaction.

The area under these current-time curves was determined after different times in the range 0 - I0 min. and the oxide coverage plotted against time and log time at each potential. The charge v. time plots were logarithmic in the range I.0 - I.5 V and the charge v. log time were consequently linear in this potential range. At higher potentials this is not true but the log charge v. log time curve was linear.

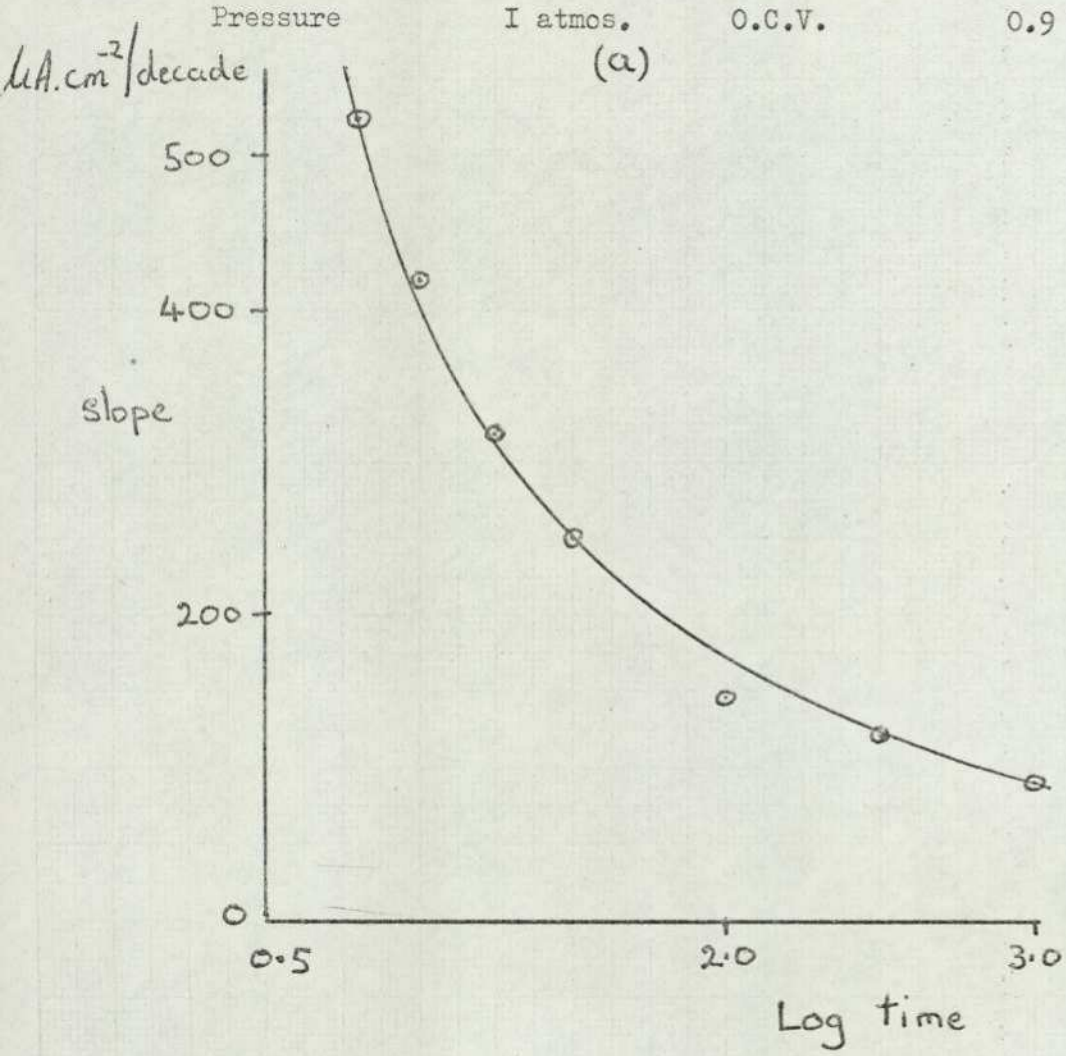
In the potential range I.0 - I.5 V the slope of the charge - log time lines is a linear function of potential as shown in graph 3I. This shows that the rate of growth of the oxide film is a linear function of potential.

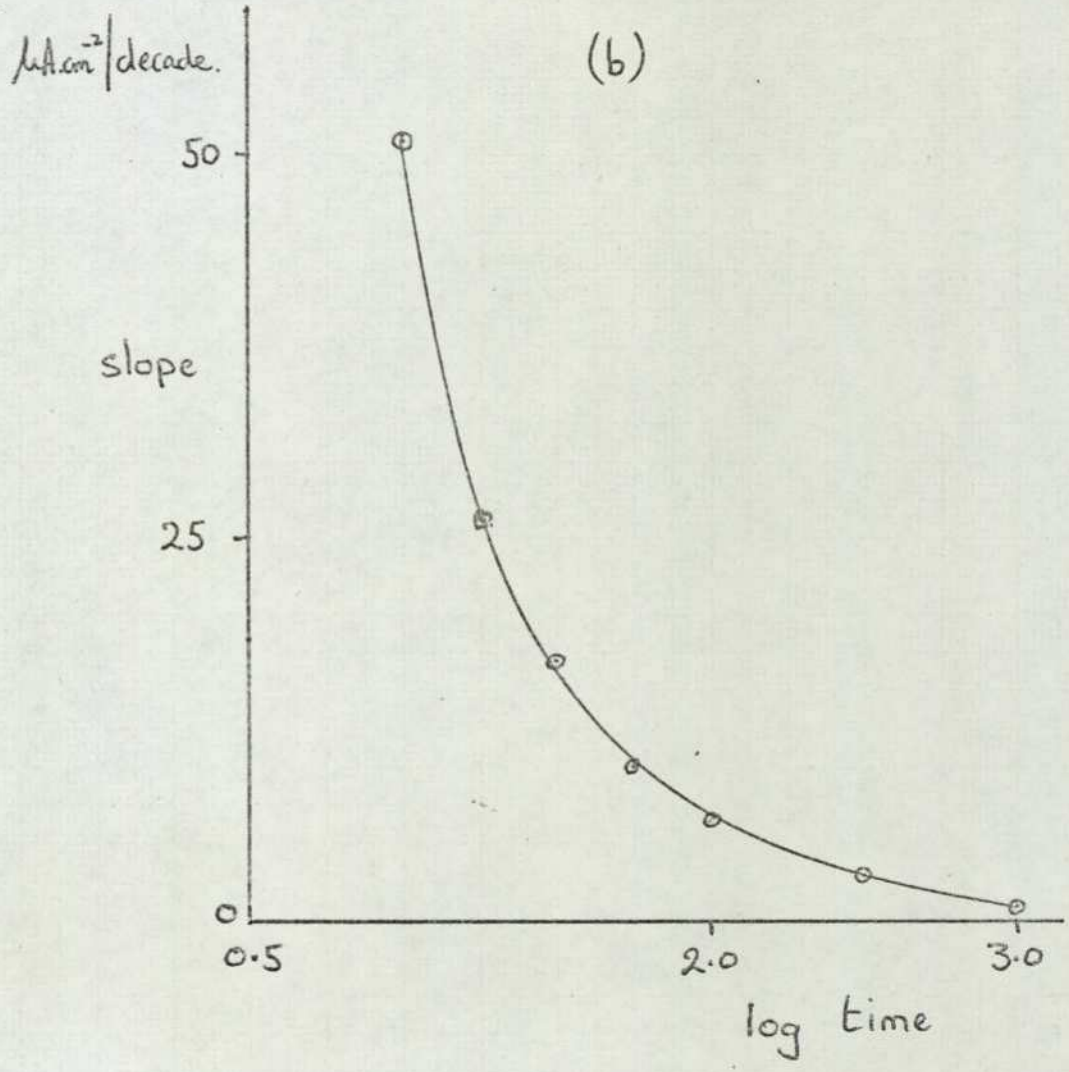
Graph 28 shows the rate of fall of current with time as a function of log time, ie. slope of i - log t curves v. log t for a given potential and graph 29 shows the rate of fall of current with log time as a function of potential at a given time ie. slope of i - log t v. E at a given time. This shows that over the entire time range the rate of fall of current with log time increases rapidly at potentials above I.80 V which is in agreement with the fact that the current density for a given time increases rapidly at potentials above I.80 V. If the only electrochemical step in the mechanism is discharge of water to form an oxide species then an increase in current density must correspond with

Graph 28.

The rate of current decay v. log time for a platinum foil electrode at a) I.9 V and b) I.40 V.

Electrolyte	5N H_2SO_4	The rate of current decay is the slope of the current - log time curve in graph 25.	
Temperature	2I°C	Resistance	0.08 ohm
Atmosphere	nitrogen	Electrocatalyst	platinum foil
Pressure	I atmos.	O.C.V.	0.9 V





Graph 29.

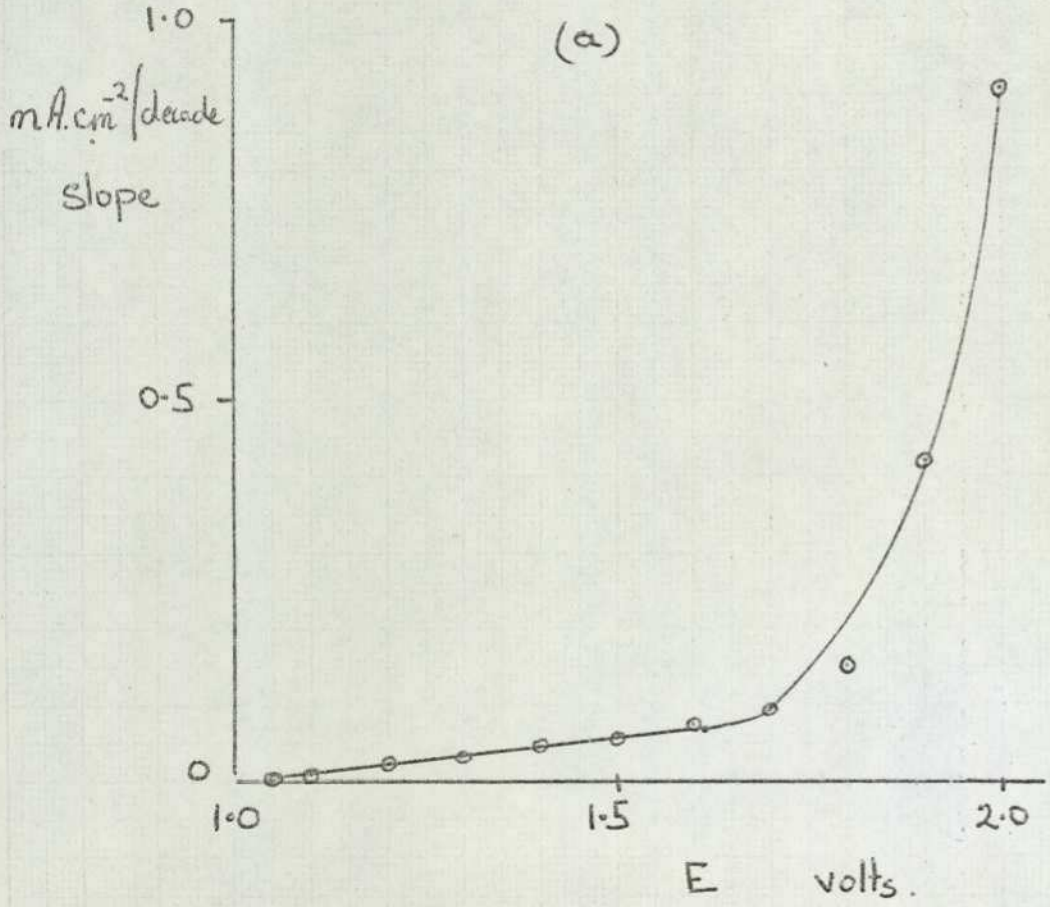
Rate of current decay v. potential on a platinum foil electrode after a) IO secs. and b) I000 secs.

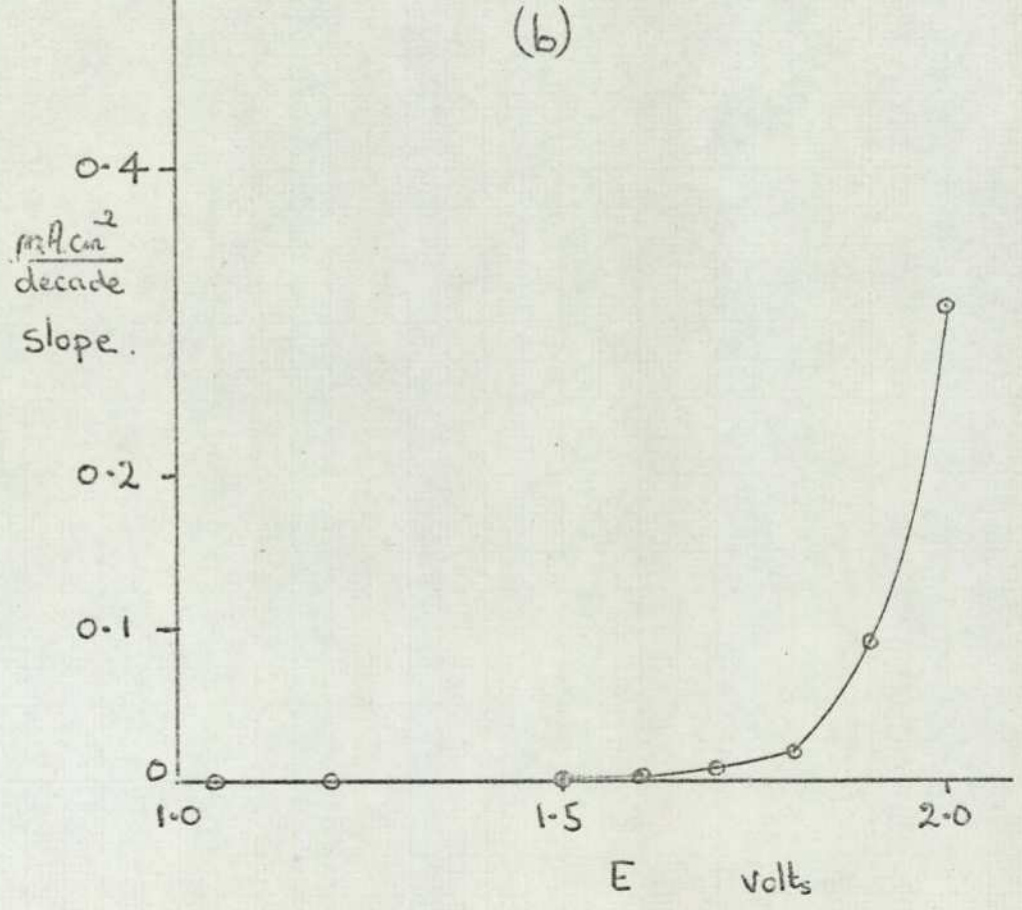
Electrolyte 5N H_2SO_4 O.C.V. 0.9 V

Temperature 2I°C Electrocatalyst platinum foil

Atmosphere nitrogen at I atmos. Resistance 0.08 ohm

Rate of current decay is the slope of the current - log time curves in graph 25.





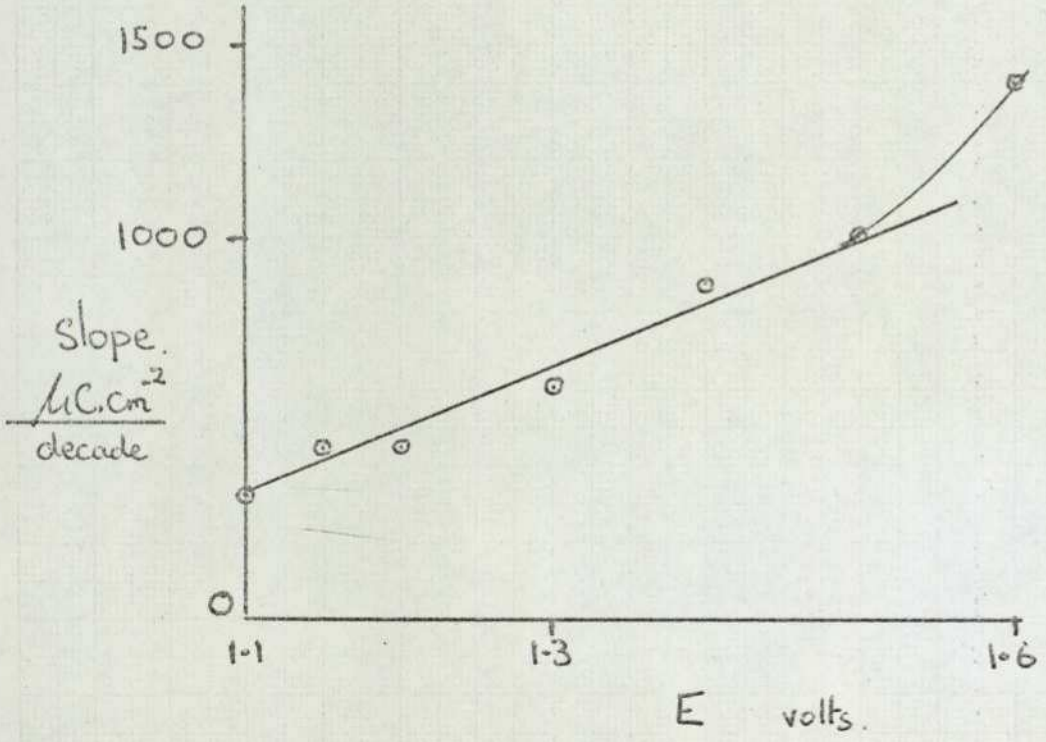
Graph 3I.

Curve of the slope of charge - log time plots (graph 25) ie. rate of growth of oxide film v. potential.

Electrolyte $5N\ H_2SO_4$

Temperature $21^{\circ}C$

Atmosphere nitrogen at I atmos.



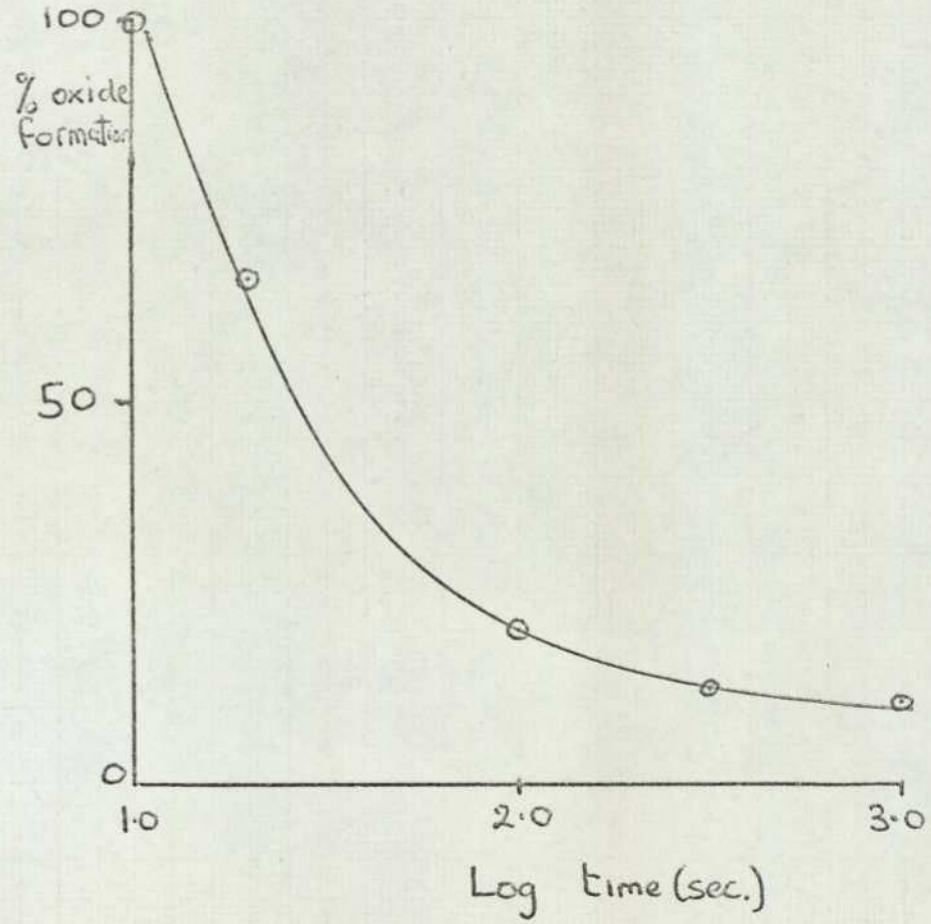
Graph 34.

Oxide formation proportion of total current v. log time at 2.00 V.

O.C.V. 0.9 V

Electrocatalyst platinum foil

Resistance 0.08 ohm



an increase in oxide coverage.

Using the above data a method has been developed for separating the oxide formation and oxygen evolution components of the total current at different times at potentials above I.50 V. The method is based on measuring the relative rate of current decay from the current - time curves. This was done by comparing the current after a time t with the current after IO sec. ($t > IO$ sec.) and representing the comparison as a ratio eg. i_t / i_{IO}. These ratios were calculated at different values of t in the potential range I.0 - 2.0 V. Between I.0 - I.5 V for a given value of t the ratio was approximately constant showing that the relative rate of current decay was constant and this would be expected at potentials where the charge-log time curve is linear. At potentials above I.50 V the ratio increases rapidly indicating a much slower relative rate of current decay. This is the potential at which oxygen evolution is first observed.

In order to separate the oxygen evolution and oxide formation currents, the current after IO sec. is read from the current-time curve at a suitable potential. It is assumed that the current after IO sec. on an initially clean platinum surface is due entirely to oxide formation. From the constant value of i_t / i_{IO} between I.0 - I.5 V the value of the oxide formation current after t seconds can be calculated and compared with the actual value of current after t seconds the difference being due to oxygen evolution. This process is repeated for different values of t and E (graph 27). This separation enables:

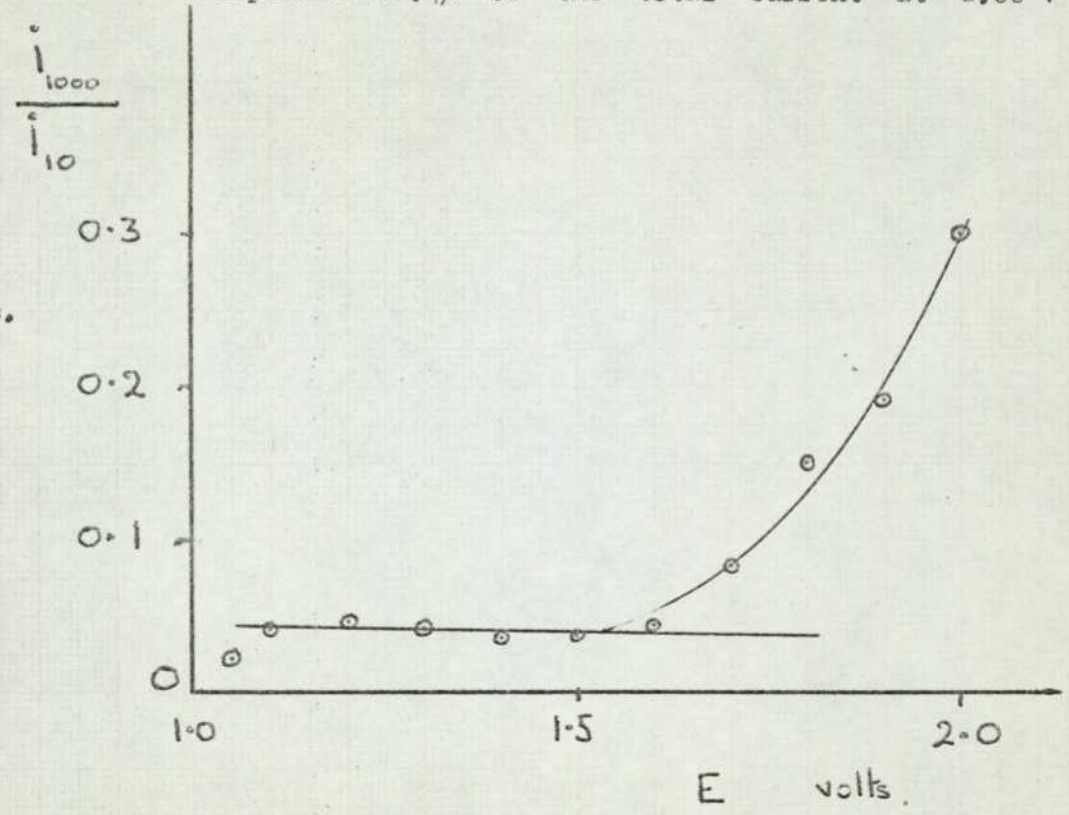
Graph 27.

Curve of the ratio of the current at I000 sec. to the current at I0 sec (relative rate of current decay) v. potential for a platinum foil electrode.

Electrolyte	5N H_2SO_4
Temperature	2I°C
Atmosphere	nitrogen
Pressure	I atmos.
O.C.V.	0.9 V
Electrocatalyst	platinum foil
Resistance	0.08 ohm
i_{I000}	current after I000 sec.
i_{I0}	current after I0 sec.

Separation of oxide formation and oxygen evolution currents.

At 2.00 V the predicted value of i_{I000} found by extrapolating the linear region of the curve to 2.00 V was 240 μA. The total actual current at 2.00 V was 2I00 μA after I000 sec., therefore oxide formation comprised II.4% of the total current at 2.00 V after I000 sec.



(I) current-time curves for oxygen evolution and oxide formation to be plotted at potentials above I.50 V. (Table 26).

(2) the oxide formation content of the total current at a given potential to be determined as a function of time. (Graph 34).

(3) the oxide coverage to be determined at potentials above I.50 V. (Graph 32).

The method was checked by plotting curves of oxide formation current v. time between I.5 and 2.0 V, measuring the area under the curve after various times and plotting a charge-log time curve which was linear ie. typical of oxide formation. Also the relative rate of current decay was the same as in the I.0 to I.5 V range, see graph 36.

Graph 32 shows the oxide coverage as a function of potential over the range I.0 - 2.0 V, the results from I.5 - 2.0 V being calculated from current time curves drawn using the oxide formation current separated from the total current. The rate of oxide film growth determined from the area under the same current-time curves is plotted against potential in graph 33. Both these graphs are linear in the range I.0 - I.5 V but deviate from linearity rapidly at potentials above I.7 V when the oxide film grows much more quickly.

If in the potential range I.5 - 2.0 V the fall of current with time is due entirely to oxide formation then the difference between the total current at t_1 and t_2 should be the same as the difference between the oxide formation component of the total current between the same times. Although this is approximately correct

Table 26.

Separation of oxygen evolution and oxide formation currents in the potential range I.6 - 2.0 V and the time interval 20 - I000 sec.

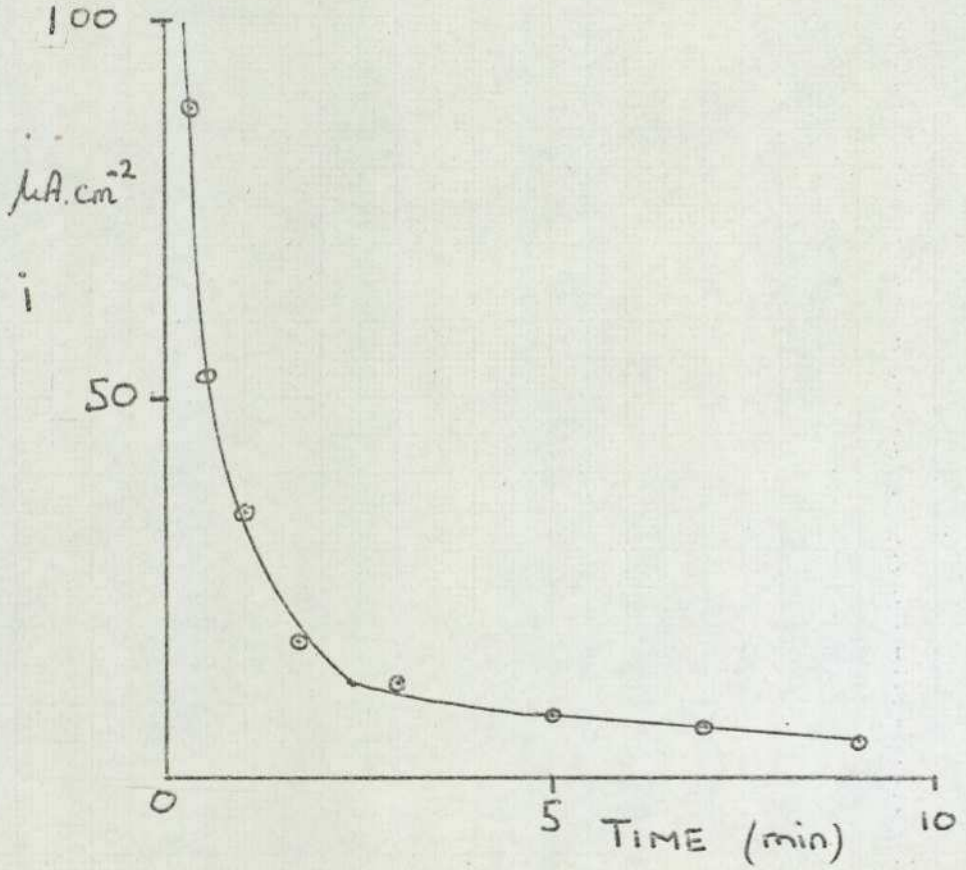
	i(total) μA	i(oxide) μA	i(O_2 evol.) μA	Time (sec)
E = 2.00 V	3800	770	3030	I00
	2I00	I82	I9I8	I000
	2800	350	2450	300
	5800	3850	I950	20
E = I.90 V	940	242	698	I00
	420	57	363	I000
	640	II0	530	300
	I700	I2I0	490	20
E = I.80 V	270	88	I82	I00
	II9	2I	98	I000
	I70	40	I30	300
	580	440	I40	20
E = I.70 V	80	33	47	I00
	25	7.8	I7.2	I000
	46	I5	3I	300
	I90	I65	25	20
E = I.60 V	40	24.2	I5.8	I00
	II	5.7	5.3	I000
	20.5	II	9.5	300
	I30	I2I	9	20

Electrolyte	5N H_2SO_4	Electrocatalyst	platinum foil
Temperature	2I°C	Resistance	0.08 ohm
Atmosphere	nitrogen	Pressure	I atmos.
O.C.V	0.9 V	Electrode area	5.0 cm^2

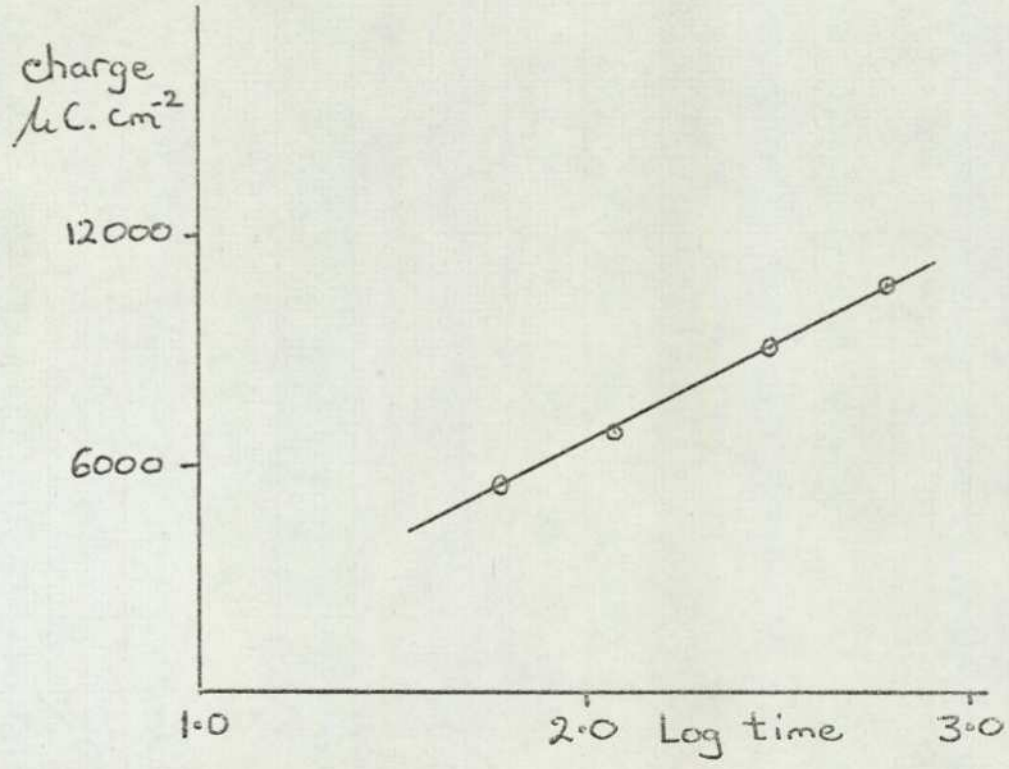
Graph 36.

Electrolyte	5N H_2SO_4	O.C.V.	0.9 V
Temperature	21°C	Electrocatalyst	platinum foil
Atmosphere	nitrogen at I atmos.	Resistance	0.08 ohm

(a) Plot of the oxide formation component of the total current at I.80 V against time for a platinum foil electrode.



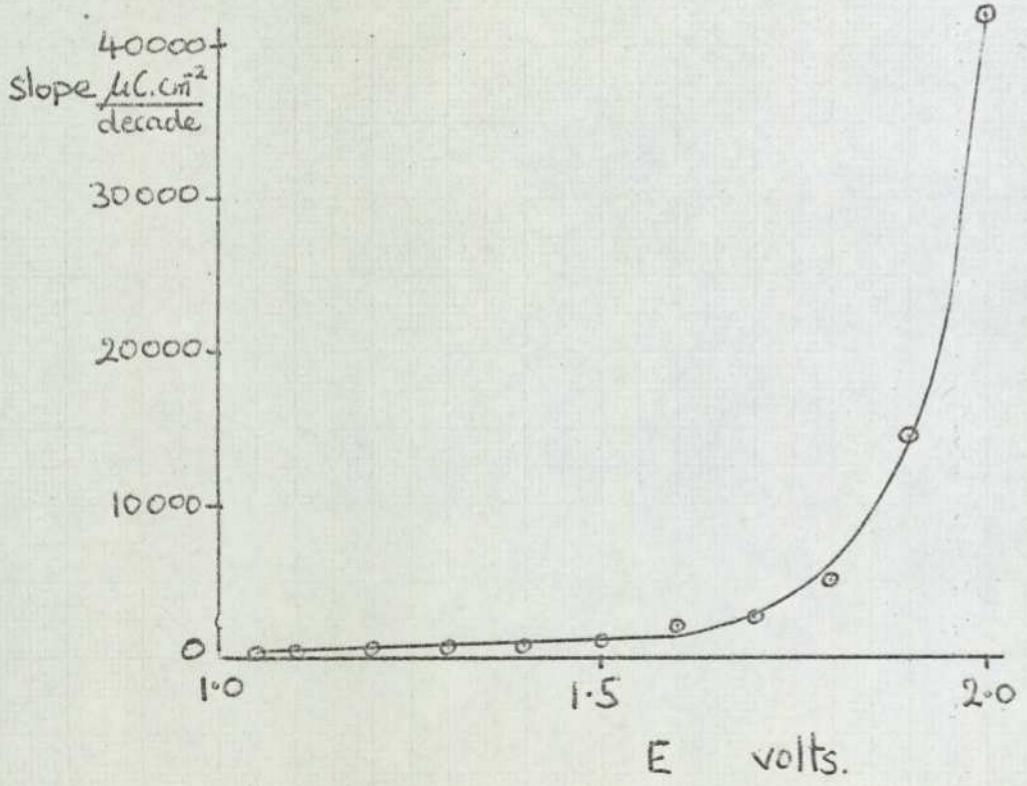
(b) Charge - log time plot for the oxide formation component of the total current at I.80 V for a platinum foil electrode



Graph 33.

Rate of growth of oxide film v. potential for a platinum foil electrode.

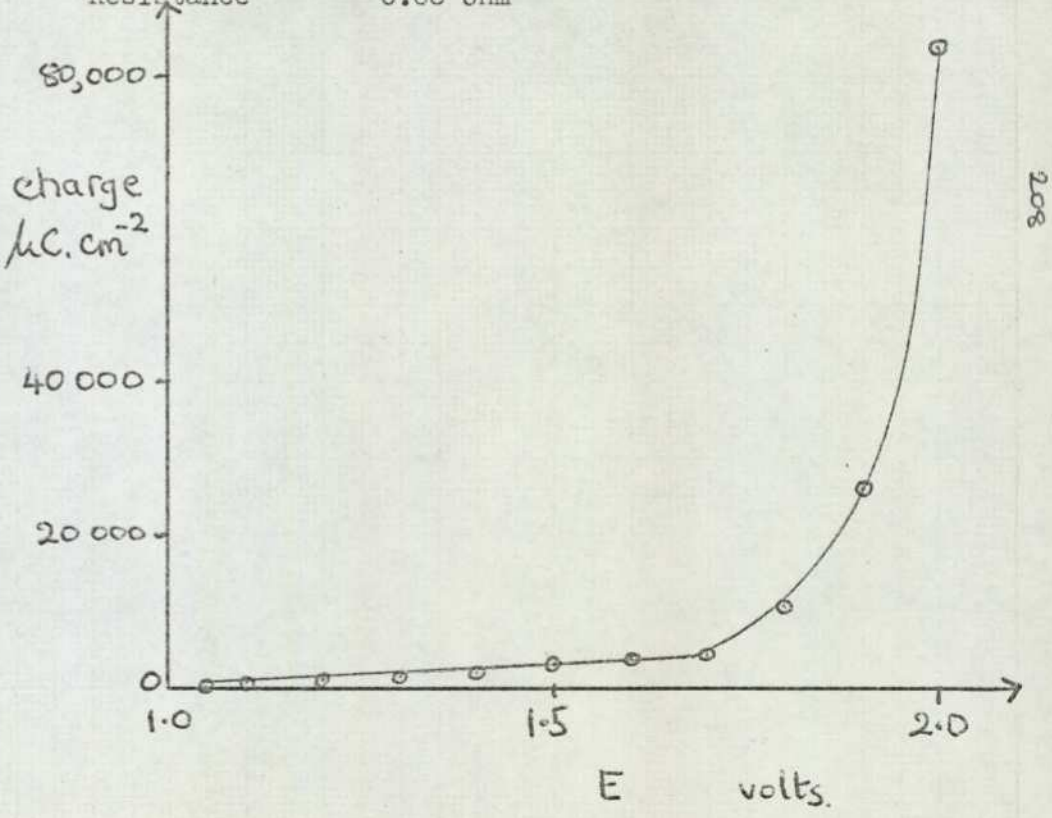
Electrolyte	5N H_2SO_4
Temperature	21°C
Atmosphere	nitrogen at I atmos.



Graph 32.

Oxide coverage v. potential for a platinum foil electrode.

O.C.V.	0.9 V
Electrocatalyst	platinum foil
Resistance	0.08 ohm



over the first 100 seconds at longer times it is found that the total current falls more than the oxide formation current, indicating that as the oxide film builds up the oxygen evolution current falls.

The method of separating the two components of the current at potentials above 1.50 V is based on the assumption that the current after 10 seconds is entirely due to oxide formation. This is not strictly true however, although the relative rate of current decay in the time range 5 - 20 seconds approximates to that predicted by Elovich kinetics. Hence the assumption is a reasonable approximation. The error will be in the form of an over compensation for the oxide current ie. the oxide proportion will be too high and the oxygen evolution proportion will be too low. The error can be reduced by measuring the current after shorter times and this can be achieved by recording potentiostatic transients over the first second.

This separation of the two main components of the anodic current from platinum electrodes at potentials above 1.50 V enables a better understanding of the anodic polarisation of platinum electrodes. For example the determination of oxide coverage at potentials above 1.50 V has been hindered by the oxygen evolution reaction occuring at the same potentials. Direct measurement by holding the electrode at a given potential for a given time followed by reducing the oxide by a cathodic current is complicated by the reduction of oxygen formed, at the anodic potential. Even constant nitrogen purging cannot overcome this difficulty since it is necessary to reduce the oxide immediately after

formation since it is only stable at its formation potential. Indirect methods such as the extrapolation of oxide coverage v. potential curve from I.0 - I.5 V up to 2.0 V are unsuitable because there is no justification for such an extrapolation.

In this study it was hoped to check the results from the separation technique by measuring the amount of oxygen formed and comparing the charge required to produce this amount of oxygen with the total charge passed, the difference being assigned to oxide formation. Unfortunately, although this technique is practically feasible it was found that a gas volume or weight detector of high sensitivity and fast response is required to follow the changes in current. The gas burette used in these experiments was not sufficiently sensitive, as although it could measure volumes reasonably accurately after extensive times at 2.00 V the oxide formation content of the total current falls rapidly with time and after only I5 min. it is less than I0%. It is hoped to calibrate some suitable capillary tubing to produce a sensitive micro gas burette to measure the very small volume changes.

The fall of anodic currents with time on platinum confirmed by the above results, shows that the Bockris mechanism cannot be correct. Bockris assumes that the oxygen evolution reaction will cease if all the platinum surface sites are converted to oxides. The following calculation shows that the oxide film can grow to a thickness of several monolayers:-

The area of a platinum site has been shown to be 8.9 $Å^2$ (187). Hence on I cm^2 of platinum surface there

will be $\frac{10^{16}}{8.9}$ platinum sites.

There are 6×10^{23} platinum sites in a gram atom of platinum.

Hence the weight of a monolayer of PtO,

$$w = \frac{10^{16}}{8.9 \times 6 \times 10^{23}} \times 211$$

The volume of a monolayer of PtO = $1\ cm^2 \times t$ where t is the monolayer thickness.

$\therefore\ t = \frac{w}{14.9}$ where 14.9 is the density of PtO.

$$t = \frac{10^{16} \times 211}{9 \times 6 \times 10^{23} \times 14.9} = 0.26 \times 10^{-7} = 2.6\ \text{Å}$$

A similar calculation to find the thickness of a monolayer of PtO_2 gives a value of 3.9 Å. (The density of PtO_2 is not known but an estimated value of $10\ g.cm^{-3}$ was used.)

The charge required to grow a monolayer of PtO is determined as follows:-

$$Pt + H_2O = PtO + 2H^+ + 2e$$

To form a monolayer $2 \times \frac{10^{16}}{8.9}$ electrons must be passed.

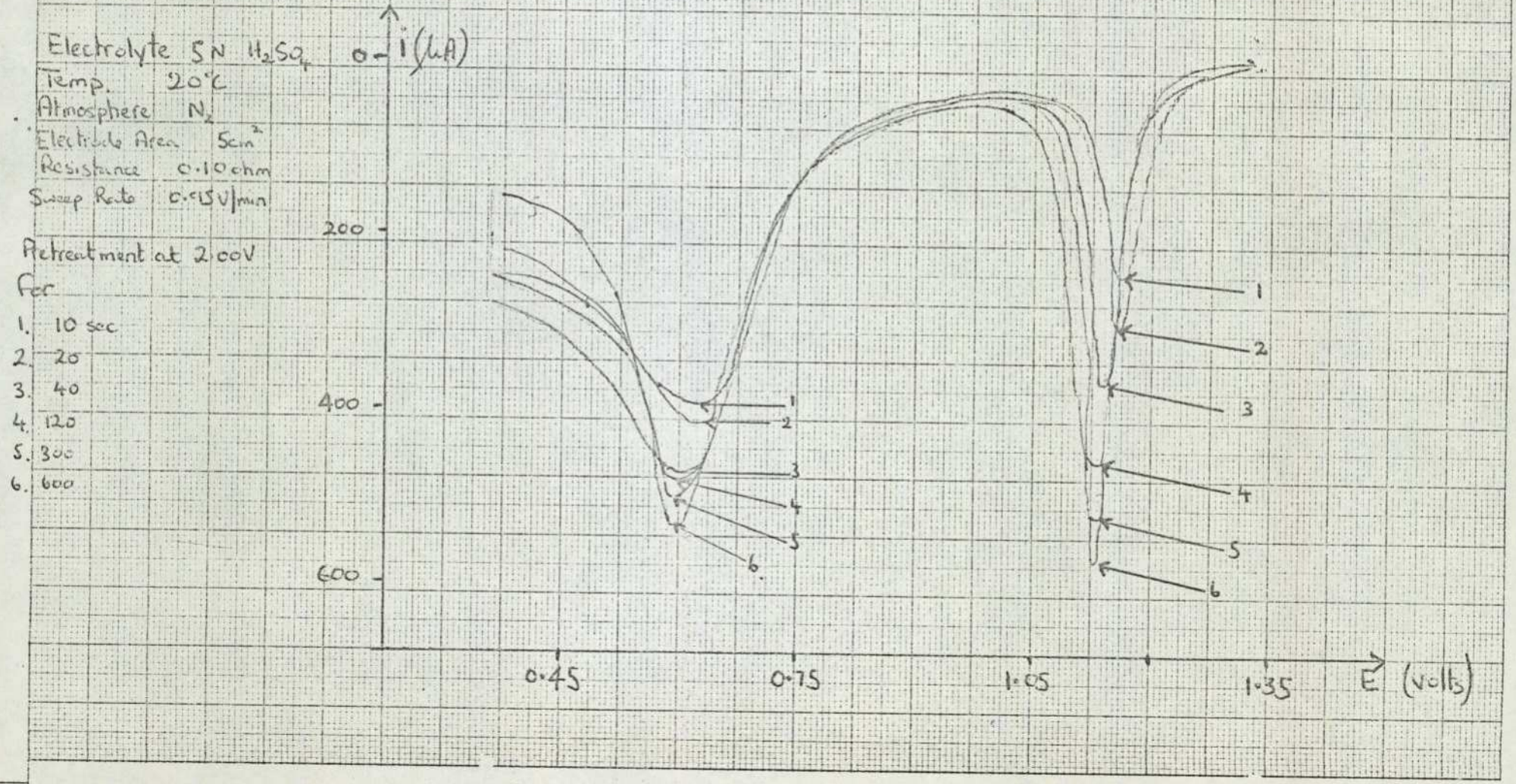
To form 1 gram molecule of PtO two Faradays ($2 \times 6 \times 10^{23}$) electrons must be passed.

$\therefore$ number of gram moles in $1\ cm^2$ monolayer $= \frac{2 \times 10^{16}}{8.9 \times 2 \times 6 \times 10^{23}}$

$= n$

$\therefore$ number of coulombs to prepare $1\ cm^2$ of monolayer of PtO = $n \times 2 \times 96{,}500 = 320\ \mu C$

GRAPH 47. The effect of anodic pretreatment time on the cathodic voltammagram under N_2.



A similar calculation for the formation of PtO_2 gives a value of 640μC.

If these values are compared with the charge v. potential curve in graph 30 it can be seen that several monolayers of the oxide can exist and that the thickness grows with time.

The decay of the oxygen evolution current with time indicates the growth of oxide even on surfaces containing more than a monolayer of oxide. When a platinum electrode was preanodised at 2.00 V for different times and then switched to a potential of I.35 V and the oxide layer stripped off the coverage was shown to increase with the time of pretreatment. Graph 47. These phenomena cannot be explained by the Bockris mechanism but they can be explained by assuming the coexistance of PtO and PtO_2 or the presence of nonstoichiometric oxides ie. no restriction on the thickness of oxide film and the thickness of the film affects the conductivity.

In order to determine x at a given potential it is necessary to know the exact thickness of the film from ellipsometer measurements, the monolayer thickness and the total oxide charge coverage. A knowledge of x would be very useful since the value of x as oxygen evolution starts at about I.45 V could be significant.

The linear relationship between the oxide coverage and log time for platinum foil in the potential range I.05 - I.50 V is similar to that commonly observed for gas chemisorption kinetics and known as Elovich kinetics. This relationship has also been found for the chemisorption of oxygen on platinum surfaces under open circuit conditions.(185)

The application of the Elovich equation,

$$\frac{dq}{dt} = ae^{-\alpha q} \qquad (I)$$

where q = amount adsorbed at time t

a and α are constants

is best made using an integrated form of equation. Assuming that q = 0 when t = 0

$$q = \frac{2.3}{\alpha} \log(1 + a\alpha t) \qquad (2)$$

or

$$q = \frac{2.3}{\alpha} \log(t + t_o) - \frac{2.3}{\alpha} \log t_o \qquad (3)$$

where $t_o = 1/\alpha a$

If a volume of gas is adsorbed instantaneously before the Elovich equation is obeyed, then equation (I) can be amended to

$$q = \frac{2.3}{\alpha} \log(t + k) - \frac{2.3}{\alpha} \log t_o \qquad (4)$$

where $k = t_o \exp \alpha q_o$

If k is negligible in comparison with t, then

$$q = \frac{2.3}{\alpha} \log t - \frac{2.3}{\alpha} \log t_o \qquad (5)$$

$$q = \frac{2.3}{\alpha} \log a\alpha t \qquad (6)$$

If $a\alpha t \gg I$ then equation (2) reduces to equation (6). If k values are practically larger than zero then the q - log t plot is not linear and must be linearised by provision of a constant, k, of suitable magnitude so that a plot of q - log(k + t) is linear. If k is negligible then equation (6) applies and the q - log t plot is linear.

From the above equations the rate of adsorption

$$\frac{dq}{dt} = \frac{2.3}{\alpha t}$$

The constant, α, being inversely proportional to the ambient rate of adsorption when $a\alpha$ is large or k or t_o very small. Hence the constant, α, can be used to describe the adsorption over its entire course.

Deviations from Elovich kinetics are sometimes observed at long times when the rate of adsorption has fallen to very low values when experimental precision is low.

Elovich kinetics can be accounted for in a number of ways:

(I) by a decrease in density of the active sites on the surface,

(2) by a decrease in adsorption energy with an increase in coverage, or

(3) by the formation of energy barriers in an electron transfer process at an interface.

In the present study it is unlikely to be (I) as suggested by Bockris,(54) since the oxide coverage can exceed monolayer proportions. It appears more likely that the energy barrier to oxide formation increases as the coverage increases.

The oxide coverage of platinum in the potential range 0.5 V to I.0 V has been reported to follow Elovich kinetics[185] and the reason given for the increase in activation energy with time is that at potentials highly anodic to the potential of zero charge, uncharged species may have considerable difficulty in reacting at the metal surface.

It was postulated that at potentials more positive than the potential of zero charge, there is strong electrostatic interaction between the negatively charged, oxygen end of the water dipole in the inner region of the double layer and metal surface. Compression of this layer of water molecules is probable due to the interaction between the outer, negatively charged ionic layers and the positive field at the interface. However, neutral species such as oxygen, containing π electrons can bond strongly to the positively charged metal surface, producing chemical bonds rather than electrostatic bonds. As a result of these strong chemical bonds the oxide film is not displaced by an adsorbed water layer at high positive potentials.

However, at potentials in the range I.0 - I.5 V the oxide film is not formed by adsorption of the oxygen molecule but by discharge of water molecules resulting in the formation of chemical metal - oxygen bonds. The results of the present investigation show that oxide is formed by electrolytic discharge of water at potentials above 0.85 V. Hence there is some doubt as to whether the oxide layer in the potential range 0.85 - I.0 V is formed by adsorption of oxygen

molecules, discharge of water or both simultaneously. It is possible that at very high positive potentials (I.45 V) the oxide film is desorbed and replaced by water molecules resulting in oxygen evolution of the desorbed oxygen, followed immediately by more oxide formation from the electrolytic discharge of water molecules and subsequent decomposition to oxygen. As the potential increases the rate of decomposition and the rate of formation of oxide increases. However, at a given potential the overall rate of formation must exceed the rate of decomposition (ie. current falls with time.)

Bockris[54] has shown a linear relationship between overvoltage and log time at a constant oxygen evolution current density. Two linear regions were observed with different gradients before the current became steady. It was assumed that when the steady current was achieved the surface was completely covered with oxide and a new rate determining step was operating. An equation of the following type was postulated:

$$i = k_{act}\, c_{OH^-}(1-\theta_t)\exp\left[\frac{\alpha \eta_t F}{RT}\right] + k_{inact}\, c_{OH^-}\theta_t \exp\left[\frac{\alpha \eta_t F}{RT}\right]$$

where k_{act} = rate constant of bare metal active sites

k_{inact} = rate constant of oxide coated metal active sites

θ_t = fraction of surface covered with oxide at time, t after commencing polarisation

The rate determining step for the reaction on the active sites results in current decay while the rate

determining step on the inactive sites results in a time invariant current. On this basis the current should become constant when a monolayer of oxide has formed. The results of the current investigation show that the current continues to fall even when the oxide coverage exceeds monolayer proportions. Bockris attributes this phenomenom to impurities in the electrolyte poisoning the catalyst. However, the electrolyte had been extensively preelectrolysed thus making this explanation improbable.

3.9. The Strength of Porous Materials.

3.9.1. Little work has been done on the mechanical strength of porous materials. In the following section four possible models are considered.

(a) a very simple model for the strength of a single pore from basic mechanical engineering theory.

(b) an empirical model based on the porosity of continuous solid phase structures.

(c) a theoretical model based on the strain energy of a pore and the gas pressure developed within it due to hydrogen evolution.

(d) a theoretical model based on the determination of the bond strength responsible for the attraction between individual aggregate particles. The effect of binders is investigated.

These models are discussed in relation to the experimental results already observed on teflon bonded electrodes and also with the effect of varying the teflon content.

(a)

Before any current is passed the electrocatalyst pores are filled with electrolyte. When a potential is applied at which hydrogen is evolved, gas is produced in these pores. This gas will escape from the pore when its pressure exceeds a certain value given by

$$p = \frac{2\sigma . \cos\theta}{r}$$

where p is the gas pressure

σ is the surface tension

r is the pore radius

θ is the contact angle

If we assume that $\theta = 0$ then the maximum pressure which can be developed in a pore of radius, r is, $2\sigma/r$. This pressure is of the order of 1000 atmos. for a 10 Å pore radius and about 100 atmos. for a 100 Å pore radius using aqueous solutions.

Consider a thin walled cylinder closed at both ends and subject to a uniform internal pressure, p. Let the wall thickness be h and the inner radius r. To determine the circumferential stress, s_c, consider a section of the cylinder of length, l, to be removed from the vessel, see Fig. (a). Fig. (b) shows the forces acting on a cross section. The horizontal components of the radial pressures cancel one another by virtue of symmetry about the vertical centre line. In the vertical direction the equilibrium equation is

$$\sum F_v = -2 s_c h l + \int_0^{\pi} pr(d\theta)(\sin\theta)l = 0$$

Integration gives

$$2 s_c h l = -prl\left[\cos\theta\right]_0^{\pi}$$

$$\therefore s_c = \frac{pr}{h} \qquad (I)$$

Fig (a)

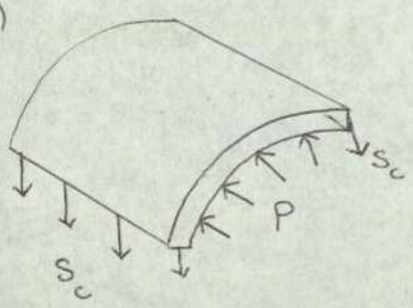
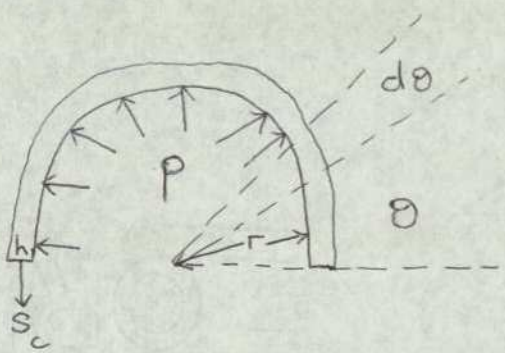


Fig (b)



Hence using the known values of s_c, r and h, it is possible to find the maximum pressure that the cylinder can endure.

For platinum black, assume s_c = 20,000 psi = tensile strength of platinum.

Let $h = 10^{-6}$ cm and $r = 2 \times 10^{-7}$ cm

For graphite assume $s_c = 6 \times 10^{7}$ dynes.cm^{-2} and $h = 10^{-6}$ cm and $r = 2 \times 10^{7}$ cm

then p for platinum black $= 6 \times 10^{3}$ atmos.

and p for graphite $= 3 \times 10^{2}$ atmos.

Hence pores of radius < 10 Å are stable in platinum black while graphite pores of radius < 50 Å are liable to rupture.

Applying the Nernst equation for the reversible hydrogen electrode in a solution of protons of unit activity

$$\eta = \frac{RT}{2F} \ln p_{H_2}$$

where η is the overpotential necessary to produce a hydrogen pressure, p, it can be taken as a crude condition of breakage.

$$p_{H_2} = e^{-2\eta F/RT} > 2\sigma/r \qquad (2)$$

The above treatment is only a very approximate likeness to a pore in a teflon bonded electrode for a number of reasons: (I) in the model it is assumed that the pore is completely surrounded by solid of a given thickness. As the pore is formed by the pushing together of several electrocatalyst particles this is not really justified unless there is some form of

metallic bonding between these particles. Probably the electrode is significantly less strong than the tensile strength value for the solid material.

(2) The tensile and compressive stresses in the cylinder wall must be uniformly distributed over the thickness of the wall and stresses must be symmetric about the axis of the cylinder.

(3) The wall thickness should be less than the radius of curvature.

(4) The argument given is quasi-thermodynamic in nature, the effects of kinetic hindrances being neglected. In this case at cathodic overpotentials greater than that given by (2), degradation is possible although its actual occurrence will depend on kinetic factors.

(b)

The effect of the amount of porosity on elastic moduli of continuous solid phase structures is given by the formula (I86)

$$\frac{I - G}{G_o} = \frac{5(3K_o + 4G_o).P + AP^2}{9K_o + 8G_o}$$

where G = rigidity modulus

K = bulk modulus

P = volume fraction of pores

A = constant

zero subscript refers to solid material

This law has been shown to be roughly obeyed by most materials, slight discrepancies being due to different types of porosity. For aluminium oxide of porosity 70% the elastic modulus is only 10% of the value of non porous aluminium oxide. Similarly for 60% porosity the

transverse strength of alumina is less than 10% of the non porous value. These changes in strength are expected to be the minimum changes with porosity, since the samples are continuous solid phase, with isolated isometric pores. Hence for porous materials made from powders the loss of strength with increasing porosity would be significantly greater.

(c)

Another possible approach, which overcomes the limitations of the thin walled cylinder calculation, is to consider the strain energy as the work done to increase the strain of the pore from $e = 0$ to $e = e$ under the action of a stress, σ, which arises from the gas pressure within the pore.

ie.

$$U_{strain} = \int_0^e \sigma \, de$$

However $\sigma = Ye$ where Y is the Young's Modulus

$$\therefore U_{strain} = \int_0^e Ye \, . \, de = \frac{Ye^2}{2} = \frac{\sigma^2}{2Y}$$

This is the strain energy per unit volume. Hence for the pore considered, the strain energy is:

$$\frac{\sigma^2}{2Y} \cdot V_{pore}$$

If the pore was a cylinder of radius, r, the volume would be $V_{pore} = \pi r^2 l$ where l is the length of the cylinder. Alternatively if we consider a spherical pore, $V_{pore} = \frac{4}{3}\pi r^3$. If we assume that the total surface energy of the crack is yA where y is the surface tension and $A = 4\pi r^2$ (sphere) or $2\pi rl$ (cylinder) then for a cylindrical pore

$$U = \frac{-\sigma^2}{2Y} \cdot \pi r^2 l + \gamma 2\pi r l .$$

If the hydrogen pressure is large enough the pore will fracture. One can find the critical value of σ and the gas pressure in the pore by finding what value of σ corresponds to:

$$\frac{du}{dr} = 0$$

$$\frac{du}{dr} = 0 = \frac{-\sigma^2}{Y} \cdot \pi l r + 2\gamma_s \pi l$$

$$\sigma = \left[\frac{2\gamma_s Y}{r}\right]^{\frac{1}{2}}$$

For a spherical pore

$$U = \frac{-\sigma^2}{2Y} \cdot \frac{4}{3}\pi r^3 + \gamma_s 4\pi r^2$$

$$\frac{du}{dr} = \frac{-4\sigma^2}{2Y} \cdot \pi r^2 + 8\gamma_s \pi r = 0$$

$$\therefore \frac{2\sigma^2}{Y} \cdot \pi r^2 = 8\gamma_s \pi r$$

$$\therefore \sigma^2 = \frac{8\gamma_s Y}{2r} = \frac{4\gamma_s Y}{r}$$

$$\sigma = \left[\frac{4\gamma_s Y}{r}\right]^{\frac{1}{2}}$$

Applying the Nearnst equation for the reversible hydrogen electrode

$$e_{H_2} = -\frac{RT}{2F} \ln P_{H_2}$$

for a unit active proton solution

$$\eta = \frac{-RT}{2F} \ln P_{H_2}$$

$$P_{H_2} = e^{-2\eta F/RT}$$

$$P_{H_2} = e^{-2\eta F/RT} > \left[\frac{2\gamma Y}{r}\right]^{\frac{1}{2}}$$ for a cylindrical pore

Hence the pressure of gas in the pore required to cause breakage is related to a certain hydrogen over-potential. Taking typical values of y, Y and r this gives a pressure of about 10^4 atmos. However, in a capillary of radius, r the maximum gas pressure which can exist is $\frac{2\gamma}{r}$ dynes.cm^{-2} which, using typical values comes to about 100 atmos. ie. less than the breaking pressure. Hence this model predicts no pore breakage and this is not in agreement with the experimental data. This model would probably apply more accurately to a material containing relatively isolated pores unlike teflon bonded porous electrodes which have a porosity in the range 60 - 90%.

(d)

The strength of porous bodies can be studied from two approaches: (I) by considering the sample to be of continuous solid phase with isolated isometric pores, or

(2) by considering the sample to be composed of individual small particles made into a pellet and held together by some type of bonding force at their points of contact. In this second approach the spaces between the individual particles can be filled with air or either partly or entirely with strength transferring material. This approach is more applicable to the situation of teflon bonded porous, gas diffusion electrodes.

Solid aggregates or agglomerates form by different kinds of bonding mechanism, namely: (I) by forming solid bridges between the particles. This type of bonding can occur by sintering, by chemical reactions, by melting and, more importantly, for porous teflon bonded electrodes, by hardening, bonding agents which can form a bridge between the grains during curing. Another important process by which solid bridges may be formed is by crystallisation ie. when solids dissolved in a liquid crystallise they can form solid bridges at the points of contact, this being more significant in that the dissolved and crystallised components may be either the electrocatalyst or foreign matter.

(2) by interfacial forces and capillary pressure in movable liquid surfaces. Intergranular liquid can influence adhesion in different ways. When the liquid has a movable surface the agglomerate can be formed in three ways:

(a) The void spaces between the particles are only partly filled with liquid which forms bridges between individual particles. At the solid - liquid - gas contact

lines, the surface tension is directed along the liquid surface while a negative capillary pressure exists in the liquid bridge, if the solid is wetted. Both these components result in mutual attraction between the particles at the liquid - gas interface.
(b) if the void space is completely filled with liquid, but the liquid does not completely envelop the agglomerate, interfacial forces exist only at the surface of the agglomerate and a negative capillary pressure exists throughout the liquid space giving the agglomerate a certain tensile strength.
(c) when the liquid completely envelops the agglomerate all interparticulate capillary bonding forces vanish and the bulk of the grains are held together only by the surface tension of the liquid droplet which envelops it.
(3) by adhesional and cohesional forces in bonding bridges which are not freely movable. With this type of bridge the following bonding mechanisms are possible: (a) thin layers of viscous binders adhering to the solid, are introduced between the particles. Such a binder will retain any surface shape given to it, because the energy required for deformation would be much greater than the decrease in surface energy. The bonding strength can be increased by several orders of magnitude, compared with the bonding strength of freely movable liquid bridges. After a certain time many viscous binders harden and form solid bridges.
(b) Adsorption layers. Capillary condensation is only observed at a pore radius greater than a certain value. Adsorption layers which are thinner than this transmit

the entire force of molecular attraction from one particle to another if they touch or penetrate one another.

(4) Even if no material bridges exist between the particles, attraction may exist and transmit tensile forces. These attractions can be molecular of electrostatic in nature. At particle distances of about 100 Å, Van der Waals forces have significant values and may occur in the agglomerate complex. Valence forces may be disregarded because of their very short range. Electrostatic charges can be picked up by particles as a result of contact friction and although charge equalisation should occur to some extent, these forces can still contribute to the agglomeration.

(5) By form - closed bonds. With suitable motion or compression, particles can interlock or mat with each other, a bond being supported by this form closure. This type of bonding is prevalent with fibrous, bulky and flat shape particles.

In practice pellets are strained by impact, compression, bending, abrasion and shear. Normally tests are designed for each particular application eg. compression tests, drop tests. If a pellet is strained by some force, tensile, pressure and shearing stresses are caused. Expansion under the pressure stress and sliding under the shear stress are not possible for most agglomerates because of their rigidity. Hence it is the tensile stresses which lead to fracture. Only very moist agglomerates are plastic where the particles are not closely packed. Rumpf (I38) has derived an approximation for the tensile strength of agglomerates

and confirmed it by measurement. This theoretical model is only an approximation giving the order of magnitude of tensile strength to be expected since the actual structure of the agglomerate cannot be considered. The main assumptions made are

(I) the number of bonds in the stressed cross section is very high.

(2) the bonds are statistically distributed across the section and over the directions in space.

(3) the particles composing the agglomerate are spherical and of uniform diameter.

(4) the particles are statistically distributed in the granule.

(5) the effective bonding forces are distributed around a mean value which can replace them in calculations.

The expression derived by Rumpf is

$$T.S = \frac{9}{8} \frac{(1-e)}{\pi d^2} kH$$

where T.S. = tensile strength

e = porosity

d = particle diameter

k = mean coordination number

H = mean bonding force at point of contact

d and e can be obtained easily from size distribution analysis and from the density of packing. The relation between k and e has been determined for spheres of uniform size and shown to be (I39)

$$ke \sim 3.I \sim \pi$$

This leaves the value of H to be determined. Estimates of this value can be obtained if the type of bonding mechanism is known.

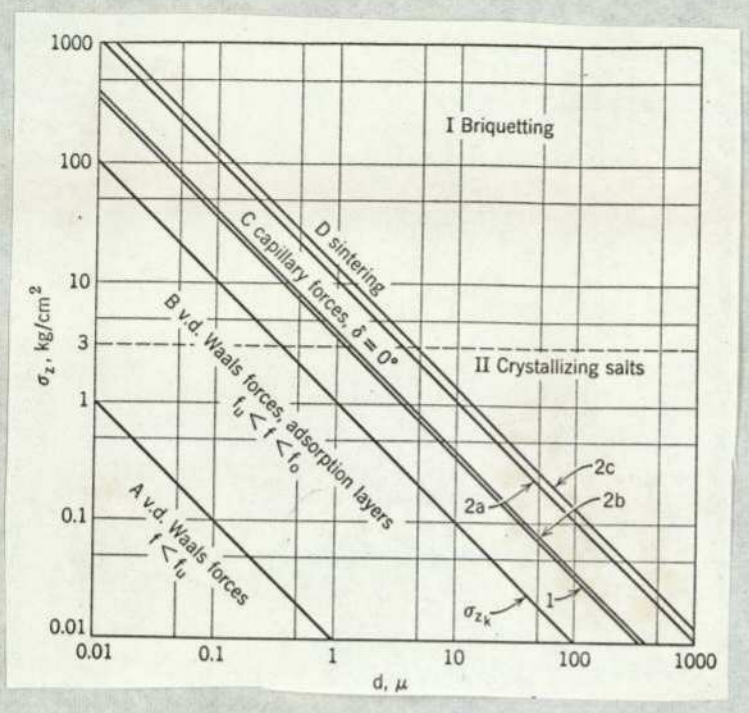
In practice a uniform particle size is not obtained and d should be replaced by d_h, the mean equivalent particle diameter which depends mainly on the fine particle size since the larger particles contribute little to the tensile strength of the agglomerate.

When the agglomerate is filled with a strength transferring material the stress distribution of a cross section strained by tension depends greatly on whether the agglomerate is filled with a movable liquid or whether the bonds are due to non movable liquid or solid binders.

The plane of fracture of agglomerates with non movable binders follows the weakest path. If the strength of the binder is much less than that of the particles, the fracture follows the particle edges. Depending on the relative strengths three possibilities for fracture exist: (I) through the particle, (2) along the boundary edges and (3) in the binder.

Van der Waals forces are able to transmit quite high tensile loads if the distance between appreciable portions of the grain surface can be reduced to less than 100 Å. eg. 10 $Kg.cm^{-2}$ when all the surface is brought to a separation distance of -17.5 Å.(133) Table 2. shows Rumpf's curve for the theoretical tensile strength of agglomerates as a function of particle size, which shows the regions for various bonding mechanisms.

Rumpf's curve.



Rumpf has confirmed this plot experimentally for the capillary pressure bonding mechanism.

The value of the mean bonding force at the point of contact can be determined for capillary forces, Van der Waals forces and electrostatic forces. Dimensional analysis for liquid bridges involving capillary pressures gives

$$H = \alpha d . f(\delta, \beta)$$

where α is the surface tension

δ is the contact angle

β is the sector angle of the liquid ring.

$f(\delta, \rho)$ has been evaluated (I40, I41) for complete wetting between $\beta = 10^\circ$ and 40° as

$$f(\delta, \beta) = 2.2 \text{ to } 2.8$$

Van der Waals forces for particle distances below 1000 Å may be obtained by the Heitler - London theory. It has been shown that for oxides or water the bonding force is given by

$$H = \left(\frac{A}{24}\right)\left(\frac{d}{a^2}\right)$$

where A is a constant equal to 10^{-12}

a is the distance between the surfaces of the two spheres.

It is known that small moisture contents greatly increase the strength of agglomerates formed from fine grained material. Under these conditions all the water is bound to the surface by adsorption and increasing thickness of these layers reduces the distances between the particle surfaces. This would result in forces greater than capillary forces. The adsorbed layer can be as thin as a monolayer and can increase in thickness until the water becomes mobile. It would seem that Van der Waals forces would have little effect on the strength unless a was consistently small throughout the agglomerate. The conditions for electrostatic bonding are very specific and this form of bonding is rarely encountered.

Some experimental work (I42) on the tensile strength of pelletised alumina has shown that up to a certain pressure the strength increases with compacting pressure although it is independent of the pressing time. The compacting pressure has little effect on the small pores but tends to reduce the size of the macropores. However, the catalytic activity and surface area were little affected by the compression. The values of tensile strength obtained were fitted to Rumpf's model and showed that the bonding forces were in the Van der Waals region.

In teflon bonded porous electrodes the possible bonding mechanisms are

(I) by the formation of solid bridges by hardening

bonding agents or by the crystallisation of dissolved material.

(2) by interfacial and capillary forces.

(3) by adhesional and cohesional forces in bonding bridges which cannot freely move ie. viscous binders and adsorption layers (note teflon is actually a solid binder).

(4) Van der Waals attraction between solid particles (before placing in the electrolyte).

The table below compares the capillary and Van der Waals bonding forces, aggregate tensile strengths and solid tensile strengths calculated from the known particle dimensions of platinum and carbon blacks.

	particle dimensions A	Ts_I Kg/cm^2	capillary bonding. H dynes	Ts_2 Kg/cm^2	Van der Waals bonding. H dynes	Ts_2 Kg/cm^2
Platinum black	a = IO d = IOO	$I.3\times IO^3$	$I.8\times IO^{-4}$	85	$4.2\times IO^{-6}$	2
carbon black	a = 200 d = 2500	30	$5\times IO^{-3}$	4	$2.6\times IO^{-7}$	$3\times IO^{-4}$

assume porosity = 0.7

a = inter particle distance within an aggregate A

d = particle diameter A

Ts_I = tensile strength of solid material Kg/cm^2

Ts_2 = tensile strength of porous material Kg/cm^2

H = bonding force dynes

The tensile strength values predicted by Rumpf assuming a porosity of 0.35 are

for 100 Å particles

Van der Waals bonding	< 1 kg/cm^2
Van der Waals adsorption layer bonding	1 - 100 kg/cm^2
Capillary forces	100 - 1000 kg/cm^2
Bonds due to scintering and solid bridges	>1000 kg/cm^2

for d = 2500 Å

Van der Waals bonding	< 0.05 kg/cm^2
Van der Waals adsorption layer bonding	0.05 - 5 kg/cm^2
Capillary forces	5 - 80 kg/cm^2
Bonds due to scintering and solid bridges	>80 kg/cm^2

Tests on the tensile strength of alumina pellets of surface area about 200 m^2/g and particle size 50 - 100 Å showed a maximum strength before compacting of 0.1 to 2 kg/cm^2 and after compacting a maximum strength of 1 - 6 kg/cm^2. (142)

Tests have shown that the compressive strength of coal pellets 20 mm in diameter composed of particles about 10^{-2} - 10^{-3} cm in diameter are in the range 0.1 - 100 kg/cm^2. (143)

3.9.2. The effect of teflon content on (a) the mechanical strength and (b) oxygen reduction performance of graphite based electrodes.

(a) Experiments on teflon bonded graphite electrodes with varying teflon contents (0 - 50% by weight) were made under anodic conditions and the current at which electrode damage was initially obeerved was noted, see table below.

Electrolyte	5N KOH	Electrocatalyst S.A.	500 m^2/g
Temperature	20 C		
Atmosphere	air	Electrocatalyst loading	10 mg.cm^{-2}
O.C.V.	0.97 V	current collector	nickel screen
		Resistance	0.15 ohm

Teflon content by weight	Breakage current $mA.cm^{-2}$	Breakage potential V
0%	2	I.3
20%	25	I.5
30%	60	I.56
40%	560	I.8
50%	>I500	>2.6

Hence it can be seen that by increasing the binder content above the 30% value which is optimum for gas dissolution reactions an electrode can be manufactured which will support high gas evolution rates without mechanical damage although a corresponding reduction in gas dissolution performance must be accepted.

Hence it would be quite a simple matter to optimise between the teflon content, gas dissolution discharge performance and the recharge rate. It can be seen that for recharge rates involving current densities not exceeding 50 $mA.cm^{-2}$ (a figure commonly quoted in connection with the overnight recharging of electric vehicles) a graphite based electrode could be conveniently used if the graphite surface oxides could be easily reduced.

(b) Teflon bonded platinised graphite electrodes containing varying teflon contents were prepared and their oxygen reduction current measured at 0.75 V under oxygen.

$i(mA.cm^{-2})$	teflon % (by weight)
I30	30
II0	40
I30	20
60	I0
I9	50

Electrolyte 5N KOH

Temperature $20^{\circ}C$

Atmosphere oxygen at I atmos.

O.C.V. I.03 V

Electrocatalyst S.A. 500 m^2/g

Electrocatalyst loading 9 $mg.cm^{-2}$

Current collector nickel screen

resistance 0.I2 ohm

These results agree quite closely with those obtained by Giner (I58) for teflon bonded platinum black electrodes. Although the current at 0.75 V does not vary much between teflon contents of 20 - 40% it should be noted that at the lower end of the range the electrode tends to sweat after long periods of use while at the upper end of the range the electrolyte takes a long time to wet the electrocatalyst causing delays before new electrodes are ready for use.

The fact that the electrode strength increases rapidly as the teflon content increases suggests that the low teflon volume concentration of the electrode is probably the cause of its low strength. If the following data is assumed :

	particle/aggregate diameter μ (17)	density
graphite	4	2.2
teflon	2 (after curing at 300°C)	4.0

Then ext. volume of graphite aggregate $= \frac{4}{3}\pi r^3 = 3.2 \times 10^{-11}$ ml

ext. volume of teflon particle $= \frac{4}{3}\pi r^3 = 4 \times 10^{-12}$ ml

mass of I graphite aggregate of porosity 0.8 $= 2.2 \times 3.2 \times 10^{-11} \times 0.8$

$= 5.6 \times 10^{-11}$ g

mass of I teflon particle of porosity 0.0 $= 1.6 \times 10^{-11}$ g

10 mg of graphite contain 0.18×10^{9} aggregates

3 mg of teflon contain 2×10^{8} particles

Volume ratio in normal teflon bonded (30% by weight) graphite electrodes is given by :

volume of teflon particle × no. of teflon particles in electrode

and volume of graphite aggregate × no. of graphite aggregates in electrode

and is found to be 88% graphite and 12% teflon by volume.

If the graphite aggregate is completely surrounded by teflon particles the structure should have maximum strength,

no. of teflon particles to surround I graphite aggregate

$$= \frac{2\pi(r + a)}{2a} \sim 20$$

where r = radius of graphite aggregate

a = radius of the teflon particle

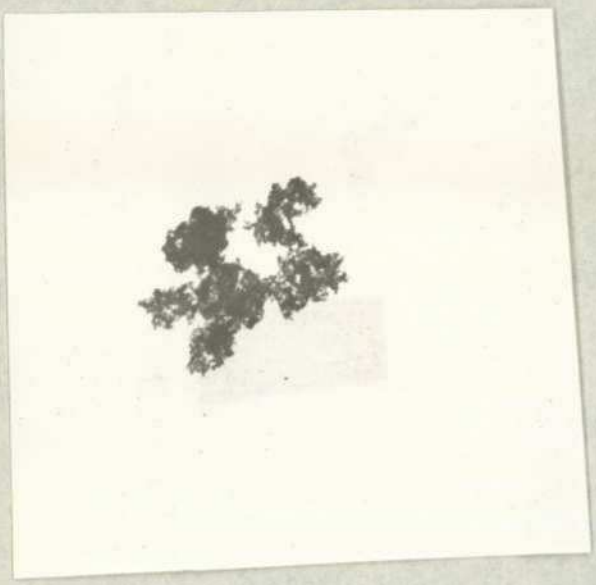
For this condition the volume ratio would be 71% teflon

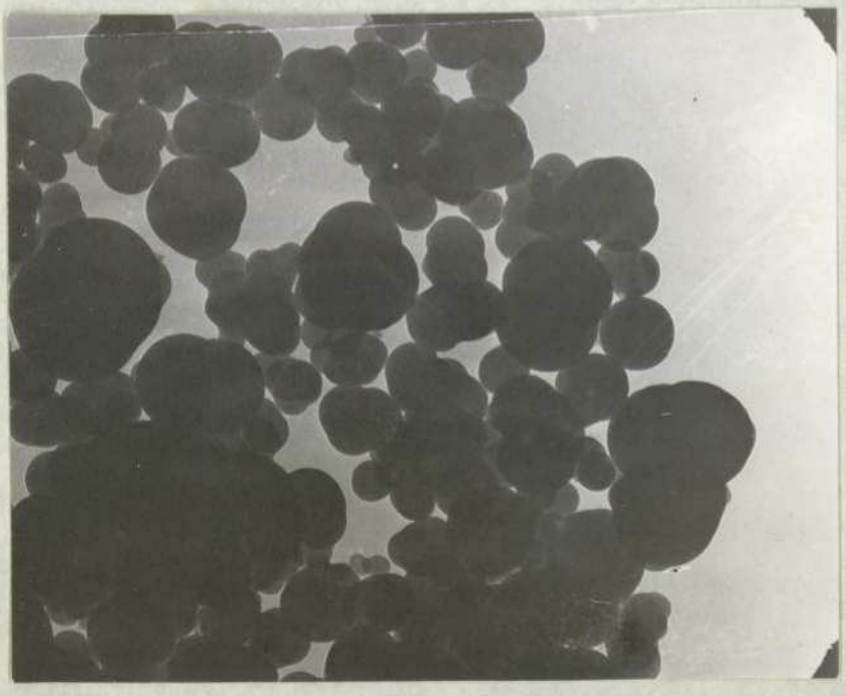
29% graphite and the mass ratio would be 85% teflon and 15% graphite.

Hence it can be seen that there is a large difference between the teflon content of the normal electrode and the teflon content of an electrode of maximum strength. The teflon particles supplied as a dispersion are approximately sperical in shape with a diameter of 0.5 micron. During the curing operation these particles grow to about 1 - 2 micron. An electron microscope study (115) of teflon bonded electrodes has shown that the teflon is in the form of fibrils and spheres and it is suggested that the fibrils are produced during the stripping of the replica from the electrode surface when platinum aggregates and individual particles of teflon become separated (replication). Fibrils formed in this way would not contribute to the strength of a teflon bonded electrode. It is however, possible that a group of adjacent teflon particles could form the source of a fibril which could be formed by expansion during curing at 300°C. The true nature of the platinum teflon bonds was notelucidated and a microscopic examination of platinum - teflon dispersions before and after curing at 300°C could show which factors are important in the bonding.

3.9.3. The effect of electrocatalyst structure on the strength of teflon bonded electrodes.

It is probable that electrocatalysts prepared by precipitation from solution form interlocked particles as the crystallites grow, resulting in a material of higher mechanical strength than an electrocatalyst produced by grinding or arc vapourisation.





Electron micrographs for carbon black and materials produced by arc vapourisation [191] show clearly that particles are not interlocked while electron micrographs for platinum black produced by precipitation show that interlocking is possible although the resolution was not sufficient to identify individual platinum crystallites clearly. This phenomenom could explain why teflon bonded carbon based electrodes are mechanically weaker than teflon bonded platinum black electrodes.

Hydrogen evolution tests on a tungsten carbide electrode containing 30% by weight of teflon showed that the electrode was not damaged at current densities up to 0.5 $A.cm^{-2}$. The tungsten carbide powder prepared by grinding should not have any interlocked particles and electrode damage might have been expected. However, the relatively low surface area 1 m^2/g of the sample could explain the greater strength ie, large pores and a higher volume concentration of teflon in the electrode.

Conclusions.

(I) The degradation of graphite based electrodes on gas evolution has been shown to be due to mechanical weakness rather than oxidation to solid and/or gaseous oxides. The gradual destruction of bulk graphite electrodes of relatively low porosity by oxygen evolution is often considered to be caused by oxidation to gaseous oxides but the present work suggests that the destruction could be caused by oxidation to solid oxides and/or mechanical rupture of the pores. The slow rate of destruction is explained by the low porosity and thickness of the electrode

(2) The surface oxide groups formed on graphite

surfaces under normal oxygen evolution conditions cannot be reduced electrochemically even by hydrogen evolution. These oxide groups reduce the oxygen reduction performance to low values. These results show that graphite electrodes could not be used as rechargeable air electrodes for metal - air cells.

(3) The surface oxide film formed under anodic recharge conditions on metal electrocatalysts is not in general reduced until potentials below that for oxygen reduction. Since these films reduce the oxygen reduction performance this limits their use as rechargeable air electrodes especially if the films are thick.

(4) Cobalt nickel oxide, a semi conducting oxide electrocatalyst, was found to be strong enough to withstand gas evolution and the higher oxides of cobalt and nickel formed during recharge are readily reduced at potentials above that for oxygen reduction. Since the oxygen reduction and evolution performances are comparable with silver on graphite and platinum black it follows that this electrocatalyst could be used successfully in a rechargeable air electrode.

(5) In order to measure the i_o value for oxygen reduction on a platinum oxide surface it is essential to ensure that the transient oxide reduction current has decayed to zero and that the surface is still covered by a monolayer of oxide before measurements are made because both oxide reduction and oxygen reduction on a clean platinum surface support much higher currents than oxygen reduction on the oxide surface.

(6) The rate of oxide formation on platinum in the potential rangeI.O - I.5 V obeyed Elovich kinetics.

chapter 4.

4.1	Introduction	242
4.2.	Model of a gas evolution electrode	244
4.3.	H_2 evolution i-E data on planar and porous platinum	247
4.4	the effect of teflon content on the performance of gas evolution electrodes	256
4.5	A comparison of gas evolution in the floating and submerged positions.	257
4.6.	The use of transient techniques to show the loss of effective surface area during H_2 evolution on Pt black	264
4.7	The effect of gas bubbles on planar gas evolution electrodes	272
4.8.	Further evidence for gas bubbles causing a loss in active surface area.	276
4.9.	Effectiveness factors of porous electrodes	284
4.10.	Intrinsic exchange current density of porous electrodes	289.

Chapter 4.

The Effect of Electrode Structure on the Activity of Gas Evolution Electrodes.

4.I. Introduction.

The feasability of using porous, high surface area materials as electrodes for fuel cells and batteries has been studied for the case of gas dissolution reactions in the liquid phase [157,158] and it has been shown that this type of electrode gives a very much better performance than the equivalent weight of the same material in the form of a planar electrode. The main advantages of the porous electrode are: (I) at a given potential it gives a much higher current than the planar electrode due to its higher surface area.

(2) it has a much higher limiting current than a planar electrode due to its favourable mass transfer properties.

(3) it provides a great saving on the cost of electrode material especially if this is expensive, as it usually is.

The main disadvantages are:

(I) the difficulty in producing powders of high surface area. This adds substantially to the cost of this type of electrode compared with a planar electrode.

(2) porous electrodes are mechanically much weaker than planar electrodes and it is usually necessary to increase the strength by using some form of binder.

The methods used for preparing high surface area powders are:

(I) grinding using a vibratory ball mill (I65)

(2) precipitation from solution (I69)

(3) freeze drying (I67)

(4) arc - vapour method (I9I)

Grinding is only suitable for materials which can be fractured by shearing, like graphite. For other substances the maximum surface area obtained by ball milling is about I m^2/g and the minimum particle size about I micron. In order to obtain finer powders more energy could be supplied by using a vibratory ball mill and smaller grinding elements. However as the particles become very small they tend to have a cushioning effect and the lowest particle sizes achieved even by vibratory ball milling are $\geq$ 0.I micron. When the particles become very small agglomeration due to welding or flocculation can also occur.

Precipitation from solution is suitable for some substances eg. metal powders, but it is necessary to take precautions if the small crystallites initially precipitated are not to grow into large particles.

Freeze drying has been found to be an excellent method for producing very high surface area powders and highly dispersed supported electrocatalysts.(see Chapter 2.)

Recently the arc - vapour method has been developed which is capable of producing very high surface area powders.

High surface area porous powders are now regularly used for fuel cells and batteries involving

a gas dissolution reaction. They are usually used with a hydrophobic binder which increases the mechanical strength and facilitates the mass transfer of the gas to the active sites of the electrocatalyst. Even though this type of electrode has a performance far superior to a planar electrode of the same material it has been reported that only a small proportion of the total surface area of the porous electrode is effectively used (see I.B).

Little work has been done on the feasability of porous electrodes for use in electrolytic gas evolution reactions, which are common industrially and of great importance. In general planar electrodes are used for this type of reaction and it is possible that porous electrodes could prove more efficient. The aim of this chapter is to study the feasability of porous electrodes for electrolytic gas evolution reactions.

4.2. Model of a gas evolution electrode.

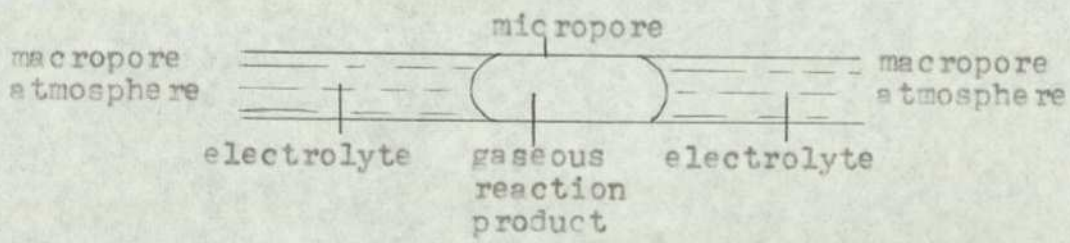
Porous electrodes prepared by using a high surface area powder have a biporous structure; that is they possess a dual scale of porosity. In the electrode the small particles of electrocatalyst of particle size of the order of 100 Å (diameter) form aggregates of particle size of the order of 1 μ. The dual scale of porosity consists of (a) the microporosity which is due to the voids within each aggregate and (b) the macroporosity which is due to the voids between the aggregates.

In general the surface area associated with the microporosity is about 100 times greater than

that associated with the macroporosity.(159) In teflon bonded porous electrodes the aggregates are held together by teflon particles situated between the aggregates and these produce hydrophobic gas channels which do not contain electrolyte. The micropores are completely filled with electrolyte.(157) These teflon bonded porous electrodes may be thought of as having certain advantages over the porous electrode containing no hydrophobic binder in that they have much greater mechanical strength and that the mass transfer rate of gaseous reaction products from the interior of the electrodes should be increased by the presence of hydrophobic gas channels. This type of electrode has been used in the present study.

This model predicts that all the gas will be produced in the micropores and consequently must find its way to the outer surface of the aggregate and then flow away down the gas channels and escape from the electrode. The problem is, how does the gas escape from the interior of an aggregate ?

If a single pore is considered



in order for the gas to escape it is necessary for a certain gas pressure to develop which depends on the pore size, the surface tension and the contact angle.

ie. $$P = \frac{2\sigma}{r} \cdot \cos\theta$$

if we assume the data to be

$$\sigma = 70 \text{ dyne.cm}^{-1}$$

$$r = 2 \times 10^{-7} \text{ cm}$$

$$\theta = 0^{\circ}$$

then $P = 7 \times 10^{8}$ dynes.cm^{-2} $\sim$ 700 atmos.

At lower pressures the only method of escape is for the gas to dissolve in the electrolyte under pressure and move to the outer surface of the aggregate by diffusion through the electrolyte. When the required pressure is reached the gas and most of the electrolyte will be forced out of the micropore. Hence it can be seen that a substantial part of the micropore surface area will not be in contact with the electrolyte for most of the time. This raises the problem of just how much of the available surface area is effectively used over a period of time. It is possible that most of the interior of the aggregates is usually dry and that the reaction only occurs on the film of liquid on the outer surface of the aggregates. If this is the case then the advantages of using porous electrodes for gas evolution reactions would be seriously questioned. For a teflon bonded platinum black electrode of typical parameters (157-8,160)

density = 20 g.cm^{-3}

microporosity = 0.9

macroporosity = 0.5

aggregate diameter = 1 μ = 10^{-4} cm

micropore radius = 20×10^{-8} cm

consider an aggregate

void volume of aggregate = $\frac{4}{3} \times 3.14 \times 125 \times 10^{-15} \times 0.9$

total micropore volume of aggregate = void volume of aggregate

ie. $\frac{4}{3} \times 3.14 \times 125 \times 10^{-15} \times 0.9 = 3.14 \times 400 \times 10^{-16} \times l$

where l = total length of pores in aggregate

$\therefore l = 3.75$ cm

surface area of 3.75 cm of pores of radius $20\ 10^{-8}$ cm

$= 2 \times 3.14 \times 20 \times 10^{-8} \times 3.75$

$= 4.7 \times 10^{-6}\ cm^2$

volume of solid in aggregate, $V = \frac{4}{3} \times 3.14 \times 1.25 \times 10^{-15} \times 0.1$

mass of solid in aggregate = $2OV = 1.06 \times 10^{-12}$ g

for an electrode of catalyst loading, 10 mg, the number of aggregates in 10 mg = $\frac{10}{1 \times 10^{-9}} = 10^{10}$

total surface area of 10 mg of microporous aggregates

$= 4.7 \times 10^{-6} \times 10^{10}$

$= 4.7 \times 10^{4}\ cm^2$

surface area of a non porous aggregate = $4 \times 3.14 \times 25 \times 10^{-10}\ cm^2$

total surface area of 10 mg of non porous aggregates

$= 31.4\ cm^2$

since the number of non porous aggregates in 10 mg is 10^9.

Hence the loss of surface area, if only the outer surface of the aggregates is used, is very great.

4.3. Comparison of hydrogen evolution polarisation curves on platinum foil and platinum black.

4.3.1. Experimental.

Steady state polarisation curves for hydrogen evolution were recorded on

(1) a sample of platinum foil of known geometric area, whose roughness factor had been determined,

(2) a teflon bonded platinum black electrode of known

TABLE 56

Current per unit electrochemical surface area for H_2 oxidation on platinum foil and black electrodes.

η (mV)	i_1	i_2	i_3
1	–	10	0.013
4	0.050	35	0.045
9	0.110	73	0.095
12	0.18	–	–
19	–	150	0.195
22	0.225		
30	–	240	0.312
44	0.260	360	0.414
59	–	485	0.630
68	0.295	–	–
119	–		
168	0.335	1320	1.71
269	–	2100	2.72

i_1 = current per unit electrochemical S.A. for platinum foil ie. corrected for roughness factor.

i_2 = current per unit geometric area for Platinum black.

i_3 = current per unit electrochemical area for platinum black.

Electrolyte	5N H_2SO_4
TEMP.	21 °C
Atmosphere	H_2
OCV foil	0.032 V
OCV black	0.029 V
roughness factor of foil	1.8.
surface area of black by H_2 stripping	$14 m^2 . g^{-1}$
loading	$5.5 mg . cm^{-2}$
current collector	Pt gauze
units of i	$mA . cm^{-2}$

TABLE 36

Current per unit electrochemical surface area for H_2 evolution on platinum foil and black electrodes.

η (mV)	i_1	i_2	i_3
1	-	-	0.012
2	0.039	-	-
3	-	-	0.029
7.5	-	-	0.062
18	-	-	0.126
27	0.133	0.098	0.181.
42	0.311	-	-
47	-	-	0.31
79	2.22	0.28	0.50
100	4.3	-	-
125	-	0.46	0.81
200	55	-	-
225	-	0.71	1.1.

i_1 = current density for platinum foil allowing for roughness factor

i_2, i_3 = current density for platinum blacks allowing for H_2 stripping area.

Electrolyte	5N H_2SO_4
Temp.	21°C
Atmosphere	H_2
OCV foil	0.050 V
ocv black(2)	0.023
" " (3)	0.029
roughness factor of foil	1.8.
Surface area of black(2)	8.1 $m^2 . g^{-1}$
" " " " (3)	14 $m^2 . g^{-1}$

geometric area, electrocatalyst loading and electrocatalyst surface area,(S.A.).

4.3.2. Results and Discussion.

Graphs 37 and 38 show that the platinum black electrode has a better performance than the platinum foil electrode over the potential range +25 mV to -300 mV, although as the potential increases the difference between the two electrodes becomes less. However, in the potential range +25 mV to -50 mV the platinum black current density is about two orders of magnitude greater than the platinum foil current, thus the porous electrode is a substantial improvement especially in the low overvoltage region. The fact that the superiority of the porous electrode is most marked in the low overvoltage region is useful in that batteries and fuel cells which operate at low overvoltages have a higher power density since the working potential is higher. It can be seen that these trends are repeated for another platinum black electrode made using a different sample of platinum black. (Graph 39).

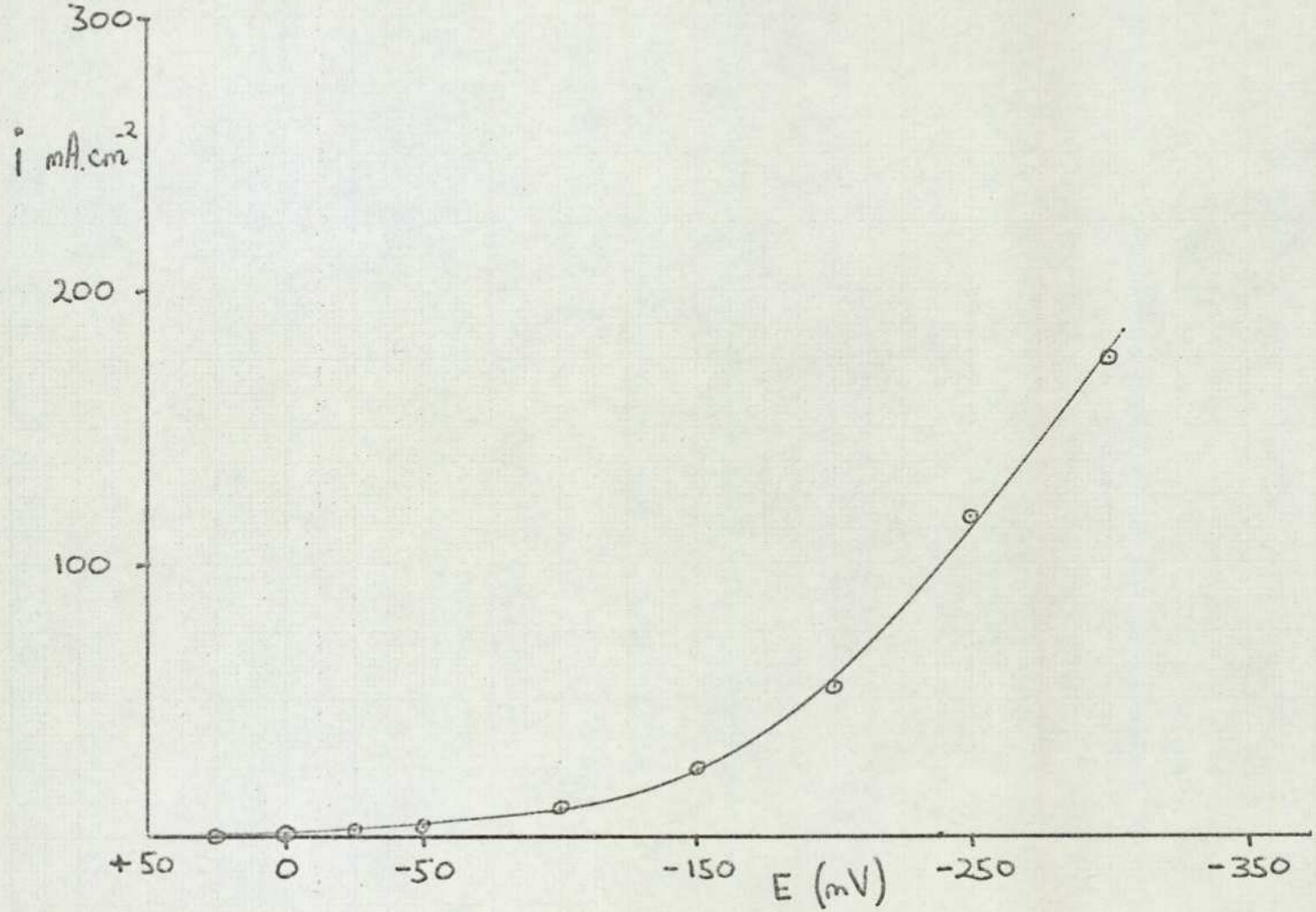
Although the current per unit geometric area is better for platinum black than platinum foil it does not follow that the true current densities ie. current per unit electrochemically active surface area are equal for porous and planar electrodes and that a quantitative scale up has been achieved. The true surface area of the platinum foil was found by determining its roughness factor by the method given in chapter 2, while the true surface area of the platinum black electrode was determined by two methods: (a) from the electrocatalyst loading and surface area which was

Graph 37.

Steady state hydrogen evolution polarisation curve on platinum foil.

Electrolyte	5N H_2SO_4
Temperature	21°C
Atmosphere	hydrogen
Pressure	I atmos.
O.C.V.	+0.052 V
Electrocatalyst	platinum foil
Roughness factor	I.8
Resistance	0.06 ohm

Surface area corrected for roughness factor.

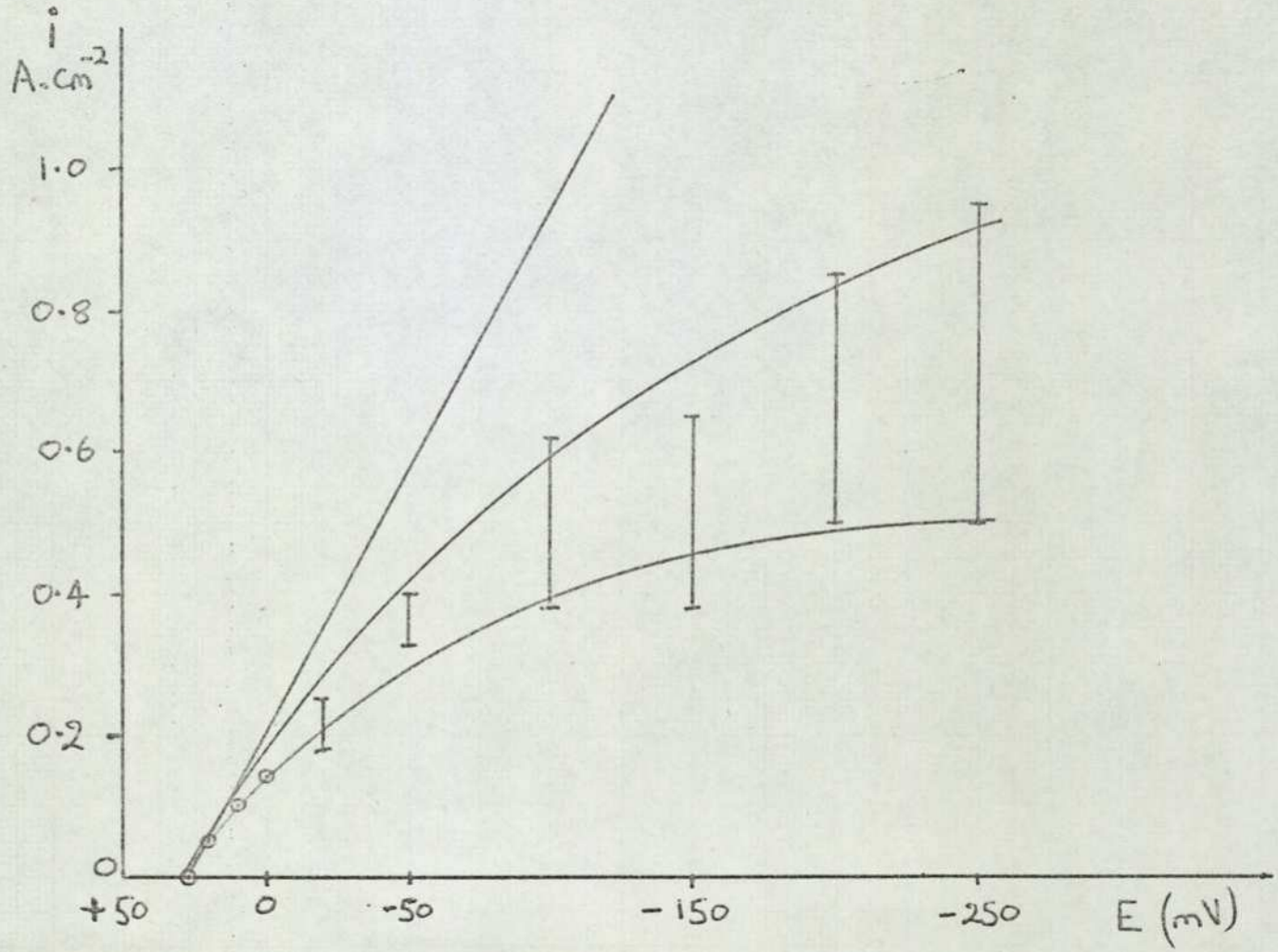


Graph 38.

Steady state hydrogen evolution polarisation curves for a teflon bonded platinum black electrode (a) floating on the electrolyte surface. (b) completely submerged.

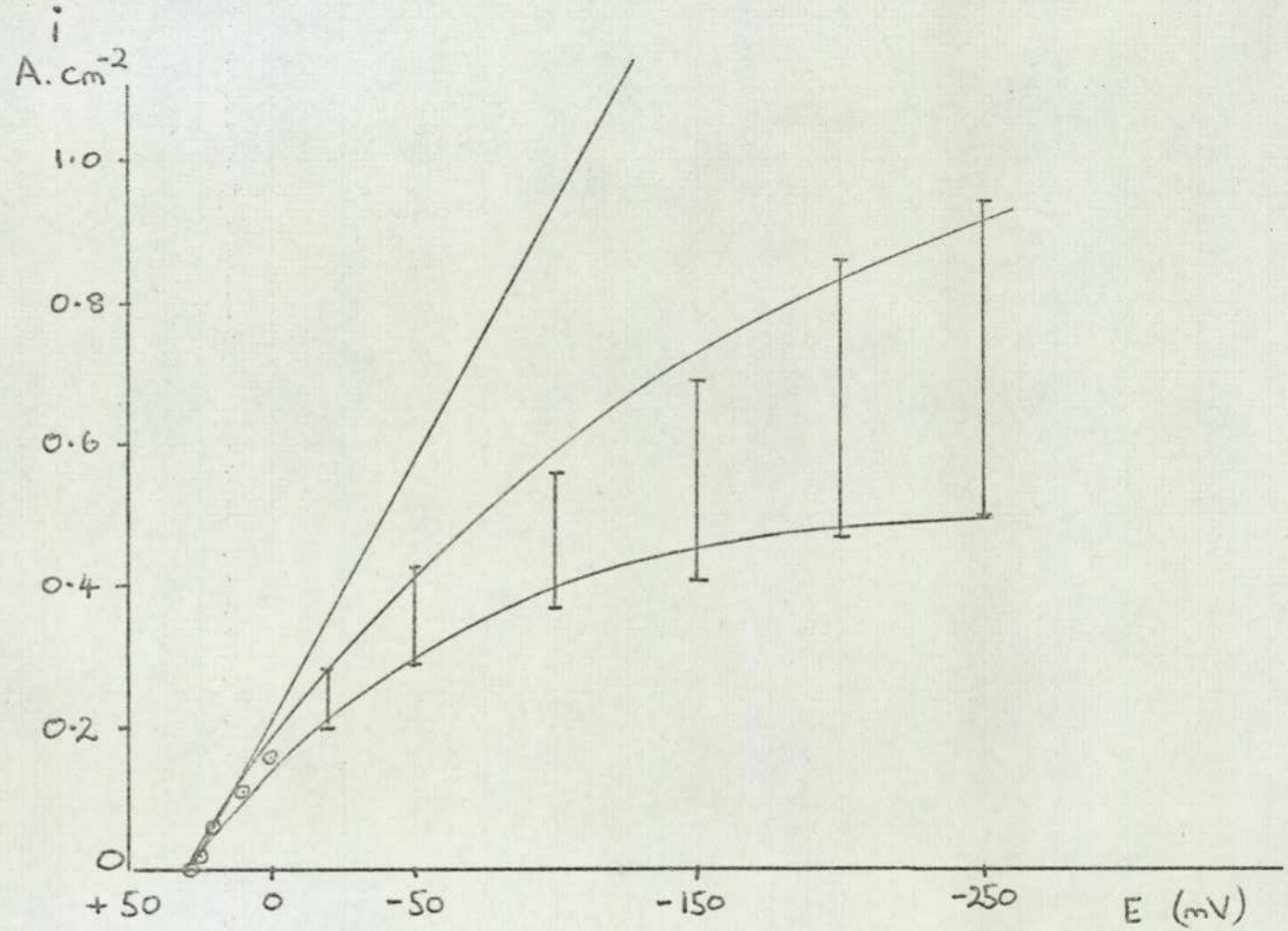
(a)

Electrolyte	5N H_2SO_4
Temperature	21 C
Atmosphere	hydrogen
Pressure	I atmos.
O.C.V.	0.022 V
Electrocatalyst	platinum black
Electrocatalyst S.A.	16 $m^2.g^{-1}$
Electrocatalyst loading	5·5 $mg.cm^{-2}$
Resistance	0.10 Ohm



250

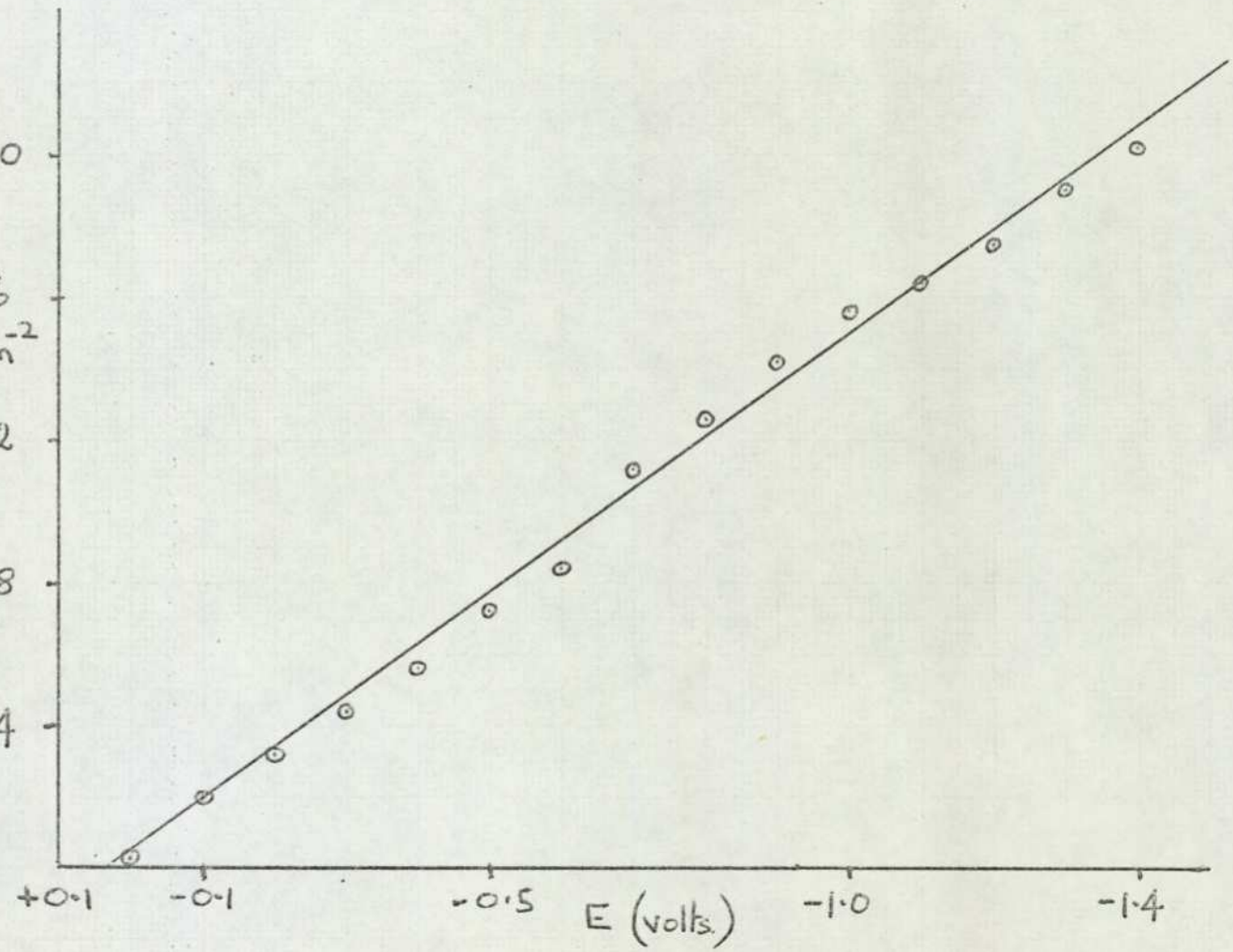
Graph 38. (b) completely submerged.



Graph 39.

Hydrogen evolution polarisation data on a platinum black, teflon bonded electrode.

Electrolyte	5N H_2SO_4
Temperature	2I C
Atmosphere	hydrogen
Pressure	I atmos.
O.C.V.	0.025 V
Electrocatalyst	platinum black
Electrocatalyst S.A.	$8.1\ m^2.g^{-1}$
Electrocatalyst loading	$10\ mg.cm^{-2}$
Resistance	0.I2 ohm



determined by the B.E.T. method, and (b) by anodic hydrogen stripping (see chapter 2.)Since the electrode fabrication technique involved heating to 300°C for one hour the B.E.T. determination was performed on platinum black which had been heated to 300°C for one hour. The results in table 27 show that the area determined by hydrogen stripping is only slightly less than that found by the B.E.T. method showing that most of the platinum black is wetted by the electrolyte. Using this data, polarisation curves of the true surface area v. potential were plotted (Table 36). From these it can be seen that the true current density for the porous electrodes is less than that for planar electrodes over the potential range +25 to -300 mV. At high overpotentials the true current density for the planar electrode is more than two orders of magnitude greater than that of the porous electrodes. Comparing the two porous electrodes prepared from different samples of platinum black it was seen that the sample of higher surface area gave the best true current density at a given potential in the range +25 to -250 mV. However the shapes of the two polarisation curves suggest that the electrode containing the high surface area platinum is approaching a limiting current condition at -250 mV while the low surface area platinum black electrode shows no limiting current region even at -I.00 V. Hence at high overpotentials (ie. high currents) the electrode with low surface area platinum black would have a higher true current density. If one assumes the hydrogen evolution activity of I cm^2 of platinum foil is the same as I cm^2 of

Table 27.

Surface area of platinum blacks.

		B.E.T.	H_2 stripping
(Johnson Matthey)	Sample A	I6 m^2/g	I4 m^2/g
(Laboratory preparation)	Sample B	8.I m^2/g	6.8 m^2/g

Loading		B.E.T. area of I cm^2 of electrode	H_2 stripping area of I cm^2 of electrode
5.5mg/cm^2	Electrode made from A	880 cm^2	770 cm^2
8.0mg/cm^2	Electrode made from B	650 cm^2	540 cm^2

Surface areas measured after I hour at 300°C in air.

platinum black (absolute surface area) then it is possible to calculate the proportion of the total platinum black surface which is not being effectively utilised. Care must be observed however, since part of the active surface area of the platinum foil is lost due to bubble coverage. Hence a straight comparison will not give very meaningful results. The difference between the hydrogen evolution performance on planar and porous electrodes in 5N sulphuric acid is probably due to the difficulty of mass transport of the hydrogen gas produced, away from the electrode. The mass transfer of hydroxonium ions into the active sites occurs at a rapid rate because of the abundant supply of these ions. The comparison between the two porous electrodes shows that the one using the higher surface area platinum black, which has the smaller micropore size, has a considerably lower limiting current than the other platinum black sample. This would be expected from the model of a porous catalyst undergoing gas evolution (4.2.). Another factor which probably affects the rate of mass transfer of hydrogen away from the electrode is the teflon content of the electrode. The higher the teflon content the more gas channels, but since the major problem is the escape of gas from the micropores this is likely to have less effect than the micropore size.

These results show that porous electrodes are superior to planar electrodes especially if the gas evolution rates are not high, but the increase in performance is not quantitative with the increased surface area. If high hydrogen evolution current

densities are required resulting in rapid gas formation it is better to use platinum foil than platinum black since a fine platinum black with high surface area and low micropore size has a fairly low limiting current and course platinum blacks with low surface area and high micropore size give a performance slightly smaller than platinum foil at high over-voltages even though their limiting current is higher than for fine platinum blacks. It is possible that a pore size could be found which would optimise between the limiting current and the slope of the linear region of the polarisation curve. These results also confirm that hydrogen evolution polarisation curves for porous electrodes are linear over a much wider potential range than for planar electrodes.(161)

The remainder of this chapter involves a more detailed investigation of the limitations of using porous electrodes for gas evolution reactions. The hydrogen evolution reaction has been chosen as the example since the other common electrolytic gas evolution reactions, namely oxygen and chlorine, both involve a change in the surface state of the platinum electrode ie. oxide film formation.

4.4. The effect of the teflon content of porous electrodes on the gas evolution performance.

4.4.I. Experimental.

For this type of electrode made from fine microporous powders, the teflon is essential for gas evolution reactions and an electrode without teflon is extremely fragile and cannot endure gas evolution. Actually the teflon content must be at least 15% if

the electrode is to sustain high gas evolution currents. In this work three teflon bonded platinum black electrodes were tested. The electrodes were prepared from the same sample of platinum black, had the same electrocatalyst loading but three different teflon contents were used ie. 20%, 30%, and 50%. Higher teflon contents could result in low electrical conductivity and severe non-wetting problems.

4.4.2. Results and Discussion.

The hydrogen evolution performance decreased slightly with increasing teflon content but the limiting current of the high teflon electrode was slightly higher (graph 40). This is not very significant since the hydrogen oxidation performance of these teflon bonded electrodes is very critically dependent on the teflon content which must be about 20 - 30% if a good performance is to be achieved. However the experiment does show that although hydrophobic gas channels do slightly help the mass transport of hydrogen away from the electrode the effect is small compared with the effect of electrocatalyst micropore size.

4.5. To investigate the use of teflon bonded gas evolution electrodes in the floating and submerged positions.

4.5.1. Introduction.

From the values of total and electrochemical surface area it can be seen that floating teflon bonded electrodes can effectively use about 85% of the available total surface area. When the electrode is submerged the electrochemical surface area should

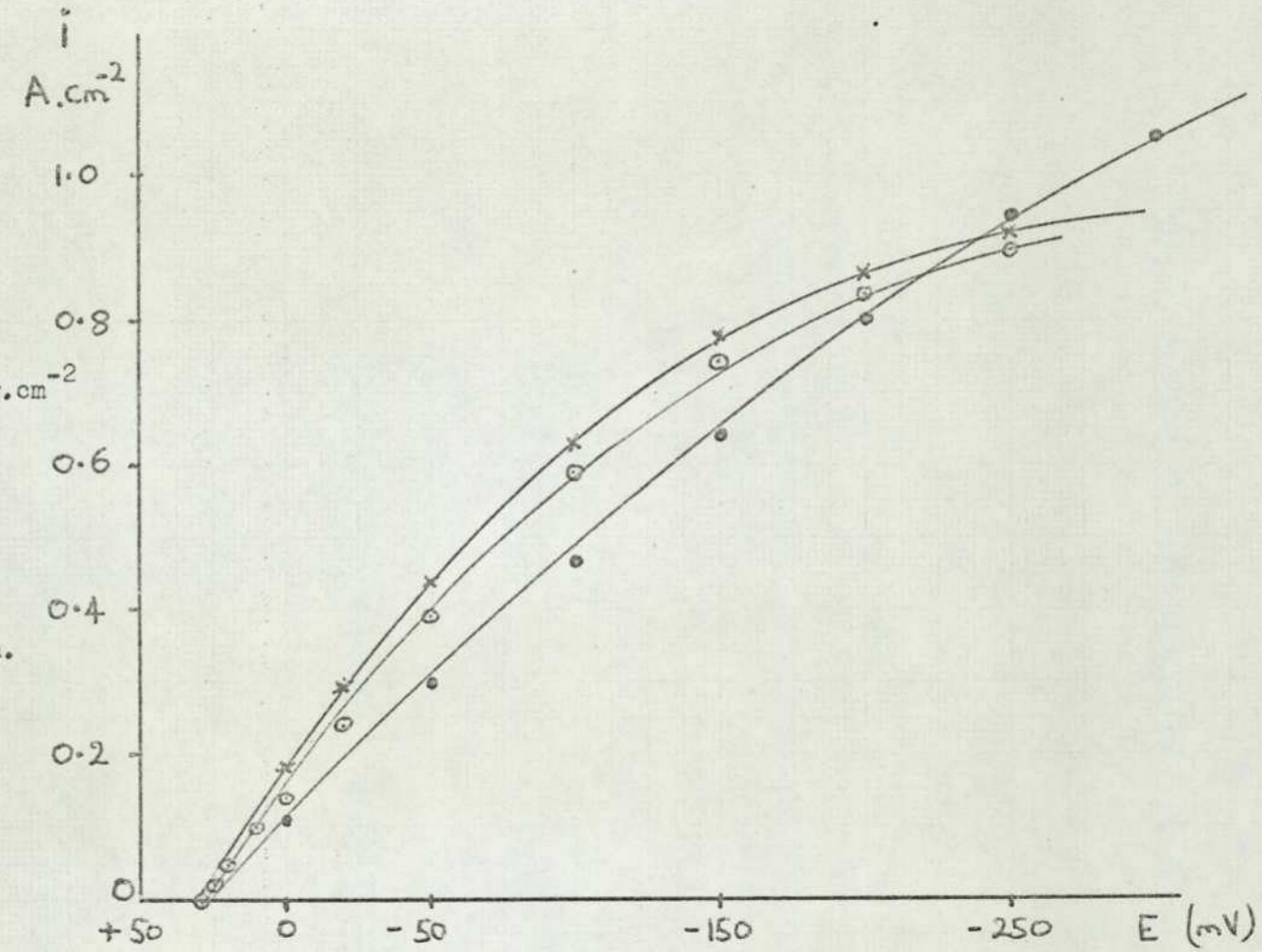
Graph 40.

The effect of varying the teflon content of a teflon bonded platinum black electrode on the hydrogen evolution polarisation curve.

Electrolyte	5N H_2SO_4
Temperature	21°C
Atmosphere	hydrogen
Pressure	I atmos.
O.C.V.	0.024 V
Electrocatalyst	platinum black
Electrocatalyst loading	6.5 mg.cm^{-2} 0.5 mg.cm^{-2}
Electrocatalyst S.A.	
Current collector	platinum gauze
Resistance	0.10 ohm 0.02 ohm

Current measured as the average over 5 min.

Key	Teflon content
•	50%
⊙	30%
×	20%



be almost the same as the total surface area especially if the electrode has been electrochemically flooded to ensure that there are no gas locks within the electrode. Hence a submerged electrode should give slightly better performance for gas evolution reactions in the initial instance. However as the gas is produced it has to escape from the electrode, which when the electrode is submerged requires a slightly higher gas pressure to overcome the liquid head than it does in the floating position, and when the gas has escaped from the micropores of the aggregate it cannot escape easily up the teflon gas channels since in the submerged position these are flooded. These two factors should decrease the performance although not by a large amount since they are relatively unimportant compared with the escape of gas from the interior of the electrocatalyst aggregate. For example the diameter of the teflon pores is about 2000 Å and consequently the escape of gas from these pores is far less hindered than the escape of gas from the micropores which have a pore diameter of about 50 Å. Hence one would not expect much difference between the performance of a gas evolution electrode in the floating and submerged positions.

4.5.2. Experimental.

The same platinum black electrode was tested in the floating and submerged positions for the hydrogen evolution potentiostatic polarisation.

The rate of fall of hydrogen evolution current with time was determined for the electrode in both positions. If the escape of gas from the submerged

electrode is more hindered than for the floating electrode then the rate of current decay should be greater.

The recovery time of the electrode was determined by evolving hydrogen at a set current and for a given time and switching off for a set time before retesting to see if any surface area was still blocked from electrolyte contact. It is likely that at the instant when the current is switched off there is gas present in the micropores at a pressure insufficient for ejection. If this is the case it is possible that this gas will be trapped and the performance of the electrode would not recover its initial value. This should be true for both floating and submerged positions although the escape of gas from the electrode interior will be even more difficult in the submerged position due to the hydrostatic head and the flooding of the teflon pores.

4.5.3. Results and Discussion.

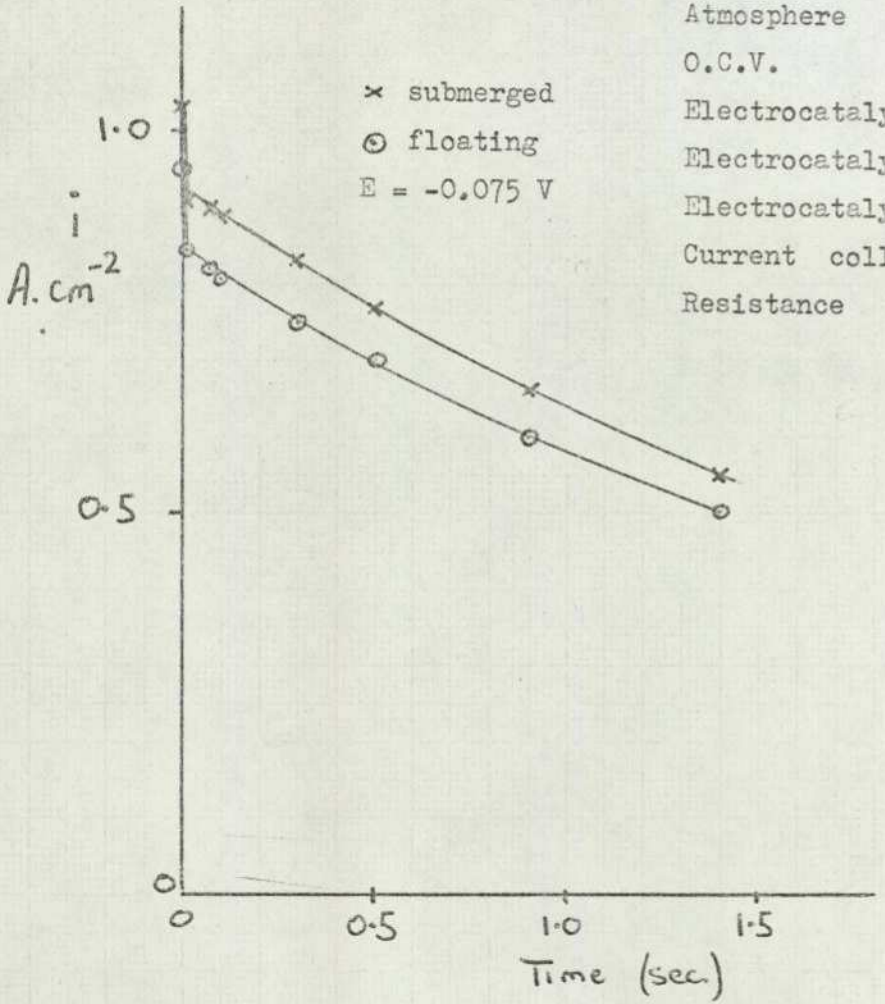
Polarisation curves for hydrogen evolution on platinum black in the floating and submerged positions are shown in graph 38. At low overpotentials the submerged electrode current density is about IO% higher than for the floating electrode probably reflecting the slightly higher surface area available in this position. At high overpotentials there is little difference in the current densities for the two positions indicating that the submerged electrode probably does trap slightly more gas within it. In general the two curves are very similar in shape and magnitude.

Graph 4I shows that the fall of hydrogen

Graph 41.

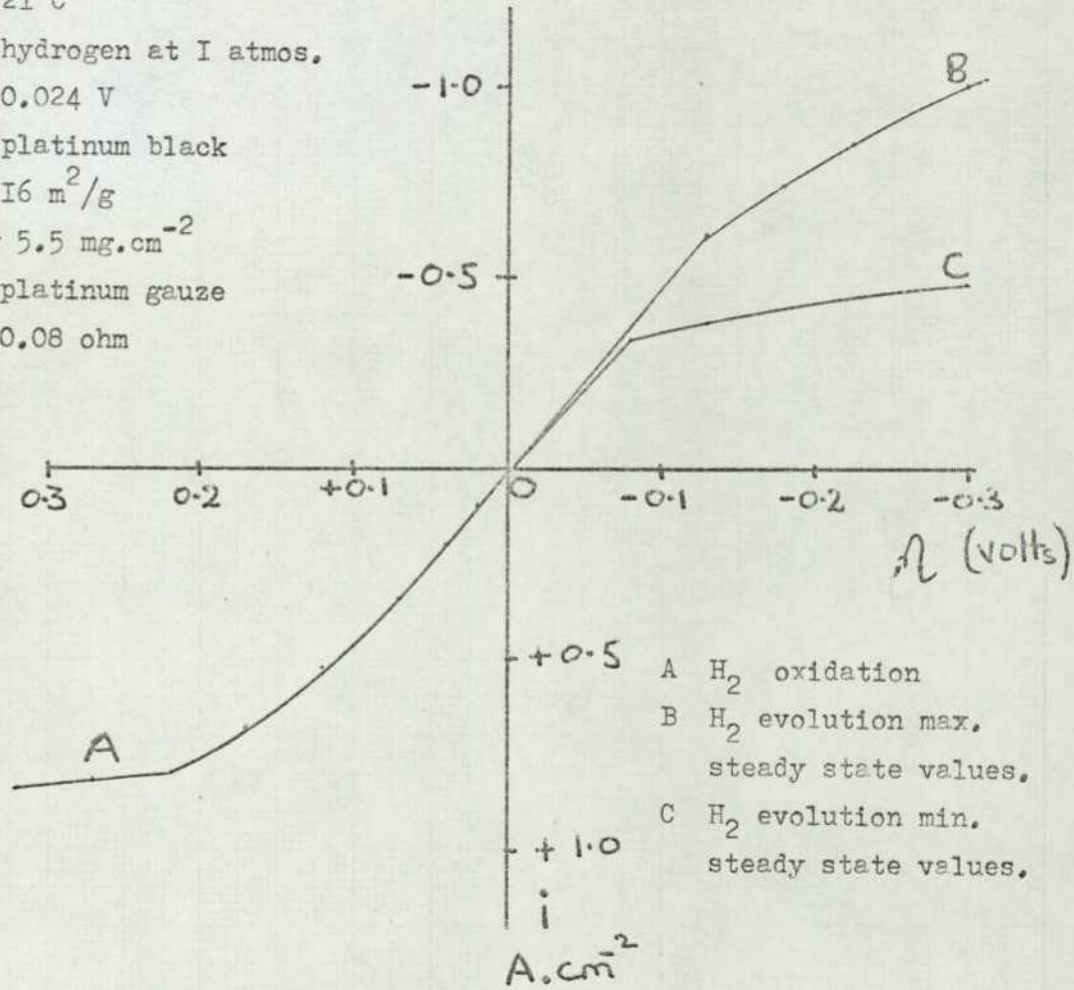
Transient current - time curves for a teflon bonded platinum black electrode in (a) the submerged position and (b) the floating position.

Electrolyte	5N H_2SO_4
Temperature	21°C
Atmosphere	hydrogen at 1 atmos.
O.C.V.	0.024 V
Electrocatalyst	platinum black
Electrocatalyst S.A.	16 m^2/g
Electrocatalyst loading	5.5 $mg.cm^{-2}$
Current collector	platinum gauze
Resistance	0.08 ohm



Graph 42.

Polarisation curves for the steady state hydrogen electrode reactions on teflon bonded platinum black.



evolution current density with time over the first second is very similar for both floating and submerged electrodes. The slightly higher surface area of the submerged electrode is responsible for the slightly higher currents from this electrode position. These results indicate that the factor hindering the escape of hydrogen gas is similar for both floating and submerged electrodes which is further evidence that the rate limiting step is the escape of hydrogen gas from the micropores within each electrocatalyst aggregate and the effect of hydrophobic gas channels in the floating position is of only minor significance in comparison. The current - time curves were measured over a very short time interval because the electrode reaches a steady state very rapidly, when the current fluctuates randomly up and down as gas is formed and escapes from the electrode. This condition is reached in approximately the same time for both floating and submerged electrodes. The currents were measured after 5 minutes at -75 mV when the floating electrode current density was 430 $mA.cm^{-2}$ while the submerged electrode was 450 $mA.cm^{-2}$ (average values measured from 4 - 6 min as the current fluctuated randomly). This shows that the submerged electrode has not trapped substantially more gas within it than the floating electrode. The current from the submerged electrode after 10 ms was 10% higher than that on the floating electrode while after 5 min it was only 5% higher, which gives some indication that the submerged electrode does trap slightly more gas than the floating electrode although the results are of limited significance owing to the

current fluctuations.

The difference between the recovery time of floating and submerged electrodes is the most obvious difference between the two electrode positions. The electrode was subjected to a potential of -75 mV for 5 min in both positions before switching off for times varying from 0.5 min - 10 min and measuring the height of a double layer charging peak for a given voltage step input. The peak height is directly proportional to the surface area and hence can monitor the reduction in surface area during and after gas evolution. This peak height was determined prior to hydrogen evolution and compared with the values obtained after hydrogen evolution. In the floating position the electrode had fully recovered within 0.5 min while in the submerged position the double layer charging peak gradually regained its original value over a period of 5 min. Hence after switching off a gas evolution current the trapped gas can leak away much more rapidly from the floating electrode than from the submerged electrode. In this case it is the hydrophobic gas channels present in the floating position which facilitate the leakage of the trapped gas within the electrode.

Since there is little difference in the loss of effective surface area on gas evolution between floating and submerged electrodes the fact that they are normally used industrially in the submerged position is not important.

4.6. The application of transient measurements to show the loss of effective surface area during hydrogen evolution on teflon bonded platinum black electrodes.

4.6.I. Experimental.

The potentiostatic transient current densities (I00 μsec - I sec) were determined over the potential range -250 to +300 mV for the hydrogen evolution and hydrogen oxidation electrode reactions and compared with the steady state polarisation data over the same potential range.

4.6.2. Results and Discussion.

Graph 42 shows the steady state polarisation curves for hydrogen evolution and hydrogen oxidation from which it can be seen that the electrode is reasonably reversible over the overpotential range $\pm$I00 mV. The hydrogen oxidation limiting current is due to mass transport of hydrogen gas molecules into the electrocatalyst active sites while the limiting current in the hydrogen evolution reaction is due to mass transport of hydrogen away from the active sites. Two curves have been drawn for hydrogen evolution representing the maximum and minimum currents observed at a given potential. It can be seen that the hydrogen oxidation limiting current lies between the two hydrogen evolution limiting currents and this deviation from reversibility is due to the irreversibility of the two limiting processes at high current densities.

This irreversibility is also shown in graph 43 where current - voltage curves are plotted at different times in the range I ms to I s. for the hydrogen oxidation and evolution reactions. For the hydrogen

Graph 43.

Hydrogen oxidation and evolution transients on a teflon bonded platinum black electrode.

(a) and (b) A 100 μs and 1 ms
B 10 ms
C 100 ms
D 1 s
E steady state values

Data for (a), (b) and (c)

Electrocatalyst loading 5.5 mg cm^{-2}

Current collector platinum gauze

Resistance 0.08 ohm

Electrolyte 5N H_2SO_4

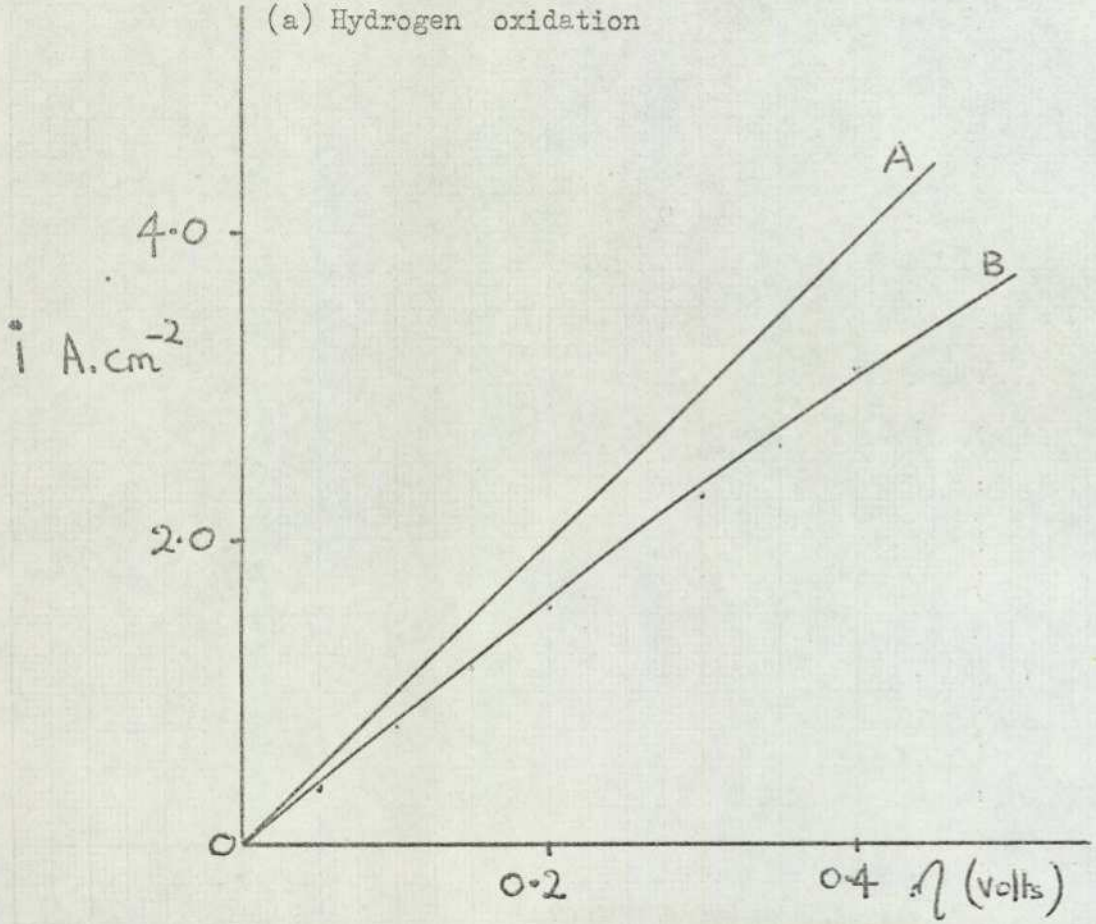
Temperature 21 °C

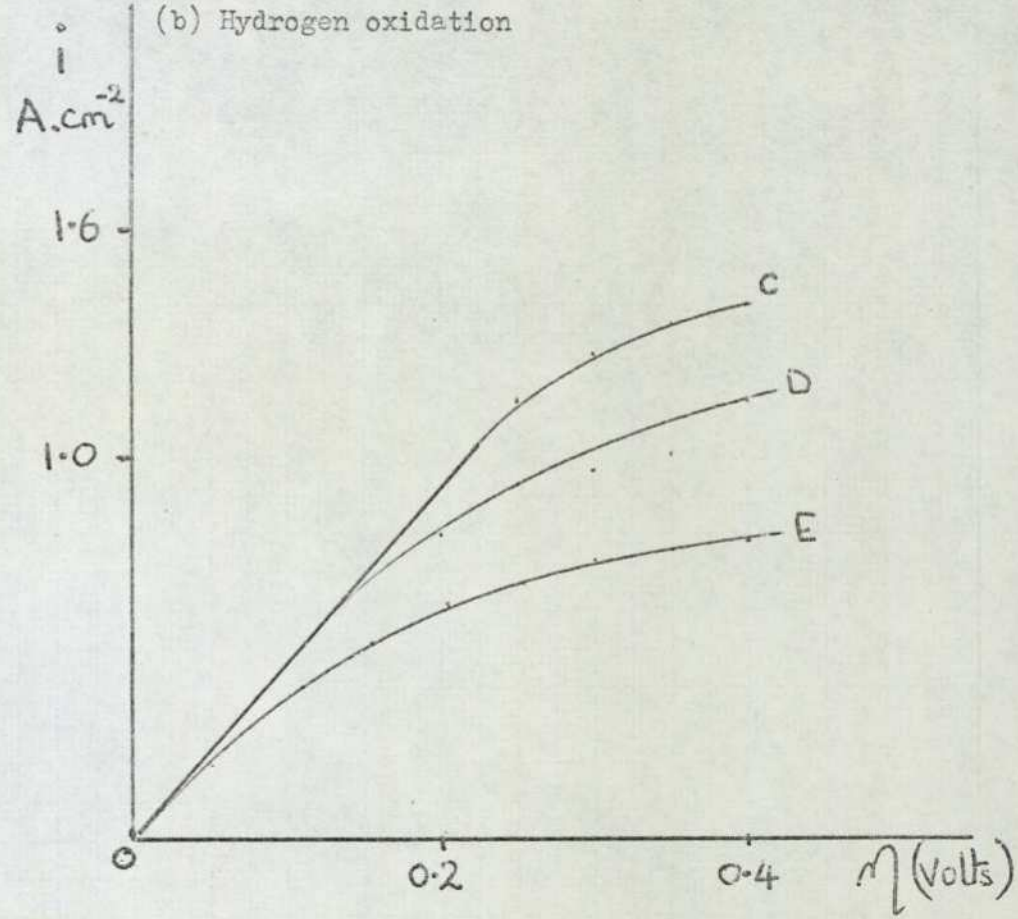
Atmosphere hydrogen at 1 atmos.

O.C.V. 0.023 V

Electrocatalyst platinum black

Electrocatalyst S.A. 16 m^2/g





Graph 43.

(c) Hydrogen evolution

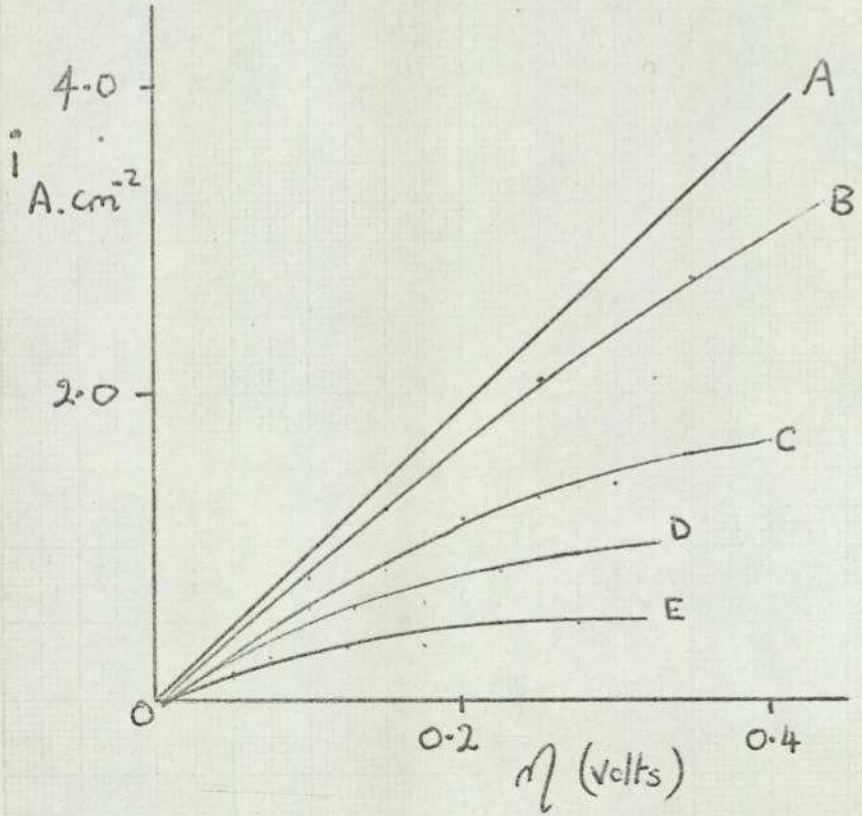
A 100 μs, 1 ms and 10 ms

B 100 ms

C 1 s

D maximum steady state values

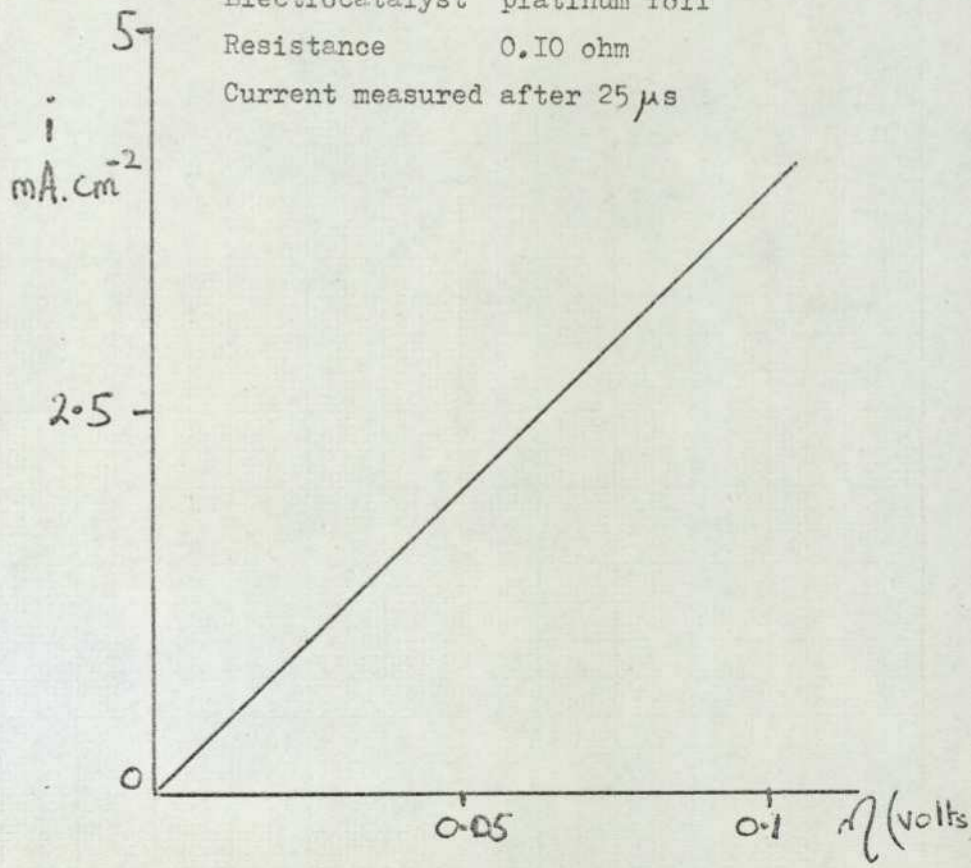
E minimum steady state values



Graph 46.

Transient hydrogen evolution polarisation curve for a platinum foil electrode.

Electrolyte	5N H_2SO_4
Temperature	22°C
Atmosphere	hydrogen at 1 atmos.
O.C.V.	0.032 V
Electrocatalyst	platinum foil
Resistance	0.10 ohm
Current measured after 25 μs	



oxidation reaction the deviation from reversibility is observed after significantly shorter times than for hydrogen evolution. A possible explanation for this is that hydrogen can escape from the electrode by two processes:

(I) by ejection as a gas from the micropores and then by passage up the hydrophobic gas channels.

(2) by dissolving in the electrolyte under the high pressures experienced in the micropores and subsequently by diffusion through the electrolyte to a region where the gas pressure is lower ie. a macropore where the hydrogen gas can easily escape to the atmosphere.

All the hydrogen diffusing to the active sites during hydrogen oxidation must initially dissolve in the electrolyte and even though the electrolyte - gas - active site interfaces are very close together this is the only means of mass transport of hydrogen to the active site.

4.6.3. Experimental.

Potentiostatic current - time transients for hydrogen evolution were measured over the potential range +28 to -250 mV. If the process was completely activation controlled the current would be independent of time. However the reaction is limited by the mass transport of hydrogen away from the electrode and the degree of limitation depends on the current density. From the current - time transients the loss in performance due to trapped gas can be estimated.

4.6.4. Results and Discussion.

The results shown in table 28 show that at low overpotentials the current falls only slightly with

Table 28.

Comparison between transient and steady state hydrogen oxidation and evolution polarisation data for a teflon bonded platinum black electrode.

(a) Hydrogen oxidation.

E(mV)	$i_{(0.1)}$	$i_{(900)}$	$i_{(ss)}$	$\frac{i_{(900)}}{i_{(0.1)}}$	$\frac{i_{(ss)}}{i_{(0.1)}}$	$\frac{i_{(ss)}}{i_{(900)}}$
	$mA.cm^{-2}$					
2	20.5	16.5	11.5	0.80	0.56	0.70
5	47.5	31.2	26	0.66	0.55	0.83
10	84	54	54	0.64	0.64	1.00
20	185	115	106	0.62	0.57	0.92
50	490	275	250	0.56	0.55	0.91
100	990	500	450	0.51	0.45	0.90
150	1475	-	620	-	0.42	-
200	2025	800	760	0.40	0.375	0.95
250	2300	940	820	0.41	0.36	0.87
300	3000	960	840	0.32	0.28	0.87
350	3425	1012	860	0.30	0.25	0.85
400	4000	1075	880	0.27	0.22	0.82

Electrolyte	5N H_2SO_4
Temperature	21°C
Atmosphere	hydrogen at 1 atmos.
O.C.V.	0.026 V
Electrocatalyst	platinum black
Electrocatalyst S.A.	16 m^2/g
Electrocatalyst loading	5.5 $mg.cm^{-2}$
Current collector	platinum gauze
Resistance	0.08 ohm

Table 28 (cont.)

(b) Hydrogen evolution.

E (mV)	$i_{(0.1)}$ / mA.cm^{-2}	$i_{(900)}$ / mA.cm^{-2}	$i_{(ss)\,max}$ / mA.cm^{-2}	$i_{(ss)\,min}$ / mA.cm^{-2}
2	20	I6	I4	-
5	58	48	32	-
I0	94	76	57	-
20	I90	I70	I00	-
50	482	365	250	I75
I00	940	600	480	360
I50	I350	850	680	400
200	2I50	II25	790	440
250	2650	I237	890	460
350	3750	I625	990	490

E (mV)	$i_{(900)}/i_{(0.1)}$	$i_{(ss)}/i_{(900)}$		$i_{(ss)}/i_{(0.1)}$	
2	0.80	0.88	-	0.70	-
5	0.83	0.66	-	0.55	-
I0	0.8I	0.75	-	0.6I	-
20	0.90	0.59	-	0.53	-
50	0.75	0.67	-	0.5I	-
I00	0.64	0.80	0.60	0.5I	0.38
I50	0.63	0.80	0.47	0.50	0.30
200	0.52	0.70	0.39	0.37	0.20
250	0.46	0.72	0.37	0.34	0.I7
300	0.43	0.6I	0.30	0.26	0.I3

$i_{(t)}$ = current after t secs and $i_{(ss)}$ = steady state current

increasing time indicating that the process is almost entirely activation controlled. In this low overpotential region the steady state current - voltage plot is linear showing that very little of the surface area of the electrode is not in electrolyte contact. It is probable that in this potential region the hydrogen escapes by dissolving in the electrolyte under pressure and then diffusing away through the electrolyte. As the current increases the hydrogen formed starts to build up within the electrode and substantial surface area is lost. At this point the current - time transient falls much more with time and the current - voltage plot is no longer linear but tends towards a limiting current. The determination of double layer capacity peak height by applying a step voltage while the electrode is evolving hydrogen at a low current when the current - voltage curve is in a linear region shows that even in this region a small amount of surface area is lost eg. fall in surface area $\sim$ 10%. In this linear region the ratio of the steady state current to the current after 100 μs is constant indicating that the hydrogen can escape by diffusion at a sufficiently fast rate and that if any surface area is lost due to gas bubbles this does not vary in this region. Also from the potentiostatic hydrogen oxidation transients for the same electrode the ratio of the steady state current to the current after 100 μs is constant over the linear region of the current - voltage plot and the value of this ratio is almost identical to the equivalent ratio for hydrogen evolution. This is further evidence that the hydrogen

gas transport mechanism is the same for both reactions.

The linear region of the current - voltage curve for both reactions is approximately from η = 0 - 50 mV. At higher potentials the current tends towards a limiting value and the ratio of steady state current to the current after 100 μs falls steadily with increasing overpotential. For hydrogen oxidation this represents the point where the concentration of hydrogen at the active sites has fallen to zero while for hydrogen evolution it represents the point where the gas bubbles start to build up. The value of the ratio in the limiting current region is different for hydrogen oxidation and hydrogen evolution suggesting a different hydrogen transport mechanism for the two processes. The gas in the interior of the electrode meets at the pore mouths and tends to form large bubbles on the outer electrode surface. These bubbles break off the electrode from time to time and as electrolyte rushes into the pores to replace the gas there is a surge of current. However, even this surge current is the result of only a partial recovery of the total surface area lost to gas bubbles and in order to compare the true current with the current assuming no loss of active surface area it is necessary to extrapolate the linear part of the current - voltage plot.

Hence it can be concluded that over the linear region of the current - voltage curve the active surface area of a hydrogen evolution electrode is constant and that the limiting current observed at higher overpotentials is due to a loss in active

surface area due to a build up of hydrogen gas. This can explain why in platinised graphite electrodes no electrode damage is observed at low hydrogen evolution currents since at low currents the hydrogen can diffuse away while at high currents the gas builds up within the electrode attaining high pressures before it can escape. These high pressures can cause the electrode to disintegrate. It can be seen that the ratio of the steady state to the 100 μs current in the limiting current region is significantly less for hydrogen evolution than for hydrogen oxidation showing that although the charge transfer process of the hydrogen electrode reaction may be reversible the mass transfer process is not. A further factor which shows the difference in mass transfer for hydrogen oxidation and evolution electrodes is the ratio between the steady state current and the current after I sec. For hydrogen oxidation this ratio is almost unity showing that after I sec a steady state has almost been obtained, while for hydrogen evolution the ratio is substantially less than unity showing that a longer time is required to achieve a steady state condition. Separate tests involving current - time curves for hydrogen evolution over periods of 5 sec to 5 min showed that in the potential range 0 - 100 mV a steady state was attained in 50 secs $\pm$5 secs, and that at higher potentials, times of up to 2 min. were needed.

4.7. The effect of gas bubbles on planar platinum foil hydrogen evolution electrodes.

4.7.I. Introduction.

In the comparison between porous and planar gas

evolution electrodes it has so far been tacitly assumed that the gas bubbles formed do not reduce the active surface area. This is unlikely to be true and the aim of this section is to determine the effect of gas bubble formation on planar electrodes so that a better comparison may be made with porous gas evolution electrodes.

4.7.2. Experimental.

Potentiostatic current - time curves were recorded in the time range 5 sec - 40 min., the fall in current over this range being due to the gradual loss of surface area to gas bubbles since for the hydrogen oxidation reaction on platinum foil a steady state is attained after about 5 sec.

The electrode was held at constant potentials and the double layer capacity charging peak height for a given potential step input was determined after different times and compared with the peak height for the electrode in the absence of gas bubbles.

4.7.3. Results and discussion.

The current - time curves (table 29) show that at low overpotentials the current falls steadily with time for 40 min. while at high overpotentials the current only falls for a few seconds before a steady value is obtained. At low overpotentials the bubbles form slowly and escape from the electrode slowly, while at high overpotentials the bubbles form and escape rapidly from the electrode. This experiment cannot be used to obtain a quantitative value for the surface area lost to gas bubbles but it does show qualitatively that as gas bubbles form the current falls and that

Table 29.

(a) The decay of hydrogen evolution currents with time on a potentiostatically controlled platinum foil electrode.

E = +0.010 V

i (mA)	time (sec)	$i_{(t)}/i_{(5)}$
I.30	5	
I.22	I0	94
I.20	I5	92
I.I5	30	88
I.07	60	82
0.95	I20	73
0.70	300	54
0.65	600	50

E = -0.07 V

i (mA)	time (sec)	$i_{(t)}/i_{(5)}$
I5.5	5	
I4.8	I0	95
I4.3	I5	92
I3.8	30	89
I3.0	60	84
I2.3	I20	79
II.0	300	7I
I0.7	720	69

E = -0.I75 V

i (mA)	time (sec)	$i_{(t)}/i_{(5)}$
55	5	
5I	I0	92
49	I5	88
52	30	94
44	60	79
52	300	94
49	600	88

E = -0.90 V

i (mA)	time (sec)	$i_{(t)}/i_{(5)}$
5.5	5	
4.8	I0	88
4.4	I5	80
4.I	30	75
3.8	60	69
3.4	I20	62
3.0	420	55
2.7	720	49

$i_{(t)}$ = current after t secs.

$i_{(5)}$ = current after 5 secs.

Table 29 .

(b) The effect of ultrasonic vibrations on the anodic performance of a platinum foil electrode.

E = I.30 V

t(sec)	i_I(μA.cm^{-2})	i_2	i_2/i_I
I0	I6	I6	I.0
90	3.0	3.0	I.0
300	0.6	0.6	I.0
700	0.4	0.4	I.0

E = I.80

t(sec)	i_I(mA.cm^{-2})	i_2	i_2/i_I
I5	0.I4	0.II	0.78
60	0.I2	0.09	0.75
I20	0.II	0.075	0.68
300	0.095	0.065	0.69
I200	0.085	0.050	0.59

E = 2.00 V

t(sec)	i_I(mA.cm^{-2})	i_2	i_2/i_I
I5	4.8	3.8	0.80
60	3.5	2.3	0.66
I20	3.I	2.0	0.65
300	2.7	I.7	0.63
900	2.5	I.5	0.60
I800	2.4	I.2	0.50

t = time

i_I = current using ultrasonic vibrator

i_2 = current not using ultrasonic vibrator

Electrolyte 5N H_2SO_4

Temperature 2I°C

Electrocatalyst platinum foil

(a) Atmosphere	hydrogen at I atmos.	(b)	air
O.C.V.	0.03 V		I.03V
Resistance	0.I0 ohm		0.I5 ohm

the faster the bubbles form the sooner a steady state condition is attained.

The double layer charging peak height for a 50 mV pulse at different hydrogen evolution currents shows that about 50% of the active surface is blocked by gas bubbles, the value tending to be slightly higher at low hydrogen evolution currents than at high hydrogen evolution currents because at low currents the bubbles tend to build up while at higher currents they break away from the electrode more easily.(Table 32.) These results are compared with those in table 33 for an experiment on a teflon bonded platinum black electrode in which
(a) the transient from O - I s was determined by pulsing from the O.C.V. to the given potential, V_I.
(b) the transient from O - I s was recorded from a potential, V_2, at which hydrogen is evolved, to the given potential, V_I. This transient is added to the steady state hydrogen evolution current at V_2.

The values from (a) and (b) should be the same and any differences are attributed to the loss of surface area in (b) due to gas bubbles. From the results it can be seen that more surface area is lost at high currents than at low currents.

4.8. Further evidence for the reduction in performance of a gas evolution electrode due to gas bubbles reducing the surface area.

4.8.I. Introduction.

The effect of gas bubbles on an oxygen evolution electrode is difficult to estimate since the oxygen evolution current decays with time due to

Table 3I.

The effect of oxygen evolution on the height of the double layer charging peak of a teflon bonded platinum black electrode.

E (V)	double layer charging peak height (cm)	i($mA.cm^{-2}$)	% reduction in peak height
I.25	0.42	50μA	0
I.40	0.42	0.7	0
I.50	0.42	I.5	0
I.60	0.39	5.5	7
I.70	0.36	27	I4
I.80	0.34	75	I9
I.90	0.30	-	29
2.00	0.29	320	3I
0.80	0.42	zero	0

Electrolyte	5N H_2SO_4
Temperature	20°C
Atmosphere	air
Electrocatalyst	platinum black
Electrocatalyst S.A.	I6 m^2/g
Electrocatalyst loading	5.5 $mg.cm^{-2}$
Current collector	platinum gauze
Resistance	0.I4 ohm
i = steady state current	
Pulse amplitude	I50 mV

Table 32.

The effect of hydrogen evolution on the double layer charging peak height of a platinum foil electrode.

E (mV)	double layer charging peak height ($mA.cm^{-2}$)	$i(mA.cm^{-2})$	% reduction in peak height
-10	2.5	2.0	58
+50	6.0	zero	0
-40	3.0	6.0	50
-100	3.8	20	37

Pulse amplitude	50 mV
Electrolyte	5N H_2SO_4
Temperature	21°C
Atmosphere	hydrogen
O.C.V.	0.05V
Electrocatalyst	platinum foil
Resistance	0.10 ohm

i = steady state hydrogen evolution current

Table 33.

The Effect of Hydrogen Evolution on the double layer charging peak heights on a Teflon Bonded Platinum Black Electrode.

E_1	i (mA)	t (msec)	$E_1-E_2=60mV$ i_p (mA)	$E_2=-40mV$ i_{ss} (mA)	$(i_{ss}+i_p)$	$\frac{(i_{ss}+i_p)}{i}$
-100mV	195	peak current	40	56	96	0.49
	180	20	36	56	92	0.51
	175	120	34	56	90	0.52
	165	400	34	56	90	0.54
	155	800	33.5	56	89.5	0.57
	190	1	39	56	95	0.56
	185	2	38	56	94	0.51
	180	6	38	56	94	0.52
	180	8	38	56	94	0.52
	195	peak current	40	56	96	0.49
-140mV			$E_1-E_2=110mV$	$E_2=-30mV$		
	250	peak current	70	40	110	0.44
	235	500μs	64	40	104	0.44
	230	1	63	40	103	0.45
	227	3	62	40	102	0.45
	225	8	60	40	100	0.44
	220	100	70	40	110	0.50
	203	300	66	40	106	0.52
	195	500	70	40	110	0.56
	190	1000	54	40	94	0.49
	178	2000	51	40	91	0.52
	165	3000	48	40	88	0.53
	150	4000	45	40	85	0.56
-210mV			$E_1-E_2=-120mV$	$E_2=-90mV$		
	490	peak current	84	100	184	0.37
	490	1	80	100	180	0.37
	456	3	76	100	176	0.38
	444	8	72	100	172	0.38
	412	30	66	100	166	0.40
	390	80	51	100	151	0.39
	370	100	46	100	146	0.40
	300	400	10	100	110	0.37
	260	900	5	100	105	0.40

Table 33 (cont.)

i_1 = current at time, t, when pulsing from O.C.V. to E_1 volts

i_{ss} = steady state hydrogen evolution current at E_2 volts.

i_p = current after time, t, when pulsing from E_2 to E_1

i_2 = peak current pulsing from O.C.V. to E_1.

Electrolyte	5N H_2SO_4
Temperature	21°C
Atmosphere	Hydrogen at 1 atmos.
O.C.V.	0.028 V
Electrocatalyst	platinum black
Electrocatalyst S.A.	16 m^2/g
Electrocatalyst loading	7 $mg \cdot cm^{-2}$
Current Collector	platinum gauze
Resistance	0.05 ohm
Electrode area	0.2 cm^2

oxide formation. On a planar electrode it is easy to remove the gas bubbles from the electrode as soon as they form by subjecting the cell to ultra sonic vibrations but it is most unlikely that this method would be effective in removing gas bubbles from the interior of porous electrodes.

The determination of double layer charging peak heights should be applicable for both planar and porous oxygen evolution electrodes, since it is a direct measure of surface area and is not affected by surface oxide ie. the formation of surface oxide does not result in an increase or a decrease in surface area as shown by tests on platinum electrodes in the potential range I.0 - I.4 V where no oxygen is evolved and all the anodic current is used for oxide formation.

4.8.2. Experimental.

(a) Oxygen evolution was carried out on a platinum foil electrode at different potentials and the currents compared with and without the ultra sonic vibrator (graph 44) operating. Assuming that when the ultra sonic vibrator was operating all the gas bubbles are removed the amount of surface area lost to gas bubbles can be calculated (table 29).

(b) the double layer charging peak height was determined for a given potential step input for a teflon bonded platinum black electrode and for a platinum foil electrode evolving oxygen at different rates and compared with the value obtained on the same electrode in the absence of gas bubbles (table 30).

Graph 44.

The effect of ultrasonic vibrations on the oxygen evolution performance of a platinum foil electrode.

Electrolyte	5N H_2SO_4
Temperature	20°C
Atmosphere	air
O.C.V.	I.04 V
Electrocatalyst	platinum foil
Resistance	0.I5 ohm
Potential	2.00V

⊙ ultrasonic vibrations

× no ultrasonic vibrations

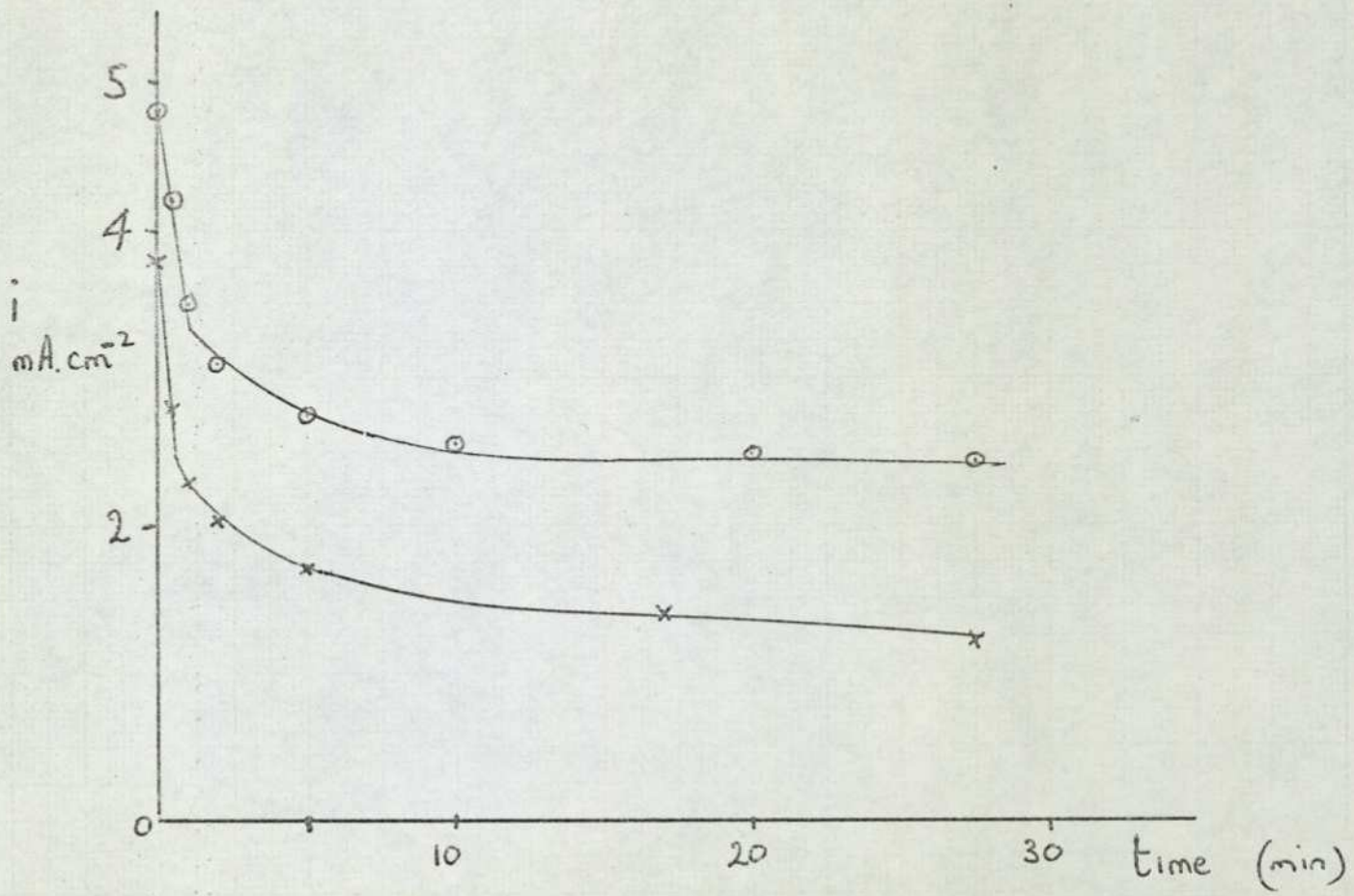


Table 30.

The effect of gas evolution on the height of the double layer charging peak of a platinum foil electrode.

E (V)	double layer charging peak height ($mA.cm^{-2}$)	$i(mA.cm^{-2})$	% reduction in peak height
I.25	I2	0.0I	0
I.40	I2	0.02	0
I.50	I2	0.03	0
I.60	I2	0.04	0
I.70	I2	0.07	0
I.80	I0.4	0.45	I4
I.90	8.8	I.3	27
2.00	8.2	3.8	30
0.80	I2	zero	0

Pulse amplitude	I00 mV
Electrolyte	5N H_2SO_4
Temperature	22°C
Atmosphere	air
O.C.V.	I.0I V
Electrocatalyst	platinum foil
Resistance	0.I2 ohm

i = steady state anodic current

4.8.3. Results and Discussion.

Both these tests on oxygen evolution electrodes confirm the results obtained for hydrogen evolution electrodes ie. that the performance is reduced owing to a loss of surface area caused by gas bubbles expelling the reacting species from the electrocatalyst active sites. A comparison of the two methods for oxygen evolution on platinum foil shows reasonable agreement. The proportion of the total surface area blocked off by gas bubbles is approximately the same for the porous and planar electrodes for the oxygen evolution reaction and hence there is a definite advantage in using the porous electrode.

A comparison of the polarisation data for hydrogen oxidation and evolution on platinum foil and platinum black electrodes, taking into account the roughness factor of the foil and the active surface area of the platinum black, shows that for hydrogen oxidation the polarisation data are very similar over the linear region of the curve. Differences occur in the potential region where the current becomes limited by mass transfer considerations. This is to be expected as mass transfer to planar and porous electrodes is very different. A similar effect is observed for the hydrogen evolution reaction. However, for a given potential in the limiting current region the ratio of the platinum foil current density to the platinum black current density is much greater for the hydrogen evolution reaction than for the hydrogen oxidation reaction. In fact the limiting current for the hydrogen oxidation is reached at a

lower overpotential and current density on platinum foil than on platinum black. For the hydrogen evolution reaction a limiting current is only observed on the platinum black and not on the platinum foil. This is because the diffusion of hydrogen gas away from the electrode is very much easier for a planar electrode than for a porous electrode. This may be compared with the hydrogen oxidation reaction where the diffusion of hydrogen gas into the electrode is much easier for the porous electrode than for the planar electrode. This clearly suggests that the mass transfer mechanism is different in both reactions, which is consistent with the assumption that in the hydrogen oxidation reaction the hydrogen gas dissolves in the electrolyte at the electrolyte - gas interface and then diffuses to the active site, while in the hydrogen evolution reaction the hydrogen gas produced collects in the micropores of a porous electrode or on the planar electrode surface and when a sufficient pressure of gas is generated it can escape directly to the atmosphere without dissolving in the electrolyte. This process would be easy on a planar electrode but in a microporous electrode it is necessary to build up high pressures before the gas can escape in this way.

4.9. The determination of effectiveness factors for porous teflon bonded electrodes.

4.9.I. Introduction.

When a reaction occurs simultaneously with mass transfer within a porous structure, a concentration gradient is established and interior surfaces are exposed to lower reactant concentrations than surfaces

near the exterior. The average reaction rate throughout a catalyst particle under isothermal conditions would almost always be less than if there were no mass trnasfer limitations. The effects of mass transfer within a porous structure on observed reaction characteristics were first analysed quantitatively by Thiele,(I62) Damkohler(I63) and Zeldovich(I64). The important result of this work is the quantitative description of factors which determine the effectiveness of a porous catalyst. The effectiveness factor, e, is defined as the ratio of the actual reaction rate to that which could occur if all the surface throughout the inside of the catalyst particle were exposed to reactant at the same concentration and temperature as that existing at the outside surface of the particle. The effectiveness factor for a first order irreversible reaction in a porous spherical particle can be related to the reaction parameters R, S, k, c^{m-1} D_{eff} by the equation

$$e = \frac{3}{\phi_s}\left[\frac{1}{\tan\phi_s} - \frac{1}{\phi_s}\right]$$

where $\phi_s = R\sqrt{\frac{S k c^{m-1}}{D_{eff.}}}$

where R = radius of particle

S = pore surface (cm^2/cm^3 of volume of the porous structure)

k = is the intrinsic reaction rate constant for a surface reaction of order, m.

c = local surface concentration inside the particle

D_{eff} = effective diffusion coefficient for a porous solid
= the ratio of flux to concentration gradient

This equation has some important practical considerations. The effectiveness of the internal surface of the porous catalyst approaches unity as an asymptote as the pellet radius or rate constant is made small or the diffusion coefficient is made large. Conversely the effectiveness becomes small for large particles, large rate constants or small diffusion coefficients. Generally the most effective use of a catalyst is attained by using the smallest possible particle size. Very active catalysts tend to have low effectiveness factors while inactive catalysts have high effectiveness factors. When a catalyst is operating at a low effectiveness factor the reactant concentration drops rapidly with distance of penetration into the interior. Hence, the catalyst in the interior contributes relatively little to the overall rate of reaction. If the active ingredient of the catalyst is expensive as is the case with substances such as platinum or palladium, it may be deposited in a thin layer on the outside portion of the pellet to maximise its usefulness. In some cases a catalyst may be so active that to obtain an effectiveness factor near unity, and hence high selectivity, the requisite particle size is so small as to be impractical. In such cases the problem may be resolved by using a thin layer of active catalyst on an inert or nonporous carrier of suitable dimensions. It should be noted that the effect of mass transfer limitations within a porous particle depends on the Thiele modulus and not on the individual values of R, k and D_{eff}.

The effectiveness factor can be determined by (a) an experimental method or (b) a theoretical method.

(a) The effectiveness factor can be experimentally determined by measuring reaction rates on several catalyst particle sizes under otherwise identical conditions. The effectiveness factor approaches unity when no increase in rate per unit quantity of catalyst occurs on subdivision. If data are available on finely divided catalyst having an effectiveness factor approaching unity, then the ratio of the rate per unit quantity of catalyst for the larger size to that for the finer is directly equal to the effectiveness factor of the larger size.

(b) If the data on the rate of reaction on a particular catalyst of one fixed size is available and it is desired to estimate the extent to which a diffusion effect may be present it is necessary to determine the intrinsic kinetic constant. This can be achieved by using the dimensionless modulus

$$\phi_s = \frac{R^2}{D_{eff}} \left(-\frac{1}{V_c} \frac{dn}{dt} \right) \frac{1}{c_s}$$

where V_c = volume of the catalyst particle

$-dn/dt$ = rate of reaction (g-mol/sec)

Even using this expression it is still necessary to know the values of R, D_{eff}, c. Hence it can be seen that both methods of determining the effectiveness factors of porous catalyst particles are quite complex necessitating the knowledge of factors such as rate data, particle size, which in practise will cover a range of values and effective diffusivity the accuracy of which, depends on the selection of the correct tortuosity factor for the porous structure.

It is particularly difficult to predict effectiveness factors due to uncertainties in predicting the effective diffusivity under reaction conditions, the nature of the intrinsic kinetics and the degree of anisotropy which exists in the catalyst structure. For complex particle shapes and structures, and intrinsic kinetics the experimental determination or theoretical prediction of effectiveness factors is very difficult.

Effectiveness factors of electrocatalysts have not been measured. However, because of the fast response of electronic circuitry a very direct method of experimentally determining effectiveness factors is available. At a given overpotential the current density is determined (a) after a time, t_1, when the value is steady and (b) after a time, t_2, when double layer charging is complete. The ratio of i at t_I to i at t_2 gives the effectiveness factor. The separation of mass transfer and charge transfer components of the total overpotential in chapter 2 enables the effectiveness factor of various electrode systems to be easily determined without a knowledge of the intrinsic kinetics, particle structure or effective diffusivity. Also the effect of electrocatalyst structure (micropore size, macropore size, pore volume) on the effectiveness factor can be determined. These electrocatalyst structure parameters can be determined by extensions of the B.E.T. technique and a range of electrocatalyst parameters can be obtained by varying the preparation conditions (see chapter 2).

4.9.2. Experimental.

Effectiveness factors have been determined at

Table 35.

Effectiveness factors for the hydrogen oxidation reacti on a teflon bonded platinum black electrode.

$i_{(ss)}$ = steady state current

i_{trans} = transient current measured after 25μsec

e = effectiveness factor.

η	$i_{(ss)}$ ($mA \cdot cm^{-2}$)	i_{trans}	e
2.5	I2	25	0.48
5	26	50	0.52
I0	53	I00	0.53
20	I04	I95	0.53
50	245	490	0.50
I00	445	990	0.50
I50	605	I480	0.4I
200	740	2020	0.37
250	803	2300	0.35
300	835	3000	0.28
350	855	3420	0.25
400	875	4000	0.22

Table 34.

Effectiveness factors for the hydrogen evolution reaction on a teflon bonded platinum black electrode.

η	$i_{(ss)}$ ($mA \cdot cm^{-2}$)	i_{trans} ($mA \cdot cm^{-2}$)	e
2.0	I3	26	0.50
5.0	32	64	0.50
I0	57	94	0.60
20	I06	I90	0.56
50	I75-250	490	0.36 - 0.5I
I00	350-480	940	0.38 - 0.5I
I50	400-680	I350	0.30 - 0.48
200	440-740	2I50	0.20 - 0.35
250	460-890	2650	0.I7 - 0.34
350	490-990	3750	0.I3 - 0.26

Data for tables 34 and 35.

Electrolyte	5N H_2SO_4
Temperature	2I°C
Atmosphere	hydrogen at I atmos.
O.C.V.	0.024 V
Electrocatalyst	platinum black
Electrocatalyst S.A.	I6 m^2/g
Electrocatalyst loading	5.5 $mg.cm^{-2}$
Current collector	platinum gauze
Resistance	0.03 ohm

$i_{(ss)}$ = steady state current

i_{trans} = transient current measured after 25μ sec

e = effectiveness factor

different potentials for the hydrogen oxidation and evolution reactions on teflon bonded platinum black electrodes.

The hydrogen electrode reactions on platinum are unusual in that the catalyst is very active and the mass transfer of hydrogen and hydrogen ions is very rapid. The experimental measurements were (a) transient current density values over the first millisecond and (b) steady state current density.

4.9.3. Results and Discussion.

The results are shown in tables 34 and 35. It can be seen that the effectiveness factor is approximately constant over the potential range in which the current - voltage curve is linear. The value in this region is similar for both hydrogen evolution and oxidation ie. about 0.5. As the steady state current tends to limiting values the effectiveness factor decreases and the value at a given overpotential for hydrogen oxidation is about the same as the maximum value for hydrogen evolution. The minimum value for hydrogen evolution falls to about half the maximum value, the difference being entirely due to gas bubbles blocking the electrode surface.

4.10. The use of the pulse technique to determine the intrinsic exchange current density.

The same measurements made for determining the effectiveness factor of a porous electrode for a given electrode reaction can be used to find the intrinsic exchange current density of the electrocatalyst. This factor is the most accurate measurement of the electrocatalytic activity of the electrocatalyst

since it takes into account the true electrochemical surface area and only considers the activation over-potential. The electrochemical surface area is found by galvanostatic hydrogen stripping while the ohmic overvoltage is corrected by using the interrupter technique and the mass transfer overvoltage is corrected by measuring the current immediately following the completion of double layer charging or more accurately from the extrapolated value of current density at $t = 0$ of an $i - t^{\frac{1}{2}}$ plot. The elimination of mass transfer and ohmic overvoltages and using the true electrochemical surface area has rarely been employed in the study of porous electrodes. This procedure is especially valuable for electrocatalysts which cannot be moulded into sheet, wire or non porous pellets. The intrinsic exchange current density of a porous electrode should be the same as that of a planar electrode of the same material. This fact was confirmed by measuring the intrinsic exchange current densities of platinum foil and platinum black electrodes for the hydrogen electrode reaction. A study of porous and planar zinc electrodes (170) in which the exchange current density was calculated using the true surface area but without correction for ohmic and mass transfer overvoltages showed that the exchange current density was constant for different zinc samples. This is suprising since mass transfer to porous and planar electrodes is unlikely to follow the same law.

The exchange current density for the oxygen reduction reaction is difficult to measure because:

(I) the Tafel equation is often not obeyed by porous electrodes and polarisation curves result which are almost linear and consequently the Tafel plot is logarithmic and not linear. This results from the reduced dissolved oxygen concentration in the micropore structure at high current densities which in part offsets the exponential increase in current with increasing polarisation. This phenomenom has been observed previously by Grens (131) who showed that the polarisation curve followed the Tafel equation more closely as the porosity was reduced.

(2) the oxygen reduction reaction which occurs in the potential range 0.6 V to I.2 V is difficult to study on the basis of kinetics since at potentials greater than 0.8 V the platinum surface is covered with an oxide film, the coverage and nature varying with potential. There is also evidence for adsorbed oxygen at lower potentials. Considering this change in the platinum surface over the entire potential range it is not suprising that the current - voltage curve does not obey the Tafel equation.

A comparison of the intrinsic exchange current densities of platinum foil and platinum black electrodes for the hydrogen evolution reaction.

Experimental.

Transients from I - 1000 μsec were measured for a platinum foil electrode and a teflon bonded platinum black electrode. The roughness factor of the platinum foil and the electrochemical surface area of the platinum black were determined. The ohmic overvoltage for each electrode was determined by the interrupter

method.

Results.

Graphs 46 & 43 show the transient current - voltage curves, corrected for the true surface area and ohmic overvoltage, for the planar and porous platinum electrodes.

The slope of these polarisation curves at low oovervoltages is used to determine the intrinsic exchange current density using the formula.

$$i'_o = \frac{i'}{\eta} \cdot \frac{\gamma RT}{nF}$$

where i'_o = intrinsic exchange current density

i' = current per unit true surface area

η = activation overpotential

γ = stoichiometric number

R = universal gas constant

T = absolute temperature

F = the Faraday

n = number of electrons associated with the rate determining step

Since the slope (i'/η) of polarisation curves for the porous and planar electrodes were 0.042 and 0.04 mA/mV respectively it follows that there is very close agreement between the i_o values for planar and porous platinum.

	i'_o mA.cm^{-2}
Platinum foil	2.04
Platinum black	2.I4

Discussion.

This experiment shows the validity of using the pulse technique to separate mass transfer

overvoltage from the activation overvoltage for microporous electrodes and although the results for platinum are not of great importance the application of this method to supported metal electrocatalysts or semiconducting oxide electrocatalysts, which cannot be moulded into a non porous form could be of significance.

Suggestions for Further Work.

(I) Comprehensive endurance tests on teflon bonded cobalt nickel oxide electrodes under both oxygen reduction and oxygen evolution conditions. The short term performance for these reactions compares favourably with other electrocatalysts in terms of both performance and cost, and if its long term endurance is satisfactory, as the oxygen evolution results predict, then it would fulfill the requirements for a rechargeable air electrode.

(2) Surface groups on carbon substrates can be investigated by infra red internal reflectance spectroscopy.(165)

Although surface oxides are known to be formed electrochemically on carbon surfaces, little work has been done on elucidating the exact nature of these groups. The results of this investigation show that oxides formed at potentials 2.8 V are reduced at potentials about 0.7 V while oxides formed at lower potentials are difficult to reduce even under extreme cathodic conditions. Hence an investigation of the nature of these oxide groups would be interesting.

(3) A more detailed study of the strength of binder electrocatalyst systems is needed. The strength of a binder - electrocatalyst - pore system depends on (a) relative particle size of electrocatalyst and solid binder, (b) the volume concentrations of the binder and electrocatalyst, and (c) the volume fraction of pores.

In general the strength of the composite system is greater than that of the binder alone and a

maximum strength is obtained at a particular volume concentration of binder ie. the voids between the aggregates are just completely filled with binder.

Since for battery and fuel cell electrodes it is desirable to use highly porous materials (porosity between 70 - 90%) it is not feasible to improve the strength by reducing the volume fraction of pores. It would however be useful to determine the ratio of the volume concentration of teflon to electrocatalyst which gives the maximum strength, to investigate the effect of teflon particle size on the strength and to test other hydrophobic particulate binders of greater mechanical strength (eg. polyethylene and P.V.C.). It is possible that a mixture of hydrophobic and hydrophilic particulate binders could be made which would have greater strength but equivalent wetting properties to the normal teflon bonded electrodes containing 30% teflon.

(4) The good electrical conductivity of platinum electrodes pretreated in such a way as to form multilayer oxide films suggests that the surface oxide is either non stoichiometric or consists of oxides with different platinum oxidation states. This possibility can be investigated by

(a) measuring the oxide film thickness by ellipsometry after a given time at a constant potential,

(b) calculating the thickness of a monolayer of PtO and PtO_2, and (c) determining the oxide coverage in Coulombs.cm^{-2} by oxide stripping after a given time at a constant potential.

The ellipsometric technique is sensitive to an

average thickness of the order of I Å and can be used to examine the electrode in solution in contrast to most other optical methods.

(5) It is possible that there is an optimum particle size for the electrocatalyst in teflon bonded electrodes. This could be investigated by preparing electrocatalyst samples over a range of particle sizes by slight variations to the reaction conditions eg. platinum black see chapter 2.

For gas dissolution reactions it is probable that an optimum particle size (hence pore size) exists since for large particles the surface area would be low while for very small particles the contact resistance could be high and it is possible that liquid phase mass transport in very small pores could be restricted.

For gas evolution reactions the escape of bubbles from large pores is easier than from small pores but this effect is balanced by surface area effect. Hence an optimum particle size should exist.

(6) It is well known that the diffusion of gases in small pores is restricted (Knudsen diffusion). Little work has been done on the diffusion of species in liquid media in small pores, although there is some evidence to suggest that it is severely impeded.

(i) when a thin tube (i.d. 2mm) filled with water, is placed in a trough of coloured solution eg. potassium permanganate, for the initial few minutes the front of the diffusing permanganate ions shows a marked upward curvature indicating that the diffusion process is slower near the walls due to the presence of

cohesive forces. At longer times the curvature disappears as radial diffusion sets in. The effect can be seen in a thin layer near the wall about 0.5 mm thick which is not dependent on the overall tube size. However, if the internal diameter (i.d.) of the tube is less than 0.5 mm one would expect the rate of diffusion to be less than that predicted by the diffusion coefficient.

(ii) The Arrhenius activation energy for proton conduction in small capillaries is considerably greater than in free solution.(154)

(iii) The surface zone of liquid in the region of a solid surface has been shown to extend from the surface for distances of the order of 100 Å in low molecular weight liquids and 1000 Å in liquids consisting of long chain molecules. X ray diffraction(193) and refractive index(194) experiments have shown the difference in the structure of liquids near solid interfaces compared with the bulk liquid. The high compressive strength of thin films of liquid also indicates a more ordered structure near solid surfaces.(194)

(iv) The viscosity of water has been shown to be increased at distances within 1.6×10^{-5} cm of a solid surface.(195) This evidence suggests that water is highly structured at distances of the order of 100 Å from a solid surface resulting in physical properties significantly different from normal water. In particular the increased viscosity will result in reduced diffusion coefficients for species diffusing through water in pores of radius less than 100 Å. Since most of the pores within an electrocatalyst aggregate are smaller than this

a reduction in mass transfer rates of the reactant to and the product from the active sites is to be expected. Experiments have been planned to measure the diffusion coefficients of common species in Corning glasses of pore radius 40 Å to 1000 Å.

References.

I. C.M. Summers, Scientific American, pI49 (I97I).

2. D.K. Adams et al., "Fuel cells - Power for the future", Harvard Business School, Harvard University, Cambridge, Mass., (I960).

3. G. Szego, Economics, Logistics and Optimisation of Fuel Cells, Institute for Defence Analysis, Res. Paper P. 208 (I965).

4. A.C.C. Tseung and W.J. King, Med. Biol. Eng. 9, I75 (I97I).

5. S.L. Chang, "Energy Conversion", Prentice Hall, Inc., Englewood Cliffs, N.J., (I963).

6. S.W. Angrist, "Direct Energy Conversion", Allyn and Bacon, Inc., Englewood Cliffs, N.J., (I964).

7. G.W. Sutton, "Direct Energy Conversion", McGraw Hill, New York, (I966).

8. J. O'M Bockris, A. Reddy, Modern Electrochemistry, 2, MacDonald (I970).

9. J.S. Newman and C.W. Tobias, J. Electrochem. Soc., I09, II83 (I962).

IO. K. Micka, Advan. Chem. Ser., 47, 73 (I965).

II. S. Srinivasan, H.D. Hurwitz and J. O'M Bockris, J. Chem. Phys., 46, 3I08 (I967).

I2. L.G. Austin, M. Ariel, R.D. Walker, G.B. Wood and R.H. Comyn, Ind. Eng. Fundamentals, 4, 32I (I965).

I3. J. O'M Bockris and BD. Cahan, J. Chem. Phys., 50, I307 (I969).

I4. A.M. Adams, F.T. Bacon, R.G.H. Watson, Ch. 4 in "Fuel Cells", W. Mitchell (ed.), Academic Press Inc., New York (I963).

I5. E. Justi and A.W. Winsel, "Kalte - Verbrennung", Franz Steiner, Verlag, Wiesbaden, Germany (I962).

I6. R. Burnstein et al., Electrochim. Acta, 9, 773 (I964).

I7. A. Tantrum and A.C.C. Tseung, Nature 22I, I67 (I969).

I8. S. Srinivasan and H.D. Hurwitz, Electrochim. Acta., I2 , 495 (I967).

I9. H.H. Ewe, E.W. Justi and A.W. Kalberlap, Energy Conversion, II, I49 (I97I).

20. A.M. Moos and N.I. Palmer, Proceedings 2Ist Annual Power sources conference, p. 5I (I967).

2I. D.A.J. Swinkels, J. Electrochem. Soc. II3, 6 (I966).

22. M. Eisenberg, Proc. Symp. Power Systems for Electric Vehicles, Columbia University, New York, April I967, p.209, U.S. Dept. of Health, Educ. and Welfare, Washington D.C.

23. J.M. Lee, 2nd semi-Ann. Report, I960, Contract DA36-039-SC-85259, U.S. Army Signal Res. and Dev. Lab., Fort Monmouth, New Jersey.

24. D.P. Gregory, "Metal - Air Batteries", Mills and Boon, London (I972).

25. A.C.C. Tseung and H.C. Bevan, J. Mat. Sci., 5, 604 (I970).

26. A.C.C. Tseung, B.S. Hobbs and A. Tantrum, Electrochim. Acta, I5, 473 (I970).

27. Private Communication, W. King, (T.C.U.).

28. P.L. Walker, Am. Scientist, 50, 259 (I962).

29. R.R. Paxton et al., J. Electrochem. Soc., II0, 933 (I963).

30. W.G. Berl, Trans. Electrochem. Soc., 83, 253 (I943).

3I. B.K. Brown and O.W. Storey, Trans. Electrochem. Soc., 53, II3 (I928).

32. R.R. Witherspoon et al., Tech. Report No 4, ONR Contract non r. 58I(00), Western Reserve Univ. (I954).

33. E. Yaeger, Ing. Vetenskaps Akad. Medd., I34, 89 (I963).

34. E. Yaeger and A. Kozawa, ASTIA Rept. no. AD429248 (Jan.I964).

35. E. Yaeger, P. Krouse and K.V. Rao, Electrochim. Acta 9,

I057 (I964).

36. R. Weisz and S. Jaff, Trans. Electrochem. Soc., 93, I28 (I948).

37. K. Kordesch and F. Martinola, Monatsh., 84, 39 (I953).

38. M.A. Davies et al., J. Electrochem. Soc., I06, 56 (I969).

39. G.W. Heise et al., Trans. Electrochem. Soc., 62, 383 (I932).

40. G.W. Heise et al., Trans. Electrochem. Soc., 92, I73 (I947).

4I. E.A. Schumacher and G.W. Heise, J. Electrochem. Soc., 99, I9Ic (I952).

42. Z. Nasarischwily, Electrokhem., 29, 320 (I923).

43. P.R. Shipps, Proc. Ann. Power Sources Conf., 20, 76 (I966).

44. F.T. Bacon, Fuel Cells, Vol. I, G.J. Young (ed.), Reinhold, New York, (I960) p.5I.

45. E.W. Justi and A.W. Winsel, Naturwiss, 47, 298 (I960).

46. M.B. Clark, W.G. Darland and K.V. Kordesch, Electrochem. Tech., 3, I66 (I965).

47. W.T. Grubb and C.J. Michalske, J. Electrochem. Soc., III, 477 (I964).

48. G.V. Elmore and H.A. Tanner, J. Electrochem. Soc., I08, 669 (I96I).

49. L.W. Niedrach and H.R. Alford, J. Electrochem. Soc., II2, II7 (I965).

50. A. Damjanovic, M.A. Genshaw, J. O'M Bockris, J. Phys. Chem., 70, 376I (I966).

5I. H. Wroblowa et al.,J. Electroanal. Chem.,I5, I39 (I967).

52. S. Schuldiner and R.M. Roe, J. Electrochem. Soc., II0, II42 (I963).

53. W. Visscher and M.A.V. Devanothon, J. Electroanal. Chem., 8, I27 (I964).

54. J. O'M Bockris and A.K.M.S. Huq, Proc. Roy. Soc., Ser. A 237, 277 (I956).

55. F. Haber and F. Fleischmain, Z. Anorg. Allgem. Chem., 51, 245 (1966).

56. T.P. Hoar, Proc. Roy. Soc., Ser.A 142, 628 (1933).

57. J.P. Hoare, J. Electrochem. Soc., 110, 1019 (1963).

58. N. Watanabe and M.A. Devanathon, J. Electrochem. Soc., 111, 615 (1964).

59. Technical data based on primary zinc - air batteries manufactured by Energy Conversion Ltd.

60. F.P. Bowden, Proc. Roy. Soc., A 125, 446 (1929).

61. F.C. Anson and J.J. Lingane, J. Am. Chem. Soc., 79, 4901 (1957).

62. A.K.N. Reddy, M.A.V. Devanathon and J. O'M Bockris, J. Electroanal. Chem., 6, 61 (1963), Proc. Roy. Soc., A 279, (1964).

63. A.K.N. Reddy and J. O'M Bockris, Proc. Symp. on the Ellipsometer and its uses, Dept. Comm. Publ. 229 (1964).

64. A.K.N. Reddy, M.A. Genshaw and J. O'M Bockris, J. Chem. Phys. 48, 671 (1968), J. Electroanal. Chem., 8, 406 (1964).

65. W. Visscher, Doctoral dissertation, Technological Univ., Sudhoven, (1968), Optik 26, 402 (1968).

66. K.I. Rozenthal, V.I. Vesdovskii, Dokl. Akad. Nauk. SSSR, 111, 637 (1956).

67. J. O'M Bockris, J. Chem. Phys., 24, 817 (1956).

68. A. Damjanovic, A. Dey and J. O'M Bockris, Electrochim. Acta, 11, 791 (1966).

69. A. Damjanovic, A. Dey and J. O'M Bockris, J. Electrochem. Soc., 113, 739 (1966).

70. J. Heyrovsky, J. Cas. cesk. lekain., 7, 242 (1927).

71. W.A.Berl, Trans. Electrochem. Soc., 83, 253 (1943).

72. M.C. Davies, M. Clark, E. Yaeger and F. Hovorka, J. Electrochem. Soc., 106, 56 (1959).

73. V.G. Levich, "Physicochemical Hydrodynamics", Prentice-Hall, Inc., Englewood Cliffs, N.J. (1962).

74. A. Damjanovic, M.A. Genshaw and J. O'M Bockris, J. Electrochem. Soc., 114, 466 (1967).

75. A. Damjanovic, M.A. Genshaw and J. O'M Bockris, J. Electrochem. Soc., 114, 1108 (1967).

76. W. Juda and D.M. Moulton, Chem. Eng. Prog., 63, 59 (1967).

77. M. Blavatnik and G.A. Tsiganov, Corrosion, 19, 421 (1963).

78. J.L. Ord and F.C. Ho, J. Electrochem. Soc., 118, 46 (1971).

79. A. Damjanovic and V. Brusic, Electrochim. Acta, 12, 615 (1967).

80. I.M. Kolthoff and E.R.Nightingale, Anal. Chim. Acta, 17, 329 (1957).

81. K.I. Rozenthal and V.I. Vaselovskii, Zh. Fiz. Khim., 27, 1163 (1953).

82. F.C. Anson, Anal. Chem., 33, 934 (1961).

83. F.C. Anson and D.M. King, Anal. Chem., 34, 362 (1962).

84. S. Gilman, J.Electroanal. Chem., 9, 276 (1965).

85. S.W. Feldberg et al., J. Electrochem. Soc., 110, 826 (1963).

86. E. Wieke and B. Weblus, Z. Elektrochem., 56, 159 (1952).

87. M.W. Breiter, Electrochim. Acta, 9, 441 (1964).

88. C.C. Lieng and A.L. Juliard, J. Electroanal. Chem., 9, 390 (1965).

89. D.T. Sawyer and L.V. Interante, J. Electroanal. Chem., 2, 310 (1961).

90. J.P. Hoare, J. Electrochem. Soc., 112, 602 (1965).

91. A.J. Appleby and A. Borucka, J. Electrochem. Soc., 116, 1212 (1969).

92. J.P. Hoare, J. Electrochem. Soc., 116, 612 (1969).

93. J.P. Hoare, ibid 110, 1019 (1963)

94. J.P. Hoare, "The Electrochemistry of Oxygen", Interscience, New York (1968).

95. S. Shibata and M.P. Sumino, Electrochim. Acta, I6, I5II (I97I).

96. S. Shibata and M.P. Sumino, ibid I6, I089 (I97I).

97. S.D. James, J. Electrochem. Soc., II6, I68I (I969).

98. J. Woltowicz, D. Gilroy and B.E. Conway, Electrochem. Acta, I4, III9 (I969).

99. L.D. Burke and A. Moyniham, Electrochem. Acta, I5, I437 (I970).

I00. W.A. Nystrom, J. Electrochem. Soc., II6, I7 (I969).

I0I. L.J.J. Janssen, J.G. Hoogland, Electrochim. Acta, I4, I097 (I969).

I02. L.I. Krishtalik and Z.A. Rotenberg, Russian J. Phys. Chem., 39, I68 (I965).

I03. B.M. Bulygin, Zhir. Prikl. Khim., 32, I22 (I959).

I04. V.I. Eberil et al., Electrokhimiya, 5, 336 (I969).

I05. M. Janes, Trans. Electrochem. Soc., 92, 23 (I947).

I06. T.S. Fillipov et al., Zh. Prikl. Khim., 40, 2488 (I967).

I07. K. Arnott and W. Fehse, Z. Elektrotech., 28, 376 (I922).

I08. V.V. Stender and O.S. Ksenzhek, Zhir. Prikl. Khim., 32, III (I959).

I09. H. Niedereither, Germ. Pat. 303 27 (I927).

II0. A.M. Adams, Electrochemical Cells As Energy Convertors, Conf. Paper no. CP 56-266, AIEE Winter Gen. Meeting, New York, (I956).

III. J.M. Lee, 2nd semi-annual report, I960, contract DA36-039-SC-85259, U.S. Army signal Res.and Dev. Lab., Fort Monmouth, New Jersey.

II2. H.H. Ewe, E.W. Justi and A.W. Kalberlah, Energy Conversion, II, I49 (I97I).

II3. E. Justi, Germ. Pat. I,I67,406 (I956).

II4. E. Justi and R. Wendtland, Aust. Pat. 265, 388 (I967).

II5. W.R. Lasko and G.P. MacCarthy, Anal. Chem., 38, 894 (I966).

II6. P.H. Emmett, Chem. Rev., 43, 69 (I948).

II7. H. Sato and H. Akamatu, Fuel, 33, I95 (I954).

II8. F.K. Schoenfield, Ind. Eng. Chem., 27, 57I (I935).

II9. R.F. Strickland-Constable, Trans. Farad. Soc., 34, I074 (I938).

I20. J.D. Lambert, Trans. Farad. Soc., 32, 452 (I936).

I2I. W.S. Hummers and R.E. Offerman, J. Am. Chem. Soc., 80, I339 (I958).

I22. E. Matuyama, J. Phys. Chem., 58, 2I5 (I954).

I23. C.A. Klein, Rev. Mod. Phys., 34, 56 (I962).

I24. E.J. Balskus, J.J. Podesta and A.J. Arvia, Electrochem. Acta, I6, I663 (I97I).

I25. D.S. Adams, Soc. Electrochem. Conf., "High Energy and High Power Density Batterries" Shell Research Centre, Thornton, Cheshire, Dec. I97I.

I26. W.T. Grubb and C.J. Michalske, J. Electrochem. Soc., III, 477 (I964).

I27. E.W. Justi and A.W. Winsel, J. Electrochem. Soc., I08, I073 (I96I).

I28. R.G. Haldeman et al., Advan. Chem., 47, I06 (I965).

I29. S.S. Tomter and A.P. Antony, Chem. Eng. Prog., 59, 47 (I963).

I30. L. Wong, Thesis-M.Phil., The City University.

I3I. E.A. Grens, Ind. Eng. Chem. Fund., 5, 542 (I966).

I32. G.F. Bianchi, F. Mazza and T. Mussini, Electrochim. Acta, 7 457 (I962).

I33. J.P. Hoare, Electrochim. Acta, II, 203 (I966).

I34. M.L.B. Rao, A. Damjanovic and J. O'M Bockris, J. Phys. Chem., 67, 2509 (I963).

I35. J.P. Hoare, J. Electrochem. Soc., II3, 846 (I966).

I36. J. Goualard and J.P. Harivel, Paper at Sixth Int. power

Sources Symp., Brighton, Sussex, Sept. I968.

I37. H.A. Christopher, Proc. Ann. Power Sources Conf., 20, I8 (I966).

I38. H. Rumpf, Chem. Ing. Tech., 30, I44 (I958).

I39. E. Monegold in "Kapillarsysteme", Verlag Strassenbau, Chem. U. Technik., Heidelberg, I955, p.524.

I40. R.A. Fischer, J. Agric. Sci., I6, 492 (I926).

I4I. W. Batel, Forsch-Ber. Wirtshafts-U. Verkehrsministeriums N. W., Dusseldorf, No. 262 (I956).

I42. S. Yamadaya et al., J. of Catalysis, I9, 264 (I970).

I43. A.J. Stirling, J. Iron and Steel Inst. (London), I77, 25 (I954).

I44. Information from Westinghouse Electric Corporation (I969).

I45. Information from Thermo Electron Engineering Corporation (I969).

I46. J.J. Loferskii, Proc. IEEE, 5I, 667 (I963).

I47. Information from Avco Everett Research Lab. (I969).

I48. S.A. Yabbe, Aviation Week, Jan.20th I969.

I49. K.V. Kordesch in "Handbook of Fuel Cell Technology", Ed. C. Berger, Prentice-Hall Inc., Englewood Cliffs, N.J. (I968).

I50. D.H. Archer et al., Proc. Ann. Power Sources Conf., I8, 36 (I964).

I5I. D.H. Archer et al., Chem. Eng. Prog., 60, 64 (I964).

I52. D.H. Archer et al., ibid 63, 55 (I967).

I53. Information from Allison Division, General Motors Corp., (I969).

I54. R.A. Horne, A.F. Day, R.P. Young and N.T. Yu, Electrochim. Acta, I3, 397 (I968).

I55. A.J. Appleby, Electroanal. Chem., 24, 97, (I970).

I56. J. O'M Bockris and S. Sirinivasan, "Fuel Cells" McGraw Hill (I969).

I57. J. Giner and C. Hunter, J. Electrochem. Soc., II6, II24 (I969).

I58. J. Giner, M. Perry, S. Smith and M. Turchan, J. Electrochem. Soc., II6, p.I692 (I969).

I59. C.N. Satterfield, "Mass Transfer in Heterogeneous Catalysis", M.I.T. Press, London (I970).

I60. F.G. Will and D.J. Bendaniel, J. Electrochem. Soc., II6, 933 (I969).

I6I. B.S. Hobbs, Ph.D. Thesis, The City University, I970.

I62. E.W. Thiele Ind. Eng. Chem., 3I, 9I6 (I939).

I63. G. Damkohler, Der Chemie-Ingenieur, 3, 430 (I937).

I64. Ya. B. Zeldovich, Acta Physiochim., U.R.S.S., I0, 583 (I939).

I65. Private Communication, M.S. Kent, The City University.

I66. W.King, Ph.D. Thesis, The City University (I972).

I67. L.Bevan, Ph.D. Thesis, The City University (I97I).

I68. H.E. Kubitschek, 'Research' I3, I78 (I960).

I69. J. Giner, J.M. Parry and S.M. Smith, Advances in Chemistry Series, No. 90, Fuel Cell Systems II, Am. Chem. Soc. (I969).

I70. R.A. Myers and J.M. Marchells, J. Electrochem. Soc., II6, 790 (I969).

I7I. J. Giner, J. Electrochem. Soc., III, 376 (I964).

I72. S. Barnett, J. Electrochem. Soc., I08, I02 (I96I).

I73. J. O'M Bockris and A.M. Azzan, Trans. Farad. Soc., 48, I45 (I952).

I74. W.J. Moore, "Physical Chemistry", Longmans Press (I965), Ch. 9 p.326.

I75. P. Delahay, "New Inst. Methods in Electrochem.",Interscience, (I966), Ch.9, p.2I7.

I76. D.P. Gregory and A.C. Riddiford,J. Chem. Soc., 3756 (I956).

I77. P. Delahay, "New Inst. Methods in Electrochem.", Ch.9 p.233.

I78. P. Delahay, ibid Ch.6 p.II5.

I79. P. Delahay, ibid Ch.I0 p.256.

I80. S.H. Maron and C.F. Prutton, "Principles of Physical Chemistry", MacMillan, (I958) Ch.7, p.2I7.

I8I. S. Brunauer and P.H. Emmett and T. Teller, J. Am. Chem. Soc., 60, 309 (I938).

I82. B.C. Lippens and M. Hermans, Powder Metallergy, 7, 66 (I96I).

I83. E.L. Fuller, H.F. Holmes, C.H. Secoy, Vacuum Microbalance Techniques Vol. 4, Plenum Press (I965) p.I09.

I84. K.R. Williams, "An introduction to Fuel Cells", Elsevier, (I966).

I85. L.D. Burke and A. Moynihan, Trans. Farad. Soc.,67, 3550 (I97I

I86. E.H. Kerner and D. MacKenzie, Proc. Phys. Soc., (London) 69B, 808 (I956).

I87. T.A. Dorling, C.J. Burlace and R.L. Moss, J. of Catalysis, I2, 207 (I968).

I88. T.A. Posey and T. Morozumi, J. Electrochem. Soc., II3, I76 (I966).

I89. H. Gerischer and M.O. Krause, Z. Phys. Chem. N.F., IO, 264, (I959).

I90. H. Gerischer and K.E. Staubach, Z. Elektrochem., 6I, 789 (I957).

I9I. W. Kuhn et al., "Ultrafine Particles", J. Wiley (I963).

I92. J. Boyes-Watson, E. Davidson and M. Perutz, Proc. Roy. Soc. (London), AI9I, 83 (I947).

I93. A.M. Taylor and A. King, Nature, I32, 64 (I933).

I94. B.V. Deryagin and M. Kusakov, Acta Physiochim. U.R.S.S., IO, 25 (I939) and IO, I53 (I939).

I95. B. Peschel, G. and K. Adlfinger, J. Colloid and Interfacial Science, 34 , 505 (I970).

I96. J. Giner and S. Smith, J. Electrochem. Technol., 5, 59 (I967).

I97. P. Delahay, "Advances in Electrochemistry and Electrochemical Engineering", Vol. I, p.265, Interscience (I96I).

I98. P. Hauck, Chemie Ing-Tech., 34, 369 (I964).

Appendix I.

The shapes of potentiostatic transients on porous electrodes.

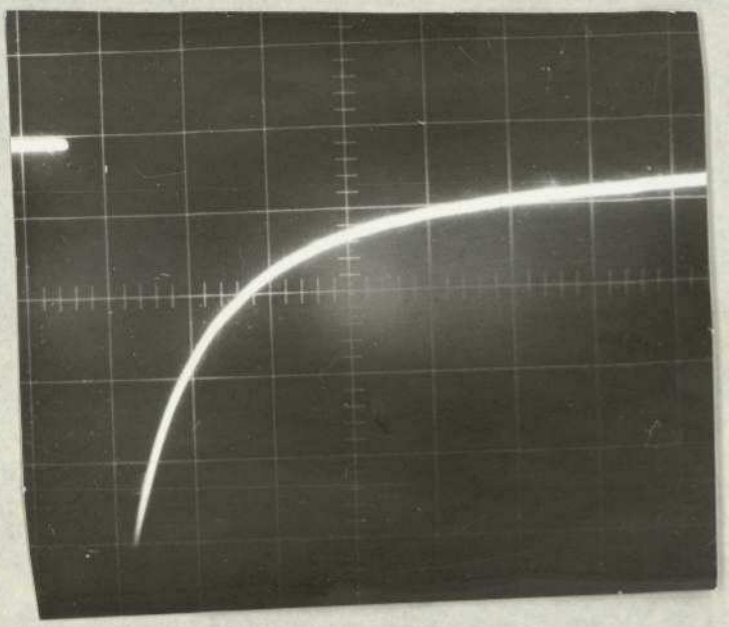
Notes.

(I) A comparison of A, B, D and E shows that the oxide reduction current falls more quickly with time.

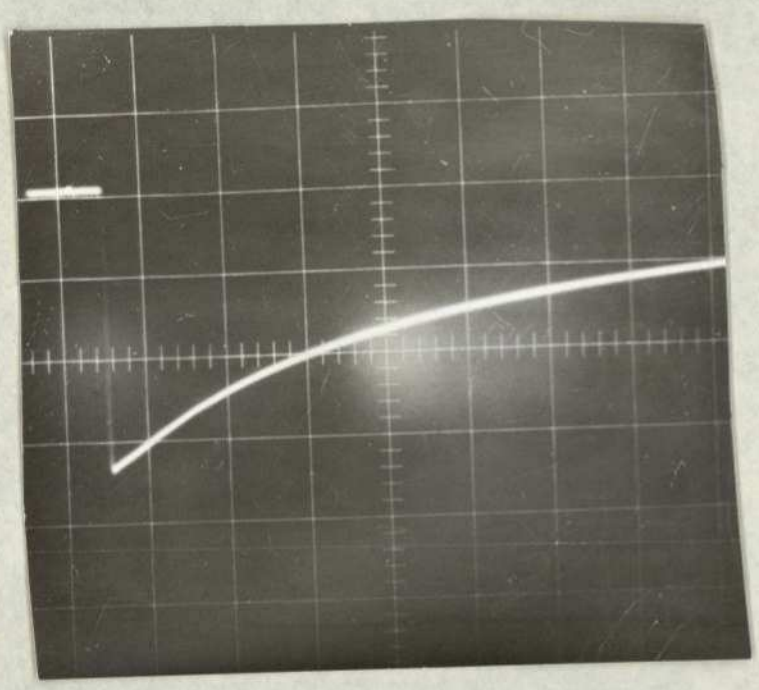
(2) The unusual slopes of cuves F,G and H for the hydrogen electrode reactions is probably caused by the very fast mass transport of the electroactive species (H_2 or H_3O^+) from the hydrophobic phase to the active site in contrast to the much slower diffusion through the bulk electrolyte. As gas at the hydrophobic phase is depleted, transition from almost zero mass transfer control to more normal conditions occurs and the current falls with time.

(3) Curves I and J show that the oxygen evolution current decays more rapidly on the clean than the preanodised surface.

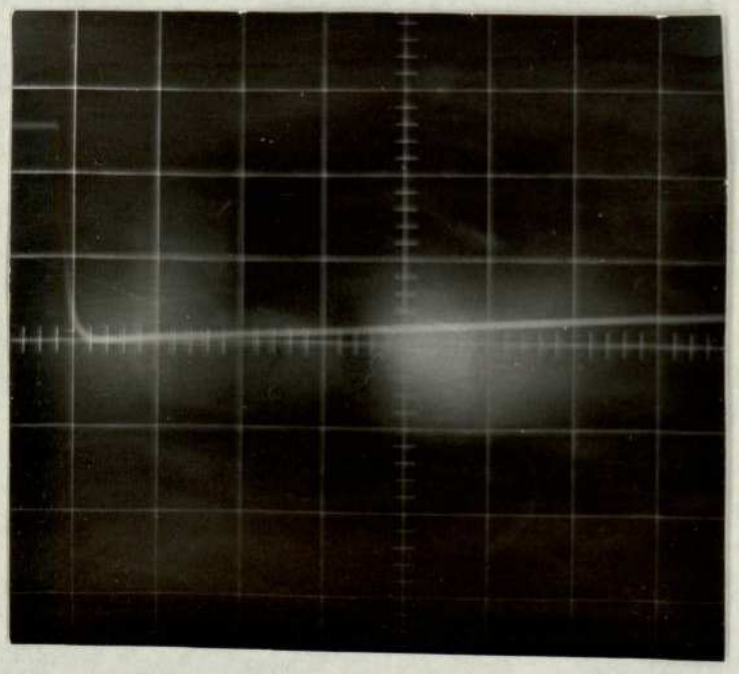
(4) A comparison of K, F and J shows the different hydrogen evolution transient shapes for platinum foil and two platinum black samples of different pore size.



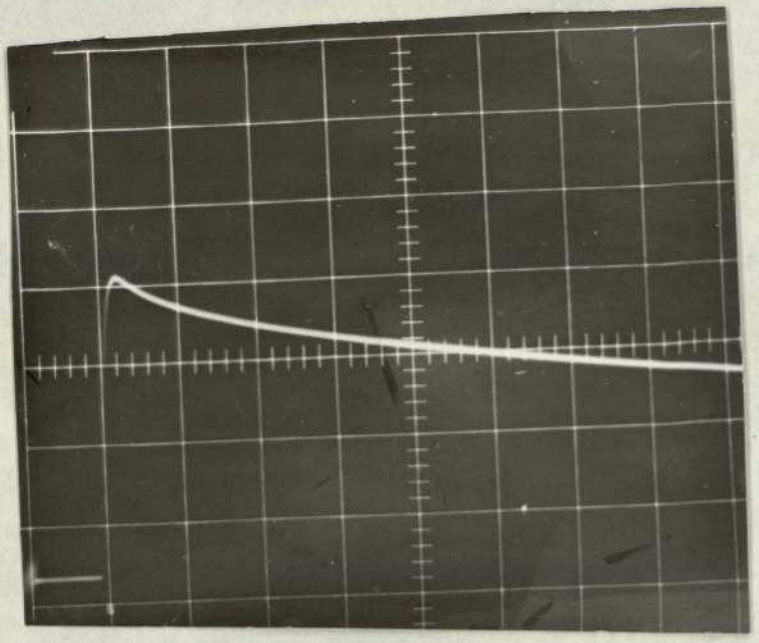
A



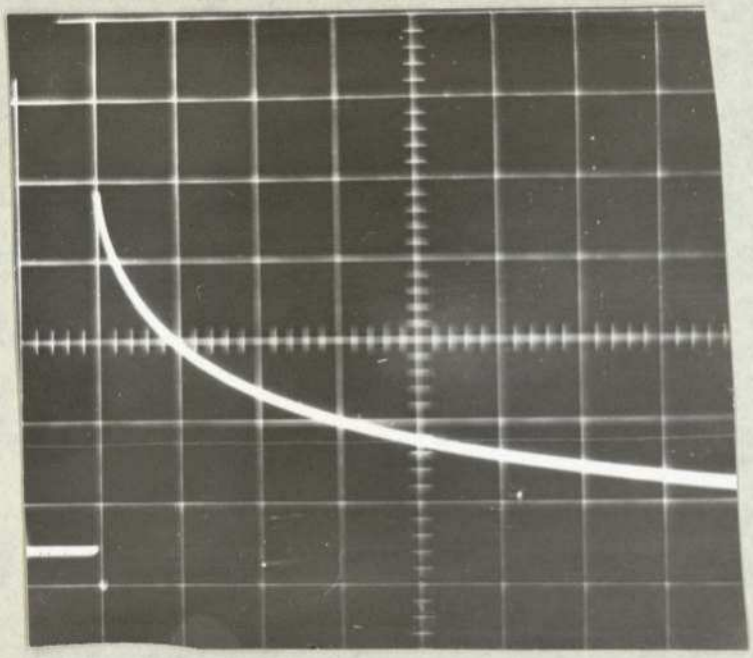
B



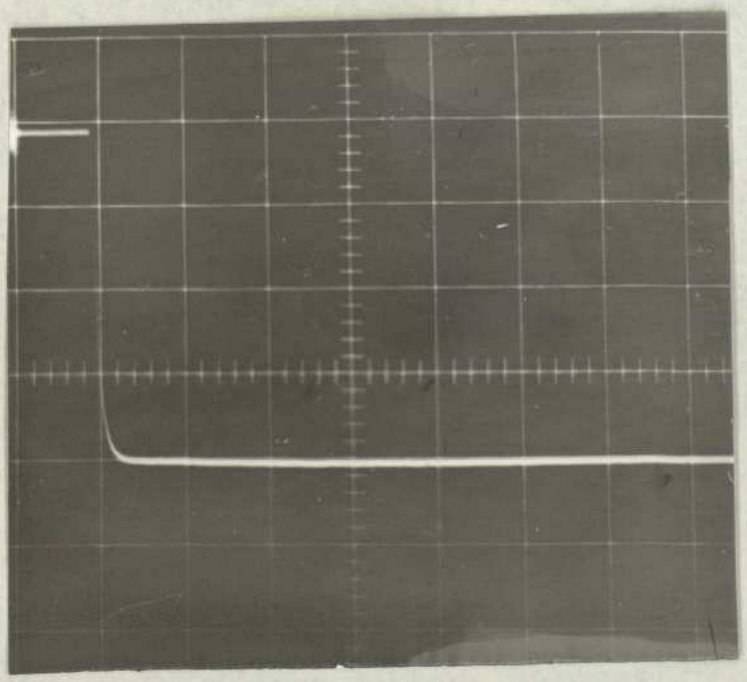
C



D



E



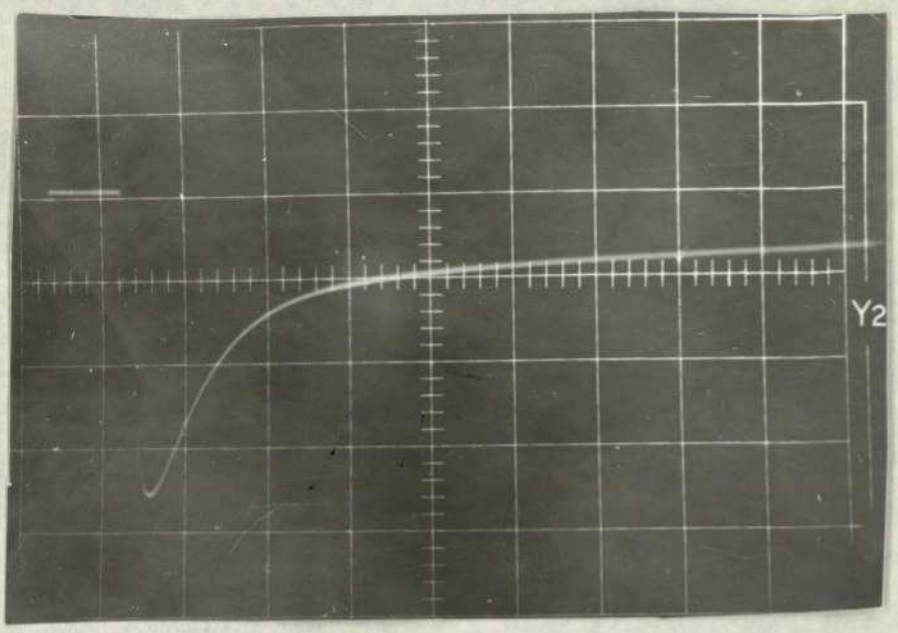
F

G

H

I

J



K

J

Key for oscilloscope traces.

Key	Reaction	Pulse (volts)	X axis time scale.
A	O_2 reduction	1·04 – 0·84	10 ms/cm.
B	" "	1·04 – 0·84	1 ms/cm
C	" "	1·04 – 0·99	0·1 ms/cm
D.	Oxide "	1·02 – 0·77	0·1 ms/cm
E	" "	1·02 – 0·82	1 ms/cm
F	H_2 evolution	0·025 – −0·025	0·1 ms/cm
G	H_2 oxidation	0·025 – 0·075	0·1 ms/cm
H	" "	0·025 – 0·075	1 ms/cm
I	O_2 evolution on oxide surface	1·02 – 1·62	1 ms/cm
J.	O_2 evolution on clean surface	1·04 – 1·84	1 ms/cm.
K	H_2 evolution	0·030 – −0·020	0·1 ms/cm
J.	H_2 evolution	0·025 – −0·075	0·1 ms/cm.

A – J teflon bonded platinum black in 5N H_2SO_4 at 20°C.
platinum black surface area $16 m^2 . g^{-1}$

K. platinum foil in 5N H_2SO_4 at 20°C

J. teflon bonded platinum black in 5N H_2SO_4 at 20°C.
platinum black surface area = $8 m^2 . g^{-1}$